BEILSTEIN JOURNAL OF ORGANIC CHEMISTRY

Progress in liquid crystal chemistry II

Edited by Sabine Laschat

Imprint

Beilstein Journal of Organic Chemistry
www.bjoc.org
ISSN 1860-5397
Email: journals-support@beilstein-institut.de

The *Beilstein Journal of Organic Chemistry* is published by the Beilstein-Institut zur Förderung der Chemischen Wissenschaften.

Beilstein-Institut zur Förderung der Chemischen Wissenschaften
Trakehner Straße 7–9
60487 Frankfurt am Main
Germany
www.beilstein-institut.de

Beilstein Journal of Organic Chemistry

Progress in liquid crystal chemistry II

Sabine Laschat

Editorial

Open Access

Address:
Institut für Organische Chemie, Universität Stuttgart, Pfaffenwaldring 55, D-70569 Stuttgart, Germany

Email:
Sabine Laschat - sabine.laschat@oc.uni-stuttgart.de

Beilstein J. Org. Chem. **2012,** *8,* 118–119.
doi:10.3762/bjoc.8.13

Received: 16 January 2012
Accepted: 17 January 2012
Published: 24 January 2012

This article is part of the Thematic Series "Progress in liquid crystal chemistry II".

Guest Editor: S. Laschat

It is a great pleasure to introduce this second Thematic Series on "Progress in liquid crystal chemistry" within the *Beilstein Journal of Organic Chemistry*. Why liquid crystals?

Liquid crystals have a major impact on our modern society, reaching from simple digital calculators to high-resolution flat-panel displays, and their market volume is expected to further increase. For example, in 2010 revenues of €1,013 million from sales of liquid crystals were reported by Merck, the world's largest supplier of liquid crystal materials for electro-optical applications. This increase of 38% on 2009 was attributed to the demand for liquid crystal displays (LCDs). Forecasts predict annual global shipments of over 268.8 million LCD television sets by 2014 [1]. However, the chemistry behind liquid crystals, and particularly the synthesis, is the platform for such tremendous technological achievements, and this is true for both calamitic (rod-like) as well as discotic (disk-shaped) or other types of liquid crystals [2-4].

Since our initial Thematic Series "Progress in liquid crystal chemistry" two years ago [5], the research field has further broadened and stretches currently from materials science, through energy conversion and storage, to life sciences. The interested reader might be directed to a very recent special issue of *Liquid Crystals* edited by John W. Goodby to find more detailed information [6].

The review articles and original research papers of this second Thematic Series in the *Beilstein Journal of Organic Chemistry*, written by known experts of their field, cover diverse topics such as novel discotic and calamitic compounds, bent-core mesogens, amphiphiles, and liquid-crystalline nanoparticles. It is our goal to give the reader insight into both synthetic aspects of liquid crystal chemistry as well as application-oriented properties, such as photoconductivity or chirality transfer, to name just a few selected examples. Finally, we would particularly like to inspire people with complementary expertise, working in different fields of chemistry, to join forces with the liquid crystal community and to introduce their specific knowledge and objectives in order to aid the further advancement of this topic.

Sabine Laschat

Stuttgart, January 2012

References

1. Merck Annual Report 2010 - Liquid Crystals. http://merck.online-report.eu/2010/ar/performancematerials/liquidcrystals.html (accessed Jan 16, 2012).
2. Goodby, J. W. *Liq. Cryst.* **2011,** *38,* 1363–1387. doi:10.1080/02678292.2011.614700
3. Hird, M. *Liq. Cryst.* **2011,** *38,* 1467–1493. doi:10.1080/02678292.2011.625126
4. Bushby, R. J.; Kawata, K. *Liq. Cryst.* **2011,** *38,* 1415–1426. doi:10.1080/02678292.2011.603262
5. Laschat, S. *Beilstein J. Org. Chem.* **2009,** *5,* No. 48. doi:10.3762/bjoc.5.48
6. Goodby, J. W. *Liq. Cryst.* **2011,** *38,* 1357–1358. doi:10.1080/02678292.2011.639938

License and Terms

Beilstein Journal of Organic Chemistry

Improved syntheses of high hole mobility phthalocyanines: A case of steric assistance in the cyclo-oligomerisation of phthalonitriles

Daniel J. Tate[1], Rémi Anémian[2], Richard J. Bushby*[1], Suwat Nanan[1], Stuart L. Warriner[3] and and Benjamin J. Whitaker[3]

Full Research Paper

Open Access

Address:
[1]Centre for Molecular Nanoscience (CMNS), University of Leeds, Woodhouse Lane, Leeds, LS2 9JT, United Kingdom, [2]Merck KGaA, Industriepark Höchst, D 65926 Frankfurt am Main, Germany and [3]School of Chemistry, University of Leeds, Woodhouse Lane, Leeds, LS2 9JT, United Kingdom

Email:
Richard J. Bushby* - R.J.Bushby@leeds.ac.uk

* Corresponding author

Keywords:
high hole mobility; phthalocyanine; steric assistance; Thorpe–Ingold effect; time-of-flight

Beilstein J. Org. Chem. **2012,** *8,* 120–128.
doi:10.3762/bjoc.8.14

Received: 23 August 2011
Accepted: 07 November 2011
Published: 24 January 2012

This article is part of the Thematic Series "Progress in liquid crystal chemistry II".

Guest Editor: S. Laschat

Abstract

It has been shown that the base-initiated cyclo-oligomerisation of phthalonitriles is favoured by bulky α-substituents making it possible to obtain the metal-free phthalocyanine directly and in high yield. The phthalocyanine with eight α-isoheptyl substituents gives a high time-of-flight hole mobility of 0.14 $cm^2 \cdot V^{-1} \cdot s^{-1}$ within the temperature range of the columnar hexagonal phase, that is 169–189 °C.

Introduction

Liquid crystalline semiconductors [1,2] are potentially useful in the fabrication of organic field-effect transistors [3,4], light-emitting devices [5-7] and photovoltaic devices [8-11]. Most of the interest has centred on using them as hole conductors and a lot of effort has been expended on designing columnar liquid crystals with high hole mobilities. There are fewer examples of good liquid crystalline electron conductors, and most of those known can only be used in an oxygen-free environment [12,13]. However, the columnar phases of 1,4,8,11,15,18,22,25-octa-octylphthalocyanine show good time-of-flight transits for both holes and electrons, together with exceptionally high mobilities (time-of-flight hole mobilities of 0.20 $cm^2 \cdot V^{-1} \cdot s^{-1}$ in the Col_r phase at 85 °C and 0.10 $cm^2 \cdot V^{-1} \cdot s^{-1}$ in the Col_h phase at 100 °C; electron mobilities of 0.30 $cm^2 \cdot V^{-1} \cdot s^{-1}$ in the Col_r phase at 85 °C and 0.20 $cm^2 \cdot V^{-1} \cdot s^{-1}$ in the Col_h phase at 100 °C) [14,15]. Furthermore, this phthalocyanine gives good time-of-flight electron transits even in an ambient atmosphere [15]. As a result, related α-alkylated phthalocyanines are attracting interest for use in organic devices, such as solar cells [16], and this stimulated our efforts to produce further examples

[17]. As part of that work we investigated cases in which the α-substituents were branched-chain types. Since we did not want to produce mixtures of diasterioisomers, we used either citronellol-based chains (enantiomerically pure substrates from the chiral pool) or symmetrical, nonchiral R_2CH-terminated chains, which we synthesised from commercially available carboxylic acids or alcohols. We discovered that bulky, branched-chain α-substituents provide steric assistance in the conversion of the phthalonitrile precursors to the phthalocyanines, thus leading to substantially enhanced yields. Just as the cyclo-oligomerisation reaction is favoured by the "pull" of a transition metal template, it can also be enhanced using the "push" of suitable α-substituents. This makes the metal-free phthalocyanines much easier to produce on a multigram scale.

Results and Discussion

Synthesis

In synthesising many different α-alkylated phthalocyanines [17] we experimented with various routes to the phthalonitrile precursors **6** (Scheme 1). The route that we originally used was one described by Cook et al. for the octaoctyl compound **7a** [18]. This involved bis-alkylation of thiophene (**1**), oxidation to the corresponding sulfone **3**, and treatment with fumaronitrile (Scheme 1, top line). However, for most of the phthalonitriles we have made, we have found that a much better route is the nickel-catalysed reaction of an alkylzinc iodide with the bistriflate of 3,6-dihydroxyphthalonitrile **5** (Scheme 1, middle line), previously described in the patent literature [19,20].

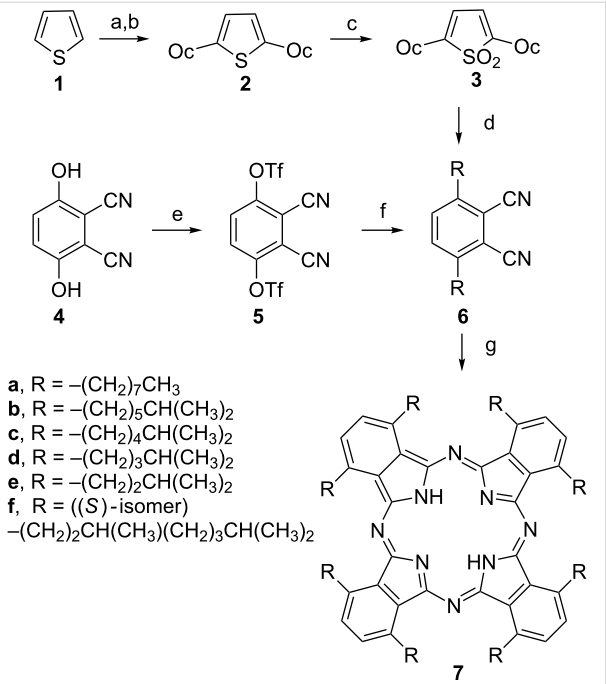

Scheme 1: (Top) original synthesis of compound **7a** from thiophene (Oc = *n*-octyl) [19]. (Below) shortened synthesis of α-alkylated derivatives through the triflate of 3,6-dihydroxyphthalonitrile. Reagents: (a) BuLi; (b) $C_8H_{15}Br$; (c) MCPBA , 35–51%; (d) fumaronitrile/Δ, 40–48%; (e) $(Tf)_2O$; (f) (i) RZnI, $NiCl_2(PPh_3)_2$, PPh_3, BuLi (ii) KBr/−78 °C; (g) (i) $Li/C_5H_{11}OH/\Delta$, (ii) AcOH.

The phthalonitriles made in this way were converted to the phthalocyanines by treating them with lithium pentoxide in refluxing pentanol [18,21-32]. Yields of phthalocyanines prepared by this route are generally poor and usually less than 25% [29-32]. This, together with the need for chromatographic purification, limits the scale on which metal-free phthalocyanine liquid crystals can be made. Such low yields are common for nontemplated phthalonitrile cyclo-oligomerisation reactions and, although high-yielding nontemplated routes have been developed for some metal-free phthalocyanines [19,33-35], for the liquid-crystalline phthalocyanines, the low yield of the cyclo-oligomerisation step is a problem. Somewhat surprisingly, for some of the branched-chain α-alkylated systems, we obtained very good yields even without using a metal template. As shown in Table 1, not only are some of these yields exceptionally high (for nontemplated phthalonitrile oligomerisation), but there is also a clear relationship between the isolated, recrystallised yield and the steric bulk of the α-substituent. As the bulk of the side-chain is increased or as the branch point in the side-chain is moved closer to the nucleus, so the yield improves. In order to check that the high yields were not the result of templating by adventitious transition metal ion impurities, the phthalocyanine **7f** was subjected to ICP-MS trace metal impurity analysis, but levels of transition metal impurities were found to be below the IPC-MS detection limit (ppb). The most likely explanation for the effect of these branched-chain substituents on the yields of these reactions is shown schematically in Scheme 2. In the intermediates **8** (Scheme 2, X = $C_5H_{11}O$, Y = growing oligomer chain) the exocyclic carbon/nitrogen double bond marked * presumably has the (*Z*)-stereochemistry shown. This is the favoured stereochemistry for most imides of aromatic ketones, although the opposite stereo-

Table 1: Isolated yields of purified phthalocyanine (chromatographed, and in the case of **7a**–**7e** crystallised) obtained by treating the corresponding phthalonitrile **6** for ca. 16 h with lithium pentoxide in refluxing pentanol. For α-alkylated phthalocyanines with *n*-alkyl substituents, the average yield obtained by this route is 22 ± 5% (based on the fourteen known examples) [29-32].

	Alkyl chain	Yield (%)
7a	$–(CH_2)_7CH_3$	17 [25]
7b	$–(CH_2)_5CH(CH_3)_2$	28
7c	$–(CH_2)_4CH(CH_3)_2$	45
7d	$–(CH_2)_3CH(CH_3)_2$	62
7e	$–(CH_2)_2CH(CH_3)_2$	78
7f	((*S*)-isomer) $–(CH_2)_2CH(CH_3)(CH_2)_2CH(CH_3)_2$	83

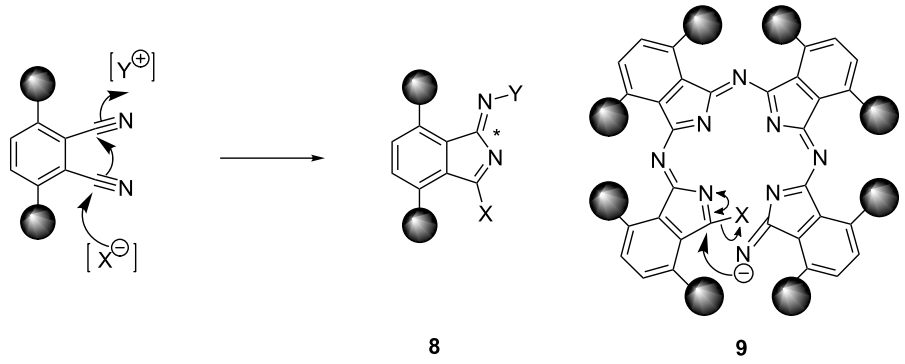

Scheme 2: Effect of bulky α-alkyl substituents on the base-initiated cyclo-oligomerisation of phthalonitriles.

chemisty is only a little bit less stable if the *ortho*-positions of the benzene ring are unsubstituted [36]. On the other hand, if these "*ortho*"-positions are substituted, this should provide a bias towards the (*Z*)-isomer. More significant in the context of phthalocyanine formation is the cumulative effect of these substituents on the conformation of the open-chain tetrameric precursor **9** (or its equivalent, Scheme 2) to the phthalocyanine nucleus. Examination of models for compound **9** shows that it is impossible for this intermediate to achieve total planarity. More important is the fact that an increase in the bulk of the alkyl substituents in the "*ortho*" positions will reinforce the preference for a (*Z*)-configuration about all of the exocyclic carbon/nitrogen partial double bonds, all six of which need to be *Z* in the cyclisation transition state. Hence, since the substituents would restrict the conformational space available to the intermediate, they would favour cyclisation. This phenomenon is clearly related to the effect of *gem*-dimethyl groups on the cyclisation of acyclic compounds (the Thorpe–Ingold effect) [37]. From the standpoint of making phthlocyanine-based liquid crystals, its importance is that it provides a simple, high-yielding route to metal-free α-alkylated phthalocyanines.

Liquid-crystal properties

The liquid-crystal behaviour of the compounds we synthesised was investigated by polarising microscopy, differential scanning calorimetry (DSC) and, in the cases of compounds **7c–7e**, by low-angle X-ray diffraction. The DSC data is summarised in Table 2, the phase behaviour of the isoalkyl series is compared graphically with that for the *n*-alkyl series in Figure 1 and typical polarizing micrographs are shown in Figure 2. Compounds **7b** and **7c** exhibit Col_h columnar mesophases. For compound **7b** the nature of the phase formed at temperatures below that for the Col_h phase (the phase formed between 112 and 124 °C) remains uncertain, but comparison of the optical textures (compare Figure 2d with Figure 2b and Figure 2f) suggests that it is crystalline rather than liquid-crystalline, and its texture is clearly very different to that of the Col_r phase of **7a** (Figure 2b). The X-ray data obtained for compound **7c** in the Col_h phase at 170–195 °C shows a 110/200 diffraction band corresponding to a = 19.2 Å and a broad band corresponding to a d spacing of 3.5–5.0 Å. For compound **7a** in its Col_h phase, Cook et al. reported a 110/200 band a = 22.6 Å, a very weak 310 band at ~13.0 Å, and a broad band corresponding to a d spacing of 3.5–5.0 Å [30]. In our case we were not able to detect the weak 310 band, but this is not unusual for the Col_h phase. The X-ray diffraction experiments confirmed that the phases formed by **7c** below 169 °C were crystalline and not columnar liquid-crystalline (not Col_r) in nature and that compounds **7d** and **7e** did not give liquid-crystalline phases.

Because suitable precursors for most isoalkyl chains are not commercially available and because (at the simplest level of

Table 2: Phase behaviour of the phthalocyanines determined by differential scanning calorimetry (second heating and first cooling cycle and a heating/cooling rate of 10 °C min^{-1}).

	Alkyl chain	Phase behaviour °C (ΔH, J·g^{-1})
7b	$–(CH_2)_5CH(CH_3)_2$	Cr_1 112 (15) Cr_2 (?)124 (9) Col_h 170 (11) I 162 (−11) Col_h 105 (−9) Cr_2 (?) 20 (−9) Cr_1
7c	$–(CH_2)_4CH(CH_3)_2$	Cr 169 (14) Col_h 189 (35) I 169 (−17) Col_h161 (−14) Cr_1 140 (−11) Cr
7d	$–(CH_2)_3CH(CH_3)_2$	Cr 237 (43) I 223 (−51) Cr
7e	$–(CH_2)_2CH(CH_3)_2$	Cr_1 238 (2) Cr_2 284 (40) I 190 (−43) Cr_1
7f	((*S*)-isomer) $–(CH_2)_2CH(CH_3)(CH_2)_2CH(CH_3)_2$	Isotropic liquid at rt

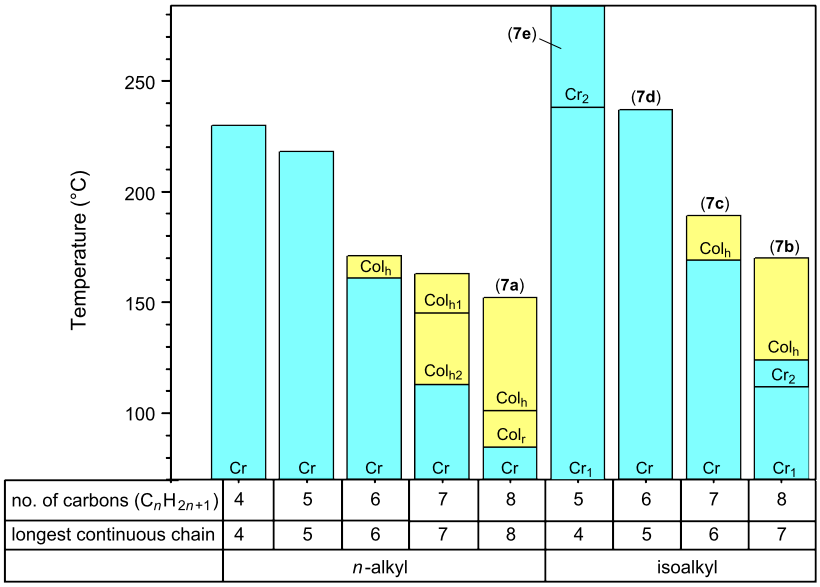

Figure 1: Comparison of the phase behaviours of the α-substituted phthalocyanines with *n*-alkyl [25] and isoalkyl side chains. The stable ranges for the crystal phases are shown in blue and those of the columnar liquid-crystalline phases in yellow.

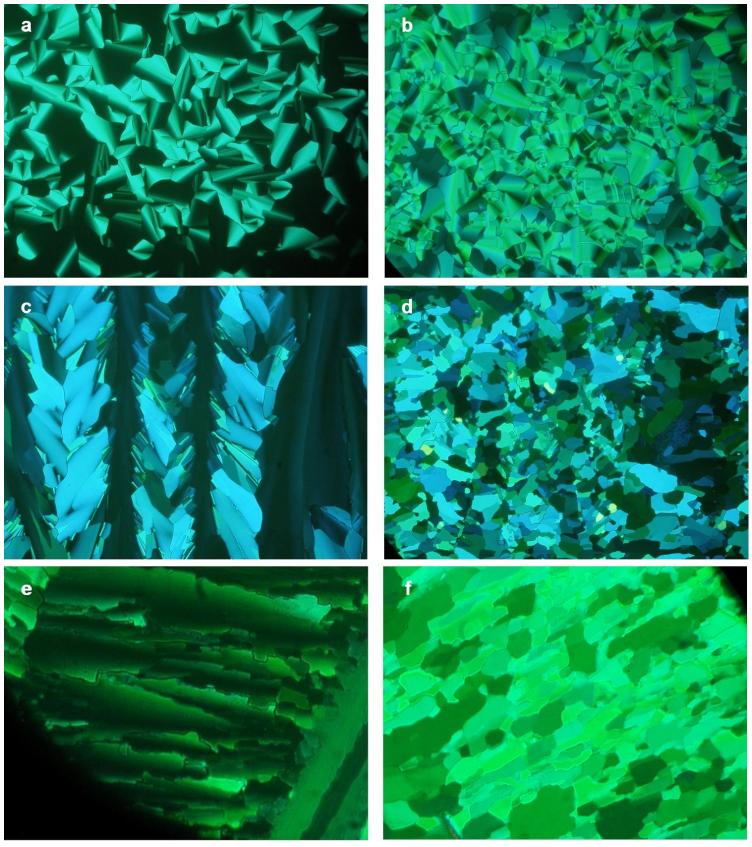

Figure 2: Optical micrographs taken with crossed polarisers and at a magnification of × 20. (a) *n*-Octyl derivative **7a** in the Col_h phase at 145 °C. (b) **7a** in the Col_r phase at 100 °C. (c) Isooctyl derivative **7b** in the Col_h phase at 170 °C. (d) **7b** in the unknown (but probably Cr) phase at 120 °C. (e) Isoheptyl derivative **7c** in the Col_h phase at 170 °C. (f) **7c** in the Cr phase at 155 °C.

theory) the space-filling properties of disordered/fluid *n*-alkyl and isoalkyl chains are expected to be "much the same", there have been few studies of the differences between the liquid-crystal properties of *n*-alkyl and isoalkyl-substituted liquid-crystal derivatives. However, Gray and Kelly have shown that in the cyanobiphenyl and cyanoterphenyl series the differences are substantial with the N/I transition temperatures being lower in the isoalkyl series by between 8 and 50 °C (on the basis of comparing chains of equal maximum length): An effect reasonably attributed to the greater lateral separation between the molecules in the isoalkyl series [38]. In the isoalkyl-substituted phthalocyanines **7** the Col–I transition temperatures are a little higher than they are in the *n*-alkyl series (by 18 or 26 °C on the basis of a comparison of chains with the same number of carbon atoms; by 7 or 18 °C on the basis of a comparison of chains of maximum equal length). This may reflect a stronger column–column interaction within the Col_h phase, and it is consistent with the observation that the column–column spacing for **7c** (the isoheptyl derivative) is rather shorter than the value extrapolated for the *n*-hexyl derivative from the values reported for the *n*-heptyl and *n*-octyl compounds [30].

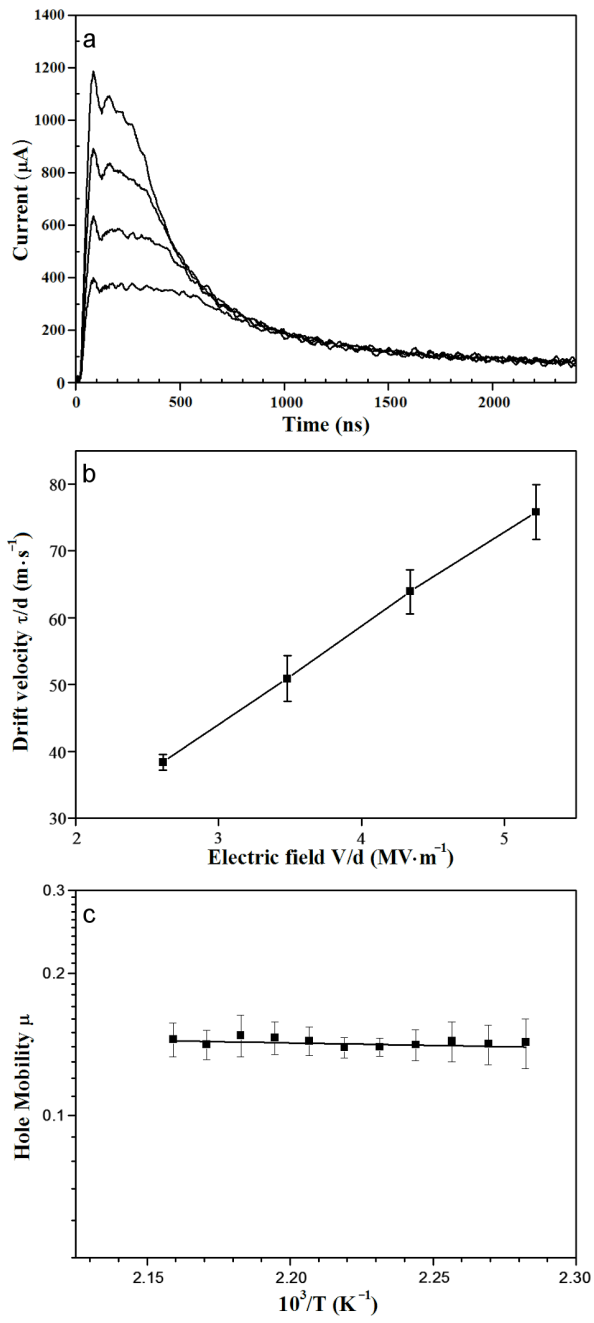

Figure 3: (a) Time-of-flight hole transits for an ITO/**7c**/ITO cell with the liquid crystal in its Col_h phase at 185 °C. Applied voltages 60 V (top trace), 80 V, 100 V, 120 V (bottom trace). (b) Drift velocity as a function of electric field (185 °C). (c) Temperature-dependence of the hole mobility within the Col_h phase. The error bars represent 2σ.

Time-of-flight photoconductivity

The hole mobility for compound **7c** was measured in its Col_h phase in the temperature range 169–189 °C. Slow cooling of a thin film sandwiched between ITO-coated glass slides readily gave the required homotropically aligned sample. However, a problem was encountered with the ToF measurements. Because the transit times are very short, the electronic noise generated by firing of the laser was found to overlap with the transient signal significantly, making it difficult to determine the transit times [39]. To overcome this problem, we found it necessary to increase the working distance between the sample and the laser. Even at the greatest practicable working distance (several metres), some noise was still seen in the first 200–300 ns of the transit, however, it was sufficiently reduced in the critical 300–800 ns region such that transit times could be determined. Figure 3a shows the time-of-flight signals for a sample of **7c** with a thickness of 23 μm at applied voltages of 60–120 V and at 185 °C. Figure 3b shows the plot of drift velocity as a function of field, each point being an average of five or more independent measurements. The mobilities were obtained from the slopes of these plots at each temperature. As shown in Figure 3c, the mobility is almost temperature-independent within the mesophase range. The hole mobility of **7c** in the Col_h phase at 185 °C was found to be 0.14 $cm^2 \cdot V^{-1} \cdot s^{-1}$, which is a little higher than that value previously reported for **7a** of 0.10 $cm^2 \cdot V^{-1} \cdot s^{-1}$ in the Col_h phase at 100 °C [14].

Conclusion

Mobilities measured by the time-of-flight method are usually significantly lower than those measured by the pulse-radiolysis time-resolved microwave conductivity (PR-TRMC) method because of the very high frequency employed in PR-TRMC. At such high frequencies the charge carriers only migrate over

microdomains, avoiding deep traps. Furthermore PR-TRMC records the combined mobilities of the holes and the electrons. Hence, although there are a number of PR-TRMC mobilities for liquid crystals that are as high as, or even higher than, that for **7c**, a value of 0.14 $cm^2 \cdot V^{-1} \cdot s^{-1}$ is one of the very highest recorded for a macrodomain (time-of-flight) hole mobility of a liquid crystal. The reason why the mobilities of these α-alkylated phthalocyanines are this high is not entirely easy to understand. Mobilities in liquid crystals are usually intermediate between those measured in crystalline and amorphous organic solids, and the mobility is primarily related to the degree of positional [40-44] or charge [45,46] disorder within the system. In most cases where a high time-of-flight mobility has been reported, the observation can be related to exceptionally high ordering in the mesophase, as revealed by X-ray diffraction (as in the Col_p phases of hexakispropyloxytriphenylene and hexakisbutyloxytriphenylene, the H phase of hexakishexylthiotriphenylene and the Col phases of CPI discotics) [40,42]. In the case of these α-alkylated phthalocyanines, there is no evidence from the X-ray studies of any particular "higher" order in the mesophase but, in comparing them to the triphenylenes, it is important to take into account the larger size of the aromatic core [47].

The steric assistance provided to the base-initiated cyclisation of α-alkylated phthalonitriles, when the α-substituents are branched-chain, enables the corresponding metal-free phthalocyanines to be made easily and on a multigram scale. Although in the examples given in this paper the compounds formed in the highest yields (for those phthalonitriles branched at the 3-position of the alkyl chain) are not liquid-crystalline, liquid-crystalline examples with branching at the 3-position could easily be designed.

Experimental

DSC Studies

DSC studies used a Perkin Elmer DSC-7 instrument calibrated with indium (mp 156.60, $\Delta H = 28.53\ J \cdot g^{-1}$) and a heating/cooling rate of 10 $°C \cdot min^{-1}$.

Time-of-flight photoconductivity studies

The cells were assembled in a laminar-flow hood to avoid contamination by dust or grease. Each ITO-coated glass slide was connected to a copper wire by epoxy resin (Aradite) and the tip of the wire was bonded to the ITO surface with silver paint (RS 186-3600). The two halves were separated by a PET spacer (Goodfellow Cambridge Limited) with a thickness of 23 μm, held in position with clips and secured with epoxy resin. The thickness of the cell (d) was accurately determined by measuring the UV–vis scattering spectrum of the empty cell. The liquid-crystal sample was filled into the cell in its isotropic phase by capillary action. The sample was heated up to a few degrees above the liquid-crystal to isotropic phase transition temperature and then was cooled into the liquid-crystal phase at 0.1 $°C \cdot min^{-1}$ to produce a monodomain, homotropically aligned sample (checked by polarising microscopy). The temperature of the cell was then controlled ± 0.1 °C on a Linkam hot stage. A field of 2.5–5.5 $MV \cdot m^{-1}$ (applied voltage, V ~ 60–120 V) was applied across the cell, a laser pulse (Nd-YAG laser, wavelength of 355 nm, intensity 30 mJ/pulse before filtering) was used to illuminate one side, and the resultant transits were recorded. Calculations show that this light is absorbed within <1 μm of the electrode surface. In some cases, a neutral density filter was used to reduce the laser power. The transit times τ were determined from the inflection point in a double logarithmic plot of the measured transient photocurrents, from a series of at least five independent experiments. The electron mobility for **7c** was not determined since the inflection in the time-of-flight signal was insufficiently distinct. As in the case of **7a**, and indeed as in the case of all other "high mobility" liquid crystals, there was no evidence for field dependence of the mobility. Hence, the mobility μ (= $d^2/V\tau$) was determined from the slope of a linear fit to the plot of drift velocity (τ/d) versus field (V/d), as shown in the example in Figure 3b.

Synthesis

General procedures

Flash chromatography was carried out on Merck (230–400 mesh) silica with HPLC grade solvent as eluent. TLC was carried out on Merck silica gel (60 Å) F_{254} coated glass plates. Melting points were recorded on a Linkam LTSE300 heating stage. IR spectra were carried out on a Perkin Elmer Spectrum 1 FT-IR spectrometer. ^1H and $^{13}C\{^1H\}$ NMR spectra were recorded on a Bruker DPX300 spectrometer. Proton and carbon signals were assigned by using a combination of $^1H/^1H$ (COSY) and $^{13}C\{^1H\}/^1H$ (HMBC and HMQC} correlation methods. Both EI and FD mass spectra were recorded on a Waters CGT micromass instrument. ES mass spectra were recorded on a Bruker Datonics Micro ToF instrument. Elemental analyses were performed in the Microanalysis Department of the School of Chemistry, University of Leeds.

3-Methylbutyl iodide [48]

To a flame-dried flask purged with argon was added triphenylphosphine (44.61 g, 0.170 mol), imidazole (16.16 g, 0.255 mol) and anhydrous diethyl ether/acetonitrile (125 mL/125 mL). The stirred reaction mixture was cooled (0 °C, ice bath) and 3-methylbutanol (7.50 g, 0.085 mol) was added. After 10 min, iodine (28.07 g, 0.111 mol) was added in portions. Upon completion of the addition the mixture was allowed to

warm to rt and stirred for a further 2 h. The mixture was diluted with pentane (200 mL), and washed sequentially with sat $Na_2S_2O_3$ (2 × 50 mL), sat $CuSO_4$ (2 × 50 mL), brine (50 mL), dried ($MgSO_4$) and concentrated in vacuo. The crude product was purified on silica gel with pentane as eluent (R_f ~0.70) to afford the title compound as a homogeneous oil (15.3 g, 91%).

IR (neat): 2956 (C–H), 2929 (C–H), 2906 (C–H), 2870 (C–H) cm^{-1}; ^1H NMR ($CDCl_3$, 300 MHz) δ 3.21 (t, J = 7.2 Hz, 2H, $(CH_3)_2CHCH_2CH_2I$), 1.74–1.69 (m, 3H, $(CH_3)_2CHCH_2CH_2I$), 0.91 (d, J = 6.37 Hz, 6H, $(CH_3)_2CH(CH_2)_2I$); ^{13}C NMR ($CDCl_3$, 75 MHz) δ 42.6 (C2), 29.1 (C3), 21.7 (C4), 5.4 (C1); HRMS–EI (70 eV) m/z: $[M - I]^+$ calcd for C_5H_{11}, 71.0860; found, 71.0854; Anal. calcd for $C_5H_{11}I$: C, 30.23; H, 5.60; I, 64.08; found: C, 30.40; H, 5.70; I, 63.80.

4-Methylpentyl iodide [49], 5-methylhexyl iodide [50,51], 6-methylheptyl iodide and (*S*)-3,7-dimethyloctyl iodide [52] were obtained in the same manner (see Supporting Information File 1).

3-Methylbutylzinc iodide

Activated zinc dust was always freshly prepared in the same glassware to be used for the subsequent stages. A suspension of zinc (7.85 g, 120 mmol) was stirred in a 2% solution of HCl (20 mL) for 2 min. The resulting dust was sequentially stirred and decanted with a 2% solution of HCl (20 mL), water (3 × 20 mL) and EtOH (2 × 20 mL). The resultant suspension was allowed to settle, decanted and washed with Et_2O (20 mL). Finally the remainder of the glassware for the reaction was assembled and the activated zinc (ca. 6.54 g, 100 mmol) was dried under vacuum (ca. 0.1 mbar), purged with argon, flame dried under vacuum (ca. 0.05 mbar) and again purged with argon ready for use.

Under an argon atmosphere, the freshly prepared activated zinc dust (16 g, 0.23 mol, 3 equiv) was stirred in anhydrous THF (30 mL). Dibromoethane (0.97 mL, 0.011 mol, 15 mol %) was added via syringe and the mixture was heated under reflux for ca. 10 min, cooled, and again heated under reflux for ca. 10 min and cooled. Trimethylsilyl chloride (1.44 mL, 0.011 mol, 15 mol %) was added and the mixture heated under reflux once more and allowed to cool. 3-Methybutyl iodide (12 g, 0.061 mol) was added via syringe and the mixture was stirred for 16 h at 40 °C. Upon completion of the reaction, the mixture was allowed to cool to rt and the excess zinc was allowed to settle. The resultant grey solution was transferred to a Schlenk tube via cannula, and the remaining zinc powder was washed with THF (30 mL) and transferred to the Schlenk tube to afford the title compound (62 mL, 0.90 M solution, assuming a ~90% conversion).

3,6-Bis(trifluoromethanesulfonyloxy)phthalonitrile (**5**) [20]

To a flame-dried flask, trifluoromethanesulfonic anhydride (24.6 mL, 149 mmol) dissolved in anhydrous DCM (20 mL) was added dropwise to a cooled (−20 °C) stirred solution of 2,3-dicyanohydroquinone (**4**) (10.0 g, 62.5 mmol) dissolved in anhydrous DCM (30 mL) and 2,6-lutidine (60 mL). Upon completion of the addition, the reaction mixture was maintained at −20 °C for 1 h and then allowed to warm to rt and stirred for a further 16 h. The reaction was quenched by the addition of water (20 mL), extracted into EtOAc (3 × 50 mL), washed successively with 10% NaOH (2 × 30 mL), 10% HCl (2 × 30 mL), brine (2 × 20 mL), dried (Na_2SO_4) and concentrated in vacuo to afford the title compound as colourless prisms (18.8 g, 71%). mp (MeOH) 109–110 °C (lit [19] 109–111 °C); IR (neat): 2252 (CN), 1471 (C=C), 1436 (C=C), 1223 (S=O) cm^{-1}; ^1H NMR ($CDCl_3$, 300 MHz) δ 7.87 (s, 2H, 4,5H); ^{13}C NMR ($CDCl_3$, 75 MHz) δ 148.9 (C3,6), 128.7 (C4,5), 114.6 (q, J = 319.5 Hz, 2 × CF_3), CN not observed; HRMS–EI (70 eV) m/z: $[M]^+$ calcd for $C_{10}H_2N_2S_2F_6O_6$, 423.9259; found, 423.9272; Anal. calcd for $C_{10}H_2N_2S_2F_6O_6$: C, 28.31; H, 0.48; N, 6.60; S, 15.12; found: C, 28.20; H, 0.35; N, 6.55; S, 15.10.

3,6-Bis(3-methylbutyl)phthalonitrile (**6e**)

To a flame-dried flask, under an argon atmosphere, were added bis(triphenylphosphine)nickel(II) dichloride (1.18 g, 1.82 mmol), triphenylphosphine (0.95 g, 3.6 mmol) and anhydrous THF (40 mL). *n*-Butyllithium (1.45 mL, 3.64 mmol, 2.5 M in hexanes) was added to the stirred mixture to afford a blood red slurry. 3,6-Bis(trifluoromethanesulfonyloxy)-phthalonitrile (7.71 g, 18.2 mmol) and KBr (6.48 g, 54.5mmol) was added under a fast stream of argon. The resultant brown solution was cooled to −78 °C. Freshly prepared 3-methylbutylzinc iodide (62.4 mL, 56.17 mmol, 0.90 M solution in THF) was added dropwise over a period of 1 h via cannula from a Schlenk flask. Upon completion of the addition, the reaction mixture was allowed to warm to rt and stirred for a further 16 h. The reaction was quenched by the careful addition of 10% HCl (10 mL) and the mixture was extracted with EtOAc (3 × 30 mL). The combined organic extracts were successively washed with 10% HCl (20 mL), 5% NaOH (20 mL), brine (20 mL), dried ($MgSO_4$) and concentrated in vacuo. The resultant yellow solid was purified by chromatography on silica gel with 5% EtOAc/hexane (v:v) as eluent until all triphenylphosphine was extracted. The title compound [24] was isolated as colourless needles (3.51 g, 72%) by increasing the polarity to 10% EtOAc/hexane (v:v). R_f ~ 0.30; mp (petroleum ether) 62–63 °C; IR (neat): 2957 (C–H), 2936 (C–H), 2872 (C–H), 2226 (CN), 1468 (C=C), 1459 (C=C) cm^{-1}; ^1H NMR ($CDCl_3$, 500 MHz) δ 7.42 (s, 2H, C4H and C5H), 2.85 (t, J = 8.1 Hz, 4H, $ArCH_2CH_2CH(CH_3)_2$), 1.64 (m, J = 6.5 Hz, 2H,

$Ar(CH_2)_2CH(CH_3)_2$), 1.54 (m, 4H, $ArCH_2CH_2CH(CH_3)_2$), 0.97 (d, J = 6.6 Hz, 12H, $Ar(CH_2)_2CH(CH_3)_2$); ^{13}C NMR ($CDCl_3$, 125 MHz) δ 146.44 (C3 and C6), 133.43 (C4 and C5), 115.60 and 115.11 (C1, C2 and CN), 39.91 (C'2), 32.38 (C'1), 27.87 (C'3), 22.33 (C'4); HRMS–EI (70 eV) m/z: $[M-CH_3]^+$ calcd for $C_{17}H_{21}N_2$, 253.1704; found, 253.1696 (100); Anal. calcd for $C_{18}H_{24}N_2$: C, 80.55; H, 9.01; N, 10.44; found: C, 79.90; H, 8.95; N, 10.30.

3,6-Bis(4-methylpentyl)phthalonitrile (**6d**), 3,6-bis(5-methylhexyl)phthalonitrile (**6c**), 3,6-bis(6-methylheptyl)phthalonitrile (**6b**) and 3,6-bis((*S*)-3,7-dimethyloctyl)phthalonitrile (**6f**) were prepared in the same manner (see Supporting Information File 1).

1,4,8,11,15,18,22,25-Octa(3-methylbutyl)phthalocyanine (**7e**)

To a flame-dried flask, under an argon atmosphere, lithium metal (0.013 g, 1.86 mmol) was added to a solution of 3,6-bis(3-methylbutyl)phthalonitrile (1.0 g, 3.73 mmol) dissolved in freshly distilled pentanol (10 mL) under reflux. Upon completion of the addition, the reaction mixture turned dark green and was stirred under reflux for 4 h. The mixture was allowed to cool to rt and acetone (5 mL) was added. Excess pentanol was removed in vacuo and the resultant dark green oil, which crystallised on standing, was purified by chromatography on silica gel with 10% DCM/hexane as eluent ($R_f \sim 0.30$) to afford the title compound [24] as fine blue-green needles, which were recrystallised from 1:1 THF/acetone (0.81 g, 81%). mp 282–284 °C; DSC (°C, J·g^{-1}): Cr 284.1 (40) I 189.9 (−43); IR (neat): 3303 (N–H), 2954 (C–H), 2931 (C–H), 2864 (C–H) cm^{-1}; ^{1}H NMR ($CDCl_3$, 500 MHz) δ 7.86 (s, 8H, C2,3,9,10,16,17,23,24H), 4.46 (t, J = 7.5 Hz, 16H, 5 $ArCH_2CH_2CH(CH_3)_2$), 1.91 (dt, J = 6.8 Hz and 8.1 Hz, 16H, $ArCH_2CH_2CH(CH_3)_2$), 1.79 (m, J = 6.6 Hz, 8H, $Ar(CH_2)_2CH(CH_3)_2$), 0.99 (d, J = 6.6 Hz, 48H, $Ar(CH_2)_2CH(CH_3)_2$); ^{13}C NMR ($CDCl_3$, 75 MHz) δ 139.5 (C1,4,8,11,15,22,25), 131.2 (C2,3,9,10,16,17,23,24), 40.4 (C'2), 30.9 (C'1), 27.9 (C'3), 23.4 (C'4); HRMS–ES$^+$ m/z: $[M]^+$ calcd for $C_{72}H_{98}N_8$, 1074.7909; found 1074.7857 (100%), 1075.7900 (75%) $[M + 1]^+$, 1076.7934 (30%) $[M + 2]^+$.

1,4,8,11,15,18,22,25-Octa(4-methylpentyl)phthalocyanine (**7d**), 1,4,8,11,15,18,22,25-octa(5-methylhexyl)phthalocyanine (**7c**), 1,4,8,11,15,18,22,25-octa(6-methylheptyl)phthalocyanine (**7b**) and 1,4,8,11,15,18,22,25-octa((*S*)-3,7-dimethyloctyl)phthalocyanine (**7f**) were all prepared in the same manner (see Supporting Information File 1).

Supporting Information

Synthesis, analytical and spectroscopic details for the alcohols, alkyl iodides, phthalonitriles **6b–6d** and **6f** and phthalocyanines **7b–7d** and **7f**.

Supporting Information File 1

Experimental details.
[http://www.beilstein-journals.org/bjoc/content/supplementary/1860-5397-8-14-S1.pdf]

Acknowledgements

We thank the EPSRC for a studentship (DJT) and the Royal Thai Government for a DPST scholarship (SN). We also thank James Cattle (supported by a Nuffield Foundation Studentship) for the optical microscopy images.

References

1. Li, Q., Ed. *Self-Organised Organic Semiconductors: From Materials to Device Applications;* Wiley: New York, 2011.
2. Bushby, R. J.; Kawata, K. *Liq. Cryst.* **2011,** *38,* 1415–1426. doi:10.1080/02678292.2011.603262
3. Pisula, W.; Menon, A.; Stepputat, M.; Lieberwirth, I.; Kolb, U.; Tracz, A.; Sirringhaus, H.; Pakula, T.; Müllen, K. *Adv. Mater.* **2005,** *17,* 684–689. doi:10.1002/adma.200401171
4. van de Craats, A. M.; Stutzmann, N.; Bunk, O.; Nielsen, M. M.; Watson, M.; Müllen, K.; Chanzy, H. D.; Sirringhaus, H.; Friend, R. H. *Adv. Mater.* **2003,** *15,* 495–499. doi:10.1002/adma.200390114
5. Seguy, I.; Destruel, P.; Bock, H. *Synth. Met.* **2000,** *111–112,* 15–18. doi:10.1016/S0379-6779(99)00405-1
6. Seguy, I.; Jolinat, P.; Destruel, P.; Farenc, J.; Mamy, R.; Bock, H.; Ip, J.; Nguyen, T. P. *J. Appl. Phys.* **2001,** *89,* 5442–5448. doi:10.1063/1.1365059
7. Hassheider, T.; Benning, S. A.; Kitzerow, H.-S.; Achard, M.-F.; Bock, H. *Angew. Chem., Int. Ed.* **2001,** *40,* 2060–2063. doi:10.1002/1521-3773(20010601)40:11<2060::AID-ANIE2060>3.0.CO;2-H
8. Schmidt-Mende, L.; Fechtenkötter, A.; Müllen, K.; Moons, E.; Friend, R. H.; MacKenzie, J. D. *Science* **2001,** *293,* 1119–1122. doi:10.1126/science.293.5532.1119
9. Schmidt-Mende, L.; Fechtenkötter, A.; Müllen, K.; Friend, R. H.; MacKenzie, J. D. *Physica E* **2002,** *14,* 263–267. doi:10.1016/S1386-9477(02)00400-9
10. Schmidtke, J. P.; Friend, R. H.; Kastler, M.; Müllen, K. *J. Chem. Phys.* **2006,** *124,* 174704. doi:10.1063/1.2194536
11. Hesse, H. C.; Weickert, J.; Al-Hussein, M.; Dössel, L.; Feng, X.; Müllen, K.; Schmidt-Mende, L. *Sol. Energy Mater. Sol. Cells* **2010,** *94,* 560–567. doi:10.1016/j.solmat.2009.11.024
12. Boden, N.; Borner, R. C.; Bushby, R. J.; Clements, J. *J. Am. Chem. Soc.* **1994,** *116,* 10807–10808. doi:10.1021/ja00102a065
13. de Leeuw, D. M.; Simenon, M. M. J.; Brown, A. R.; Einerhand, R. E. F. *Synth. Met.* **1997,** *87,* 53–59. doi:10.1016/S0379-6779(97)80097-5
14. Iino, H.; Hanna, J.-i.; Bushby, R. J.; Movaghar, B.; Whitaker, B. J.; Cook, M. J. *Appl. Phys. Lett.* **2005,** *87,* No. 132102. doi:10.1063/1.2056608

15. Iino, H.; Takayashiki, Y.; Hanna, J.-i.; Bushby, R. J. *Jpn. J. Appl. Phys.* **2005,** *44,* L1310–L1312. doi:10.1143/jjap.44.L1310
16. Hori, T.; Miyake, Y.; Yamasaki, N.; Yoshida, H.; Fujii, A.; Shimizu, Y.; Ozaki, M. *Appl. Phys. Express* **2010,** *3,* 101602–101624. doi:10.1143/APEX.3.101602
17. Tate, D. J. Applications of Discotic Liquid Crystals in Organic Electronics. Ph.D. Thesis, University of Leeds, 2008.
18. McKeown, N. B.; Chambrier, I.; Cook, M. J. *J. Chem. Soc., Perkin Trans. 1* **1990,** 1169–1177. doi:10.1039/P19900001169
19. Uchida, H.; Yoshiyama, H.; Reddy, P. Y.; Nakamura, S.; Toru, T. *Bull. Chem. Soc. Jpn.* **2004,** *77,* 1401–1404. doi:10.1246/bcsj.77.1401
20. Cook, M. J.; Heeney, M. J. Substituted phthalocyanines and their precursors. PCT Patent WO 20011042368A1, June 14, 2001.
21. Pawlowski, G.; Hanack, M. *Synthesis* **1980,** 287–289.
22. Piechocki, C.; Simon, J.; Skoulios, A.; Guillon, D.; Weber, P. *J. Am. Chem. Soc.* **1982,** *104,* 5245–5247. doi:10.1021/ja00383a050
23. Ohta, K.; Watanabe, T.; Tanaka, S.; Fujimoto, T.; Yahamoto, I.; Bassoul, P.; Kucharczyk, N.; Simon, J. *Liq. Cryst.* **1991,** *10,* 357–368. doi:10.1080/02678299108026282
24. McKeown, N. B.; Painter, J. *J. Mater. Chem.* **1994,** *4,* 1153–1156. doi:10.1039/JM9940401153
25. Cook, M. J.; Daniel, M. F.; Harrison, K. J.; McKeown, N. B.; Thomson, A. J. *J. Chem. Soc., Chem. Commun.* **1987,** 1086–1088. doi:10.1039/C39870001086
26. Cook, M. J.; McKeown, N. B.; Thomson, A. J.; Harrison, K. J.; Richardson, R. M.; Davies, A. N.; Roser, S. J. *Chem. Mater.* **1989,** *1,* 287–289. doi:10.1021/cm00003a001
27. Cammidge, A. N.; Cook, M. J.; Haslam, S. D.; Richardson, R. M.; Harrison, K. J. *Liq. Cryst.* **1993,** *14,* 1847–1862. doi:10.1080/02678299308027720
28. Cammidge, A. N.; Bushby, R. J. Discotic Liquid Crystals: Synthesis and Structural Features. In *Handbook of Liquid Crystals: Low Molecular Weight Liquid Crystals II;* Demus, D.; Goodby, J.; Gray, G. W.; Spiess, H.-W.; Vill, V., Eds.; Wiley-VCH: Weinheim, Germany, 1998; Vol. 2B, pp 693–748. doi:10.1002/9783527620623.ch4
29. McKeown, N. B.; Chambrier, I.; Cook, M. J. *J. Chem. Soc., Perkin Trans. 1* **1990,** 1169–1177. doi:10.1039/P19900001169
30. Cherodian, A. S.; Davies, A. N.; Richardson, R. M.; Cook, M. J.; McKeown, N. B.; Thomson, A. J.; Feijoo, J.; Ungar, G.; Harrison, K. *Mol. Cryst. Liq. Cryst.* **1991,** *196,* 103–114. doi:10.1080/00268949108029690
31. Swarts, J. C.; Langner, E. H. G.; Krokeide-Hove, N.; Cook, M. J. *J. Mater. Chem.* **2001,** *11,* 434–443. doi:10.1039/b006123i
32. Cammidge, A. N.; Cook, M. J.; Hughes, D. L.; Nekelson, F.; Rahman, M. *Chem. Commun.* **2005,** 930–932. doi:10.1039/b414820g
33. Kharisov, B. I.; Méndez, U. O.; Garza, J. L. A.; Rodríguez, J. R. A. *New J. Chem.* **2005,** *29,* 686–692. doi:10.1039/b415712p
34. Chauhan, S. M. S.; Agarwal, S.; Kumari, P. *Synth. Commun.* **2007,** *37,* 2917–2925. doi:10.1080/00397910701470768
35. Uchida, H.; Tanaka, H.; Yoshiyama, H.; Reddy, P. Y.; Nakamura, S.; Toru, T. *Synlett* **2002,** *10,* 1649–1652. doi:10.1055/s-2002-34237
36. Clark, P. F.; Elvidge, J. A.; Golden, J. H. *J. Chem. Soc.* **1956,** 4135–4143. doi:10.1039/JR9560004135
37. Jung, M. E.; Piizzi, G. *Chem. Rev.* **2005,** *105,* 1735–1766. doi:10.1021/cr940337h
38. Gray, G. W.; Kelly, S. M. *Mol. Cryst. Liq. Cryst.* **1984,** *104,* 335–345. doi:10.1080/00268948408070435
39. Kashima, K.; Sato, H.; Musha, K.; Kanno, K.-i.; Takahashi, T. *Anal. Sci.* **2007,** *23,* 1249–1251. doi:10.2116/analsci.23.1249
40. Adam, D.; Schuhmacher, P.; Simmerer, J.; Häussling, L.; Siemensmeyer, K.; Etzbachi, K. H.; Ringsdorf, H.; Haarer, D. *Nature* **1994,** *371,* 141–143. doi:10.1038/371141a0
41. Hirai, Y.; Monobe, H.; Mizoshita, N.; Moriyama, M.; Hanabusa, K.; Shimizu, Y.; Kato, T. *Adv. Funct. Mater.* **2008,** *18,* 1668–1675. doi:10.1002/adfm.200701313
42. Wegewijs, B. R.; Siebbeles, L. D. A.; Boden, N.; Bushby, R. J.; Movaghar, B.; Lozman, O. R.; Liu, Q.; Pecchia, A.; Mason, L. A. *Phys. Rev. B* **2002,** *65,* 245112. doi:10.1103/PhysRevB.65.245112
43. Paraschiv, I.; de Lange, K.; Giesbers, M.; van Lagen, B.; Grozema, F. C.; Abellon, R. D.; Siebbeles, L. D. A.; Sudhölter, E. J. R.; Zuilhof, H.; Marcelis, A. T. M. *J. Mater. Chem.* **2008,** *18,* 5475–5481. doi:10.1039/b805283b
44. Gearba, R. I.; Lehmann, M.; Levin, J.; Ivanov, D. A.; Koch, M. H. J.; Barberá, J.; Debije, M. G.; Piris, J.; Geerts, Y. H. *Adv. Mater.* **2003,** *15,* 1614–1618. doi:10.1002/adma.200305137
45. Iino, H.; Hanna, J.-i.; Bushby, R. J.; Movaghar, B.; Whitaker, B. J. *J. Appl. Phys.* **2006,** *100,* 043716. doi:10.1063/1.2219692
46. Ochse, A.; Kettner, A.; Kopitzke, J.; Wendorff, J. H.; Bässler, H. *Phys. Chem. Chem. Phys.* **1999,** *1,* 1757–1760. doi:10.1039/A808615J
47. van de Craats, A. M.; Warman, J. M. *Adv. Mater.* **2001,** *13,* 130–133. doi:10.1002/1521-4095(200101)13:2<130::AID-ADMA130>3.0.CO;2-L
48. Chiles, M. S.; Jackson, D. D.; Reeves, P. C. *J. Org. Chem.* **1980,** *45,* 2915–2918. doi:10.1021/jo01302a035
49. Page, P. C. B.; McKenzie, M. J.; Allin, S. M.; Klair, S. S. *Tetrahedron* **1997,** *53,* 13149–13164. doi:10.1016/S0040-4020(97)00837-5
50. Berkenbusch, T.; Brückner, R. *Tetrahedron* **1998,** *54,* 11461–11470. doi:10.1016/S0040-4020(98)00687-5
51. Levene, P. A.; Allen, C. H. *J. Biol. Chem.* **1916,** *27,* 433–462.
52. Chen, C. Y.; Nagumo, S.; Akita, H. *Chem. Pharm. Bull.* **1996,** *44,* 2153–2156.

License and Terms

Beilstein Journal of Organic Chemistry

Laterally substituted symmetric and nonsymmetric salicylideneimine-based bent-core mesogens

Sonja Findeisen-Tandel[1], Wolfgang Weissflog*[1], Ute Baumeister[1], Gerhard Pelzl[1], H. N. Shreenivasa Murthy[1] and Channabasaveshwar V. Yelamaggad[2]

Full Research Paper

Open Access

Address:
[1]Martin-Luther-Universität Halle-Wittenberg, Institut für Chemie, Physikalische Chemie, von-Danckelmann-Platz 4, 06120 Halle, Germany and [2]Centre for Soft Matter Research, Jalahalli, Bangalore 560 013, India

Email:
Wolfgang Weissflog* - weissflog@chemie.uni-halle.de

* Corresponding author

Keywords:
antiferroelectric smectic phases; bent-core mesogens; electro-optical behaviour; liquid crystals; salicylideneanilines

Beilstein J. Org. Chem. **2012,** *8,* 129–154.
doi:10.3762/bjoc.8.15

Received: 14 September 2011
Accepted: 29 November 2011
Published: 24 January 2012

This article is part of the Thematic Series "Progress in liquid crystal chemistry II".

Guest Editor: S. Laschat

Abstract

Bent-core mesogens have gained considerable importance due to their ability to form new mesophases with unusual properties. Relationships between the chemical structure of bent-core molecules and the type and physical properties of the formed mesophases are relatively unknown in detail and differ strongly from those known for calamitic liquid crystals. In this paper symmetric and nonsymmetric five-ring salicylideneaniline-based bent-core mesogens are presented, and the effect of lateral substituents attached at the outer phenyl rings (F, Cl, Br) or the central phenyl ring (CH_3) on the liquid-crystalline behaviour and on the physical properties is studied. Corresponding benzylideneaniline-based compounds were additionally prepared in order to study the influence of the intramolecular hydrogen bond. The occurring mesophases were investigated by differential scanning calorimetry, polarising microscopy, X-ray diffraction and dielectric and electro-optical measurements. The paper reports on new findings with respect to the structure–property relationships of bent-core mesogens. On one hand, the disruptive effect of laterally substituted halogen atoms, F, Cl and Br, on the mesophase behaviour of three isomeric series was much lower than expected. On the other hand, an increase of the clearing temperature by 34 K was observed, caused by small lateral substituents. The electro-optical behaviour, especially the type of polar switching and corresponding molecular movements, is sensitive to variations in the molecular structure.

Introduction

For a long time there was a general perception that molecules capable of exhibiting liquid crystal (LC) phases have to be rodlike, so-called calamitic LCs. As is well known, such compounds exhibit nematic and smectic phases, which are commonly referred to as “calamitic phases”. However, the inherent fallacy of this notion was pointed out in the middle of the seventies when columnar (Col) phases were discovered in disklike (discotic) mesogens; such mesogens also exhibit

nematic behaviour like that of calamitics. In fact, a survey of the literature shows clearly that molecules with a bent (banana) shape prepared earlier than discotics by Vorlaender (in 1929) possess the ability to exhibit mesomorphism. Interest in such nonconventional mesogens increased remarkably in the mid-1990s following the report by Niori and co-workers [1] that the mesophases (banana phases) formed by 1,3-disubstituted benzenes hold unusual properties. As a result, a large number of banana-shaped compounds have been synthesized with various combinations of structural fragments, and thus, they represent a new subfield of liquid crystals. Generally speaking, these mesogens prefer to pack in layers so as to yield smectic phases. Due to their bent shape there is a lateral correlation of molecular dipoles yielding a polar order within the layers, which can be switched on application of an electric field. The molecular arrangement of bent-core molecules, with respect to the tilt and the polarity in adjacent layers of a SmCP phase, is shown in Supporting Information File 1, Figure S1. An explanation of the suffixes **P**, **A**, **F**, **s**, and **a**, used for the characterization of banana phases, is also given there. In the SmCP phase the molecular long axis is tilted with respect to the layer normal, which corresponds to a C_2 symmetry of the smectic layers. The combination of director tilt and polar order leads to a chirality of the smectic layers, although the constituent molecules are achiral [2]. In this context it should be noted that there is a tilted smectic "banana phase" designated as SmCG, which exhibits chiral smectic layers with C_1 symmetry [3,4].

In order to avoid a macroscopic polar order, in most cases the polar axes in adjacent layers are antiparallel such that, in general, antiferroelectric $SmCP_A$ phases occur, which can be switched into the corresponding ferroelectric state. This switching, and also the switching between opposite ferroelectric states, usually takes place by the collective rotation of the molecules around the tilt cone. It is seen from Supporting Information File 1, Figure S1 that during this switching, the chirality of the layers does not change. However, there are SmCP phases where the switching is based on a collective rotation of the molecules around their long molecular axes. In this case the chirality of the smectic layers is changed by the switching process, which is a prominent feature observed in the present investigation.

The formation of simple layer structures is disrupted if the amount of space required by the rigid cores and the flexible terminal chains is too different. Together with certain polar forces, such connection can result in undulating tilted smectic phases designated as USmCP, or columnar phases of different structure. The columns are represented by polar-layer fragments. Two examples are given: In the B_1 phase, the columns form a 2D rectangular cell. However, the structural feature of B_7 phases is a splay of polarization, which gives rise to an undulation of smectic layers or two-dimensionally ordered layer fragments [5].

Due to such unusual behaviour banana-shaped liquid crystals have emerged as a special topic in the field of liquid crystals. It should be pointed out here, that polar banana phases have only been formed by bent molecules up until now. Although a bent conformation is also exhibited by dimesogens due to the presence of odd-parity central spacer, they do not spontaneously form polar banana phases [6,7].

In general, banana-shaped molecules consist of five or more aromatic rings, in which two wings (rodlike arms) are attached to the 1,3-positions of a central phenyl ring. The vast majority of the banana-shaped mesogens contain ester and/or azomethine linking groups. It is remarkable that derivatives containing an azomethine group (Schiff bases) often show interesting polymorphism. Relationships between molecular structure and the formation of banana phases have been summarized, together with the structure and the behaviour of these phases, in several reviews, see e.g., [8-11].

It is well-known that a hydroxy group in ortho-position to the CH=N (azomethine) unit not only enhances the photochemical and hydrolytic stability due to intramolecular H-bonding, but also increases the clearing temperature of liquid crystals. Therefore, the introduction of salicylideneimine fragment(s) in the LC molecular architecture has attracted significant attention. Several examples demonstrate this, as many salicylideneanilines exhibiting mesophases are listed, see e.g., [12,13]. These salicylideneanilines, but also salicylideneimines, can form metallomesogens by complexation with d- and f-block elements, [14-17]. Tris(salicylideneanilines) having a discotic shape exhibit a room-temperature columnar mesophase [18,19]. Dendromesogens containing up to 64 peripheral mesogenic salicylideneimine fragments have also been reported [20]. Antiferroelectric behaviour has been claimed by Yablonski et al. to be exhibited by achiral liquid-crystalline monomer–polymer mixtures containing salicylideneaniline moieties [21,22].

Interesting examples of bent molecules are given by the following: Two salicylideneimine moieties can be connected to each other to form twin molecules (Scheme 1A). In the case of an odd-numbered spacer these dimers exhibit a bent shape and form nematic, columnar nematic, smectic and columnar phases. Columnar phases were not found for the dimers having even-numbered spacers, because these molecules are more linear [23-27]. Interestingly, for a nonsymmetric chiral dimer the reentrant-phase behaviour SmA–SmA_b–SmA was reported [28].

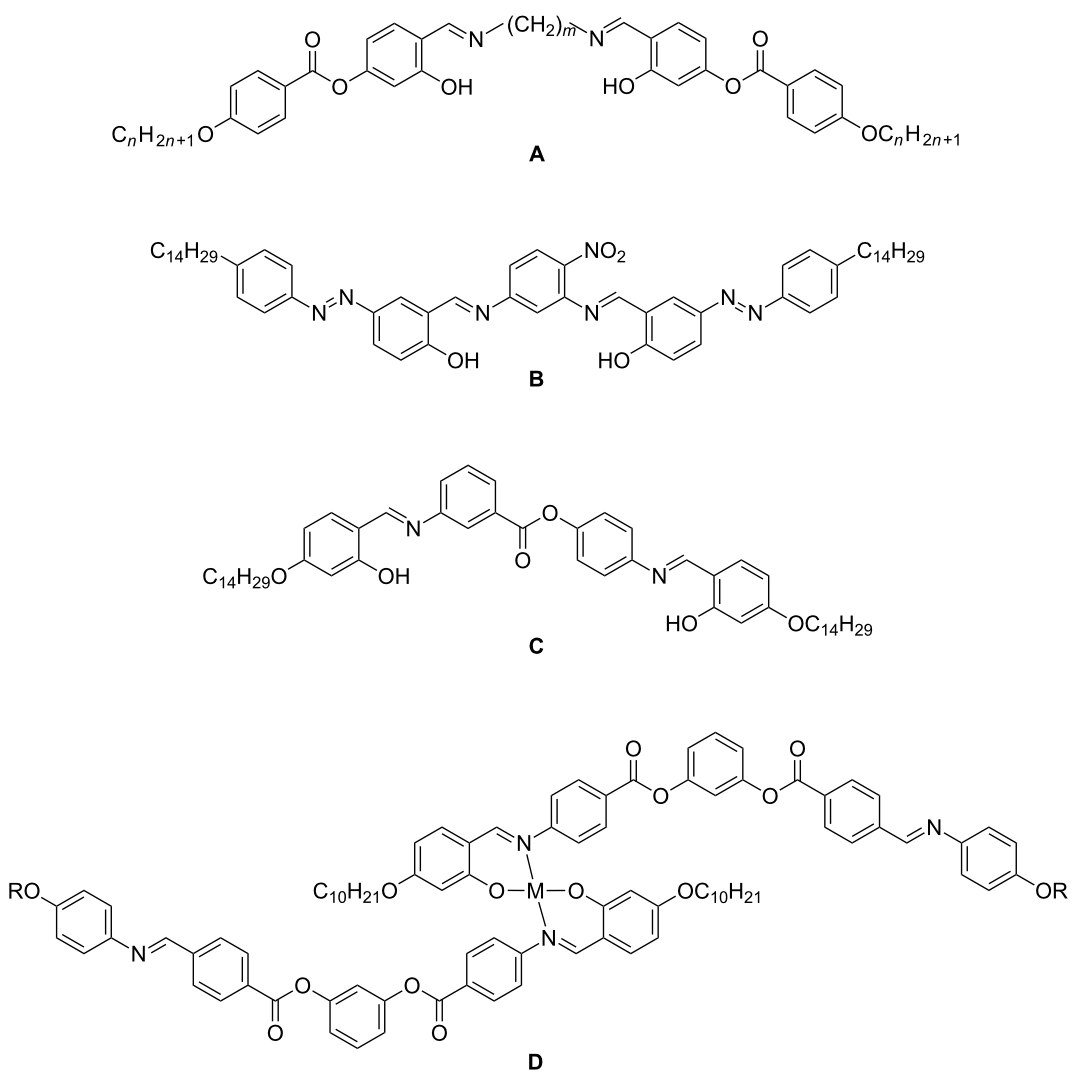

Scheme 1: Examples for bent mesogens containing salicylideneimine moieties.

Rao et al. postulated a new chiral smectic phase formed by W-shaped achiral molecules that contain two salicylideneaniline units (Scheme 1B) [29,30]. Recently, new achiral four-ring molecules were reported by Deb et al., in which two substituted salicylideneaniline moieties are linked by an ester group (Scheme 1C). These compounds, which show a strong photoluminescence, exhibit typical banana phases B_1 and B_7 [31]. Yelamaggad et al. reported V-shaped five-ring mesogens: Two salicylideneaniline moieties are linked by ester groups to the 1,2-positions of a phenyl ring. Due to the low bending angle of about 70°, the molecules form a partially intercalated SmA phase instead of banana phases [32].

Banana phases can be expected when the bending angle is opened to about 120°. Already several bent-core mesogens with salicylideneaniline moieties have been reported. The molecules can have a symmetric or nonsymmetric structure. If the aromatic core consists of five phenyl rings containing one and two salicylideneaniline moieties we speak about mono- or disalicylideneaniline compounds.

Monosalicylideneaniline compounds with different chain lengths in the terminal positions have been reported. Additionally, the effect of a nitro group neighbouring the hydroxy group has been studied. A mixture of one of these derivatives with a chiral twin compound was investigated by dielectric methods [33,34]. Yelamaggad et al. [35] reported nonsymmetric molecules having two fluorine atoms in the 2,3-position of one outer phenyl ring. SmCP phases with an unusual electro-optical switching behaviour were observed. The SmCP phase of bidendate bent-core ligands disappears in the corresponding Cu(II) and Pd(II) metal complexes (Scheme 1D) [36].

In 2001, homologues of a series of symmetric compounds bearing both azomethine groups between the outer and the next neighbouring inner phenyl rings were reported for the first time by Yelamaggad et al. [37-39] who also investigated the phase behaviour under pressure and the effect of light on the polarization of a mixture of these salicylideneanilines with a photoactive azo compound. The observation of a B_7 mesophase on the hexadecyloxy compound is surprising, because the central phenyl ring was not substituted by a nitro or cyano group as is the case for most of the other banana-shaped liquid crystals that form this phase type [40]. The nonyloxy homologue was studied in detail by Walba et al. For this compound, also abbreviated as NORABOW, the existence of the very rare SmCG mesophase was claimed [41]. Achten et al. compared the phase behaviour of the complete homologous series with that of the corresponding 1,5-pentylene connected dimers [27]. In 2007, we reported systematic investigations on the influence on the mesophase behaviour of lateral groups attached to the central phenyl ring of several homologous series [42].

Isomeric compounds, symmetric in the aromatic core, result when both azomethine groups are linked to the central phenyl ring. The influence on the mesomorphism of a fluoro substituent at the central phenyl ring was studied by Rao et al. [43]. Three years ago, we reported the synthesis and a remarkable electro-optical behaviour of three bent-core compounds derived from 2-methyl-1,3-phenylenediamine. The unusual current response showed five peaks per half period. Such multistage switching was measured for the first time on banana-shaped liquid crystals and has been proved by different electro-optical methods and optically observed by a high-speed camera [44,45].

It is not surprising that bent-core compounds having six phenyl rings can also form banana phases. Recently, the central phenyl ring of a salicylideneaniline based five-ring bent-core compound was replaced by a biphenyl moiety, leading to SmCP phases [46].

In continuation of our work on salicylideneaniline-based banana-shaped mesogens, we herein report a study of the effect of lateral substituents on the mesophase behaviour of symmetric and nonsymmetric five-ring bent-core mesogens. Up to now there have only been systematic investigations on the effect of atoms and groups introduced at the central phenyl ring. In our work, we now attach halogen atoms at the outer phenyl rings. When nonsymmetric compounds are laterally substituted with one halogen atom, this can be introduced in either one of both of the molecular legs, giving isomeric compounds, which will allow a detailed comparison. A further goal of the present work is the synthesis of bent-core salicylideneaniline compounds bearing a lateral methyl group at the central phenyl ring, in search of further materials that may also show the unusual multistage switching as mentioned above. To assess the effect of the intramolecular hydrogen bond on the mesophase behaviour, corresponding compounds without hydroxy groups were additionally prepared. In order to focus the study on the effect of lateral substituents, the hydrocarbon chains at both terminal phenyl rings were fixed with dodecyloxy groups.

Results and Discussion

Monosalicylideneaniline compounds **OH 1** bearing the azomethine group between an outer phenyl ring and its neighbour

Synthesis of the compounds **OH 1**

The synthesis of the compounds **OH 1**, which contain the azomethine connection group between an outer phenyl ring and the adjacent ring of the five-ring bent-core mesogens, is sketched in Scheme 2. The 4-(4-dodecyloxy-3-halogenobenzoyloxy)benzoic acids **2** were prepared by acylation of 4-hydroxybenzaldehyde with the corresponding 4-dodecyloxy-3-halogenobenzoic acids following oxidation of the formyl compounds **1**. The phenolic intermediates **3** were obtained by reaction of 3-benzyloxyphenol with the substituted benzoic acids **2** and hydrogenolytic deprotection of the hydroxy group according to [47]. The final products **OH 1a–c** were obtained by esterification of the phenols **3** with 4-(4-dodecyloxy-2-hydroxybenzylideneamino)benzoic acid (**4**), which exhibits a liquid-crystalline phase itself (Cr 204 N 269 I) [42]. It should be mentioned that Yelamaggad et al. [36] preferred a condensation step between the 4-*n*-alkyloxy-2-hydroxybenzaldehyde and the related four-ring amino compound for the synthesis of short-chain homologues of the laterally unsubstituted compound **OH 1a** to study the complexation with Cu(II) and Pd(II).

Mesophase behaviour of the compounds **OH 1**

The transition temperatures and associated enthalpies of the compounds **OH 1** are summarized in Table 1. The introduction of the hydroxy group causes an increase of the clearing temperature by approximately 30 K (compare, e.g., compounds **H 1a** and **OH 1a**). This stabilization effect is already well-known from calamitic Schiff bases and is caused by the intramolecular hydrogen bond, which could also reduce the flexibility of this molecular leg. Halogen substituents in position X have only a modest effect on the mesophase stability. A slight decrease in the clearing temperature with increasing size of the substituent is observed. We had expected a stronger effect caused by a lateral chlorine or bromine atom.

By cooling the isotropic liquid of **H 1a** and **OH 1a** a birefringent grainy texture together with areas showing a Schlieren

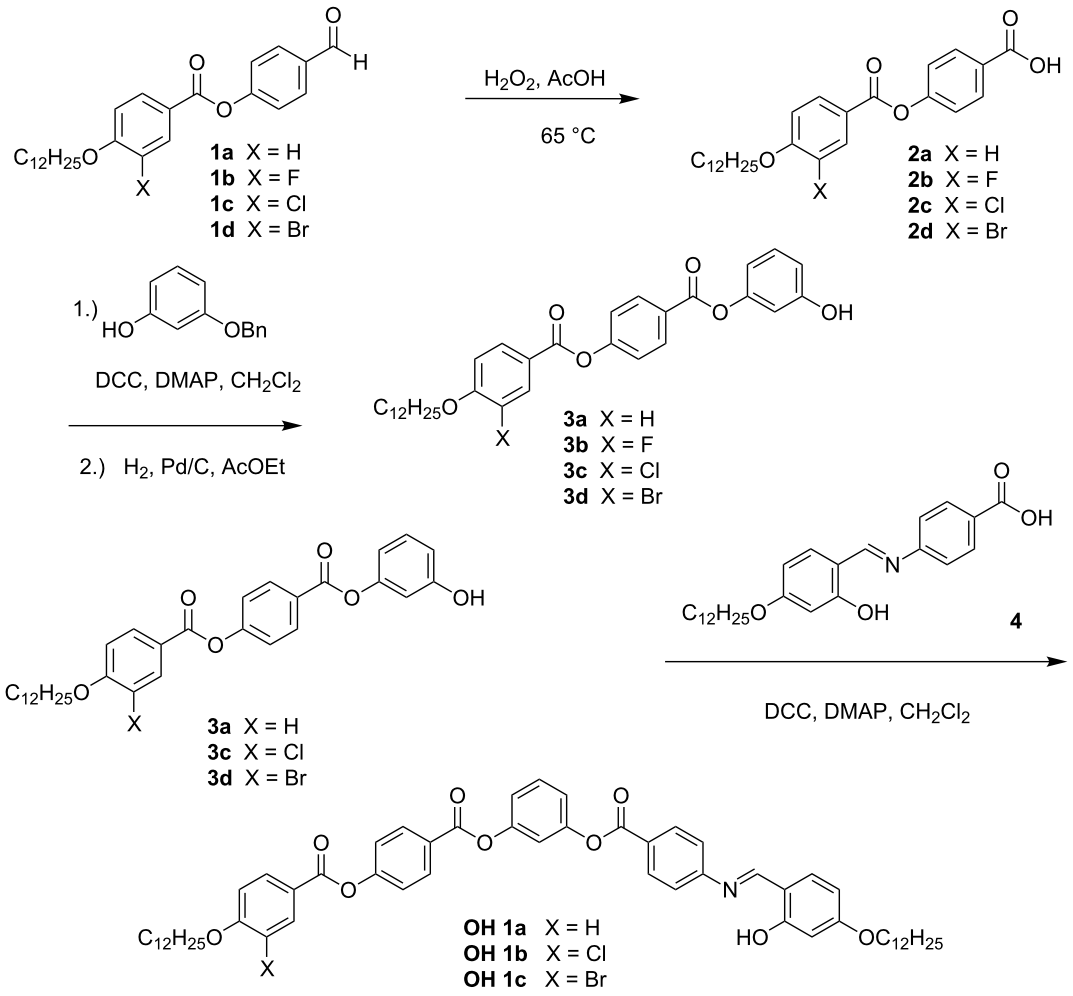

Scheme 2: Synthetic pathway to prepare compounds **OH 1**.

Table 1: Mesophase behaviour, transition temperatures (°C) and enthalpies [kJ/mol], and P_S values (nC/cm^2) of compounds **OH 1** and **H 1a**.

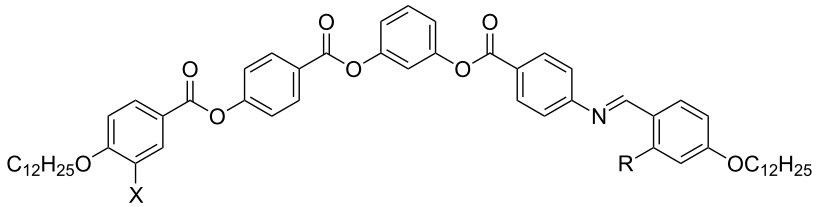

No.	R	X	Cr		SmCP$_A$		I	P_S
H 1a	H	H	•	92 [62.3]	•	111 [19.8]	•	750
OH 1a	OH	H	•	80 [44.7]	•	142 [22.4]	•	900
OH 1b	OH	Cl	•	82 [22.5]	•	140 [19.2]	•	390
OH 1c	OH	Br	•	85 [22.1]	•	134 [16.9]	•	250

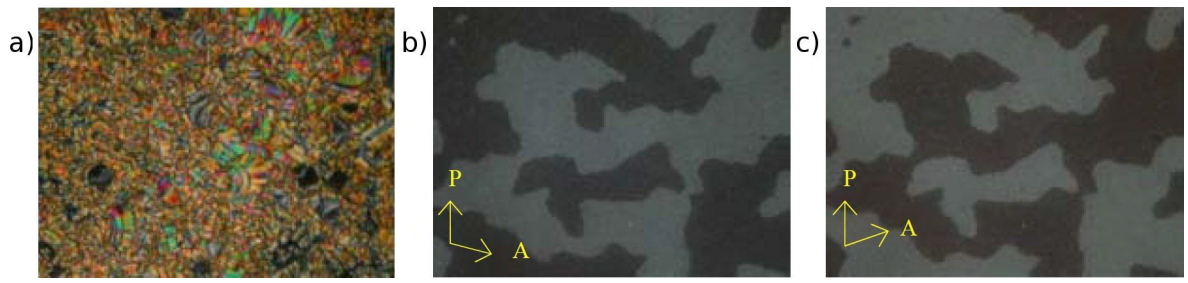

Figure 1: Polarising optical microscopy images. a) Compound **OH 1a**: Grainy texture with smectic Schlieren areas at 130 °C; b), c) compound **OH 1c**: Chiral domains of opposite handedness at 125 °C; polarisers decrossed from 90° by about +/-5°.

texture were observed by polarising optical microscopy (Figure 1a), which is a hint for a layer structure. In contrast, the mesophases of the halogen-substituted compounds **OH 1b** and **OH 1c** appeared optically isotropic with crossed polarisers. By rotation of one of the polarisers clockwise from the crossed (90°) position, bright and dark domains became visible (Figure 1b). Rotating the polariser anticlockwise by the same angle made the dark domains bright, and vice versa (Figure 1c). Obviously domains of opposite handedness occur. One explanation is the bookshelf geometry of smectic layers in which an anticlinic arrangement with a tilt angle of 45° leads to an orthoconic structure. This state is nonbirefringent [48,49].

X-ray diffraction experiments on powderlike samples of **OH 1a** and **OH 1b** showed first and second order layer reflections and a diffuse outer scattering, revealing a simple layer structure having a liquidlike state within the layers (Figure 2). The layer thicknesses amount to d = 4.0 nm (**OH 1a**) and d = 4.2 (**OH 1b**). Based on a calculated molecular length of L ~ 5.4 nm, the molecular long axes are tilted with respect to the layer normal by about 42°, excluding an intercalation of the terminal chains.

EHC cells consisting of two thin glass plates with a conductive surface (ITO) were used for electro-optical investigations. After the cell is filled with the material under study, the application of an electric field gives information on the dielectric properties and polar switching processes. The current response curve of a low-frequency triangular wave voltage shown in Figure 3a gives evidence that the tilted smectic phase exhibits an antiferroelectric switching behaviour. Cooling the isotropic liquid in the presence of a D.C. field leads to the formation of circular domains, in which the layers are arranged cylindrically. In the ground state the extinction brushes are parallel to polariser and analyser, see Figure 3c. From this observation it follows that the antiferroelectric SmCP phase exhibits an anticlinic arrangement (SmC_aP_A). By application of an electric field the extinction brushes rotate clockwise or anticlockwise depending on the polarity of the field, see Figure 3b and Figure 3d. Under the

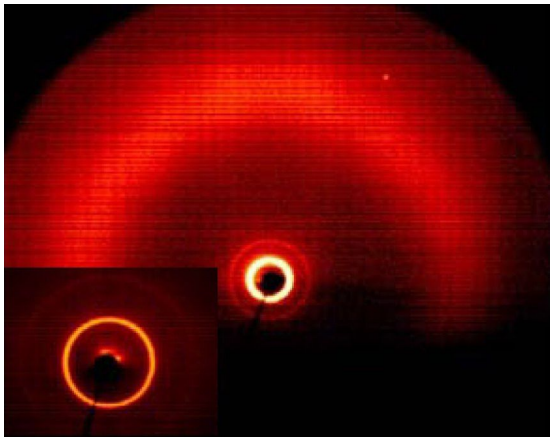

Figure 2: X-ray diffraction pattern of a powderlike sample of **OH 1b** at 131 °C (inset: Small angle region; lower part of the patterns shadowed by the heating stage).

field the molecules are arranged with the polar axes in the field direction such that a synclinic and ferroelectric state results. When the field is switched off, the molecules rotate back to the antiferroelectric ground state. The arrangement of the molecular long axes in two adjacent layers is sketched below the textures in Figure 3. This behaviour was found for all compounds **OH 1a–c**. The values of the spontaneous polarization are given in Table 1.

The switching behaviour of the compound **H 1a** without the hydroxy group is more complicated (Figure 4). When an electric field is applied, circular domains are formed (Figure 4b). In the circular domains the smectic layers are cylindrically arranged around the centre of the domains. This arrangement is indicated by the occurrence of extinction crosses. For tilted smectic phases the angle between the extinction crosses and the crossed polarisers corresponds to the tilt angle of the smectic phase. As shown in Figure 4b, circular domains appear under application of a sufficiently high electric field. After removal of the electric field, the relaxation of the field-induced circular

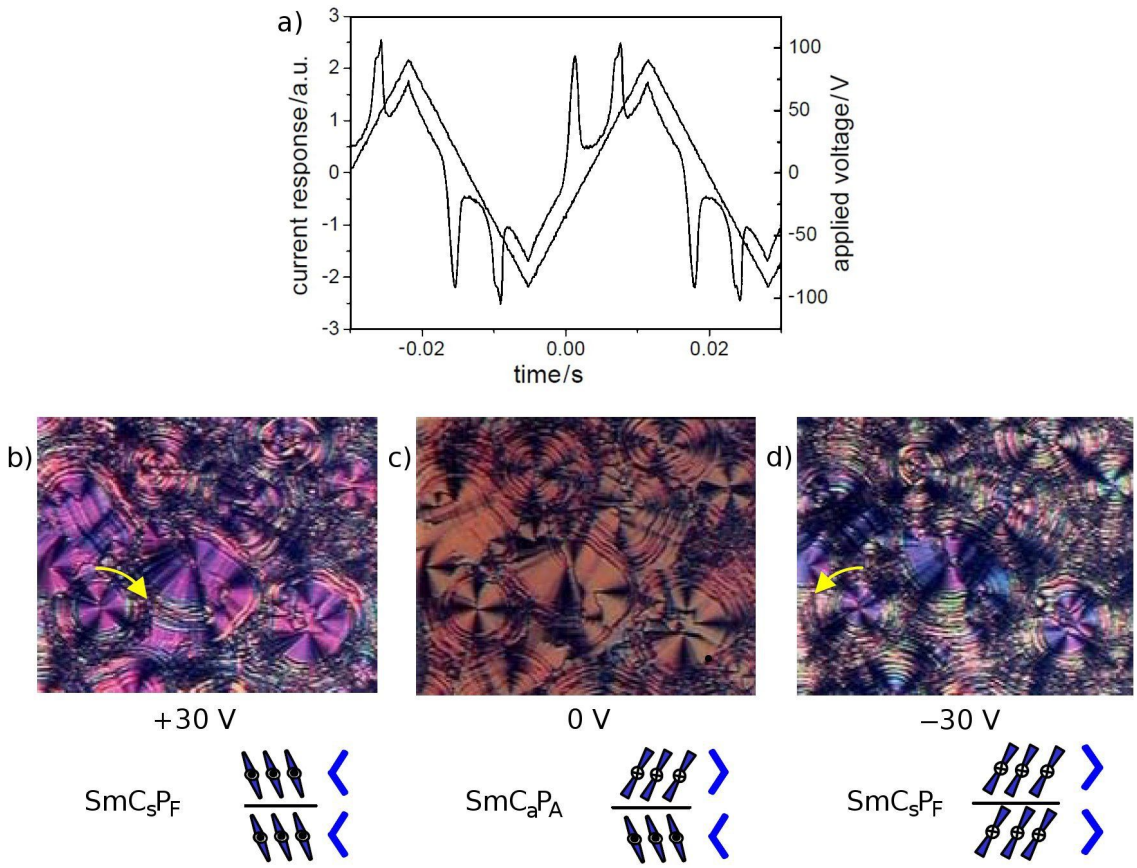

Figure 3: Electro-optical behaviour of compound **OH 1a**: a) current response curve (U = 182 V_{pp}, f = 30 Hz, T = 112 °C, d_{cell} = 6 µm, P_S = 900 nC/cm^2); b–d) tristable switching of circular domains by a D.C. voltage. T = 112 °C, d_{cell} = 6 µm; c) 0 V, extinction crosses parallel to the crossed polariser; b) +30 V, clockwise rotation of the extinction crosses (see yellow arrow); d) −30 V, anticlockwise rotation of extinction crosses (see yellow arrow).

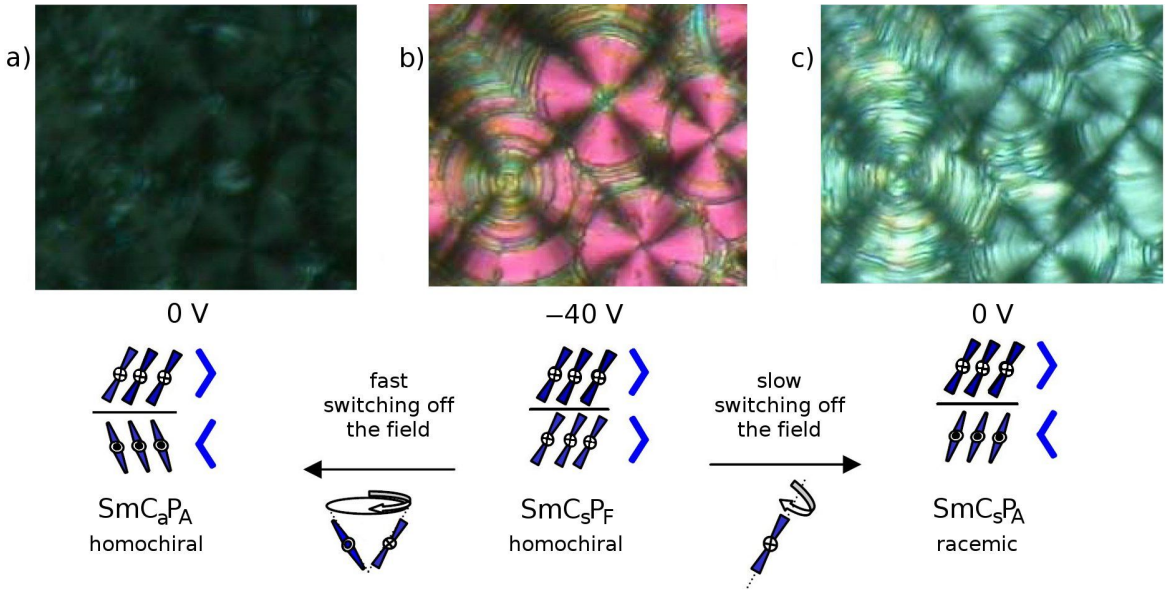

Figure 4: Switching behaviour of compound **H 1a**, which depends on how quickly the electric field is switched off.

domains strongly depends on the experimental conditions. When the electric field is removed quickly, the extinction crosses rotate back to the crossed polariser position. The texture becomes dark and the crosses are difficult to recognize, as shown in Figure 4a. The reason for this is that for smectic layers perpendicular to the substrate an antiferroelectric arrangement with a tilt angle of about 45° leads to an orthoconic structure. This state is nonbirefringent in the direction perpendicular to the substrate and therefore dark between crossed polarisers [49]. Upon reapplication of the electric field, the crosses rotate back to the 45° positions (Figure 4a and Figure 4b). When the field is removed very slowly (about 2 V/s) the circular domains do not change, and only a slight decrease in the birefringence is seen (Figure 4c). When the electric field is applied again, the extinction crosses do not rotate. Different movements of the molecular long axis are responsible for such distinct behaviour: In most cases the molecular long axes rotate on a cone, as sketched in Figure 4 below the texture. In the other case, the crosses do not change when the molecules of each second layer rotate by 180° about their long axes (sketch on the right below the textures in Figure 4).

In this case, of rotation about the long axes, the chirality changes from the chiral SmC_sP_F phase to the racemic SmC_sP_A phase. This means that the chirality is changed in every second layer. Such flipping of chirality has been reported by Schröder et al. in 2004 [48] for the SmCP phases and by Szydlowska et al. in 2003 [50] for the B_1 phase. Both processes of molecular movement require different energies, which correspond to different coefficients of viscosity for both molecular movements [51].

Monosalicylideneaniline compounds **OH 2** bearing the azomethine group between the central phenyl ring and one neighbouring ring

Synthesis of the compounds **OH 2**

The compounds **OH 2** have one azomethine linking group between the central phenyl ring and the adjacent ring bearing a hydroxy group. Two reaction pathways to prepare these compounds are sketched in Scheme 3. The basic intermediates were the 4-formyl-3-hydroxyphenyl 4-*n*-dodecyloxy-3-substituted-benzoates **5a–d**, which were synthesized by acylation of 2,4-dihydroxybenzaldehyde with the corresponding 4-*n*-dodecyloxy-3-substituted-benzoyl chlorides prepared by use of oxalyl chloride. Following pathway **A** the condensation of the salicylaldehydes **5a–d** with 3-aminophenyl 4-(4-*n*-dodecyloxy-3-substituted-benzoyloxy)benzoates **6** yielded the final compounds according to [33].

Following pathway **B**, the salicylidene intermediates **5a–d** were reacted with 3-aminophenols to give the phenols **7a**,**b**. Subsequently, their esterification with 4-(4-*n*-dodecyloxy-3-substituted-benzoyloxy)benzoic acids **2** was the final step needed to afford the compounds **OH 2b**, **2e**, **2g**. The selection of route **A** or **B** was determined by the better purity of the final products, but short reaction paths for the expensive intermediates, e.g., the fluoro-containing compounds, were also an important consideration.

Mesophase behaviour of the compounds **OH 2**

Transition temperatures and corresponding enthalpies from calorimetric measurements are summarized in Table 2. For comparison, the compound **H 2a** without the hydroxy group is added.

All compounds **OH 2** form a SmCP phase. The clearing temperature of the benzylideneaniline **H 2a** is increased by 29 K by introduction of the hydroxy group in the ortho position of the azomethine linking group, to give **OH 2a**. The effect of a methyl group on the mesophase stability depends on the position on the central phenyl ring. The lowering of the smectic–isotropic phase-transition temperature by introduction of the lateral methyl group in the 6-position, **OH 2b**, amounts to 31 K. The influence of a methyl group in the obtuse angle of **OH 2c**, that is in position 2, can be virtually ignored, and surprisingly also the combination with a chlorine atom laterally attached to one of the outer rings in **OH 2d** has little effect. Comparing the different sizes and polarities of the halogen atoms in the compounds **OH 2e–j**, a fluorine atom increases the clearing temperatures by about 6 K (**2e**, **2h** in comparison to the laterally nonsubstituted compound **OH 2a**). The chlorine- and bromine-substituted compounds have transition temperatures that are only a little lower. Although the bromine atom is a relatively large substituent, the clearing temperatures are, surprisingly, depressed by only few degrees. Furthermore, the disrupting effect is comparable for the both series **OH 2e–g** and **OH 2h–j**, which are isomeric to each other. Here, the halogen atoms are attached to the "left" or "right" arms, which are chemically different. It should also be mentioned that by introduction of one halogen atom in these nonsymmetric molecules the melting temperatures can strongly decrease. Therefore, relatively broad enantiotropic mesophase ranges result, for example, 77 K for compound **OH 2j**.

Observation by polarising optical microscopy shows textures typical for SmCP phases, for example fan-shaped, ribbonlike and Schlieren textures (Figure 5).

X-ray diffraction studies on **OH 2a** give evidence for a layer structure with a liquidlike order within the layers. The layer distance, with $d = 3.8$ nm, is significantly smaller than the calculated molecular length ($L \sim 5.4$ nm). According to $\cos\theta = d/L$, a

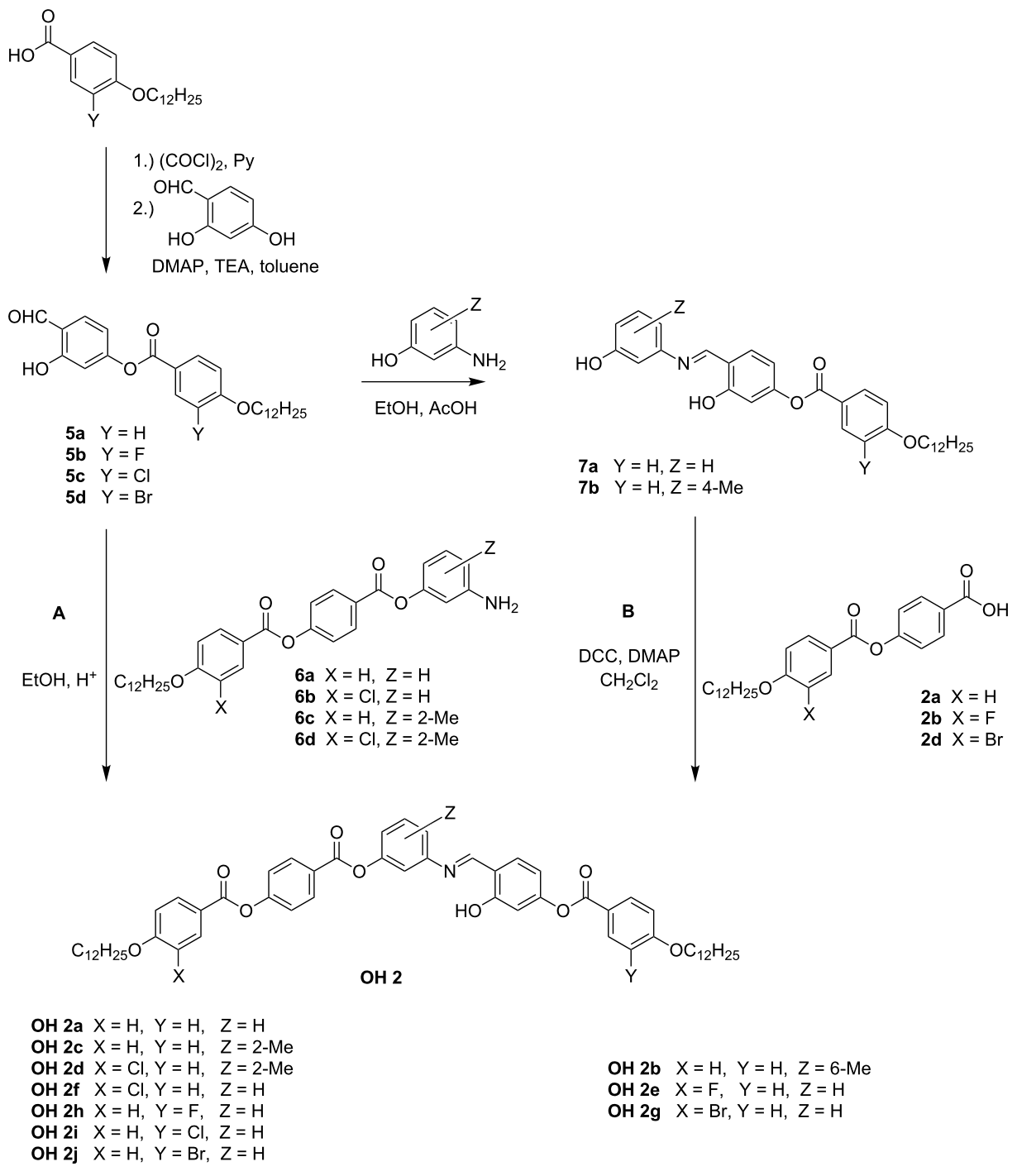

Scheme 3: Reaction pathways to prepare the monosalicylideneaniline compounds **OH 2a–j**.

tilt angle of the molecular long axis with respect to the layer normal of 45° results at a temperature of 130 °C. A similar tilt angle of 42° was determined from the mutual positions of the maxima of the outer diffuse scattering and of the small-angle reflections in the 2D diffraction patterns (Figure 6). The significant difference in the intensities of the two maxima of the outer diffuse scattering is a hint to a synclinic arrangement of the molecules in adjacent layers.

Electro-optical measurements on **OH 2a** by using a triangular wave voltage show a current response consisting of two repolarization peaks, which proves an antiferroelectric ground state.

Table 2: Mesophase behaviour, transition temperatures (°C), transition enthalpies [kJ/mol] and P_S [nC/cm^2] values of the compounds **OH 2** and **H 2a**.

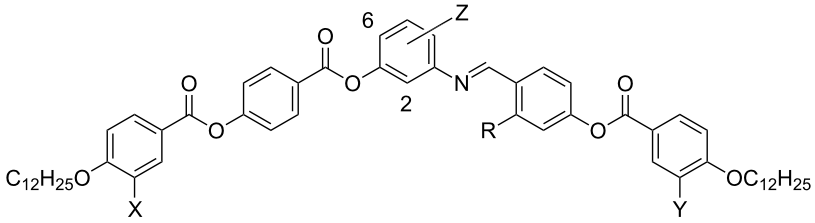

No.	R	X	Z	Y	Cr		SmCP$_A$		I	P_S
H 2a	H	H	H	H	•	111 [65.5]	•	(107) [16.9]	•	920
OH 2a [33]	OH	H	H	H	•	105 [63.1]	•	136 [22.4]	•	670
OH 2b	OH	H	6-CH_3	H	•	83 [32.0]	•	105 [16.3]	•	630
OH 2c	OH	H	2-CH_3	H	•	125 [27.4]	•	132 [19.5]	•	—[a]
OH 2d	OH	Cl	2-CH_3	H	•	125 [11.7]	•	133 [18.9]	•	420
OH 2e	OH	F	H	H	•	107 [47.4]	•	142 [21.2]	•	730
OH 2f	OH	Cl	H	H	•	68 [22.1]	•	138 [20.7]	•	730
OH 2g	OH	Br	H	H	•	66 [24.8]	•	132 [18.9]	•	470
OH 2h	OH	H	H	F	•	107 [30.4]	•	143 [21.8]	•	660
OH 2i	OH	H	H	Cl	•	79 [56.9]	•	135 [21.7]	•	640
OH 2j	OH	H	H	Br	•	56 [24.3]	•	133 [20.1]	•	590

[a]Despite many purification procedures, P_S could not be reproducibly measured due to the high conductivity of the compound.

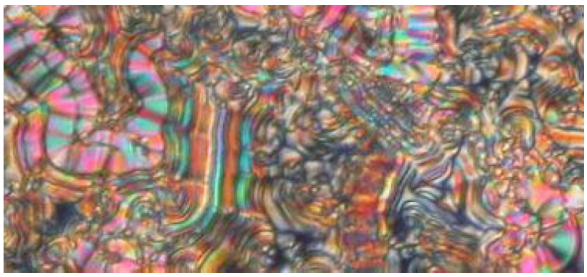

Figure 5: Compound **OH 2a**: Texture of the SmCP phase at 126 °C.

Figure 7 shows the switching behaviour and corresponding textures. The extinction crosses rotate to the right or left in response to the polarity of the electric field. This behaviour is characteristic of a tristable switching process between the tilted anticlinic antiferroelectric (SmC_aP_A) and the synclinic ferroelectric (SmC_sP_F) states. The value of the spontaneous polarization was calculated from the area under the repolarization peaks to be 660 nC/cm^2. The switching behaviour of **OH 2a** is representative for all compounds **OH 2a–j**. The P_S values are given in Table 2.

Disalicylideneaniline compounds **OH 3** and **OH 4** bearing the azomethine groups between the outer and neighbouring phenyl rings

Synthesis of the compounds **OH 3** and **OH 4**

Compounds **OH 3** and **OH 4** consist of two 4-*n*-dodecyloxysalicylideneaniline moieties, which are connected to the central phenyl ring by ester groups. These linking groups have different directions in the compounds **OH 3** and **OH 4**. Esterification of the carboxylic acid **4** or of the phenolic intermediate **8** with the corresponding resorcinols and isophthalic acids, yielded the compounds **OH 3** and **OH 4**, respectively, as sketched in Scheme 4.

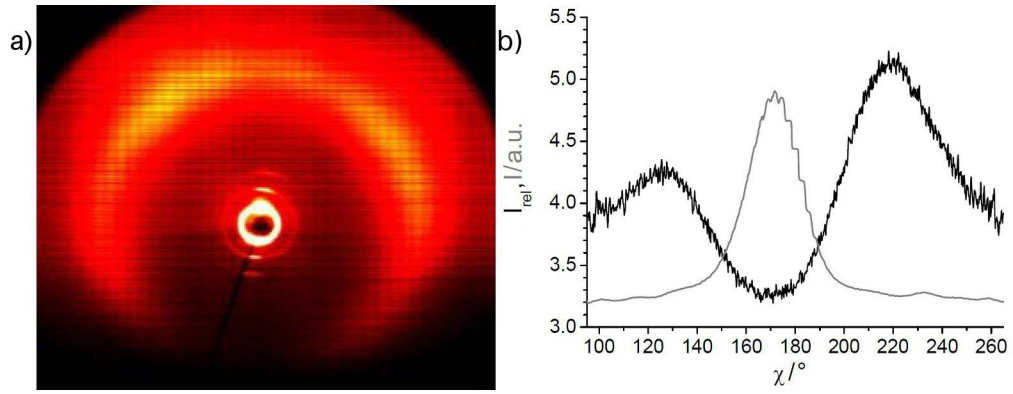

Figure 6: a) 2D X-ray pattern of a surface-aligned sample of compound **OH 2a** at 128 °C (lower part of the pattern shadowed by the heating stage); b) χ scan for the outer diffuse scattering with maxima at χ ≈ 125 and 220° [I_{rel} = I(128 °C)/I(140 °C, isotropic liquid], and the position of the layer reflections for comparison (gray line).

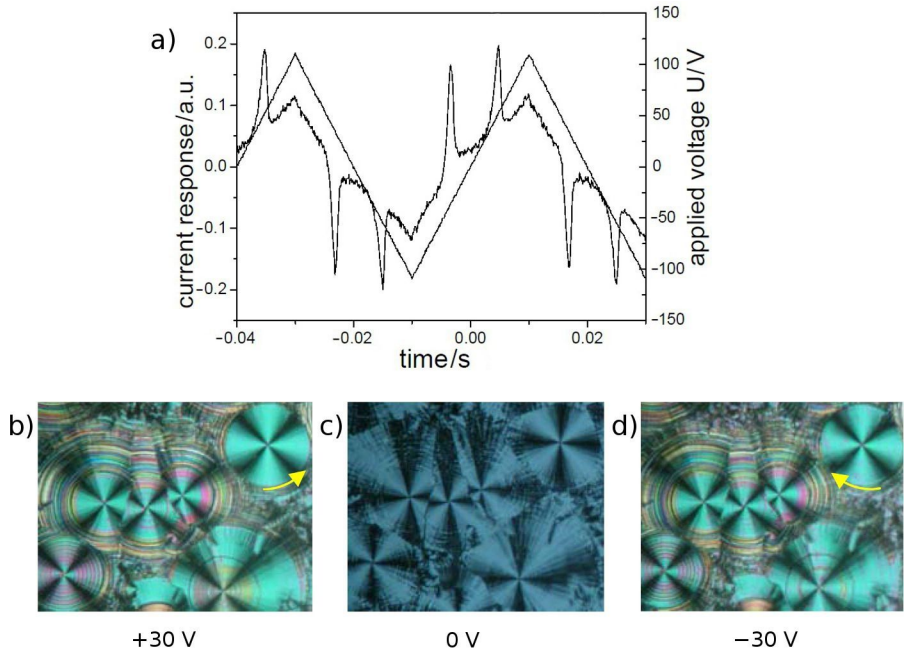

Figure 7: Electro-optical switching behaviour of compound **OH 2a**: a) current response (U = 230 V_{pp}, f = 25 Hz, T = 106 °C, d_{cell} = 6 µm; P_S = 660 nC/cm^2); b–d) tristable switching on homogeneous chiral domains; starting from texture c) where the extinction crosses are parallel to the crossed polariser, the extinction crosses rotate anticlockwise in b) and clockwise in d) in dependence on the polarity of the D.C. electric field.

Mesophase behaviour of the compounds OH 3

Table 3 shows the transition temperatures of the isophthalic acid derivatives **OH 3a–c** together with those of the corresponding esters **H 3a–c**, which do not exhibit an ortho-hydroxy group, for comparison.

Liquid-crystalline phases were not observed for the benzylidene derivative **H 3a**. The introduction of the hydroxy groups enables the salicylideneaniline compound **OH 3a** to form a mesophase. The clearing temperature of the bromine-substituted compound **OH 3b** increases due to the presence of hydroxy groups, in comparison to **H 3b**, by 34 K. Liquid-crystalline behaviour was not observed for either of the nitro derivatives **H 3c** or **OH 3c**, probably because the 5-position of the nitro group, which is at the top of the bent molecules, is sterically unfavourable in most cases. Generally, melting temperatures and phase-transition temperatures of isophthalic acid derivatives are much higher in comparison to those of the

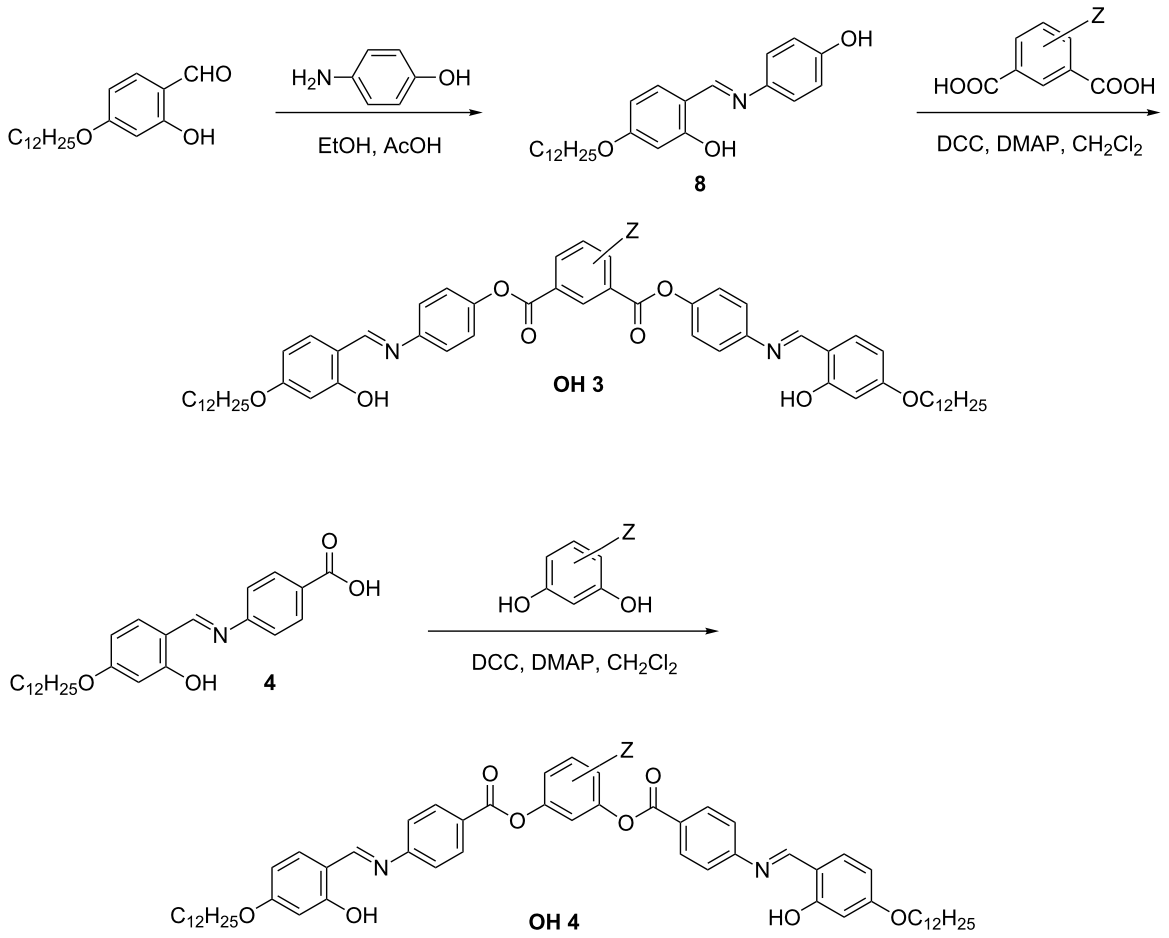

Scheme 4: Synthetic steps followed to prepare the compounds **OH 3** and **OH 4**.

Table 3: Mesophase behaviour, transition temperatures (°C) and enthalpies [kJ/mol] of compounds **OH 3** (on the right) and compounds **H 3** (on the left).

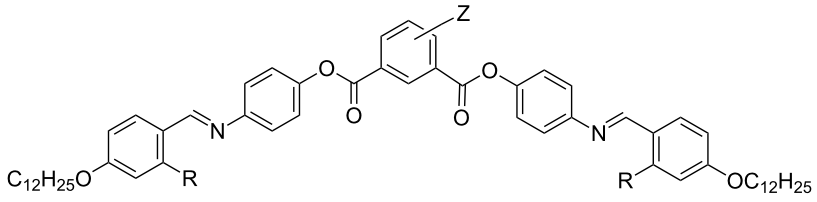

Mesophase behaviour	R = H	Z	R = OH	Mesophase behaviour
Cr 190 [98.0] I	**H 3a**	H	**OH 3a**	Cr 179 [63.5] $SmCP_A$ 223 [22.5] I
Cr 163 [84.2] ($SmCP_A$ 155 [28.2]) I	**H 3b**	4-Br	**OH 3b**	Cr 136 [40.8] $SmCP_A$ 189 [21.6] I
Cr 193 [57.5] I	**H 3c**	5-NO_2	**OH 3c**	Cr 224 [61.9] I

isomeric resorcinol derivatives (see compounds **OH 4**), as also proved for two other series of isomeric five-ring mesogens containing only ester linking groups [47].

Helical filaments and circular domains grow upon cooling of the isotropic liquid of compound **OH 3a** (Figure 8a), which coalesces into a nonspecific texture. Such spiral germs could be

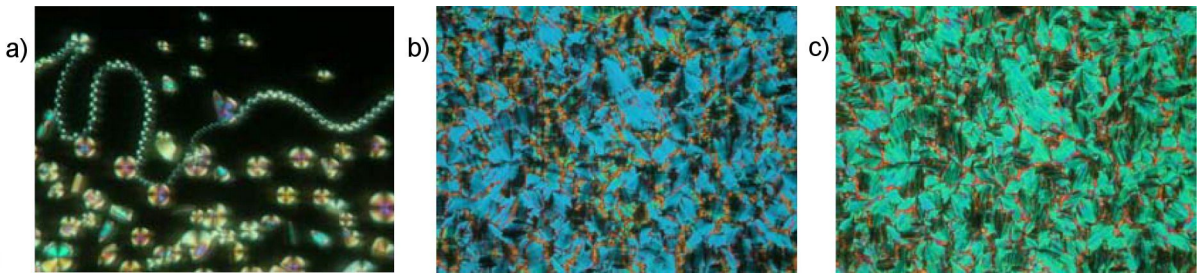

Figure 8: Optical photomicrographs of compound **OH 3a**: a) On cooling of the isotropic liquid; c) U = 0 V; b) $U_{D.C.}$ = ±67 V, T = 172 °C, d_{cell} = 6 µm.

a hint for undulated layer structures or a B_7 phase. X-ray patterns on nonoriented samples display two orders of layer reflections (d = 4.7 nm), however do not provide any evidence for a modulation or undulation of the layers.

Upon application of an electric field, the birefringence slightly changes, as shown in Figure 8b and Figure 8c for a D.C. field. In Figure 9b, the parallel arrangement of extinction crosses with respect to the position of the crossed polarisers indicates an anticlinic arrangement of the molecules in adjacent layers. With high fields, two repolarization peaks per half period were separated, which is typical for an antiferroelectric switching of a SmC_aP_A phase (Figure 9a). The extinction crosses do not rotate and the electro-optical behaviour is independent of the polarity of the electric field. This behaviour suggests that the position of the optical axis and hence the direction of the molecular long axes does not change. Therefore, the switching process can be explained by a collective rotation of the molecules about their long axis.

Substitution of the central phenyl ring with a bromine atom (Z = 4-Br) results in a broader mesophase range at lower temperatures for **OH 3b**. Upon cooling of the isotropic liquid, lancetlike filaments grow into a fan-shaped texture exhibiting some cross-stripes (Figure 10).

X-ray patterns from partially aligned samples of the 4-bromo-isophthalic acid derivative **OH 3b** display up to five orders of the layer reflections on the meridian of the 2D-pattern (Figure 11a), which is evidence for a layer structure with well defined layers (d = 4.8 nm at 160 °C). From the position of the maxima of the outer diffuse scattering at approximately 115 and

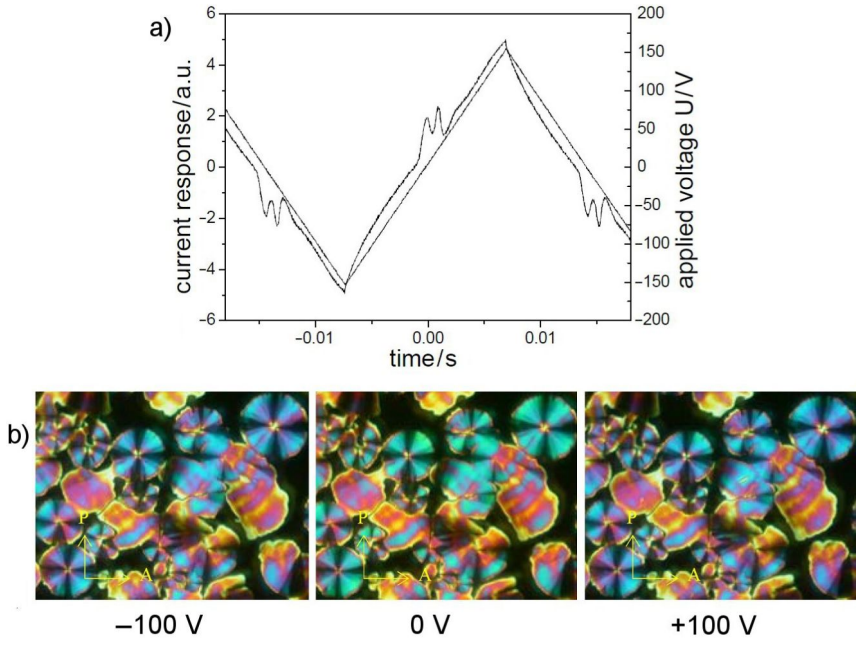

Figure 9: Electro-optical behaviour of compound **OH 3a**: a) Current response curve (U = 308 V_{pp}, f = 35 Hz, T = 172 °C, d_{cell} = 6 µm, P_S = 370 nC/cm^2); b) texture of the $SmCP_A$ phase depending on the polarity of the applied field.

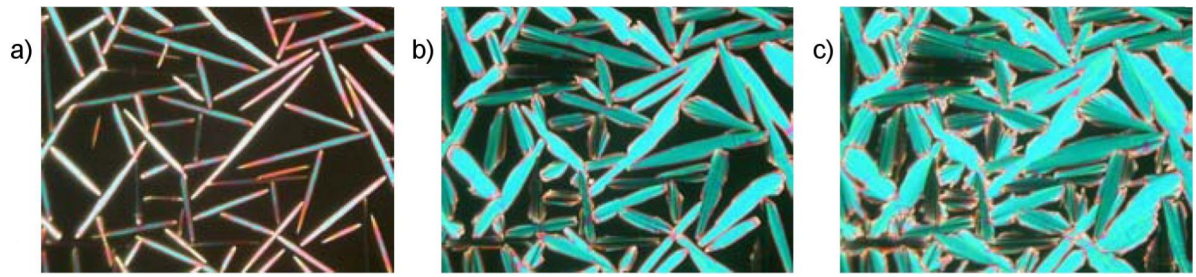

Figure 10: Growth of a fan-shaped texture from lancetlike filaments upon cooling of the isotropic liquid of compound **OH 3b**.

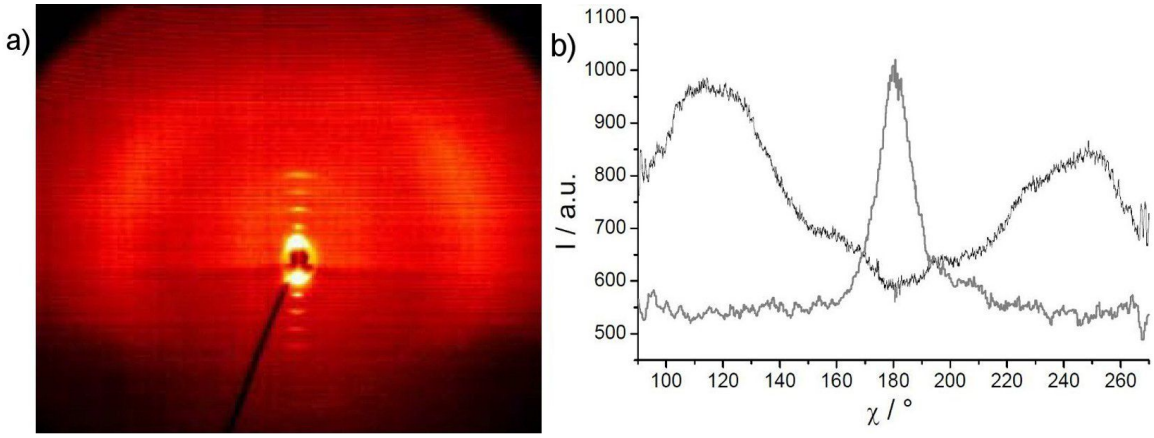

Figure 11: a) 2D X-ray pattern of a surfaced-aligned sample of compound **OH 3b** at 160 °C (lower part of the pattern shadowed by the heating stage); b) χ-scan for the diffuse scattering (black line), compared to the position of the layer reflections on the meridian (grey line).

245° in the χ scan (Figure 11b), an average tilt angle of about 25° towards the layer normal was found.

Initial electro-optical investigations employing an A.C. field (U = 260 V_{pp}, f = 20 Hz, T = 106 °C, d_{cell} = 6 µm, P_S = 180 nC/cm^2) yielded a current response with one repolarization peak per half period only. This would normally be a hint for ferroelectric properties of compound **OH 3b**, but it is in contradiction to the optical behaviour shown in Figure 12. A tristable switching process is observed, and after the electric field is switched off the texture is clearly changed (Figure 12b). In the case of a ferroelectric response, the compound would switch between the states (Figure 12a and Figure 12c), and after the field is switched off one of these textures would be remain. By extensive electro-optical studies employing lower frequencies and a modified triangular wave voltage, the current

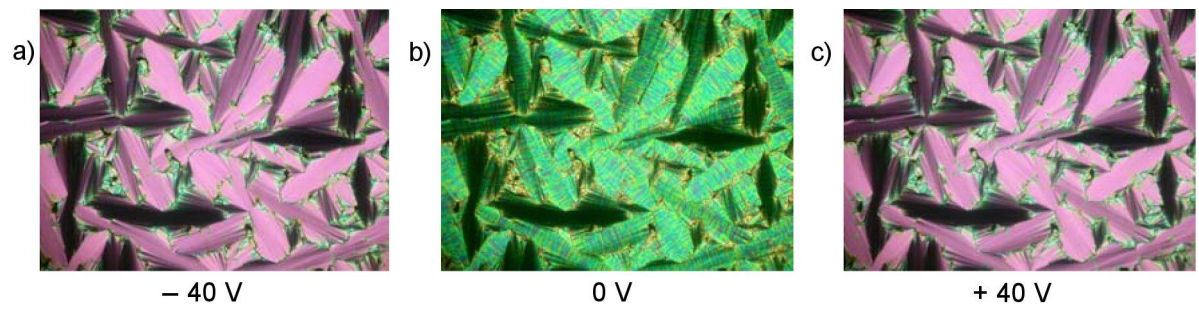

Figure 12: Compound **OH 3b**: Texture of the $SmCP_A$ phase in dependence on the polarity of the applied D.C. field.

response peaks split. Thus, the results of the electro-optical studies are consistent with each other, and the mesophase of compound **OH 3b** can be assigned as $SmCP_A$ phase.

Mesophase behaviour of the compounds OH 4

The carboxylic groups attached to the central phenyl ring of the molecules **OH 4** have an inverse direction in comparison to those of the compounds **OH 3**. The basic series **OH 4**, i.e., without lateral substituents, has been an object of interest for several research groups [27,37-41]. Some time ago, the influence of lateral substituents on six complete homologous series, in which the aromatic five-ring core corresponds to formula **OH 4**, was investigated by us. The effect of atoms and groups laterally attached to different positions on the central phenyl ring was studied [42]. Therefore, Table 4 shows only a few examples of interest for the present paper.

Compounds **H 4a–d** and **OH 4b** and **4d** are new materials. As seen from Table 4, the nature of the mesophase changes upon introduction of the hydroxy groups, from a crystal-like B_X phase to a SmCP phase (**H 4c** to **OH 4c**) and from a nematic phase to an undulated SmCP phase (**H 4b** to **OH 4b**). In the case of the 5-methoxy-substituted compound **OH 4d**, liquid-crystalline behaviour was induced by introduction of the hydroxy groups. The increase of the clearing temperatures by the introduction of two ortho-hydroxy groups in compounds **OH 4** depends strongly on the pattern of substitution; compare compounds **H 4a–d** with **OH 4a–d.** The increase amounts to 69 K for the laterally nonsubstituted compounds **H 4a**/**OH 4a**, but is reduced to 33 K for 4,6-dichloro-substituted compounds (see Supporting Information File 1, Table S4).

The 4-bromoresorcinol derivative **OH 4b** (Z = 4-Br) is isomeric to the 4-bromoisophthalic acid ester **OH 3b**. The texture of the mesophase of compound **OH 4b** is quite different from that of **OH 3b**. It shows spherolitic, lancetlike filaments and regions of a growing Schlieren texture upon cooling the isotropic liquid (Figure 13).

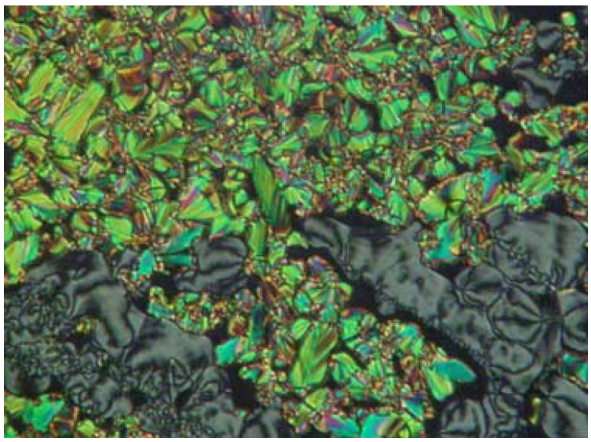

Figure 13: Compound **OH 4b,** exhibiting a fan-shaped texture together with a Schlieren texture upon cooling of the isotropic liquid, *T* = 145 °C.

Table 4: Mesophase behaviour, transition temperatures (°C) and -enthalpies [kJ/mol] of compounds **OH 4** (on the right) and corresponding compounds **H 4** (on the left).

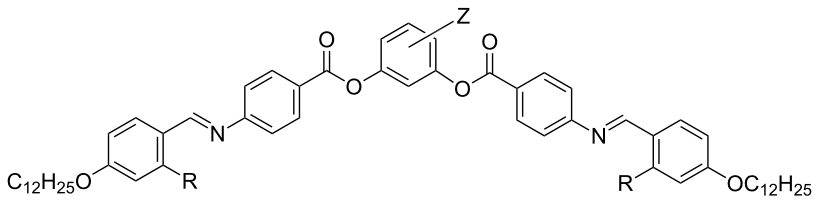

Mesophase behaviour					R = H	Z	R = OH	Mesophase behaviour					P_S[c]
Cr	124 [73.4]	($SmCP_A$	110) [—[a]]	I	**H 4a**	H	**OH 4a** [27]	Cr	114 [21.1]	$SmCP_A$	179 [21.6]	I	500
Cr	88 [37.3]	N	95 [21.5]	I	**H 4b**	4-Br	**OH 4b**	Cr	112 [18.0]	$USmCP_A$	146 [12.2]	I	600
Cr	125 [80.9]	(B_X	116)[b] [—[a]]	I	**H 4c**	2-Me	**OH 4c**	Cr	148 [36.3]	$SmCP_A$	171 [22.1]	I	640
Cr	98 [45.7]	I			**H 4d**	5-OMe	**OH 4d**	Cr	134 [73.2]	($SmCP_A$	127) [20.1]	I	590

[a]could not be found by calorimetric measurements due to crystallization.
[b]B_X phase: Preliminary assignment as crystal-like phase.
[c]in [nC/cm²]

In addition, the X-ray patterns show significant differences in the structures of the mesophases for both compounds. Partially surface-aligned samples of **OH 4b** show additional very weak X-ray reflections next to the first-order layer reflections (Figure 14), which suggest a two-dimensionally modulated electron density, i.e., an undulated or modulated layer structure (layer spacing d = 4.5 nm). The position of the reflections implies an oblique 2D lattice for this modulation, but only partial alignment was achieved, and the very strong ringlike-layer reflection affects the measurements of the other very weak ones. Therefore, further quantitative conclusions are rather speculative. One plausible interpretation of the data is given in Supporting Information File 1, Figure S2.

The designation as a polar phase results from electro-optical investigations. Two repolarization peaks per half period of an applied triangular wave voltage are generated (Figure 15a). The spontaneous polarization amounts to 600 nC/cm^2. The extinction crosses rotate clockwise (Figure 15b) or anticlockwise (Figure 15d) depending upon the polarity of the electric field, by an angle of about 20°. According to the electro-optical switching behaviour and the results of the X-ray measurements, the mesophase was assigned as a USmCP$_A$ phase

The 2-methyl-substituted compound **OH 4c** is isomeric with **OH 5b**, which exhibits an interesting multistage switching [44].

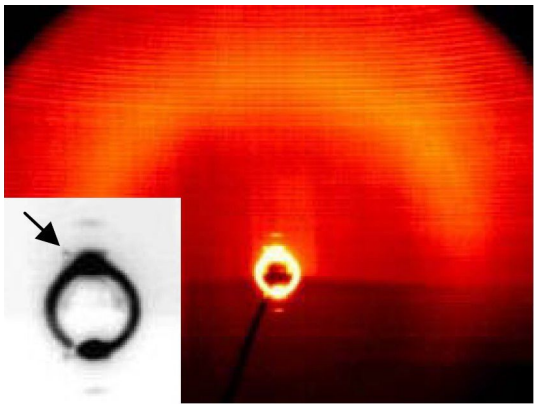

Figure 14: 2D X-ray diffraction pattern of a partially surface-aligned sample of **OH 4b** at 115 °C (inset: Small angle region, the arrow points to one of the additional non-layer reflections).

However, electro-optical studies on **OH 4c** show two peaks in the current response, as usually found for a SmCP$_A$ phase.

In compound **OH 4d** a methoxy group is attached at the top of the central phenyl ring; this 5-position is often sterically unfavourable for the formation of banana phases. Nevertheless, a metastable SmCP phase was observed and investigated. The growth of a fringe pattern typical for a SmCP phase can be seen in Figure 16a.

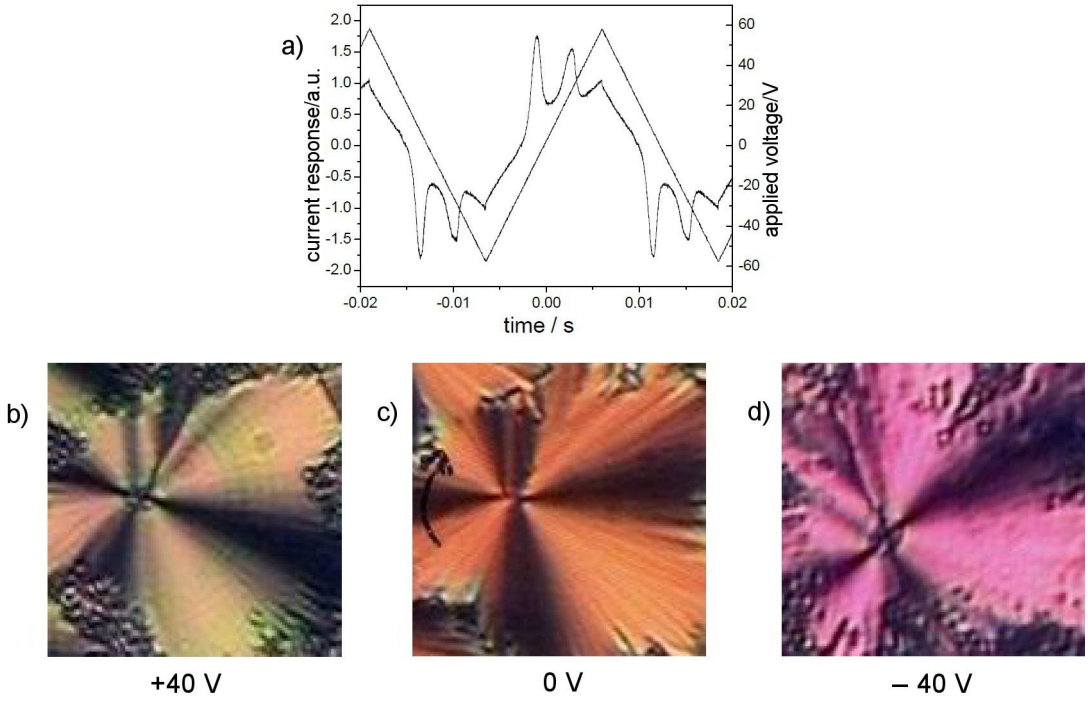

Figure 15: Switching behaviour of compound **OH 4b** at 120 °C: a) Current response curve (U = 116 V$_{pp}$, f = 40 Hz, T = 120 °C, d_{cell} = 6 µm, P_S = 600 nC/cm^2); b) tristable switching observed on circular domains applying a D.C. voltage (U = ± 40 V, T = 122 °C, d_{cell} = 6 µm).

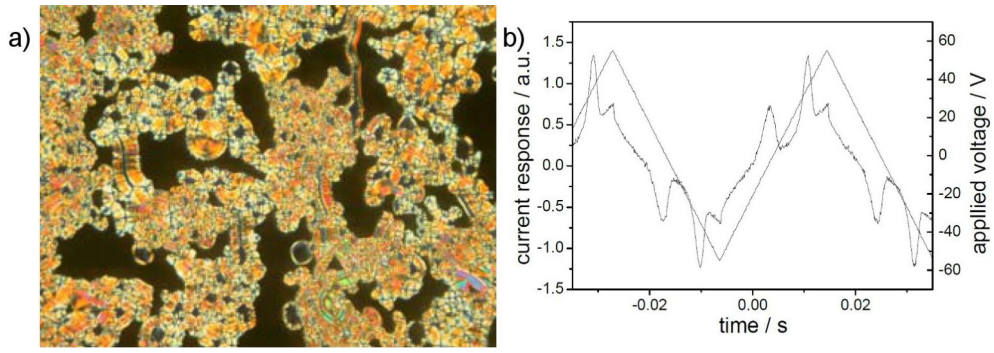

Figure 16: Compound **OH 4d**: a) Microphotograph of a growing fringe pattern of a SmCP phase upon cooling of the isotropic liquid; b) current response curve showing antiferroelectric behaviour (U = 19 V/µm, 20 Hz, d_{cell} = 6 µm, P_S = 500 nC/cm^2).

The current response shows two peaks per half period, which is typical for an antiferroelectric switching. The spontaneous polarization amounts to 500 nC/cm^2 (Figure 16b). Action of an electric D.C. field shows a transition from a striped, fan-shaped texture to a smooth one (Figure 17).

The X-ray diffraction measurements on the monotropic liquid-crystalline phase of **OH 4d** show the patterns of a tilted smectic layer structure with a layer spacing of 4.3 nm and a 30° tilt of the long molecular axes with respect to the layer normal (Figure 18), from which an effective molecular length of $L_{eff} = d/\cos\theta = 5.0$ nm results, which is significantly shorter than the molecular length $L_{calc} = 5.5$ nm estimated by molecular models. The difference may be caused by a deviation of the molecular configuration from that assumed in the model calculations (e.g., by another bending angle or a high proportion of gauche conformers), or by an interdigitation of the terminal chains (see discussion for **OH 4b** in Supporting Information File 1).

Figure 17: Electro-optical behaviour observed on the fan-shaped texture of compound **OH 4d**; $U_{D.C.}$ = 47 V; T = 123 °C; a) −47 V; b) 0 V; c) +47 V.

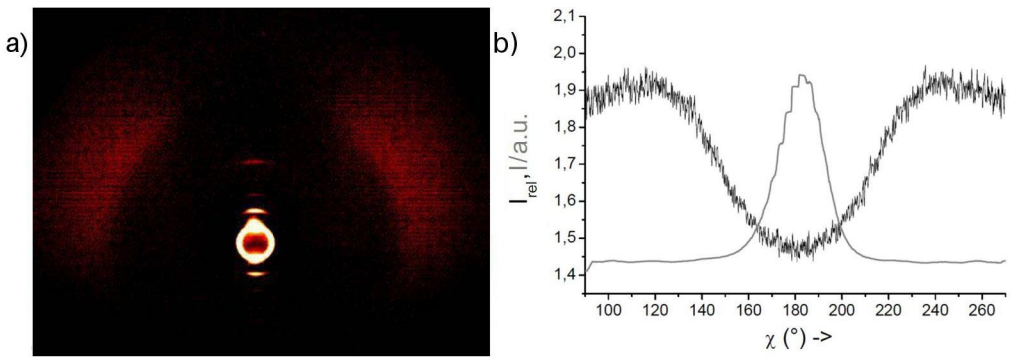

Figure 18: a) 2D X-ray diffraction pattern for a surface-aligned sample of **OH 4d** at 122 °C on cooling; b) χ-scan for the outer diffuse scattering with maxima at about 120 and 240° (I_{rel} = I(122 °C)/I(140 °C, isotropic liquid).

The results of electro-optical, microscopic and X-ray diffraction studies prove the existence of a $SmCP_A$ phase.

Disalicylideneimine compounds **OH 5** and **OH 6** bearing the azomethine groups between the central phenyl ring and the neighbouring rings

Synthesis of the compounds **OH 5** and **OH 6**

The 1,3-phenylenediamine derivatives **OH 5** and **OH 6** were prepared by condensation of the corresponding 1,3-phenylenediamines with 4-formyl-3-hydroxyphenyl 4-*n*-dodecyloxy-3-substituted-benzoates **5** and 4-formyl-3-hydroxyphenyl 4-*n*-dodecyloxycinnamate (**9**), respectively, as sketched in Scheme 5. Compound **9** was obtained by esterification of 2,4-dihydroxybenzaldehyde with 4-*n*-dodecyloxycinnamic acid, under the same conditions as reported for the salicylaldehydes **5**.

Mesophase behaviour of the compounds **OH 5** and **OH 6**

The influence of the pattern of substitution at the outer and/or the central phenyl ring on the phase-transition temperatures and phase type of the compounds **OH 5** and **OH 6** can be seen from Table 5. For comparison, corresponding compounds having the same aromatic core but without the hydroxy groups are given.

The phase-transition behaviour shown in Table 5 demonstrates the strong influence of the ortho-hydroxy groups on the mesophase type and the mesophase stability. The comparison of the compounds **H 5a–g** with **OH 5a–g** shows that in all cases the clearing temperatures are increased by about 60 K or liquid-crystalline behaviour is induced.

Compound **OH 5a** exhibits a very high melting point; the occurrence of the metastable columnar phase is established by means of typical textures only. It should be mentioned that the B_6 banana phase was first reported for short-chain members of the homologous series of **H 5a** [52]. The effect of lateral substituents X and Z is remarkable. Introduction of a methyl group into the 2-position of the central phenyl ring of **OH 5a** not only decreases the melting temperature by 54 K but also increases the clearing point by 21 K for **OH 5b**. Additional attachment of fluorine atoms at the outer phenyl rings increases the smectic–isotropic phase-transition temperature again by 13 K for **OH 5c**. That means that the laterally substituted com-

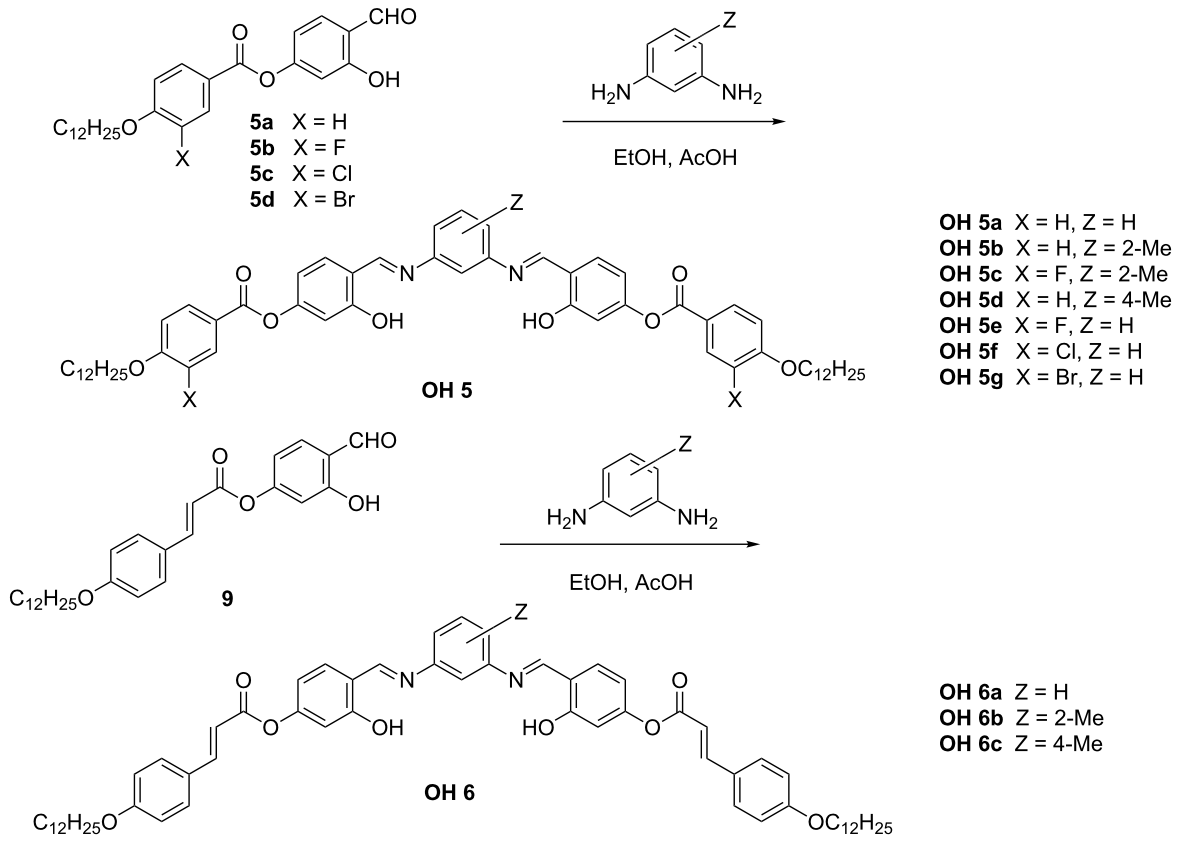

Scheme 5: Reaction steps employed for the preparation of the compounds **OH 5** and **OH 6**.

Table 5: Mesophase behaviour, transition temperatures (°C) and enthalpies [kJ/mol] of compounds **OH 5** and **OH 6** (on the right) and corresponding compounds **H 5** and **H 6** (on the left).

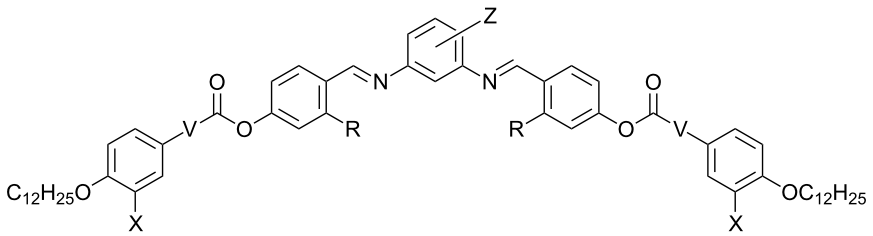

Mesophase behaviour					R = H	V	X	Z	R = OH	Mesophase behaviour				
Cr	120 [48.9]	(SmCP	114) [17.1]	I	**H 5a** [52]	—	H	H	**OH 5a**	Cr	177 [45.2]	(Col	172) [—[a]]	I
Cr	128 [26.2]	I			**H 5b**	—	H	2-Me	**OH 5b** [44]	Cr	123 [71.2]	$SmCP_A$	193 [19.5]	I
							F	2-Me	**OH 5c**	Cr	105 [63.2]	$SmCP_A$	206 [20.4]	I
Cr	98 [58.0]	I			**H 5d**	—	H	4-Me	**OH 5d**	Cr	97 [8.5]	B_X	126 [32.1]	I
Cr	127 [75.1]	(SmCP	124) [8.6]	I	**H 5e**	—	F	H	**OH 5e**	Cr	179 [25.9]	USmC	186 [26.7]	I
Cr	116 [74.1]	(SmCP	108) [13.5]	I	**H 5f**	—	Cl	H	**OH 5f**	Cr	165 25.1	USmC	173 [22.2]	I
Cr	79 [14.1]	SmCP	92 [6.2]	I	**H 5g**	—	Br	H	**OH 5g**	Cr	143 [17.6]	USmC	161 [13.5]	I
Cr	146 [56.8]	I			**H 6a**	HC=CH	H	H	**OH 6a**	Cr	189 [54.4]	($SmCP_A$	183) [—[a]]	I
Cr	136 [67.6]	N	140 [0.5]	I	**H 6b**	HC=CH	H	2-Me	**OH 6b**	Cr	131 [74.1]	$SmCP_A$	202 [16.9]	I
Cr	107 [40.8]	I			**H 6c**	HC=CH	H	4-Me	**OH 6c**	Cr	114 [23.4]	$SmCP_A$	134 [14.4]	I

[a]Could not be found by calorimetric measurements due to crystallization.

pound **OH 5c** exhibits a transition temperature to the isotropic phase that is 34 K higher than the laterally unsubstituted parent compound **OH 5a**. This is a really exciting result.

Upon shifting of the methyl groups of **OH 5b** from the 2-position into the 4-position, the clearing temperature decreases by 67 K for the isomeric compound **OH 5d**. By cooling the isotropic liquid of **OH 5d**, an intensive blue colour arises. Furthermore, chiral domains of different handedness are visible in the texture (Figure 19a and Figure 19b). Both appearances could be a hint for a B_4 banana phase [8,53,54]. X-ray patterns show slightly broadened layer reflections (d = 4.0 nm) and additional weak and sharp reflections together with broadened ones over the entire diffraction range (Figure 19c), which are also arguments for a B_4 or another soft-crystal-like B_X phase of **OH 5d**.

The methyl-substituted compound **OH 5b** is of special interest. The X-ray patterns of nonoriented samples show a strong reflection in the small-angle region with a very weak second order reflection and a diffuse scattering in the wide-angle region indicating a simple layer structure without in-plane ordering. The layer spacing of 3.8 nm is clearly smaller than the molecular length L = 5.4 nm as estimated by commercial molecular modelling software (Cerius 2) and thus from $\cos\theta = d/L$ = 3.8 nm/5.4 nm a tilt angle of about 45° was estimated. Such a tilt angle explains the optical behaviour. Upon cooling of the isotropic liquid, the SmCP phase occurs as nonbirefringent black texture. After slight decrossing of the polarisers, however, optically active domains become visible, as shown in Figure 20a and Figure 20b. Under the action of an A.C. electric field, nucleation of a birefringent texture starts, which coalesces to a non-specific or broken fan-shaped texture (Figure 20c).

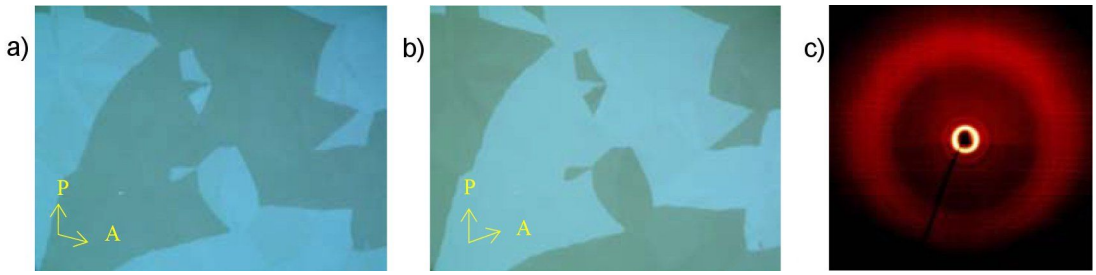

Figure 19: Compound **OH 5d**: Optical photomicrographs of chiral domains at 122 °C; polariser and analyser are uncrossed by about a) −8° and b) +8° from the 90° position; c) X-ray pattern of a powderlike sample at 110 °C.

This state of compound **OH 5b** exhibits an interesting current response consisting of five or more peaks per half period (Figure 20d).

Such a multistage switching is unique for bent-core compounds and was reported by us some time ago [44]. This switching cannot be explained by using a simple layer structure of the SmCP phase. Therefore, a structure model for an intermediate field-induced ferrielectric state was proposed [45]. In the present work it is helpful to search for further bent-core compounds exhibiting a multistage switching. Hence, the molecular structure was changed in a stepwise manner. Starting from compound **OH 5b**, the attachment of fluoro atoms on the outer rings results in compound **OH 5c**, which also exhibits a $SmCP_A$ phase. However, a two-peak current response typical of an antiferroelectric switching is found. As mentioned above, compound **OH 5d** isomeric with **OH 5b**, shows a crystal-like phase only. That means that simple changes of the molecular structure can prevent the unusual multistage switching found for **OH 5b**.

Substitution by fluorine, chlorine, and bromine atoms at both outer phenyl rings of compound **OH 5a** results in **OH 5e–g**. The following tendency of clearing temperatures is found: X = H (172 °C), F (186 °C), Cl (173 °C), Br (161 °C). It is very surprising that compound **OH 5f**, bearing two chlorine atoms in lateral positions, exhibits mesophase stability similar to the laterally unsubstituted parent compound **OH 5a**.

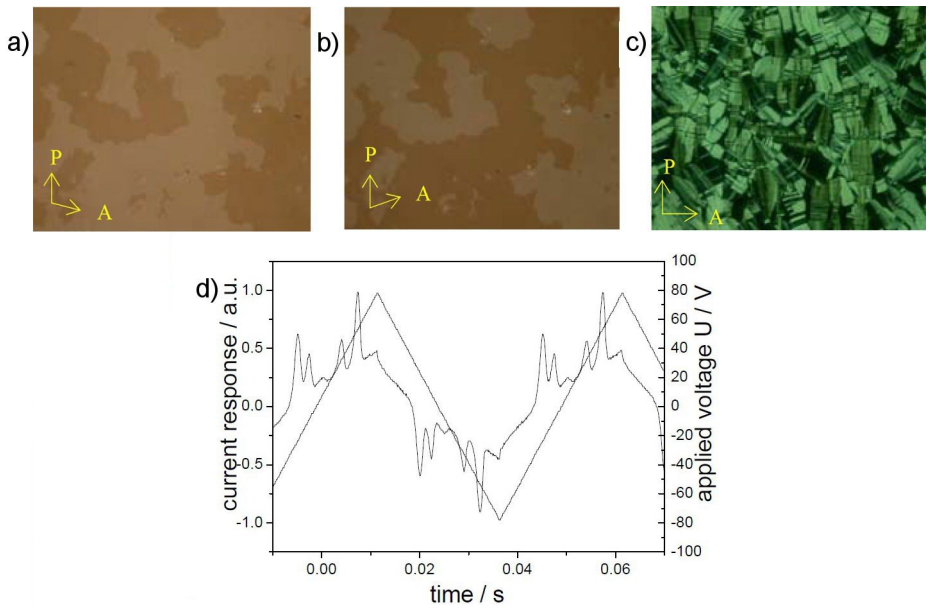

Figure 20: Compound **OH 5b:** a), b) Chiral domains at 175 °C, 0 V, polarisers uncrossed by about ±8° from the 90° position; c) birefringent texture formed under an electric field (U = 100 $V_{A.C.}$); d) current response (U = 158 V_{pp}, f = 20 Hz, T = 174 °C, d_{cell} = 6 µm).

X-ray diffraction patterns for the halogen-substituted compounds **OH 5e–g** show several sharp small-angle reflections and a diffuse outer scattering (Figure 21). The sample of **OH 5f** was partially surface-aligned and the diffraction angles of four reflections were determined. Thus the reflections were indexed to an oblique 2D lattice (for parameters see Table 6). In the same way the small-angle reflections of the other two compounds can be interpreted. Comparing the molecular volume with the volume of a hypothetical 3D unit cell with a thickness of 0.52 nm, corresponding to the assumed stacking distance of the molecules in bending direction, the number of molecules in the cross section of the unit cell, i.e., in the blocks of the modulated structure, was calculated (see Table 6 and Supporting Information File, Table S3). These structural parameters for the liquid-crystalline phases of the three compounds closely resemble each other. There are several packing models for the molecules that fit these data, namely the undulated-layer model (USmC phase), the broken-layer (columnar) model (Col_{ob} phase), and the polarization-modulation model, and several modes within these models depending on the direction of the polarization between the layers, which cannot be decided based on our X-ray results [5,9]. Since no sufficient alignment of the samples was achieved, the tilt angle of the molecules with respect to the axes of the 2D lattice could not be determined.

Table 6: Structural parameters for the modulated-layer phases of compounds **OH 5e**, **5f** and **5g:** Temperature, *T* (°C) on cooling, 2D lattice parameters *a*, *b* (nm), and γ (°), molecules in the cross section of the unit cell n_{lc}.

Compound	*T*	*a*	*b*	γ	n_{lc}
OH 5e	177	14.0	4.9	116	22
OH 5f	158	14.8	4.5	112	21
OH 5g	150	17.0	4.4	112	24

In principle the appearance of spiral germs upon slow cooling of the isotropic liquid of the compounds **OH 5** hints at an undulated smectic phase or a B_7 banana phase, see Figure 22a. However, in the presence of an electric D.C. field, a texture with chiral domains is observed, with a change in contrast seen upon rotation of one polariser from the 90° position by several degrees (Figure 22). Surprisingly, it was not possible to find a

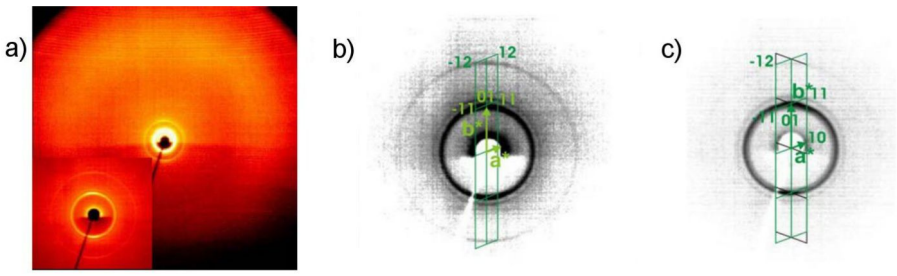

Figure 21: X-ray diffraction patterns of compounds **OH 5**: a) Pattern of a powderlike sample of compound **OH 5g** at 150 °C on cooling (inset: small-angle region); b) small-angle pattern of **OH 5g** showing the reciprocal 2D lattice and the indexing of the observed reflections; c) small-angle pattern of a partially surface-aligned sample of compound **OH 5f** at 158 °C on cooling, showing the two preferred orientations of the reciprocal 2D lattice in the sample and the indexing of the observed reflections.

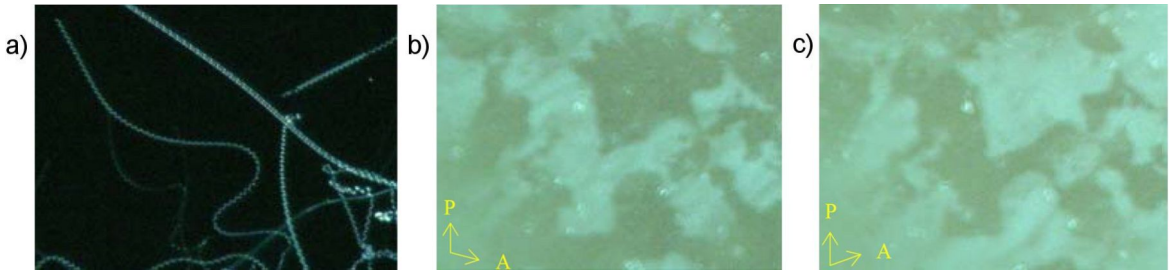

Figure 22: Photomicrographs of compound **OH 5f**: a) Appearance of spiral filaments on slow cooling of the isotropic liquid at 171 °C; b), c) cooling from the isotropic phase in the presence of an electric field of 15 V/µm results in a texture with chiral domains, which are visible by rotation of one polariser clockwise or anticlockwise by several degrees from the crossed position; *T* = 165 °C.

current response typical for a polar banana phase. The birefringence of the sample changed depending on the power of the electric field. Although the chemical structure and the molecular shape suggest that the compounds might be capable of forming banana phase(s), the polar character of the mesophases could not be unambiguously determined. Therefore, the mesophases of the compounds **OH 5e–g** are designated as USmC phases.

A further slight modification of the chemical structure of the series **OH 5** is the insertion of C=C groups between the outer and the neighbouring phenyl rings, giving **OH 6a–c**. Of all three hydroxy group-free compounds, **H 6a–c**, only the 2-methyl-substituted compound shows liquid-crystalline behaviour. A nematic phase is observed, which is very surprising for this mesogen having a molecular shape characteristic of banana-shaped liquid crystals. Although both legs of the bent-core molecules are extended by the C=C units, the clearing temperatures increase only by about 10 K. Introduction of a lateral methyl group on the central phenyl ring drastically decreases the melting temperatures. Therefore, broad SmCP phase ranges exist for **OH 6b** and **OH 6c** in comparison to the laterally unsubstituted derivative **OH 6a**. That also means that the nematic phase of **H 6b** changes to a polar smectic phase in **OH 6b** by insertion of the C=C units.

The mesophase behaviour of compound **OH 6b** is characteristic for a $SmCP_A$ phase. On cooling, the isotropic liquid fringe textures as well as Schlieren textures are observed. The current response shows two peaks per half period (Figure 23). The spontaneous polarization amounts to 220 nC/cm^2. However, notably, the multistage switching found for the corresponding compound **OH 5b** disappears.

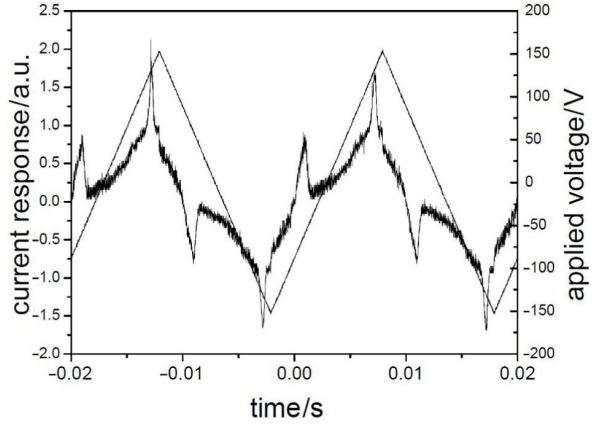

Figure 23: Current response of compound **OH 6b** exhibiting two repolarisation peaks proving an antiferroelectric switching ($U_{A.C.}$ = 15 V/µm, f = 50 Hz, T = 174 °C, d_{cell} = 6 µm).

By shifting the methyl group from the 2-position in **OH 6b** to the 4-position of the central phenyl ring of compound **OH 6c**, the clearing temperature decreases by 68 K. Nevertheless, an enantiotropic mesophase exists and can be investigated. Microscopic pictures show textures typical for SmCP phases (Figure 24).

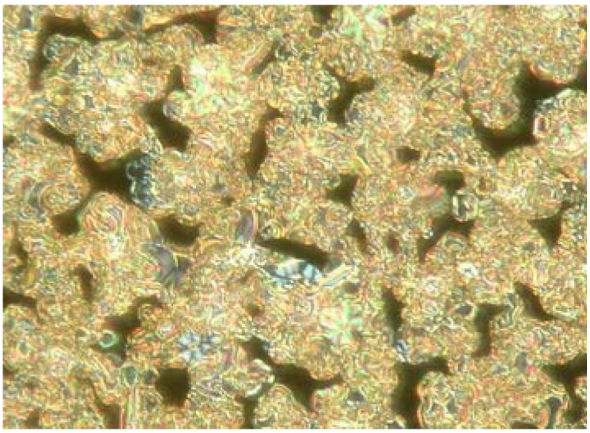

Figure 24: On cooling the isotropic liquid phase of compound **OH 6c**; a Schlieren texture together with fringe pattern appears characteristic for $SmCP_A$ phases.

Guinier X-ray patterns of a powderlike sample of **OH 6c** show first and second order layer reflections and a diffuse outer scattering indicating a smectic layer structure with a layer spacing of 4.0 nm. Electro-optical studies of the mesophase of compound **OH 6c** support the assignment as a $SmCP_A$ phase. Figure 25 shows the current response curve and microscopic pictures, which demonstrate the switching between SmC_aP_A to SmC_sP_F upon application of a D.C. electric field.

Conclusion

The use of salicylideneaniline moieties in five-ring bent-core mesogens is shown to be helpful in deriving the relationship between the chemical structure and the mesophase behaviour. Here, the effect of fluorine, chlorine, and bromine atoms laterally attached to the outer phenyl rings, the influence of the hydroxy group in ortho-position to azomethine units, and the effect of a methyl group situated at the central phenyl ring on the liquid-crystalline behaviour and physical properties were studied.

For most of the salicylideneaniline compounds synthesized, the corresponding benzylideneaniline derivatives were prepared for a comparative study. As expected, the clearing temperatures generally increase due to the presence of the ortho-hydroxy group. The increase amounts to about 30 K for mono-salicylide-

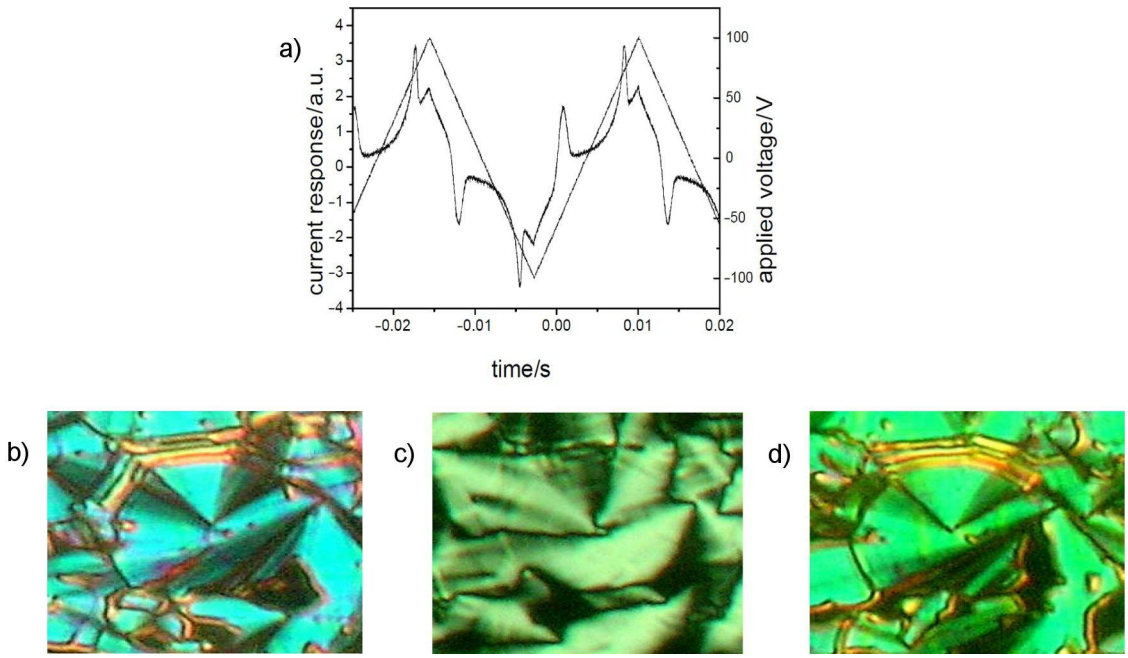

Figure 25: Electro-optical behaviour of compound **OH 6c**: a) Current response ($U_{A.C.}$ = 17 V/µm, f = 39 Hz, T = 123 °C, d_{cell} = 6 µm, P_S = 520 nC/cm^2); c) 0 V, ground state SmC_aP_A; b) and d) formation of the SmC_SP_F phase upon application of a D.C. field of different sign: b) +7 V/µm; d) −7 V/µm.

neaniline compounds **OH 1** and **OH 2**, and can be up to 60 K for the mesogens containing two salicylideneaniline moieties, namely **OH 4**, **OH 5**, **OH 6**. As shown in Table 1–Table 5 and Supporting Information File 1, Table S4, the definite increase of the clearing temperature can be much lower depending on the size of the molecules, the length of the terminal chains, and the presence of further lateral substituents and their positions at the different phenyl rings. More importantly, in many cases the introduction of the hydroxy group induces liquid-crystalline behaviour, which was not observed for the corresponding benzylideneaniline compounds. There are other cases where the type of mesophase also changed, for example from nematic to SmCP, nematic to USmCP, B_X to SmCP, and SmCP to columnar.

The influence of one halogen atom attached at the outer phenyl rings was investigated in several nonsymmetric molecules. The mono-halogen derivatives of three series are isomeric to each other (**OH 1b–c**, **OH 2e–g**, **OH 2h–j**). All these compounds exhibit SmCP phases. The lowering of the clearing temperatures by a lateral fluorine, chlorine, or bromine atom is unexpectedly low and nearly independent of the different chemical structure of the aromatic cores of the compounds **OH 1** and **OH 2**. For example, the clearing temperatures of the isomeric mono-chlorinated compounds (**OH 1b** 140 °C; **OH 2f** 138 °C; **OH 2i** 135 °C) have nearly the same values as those of the corresponding laterally unsubstituted compounds (**OH 1a** 142 °C; **OH 2a** 136 °C) The replacement of the chlorine atom by the larger bromine atom additionally decreases the clearing temperatures by only 2–6 K.

Looking at the compounds **OH 5e–g**, which have two halogen atoms, i.e., one halogen atom at each leg, the lowering of the clearing points found for mono-halogen derivatives is approximately doubled. Nevertheless, the effect of lateral halogen atoms on the mesophase stability is much lower for the salicylideneanilines under study, as reported for comparable derivatives in the original banana series. There, in dependence on further substituents at the central phenyl ring, the clearing temperatures of corresponding terminally dodecyloxy-substituted derivatives decreased by the introduction of chlorine atoms, by 18–34 K. For related octyloxy-substituted homologues the effect was much stronger [55,56]. The reason for such differences found in different series of bent-core mesogens is not clear up to now.

Comparing the compounds **OH 5a–c**, an unusually strong increase of the mesophase stability caused by lateral substituents was found. In comparison to the salicylideneimine-based compound **OH 5a** (clp 172 °C), the clearing point of the 2-methyl-substituted compound **OH 5b** increases to 193 °C; compound **OH 5c** having additional fluorine atoms at the outer phenyl rings exhibits a SmCP–isotropic phase-transition temperature of 206 °C.

In relation to this it should be mentioned that the cinnamic ester **H 6b**, having a methyl group in the same position, exhibits a nematic phase. The formation of nematic and nonpolar smectic phases by bent-core mesogens can be explained by flexible molecular fragments, and especially by a bending angle clearly above 120° [57]. Such molecules have a more rodlike shape, and therefore "calamitic phases" can be formed. The 4-bromoresorcinol derivative **H 3c** also shows a nematic phase. It is known from NMR studies of other related bent-core mesogens that halogen atoms in the 4-position extend the bending angle to about 135°, and hence this would explain the nematic phase in compound **H 3c**. The influence of a methyl group in the 2-position of the central phenyl ring on the bending angle of bent-core mesogens depends on the chemical structure and on the direction of the linking groups, which connect both molecular legs to the central phenyl ring, as we know from solid state NMR studies. For 2-methylresorcinol bisbenzoates, for example, the bending angle amounts to about 120° [58]. In contrast, for isomeric diphenyl 2-methylisophthalates the bending angle is extended to about 145° [59]. Transferring this knowledge to the methyl-substituted compound **H 6b** would mean that the existence of a nematic phase strongly hints at a bending angle larger than 120°. However, the evidence can only be delivered by NMR studies of the liquid-crystalline state.

The electro-optical behaviour of the salicylideneaniline compounds can change in comparison to that of the corresponding compounds without a hydroxy group. Upon action of an electric field on a SmCP phase, the tilted molecules can rotate on a cone or can rotate about their long axis. Only the latter movement changes the chirality of the layers. In a few cases both molecular processes have been observed for the same material, in dependence on the frequency, temperature and/or the field [48,50,51]. For compound **H 1a** both molecular movements exist depending on how rapidly the electric field is removed. This interesting behaviour disappears in compound **OH 1a** by the substitution with an ortho-hydroxy group.

A further motivation for the present work was the exciting multistage switching reported for the 2-methyl-substituted compound **OH 5b** (and for two longer-chain homologues) bearing two salicylidene legs [44]. Therefore, the chemical structure of this molecule was varied step by step. Liquid-crystalline behaviour was not observed for the corresponding compound without an ortho-hydroxy group, **H 5b**. In compound **OH 4c** only the COO and CH=N linking groups are exchanged in comparison to the isomeric compound **OH 5b**; however, the characteristic electro-optical behaviour of a $SmCP_A$ phase was found. Furthermore, the chemical structure of compound **OH 5b** was varied by substitution with fluorine atoms at the outer phenyl rings (**OH 5c**), by shifting the methyl group to the 4-position of the central phenyl ring (**OH 5d**), by insertion of C=C units (**OH 6b** and **OH 6c**) and by preparation of a corresponding compound having only one salicylideneaniline moiety together with a methyl group in the 2-position (**OH 2c**). Unfortunately, the creation of new compounds exhibiting a multistage switching was not successful.

The studies on the influence of lateral halogen atoms, and also of a lateral methyl group, on the mesophase behaviour and further physical properties of salicylideneimine-based bent-core mesogens show that the relationships strongly differ from those reported for calamitic liquid crystals, and that they also vary in comparison to other similar five-ring bent-core mesogens.

Experimental

The thermal transition behaviour was investigated by using a Perkin Elmer DSC Pyris 1 differential scanning calorimeter. Texture observations of liquid-crystal films sandwiched between two glass plates were carried out with a Leitz polarizing microscope (Laborlux 12 Pol S, Germany). For the electro-optical measurements we used commercial sandwich cells (E.H.C., Japan) with thickness of 6 μm, having a rubbed polyimide coating for planar surface alignment. The cells were observed in transmission by using a Leica (DMRXP, Germany) polarizing microscope equipped with a digital camera (Nikon Coolpix 4500, Japan). The cells are mounted on a heating stage (Linkam LTS 350, UK, and Mettler FP82HT and FP90, UK) for temperature control. The magnitude of the spontaneous polarization was measured by integrating the polarization-reversal current peak obtained by switching the sample with a triangular electric field.

X-ray diffraction measurements on powderlike samples in glass capillaries kept in a temperature-controlled heating stage were performed by using a Guinier film camera (Huber Diffraktionstechnik GmbH) and quartz-monochromatized Cu Kα radiation. 2D diffraction patterns were recorded on an area detector (HI-Star, Siemens/Bruker) from Ni-filtered Cu Kα radiation. Surface aligned fibrelike disordered samples were obtained by slowly cooling a drop of the isotropic liquid placed on a glass plate on a temperature-controlled heating stage.

Reaction pathways to prepare the final compounds **OH 1–6** are sketched in Scheme 2–Scheme 5.

Generally, all compounds **H1–H6**, which do not bear the ortho-hydroxy group, were prepared by following the same reaction pathways sketched in Scheme 2–Scheme 5, but instead of the salicylidene intermediates the corresponding benzylidene intermediates were used. Further details are given in Supporting Information File 1.

Supporting Information

Supporting Information File 1

Schematic presentation of the SmC_aP_A phase, additional X-ray data, mesophase behaviour of selected compounds and synthesis of compounds (experimental procedures and analytical data).
[http://www.beilstein-journals.org/bjoc/content/supplementary/1860-5397-8-15-S1.pdf]

Acknowledgements

The authors are indebted to the Deutsche Forschungsgemeinschaft for financial support.

References

1. Niori, T.; Sekine, T.; Watanabe, J.; Furukawa, T.; Takezoe, H. *J. Mater. Chem.* **1996,** *6,* 1231–1233. doi:10.1039/jm9960601231
2. Link, D. R.; Natale, G.; Shao, R.; Maclennan, J. E.; Clark, N. A.; Körblova, E.; Walba, D. M. *Science* **1997,** *278,* 1924–1927. doi:10.1126/science.278.5345.1924
3. Brand, H. R.; Cladis, P. E.; Pleiner, H. *Eur. Phys. J. B* **1998,** *6,* 347–353. doi:10.1007/s100510050560
4. Bedel, J. P.; Rouillon, J. C.; Marcerou, J. P.; Nguyen, H. T.; Achard, M. F. *Phys. Rev. E* **2004,** *69,* 061702. doi:10.1103/PhysRevE.69.061702
5. Coleman, D. A.; Fernsler, J.; Chattham, N.; Nakata, M.; Takanishi, Y.; Körblova, E.; Link, D. R.; Shao, R.-F.; Jang, W. G.; Maclennan, J. E.; Mondainn-Monval, O.; Boyer, C.; Weissflog, W.; Pelzl, G.; Chien, L.-C.; Zasadzinski, J.; Watanabe, J.; Walba, D. M.; Takezoe, H.; Clark, N. A. *Science* **2003,** *301,* 1204–1211. doi:10.1126/science.1084956
6. Izumi, T.; Kang, S.; Niori, T.; Takanishi, Y.; Takezoe, H.; Watanabe, J. *Jpn. J. Appl. Phys.* **2006,** *45,* 1506–1514. doi:10.1143/JJAP.45.1506
7. Takanishi, Y.; Toshimitsu, M.; Nakata, M.; Takada, N.; Izumi, T.; Ishikawa, K.; Takezoe, H.; Watanabe, J.; Takahashi, Y.; Iida, A. *Phys. Rev. E* **2006,** *74,* 051703. doi:10.1103/PhysRevE.74.051703
8. Pelzl, G.; Diele, S.; Weissflog, W. *Adv. Mater.* **1999,** *11,* 707–724. doi:10.1002/(SICI)1521-4095(199906)11:9<707::AID-ADMA707>3.0.CO;2-D
9. Amaranatha Reddy, R.; Tschierske, C. *J. Mater. Chem.* **2006,** *16,* 907–961. doi:10.1039/b504400f
10. Hird, M. *Liq. Cryst. Today* **2005,** *14,* 9–21. doi:10.1080/14645180500274347
11. Takezoe, H.; Takanishi, Y. *Jpn. J. Appl. Phys.* **2006,** *45,* 597–625. doi:10.1143/JJAP.45.597
12. LiqCryst database, 5.0; LCI Publisher GmbH, 2011.
13. Vill, V. Liquid Crystals. In *Macroscopic properties of matter;* Thiem, J., Ed.; Landolt-Börnstein, New Series, Group IV, Vol. 7; Springer: Berlin, Heidelberg, New York, 2003.
14. Serrano, K. L. *Metallomesogens. Synthesis, Properties and Applications;* Wiley-VCH: Weinheim, Germany, 1996.
15. Donnio, B.; Guillon, D.; Deschenaux, R.; Bruce, D. W. Metallomesogens. In *Comprehensive Coordination Chemistry II;* McCleverty, J. A.; Meyer, T. J., Eds.; Pergamon: Oxford, 2003; Vol. 7, pp 357–627.
16. Yelamaggad, C. V.; Prabhu, R.; Shanker, G.; Bruce, D. W. *Liq. Cryst.* **2009,** *36,* 247–255. doi:10.1080/02678290902818826
17. Pucci, D.; Aiello, I.; Bellusci, A.; Crispini, A.; Ghedini, M.; La Deda, M. *Eur. J. Inorg. Chem.* **2009,** 4274–4281. doi:10.1002/ejic.200900536
18. Yelamaggad, C. V.; Achalkumar, A. S. *Tetrahedron Lett.* **2006,** *47,* 7071–7075. doi:10.1016/j.tetlet.2006.07.102
19. Yelamaggad, C. V.; Achalkumar, A. S.; Rao, D. S. S.; Prasad, S. K. *J. Org. Chem.* **2009,** *74,* 3168–3171. doi:10.1021/jo9001933
20. Barberá, J.; Marcos, M.; Serrano, J. L. *Chem.–Eur. J.* **1999,** *5,* 1834–1840. doi:10.1002/(SICI)1521-3765(19990604)5:6<1834::AID-CHEM1834>3.0.CO;2-A
21. Soto Bustamante, E. A.; Yablonski, S. V.; Ostrovski, B. I.; Beresnev, L. A.; Blinov, L. M.; Haase, W. *Liq. Cryst.* **1996,** *21,* 829–839. doi:10.1080/02678299608032899
22. Yablonski, S. V.; Soto Bustamante, E. A.; Vergara-Toloza, R. O.; Haase, W. *Adv. Mater.* **2004,** *16,* 1936–1939. doi:10.1002/adma.200306622
23. Hsieh, C.-C.; Liu, K.-T.; Lai, C. K. *J. Chin. Chem. Soc.* **2006,** *53,* 1397–1404.
24. Šepelj, M.; Lesac, A.; Baumeister, U.; Diele, S.; Bruce, D. W.; Hameršak, Z. *Chem. Mater.* **2006,** *18,* 2050–2058. doi:10.1021/cm0526213
25. Yelamaggad, C. V.; Nagamani, S. A.; Hiremath, U. S.; Shankar Rao, D. S.; Prasad, S. K. *Liq. Cryst.* **2002,** *29,* 1401–1408. doi:10.1080/0267829021000029480
26. Yelamaggad, C. V.; Mathews, M.; Hiremath, U. S.; Nair, G. G.; Shankar Rao, D. S.; Prasad, S. K. *Liq. Cryst.* **2003,** *30,* 899–907. doi:10.1080/0267829031000138587
27. Achten, R.; Koudijs, A.; Karczmarzyk, Z.; Marcelis, A. T. M.; Sudhölter, E. J. R. *Liq. Cryst.* **2004,** *31,* 215–227. doi:10.1080/02678290310001642531
28. Yelamaggad, C. V.; Tamilenthi, V. P.; Shankar Rao, D. S.; Nair, G. G.; Prasad, S. K. *J. Mater. Chem.* **2009,** *19,* 2906–2908. doi:10.1039/b906315c
29. Rao, N. V. S.; Paul, M. K.; Miyake, I.; Takanishi, Y.; Ishikawa, K.; Takezoe, H. *J. Mater. Chem.* **2003,** *13,* 2880–2884. doi:10.1039/b304964g
30. Choi, S.-W.; Ha, N. Y.; Shiromo, K.; Rao, N. V. S.; Paul, M. K.; Toyooka, T.; Nishimura, S.; Wu, J. W.; Park, B.; Takanishi, Y.; Ishikawa, K.; Takezoe, H. *Phys. Rev. E* **2006,** *73,* 021702. doi:10.1103/PhysRevE.73.021702
31. Deb, R.; Nath, R. K.; Paul, M. K.; Rao, N. V. S.; Tuluri, F.; Shen, Y.; Shao, R.; Chen, D.; Zhu, C.; Smalyukh, I. I.; Clark, N. A. *J. Mater. Chem.* **2010,** *20,* 7332–7336. doi:10.1039/c0jm01539c
32. Yelamaggad, C. V.; Shashikala, I.; Shankar Rao, D. S.; Prasad, S. K. *Liq. Cryst.* **2004,** *31,* 1027–1036. doi:10.1080/02678290410001716015
33. Majumdar, K. C.; Chakravorty, S.; Pal, N. *Mol. Cryst. Liq. Cryst.* **2009,** *503,* 112–125. doi:10.1080/15421400902841445
34. Bhattacharyya, S. S.; Mukherjee, A.; Chaudhuri, B. K. *Mol. Cryst. Liq. Cryst.* **2010,** *528,* 23–31. doi:10.1080/15421406.2010.504512
35. Yelamaggad, C. V.; Shashikala, I. S.; Hiremath, U. S.; Liao, G.; Jakli, A.; Shankar Rao, D. S.; Prasad, S. K.; Li, Q. *Soft Matter* **2006,** *2,* 785–792. doi:10.1039/b608278e
36. Yelamaggad, C. V.; Nagamani, S. A.; Nair, G. G.; Shankar Rao, D. S.; Prasad, S. K.; Jakli, A. *Liq. Cryst.* **2002,** *29,* 1181–1185. doi:10.1080/02678290210155561
37. Yelamaggad, C. V.; Hiremath, U. S.; Nagamani, S. A.; Shankar Rao, D. S.; Prasad, S. K. *J. Mater. Chem.* **2001,** *11,* 1818–1822. doi:10.1039/b100022p

38. Prasad, S. K.; Maeda, Y.; Shankar Rao, D. S.; Nagamani, S. A.; Hiremath, U. S.; Yelamaggad, C. V. *Liq. Cryst.* **2003,** *30,* 1277–1283.
39. Nair, G. G.; Prasad, S. K.; Hiremath, U. S.; Yelamaggad, C. V. *J. Appl. Phys.* **2001,** *90,* 48–52.
40. Shankar Rao, D. S.; Nair, G. G.; Prasad, S. K.; Nagamani, S. A.; Yelamaggad, C. V. *Liq. Cryst.* **2001,** *28,* 1239–1243. doi:10.1080/02678290110051567
41. Walba, D. M.; Körblova, E.; Shao, R.; Clark, N. A. *J. Mater. Chem.* **2001,** *11,* 2743–2747. doi:10.1039/b102732h
42. Yelamaggad, C. V.; Mathews, M.; Nagamani, S. A.; Shankar Rao, D. S.; Prasad, S. K.; Findeisen, S.; Weissflog, W. *J. Mater. Chem.* **2007,** *17,* 284–298. doi:10.1039/b610758c
43. Rao, N. V. S.; Deb, R.; Paul, M. K.; Francis, T. *Liq. Cryst.* **2009,** *36,* 977–987. doi:10.1080/02678290903165979
44. Findeisen-Tandel, S.; Schröder, M. W.; Pelzl, G.; Baumeister, U.; Weissflog, W.; Stern, S.; Nemes, A.; Stannarius, R.; Eremin, A. *Eur. Phys. J. E* **2008,** *25,* 395–402. doi:10.1140/epje/i2007-10306-1
45. Stern, S.; Stannarius, R.; Eremin, A.; Weissflog, W. *Soft Matter* **2009,** *5,* 4136–4140. doi:10.1039/b903659h
46. Liao, C.-T.; Liu, J.-Y.; Jiang, M.-H.; Zou, S.-F.; Wu, N.-C.; Wu, Z.-L.; Lee, J.-Y. *Mol. Cryst. Liq. Cryst.* **2010,** *533,* 115–125. doi:10.1080/15421406.2010.504657
47. Weissflog, W.; Naumann, G.; Kosata, B.; Schröder, M. W.; Eremin, A.; Diele, S.; Vakhovskaya, Z.; Kresse, H.; Friedemann, R.; Rama Krishnan, S. A.; Pelzl, G. *J. Mater. Chem.* **2005,** *15,* 4328–4337. doi:10.1039/b508488a
48. Schröder, M. W.; Diele, S.; Pelzl, G.; Weissflog, W. *ChemPhysChem* **2004,** *5,* 99–103. doi:10.1002/cphc.200300904
49. Lagerwall, S. T.; Dahlgren, A.; Jägemalm, P.; Rudquist, P.; D'havé, K.; Pauwels, H.; Dabrowski, R.; Drzewinski, W. *Adv. Funct. Mater.* **2001,** *11,* 87–94. doi:10.1002/1616-3028(200104)11:2<87::AID-ADFM87>3.0.CO;2-E
50. Szydlowska, J.; Mieczkowski, J.; Matraszek, J.; Bruce, D. W.; Gorecka, E.; Pociecha, D.; Guillon, D. *Phys. Rev. E* **2003,** *67,* 031702. doi:10.1103/PhysRevE.67.031702
51. Nakata, M.; Shao, R.-F.; Maclennan, J. E.; Weissflog, W.; Clark, N. A. *Phys. Rev. Lett.* **2006,** *96,* 067802. doi:10.1103/PhysRevLett.96.067802
52. Weissflog, W.; Wirth, I.; Diele, S.; Pelzl, G.; Schmalfuss, H.; Schoss, T.; Würflinger, A. *Liq. Cryst.* **2001,** *28,* 1603–1609. doi:10.1080/02678290110075075
53. Sekine, T.; Niori, T.; Watanabe, J.; Furukawa, T.; Choi, S. W.; Takezoe, H. *J. Mater. Chem.* **1997,** *7,* 1307–1309. doi:10.1039/a702026k
54. Martínez-Perdiguero, J.; Alonso, I.; Folcia, C. L.; Etxebarria, J.; Ortega, J. *J. Mater. Chem.* **2009,** *19,* 5161–5166. doi:10.1039/b900832b
55. Weissflog, W.; Nádasi, H.; Dunemann, U.; Pelzl, G.; Diele, S.; Eremin, A.; Kresse, H. *J. Mater. Chem.* **2001,** *11,* 2748–2758. doi:10.1039/b104098g
56. Dunemann, U.; Schröder, M. W.; Amaranatha Reddy, R.; Pelzl, G.; Diele, S.; Weissflog, W. *J. Mater. Chem.* **2005,** *15,* 4051–4061. doi:10.1039/b507458d
57. Pelzl, G.; Weissflog, W. Mesophase behaviour at the borderline between clamitic and banana-shaped mesogens. In *Thermotropic Liquid Crystals;* Ramamoorthy, A., Ed.; Springer: Berlin, 2007; pp 1–58.
58. Diele, S.; Grande, S.; Kruth, H.; Lischka, C.; Pelzl, G.; Weissflog, W.; Wirth, I. *Ferroelectrics* **1998,** *212,* 169–177. doi:10.1080/00150199808217363
59. Weissflog, W.; Baumeister, U.; Tamba, M.-G.; Pelzl, G.; Kresse, H.; Friedemann, R.; Hempel, G.; Kurz, R.; Roos, M.; Merzweiler, K.; Jákli, A.; Zhang, C.; Diorio, N.; Stannarius, R.; Eremin, A.; Kornek, U. *Soft Matter* **2012,** in press. doi:10.1039/c2sm07064b

License and Terms

Beilstein Journal of Organic Chemistry

The interplay of configuration and conformation in helical perylenequinones: Insights from chirality induction in liquid crystals and calculations

Elisa Frezza[1], Silvia Pieraccini[2], Stefania Mazzini[3], Alberta Ferrarini[*1] and Gian Piero Spada[*2]

Full Research Paper

Open Access

Address:
[1]Department of Chemical Sciences, University of Padova, via Marzolo 1, 35131 Padova, Italy, [2]Dipartimento di Chimica Organica "A. Mangini", Alma Mater Studiorum – Università di Bologna, via San Giacomo 11, 40126 Bologna, Italy and [3]Dipartimento di Scienze Molecolari Agroalimentari, Università degli Studi di Milano, via Celoria 2, 20133 Milano, Italy

Email:
Alberta Ferrarini[*] - alberta.ferrarini@unipd.it; Gian Piero Spada[*] - gianpiero.spada@unibo.it

* Corresponding author

Keywords:
chirality; conformational analysis; DFT calculations; helical twisting power; nematic liquid crystals

Beilstein J. Org. Chem. **2012,** *8,* 155–163.
doi:10.3762/bjoc.8.16

Received: 03 October 2011
Accepted: 30 December 2011
Published: 24 January 2012

This article is part of the Thematic Series "Progress in liquid crystal chemistry II".

Guest Editor: S. Laschat

Abstract

The chirality transfer in liquid crystals induced by two helical perylenequinones (namely, the natural compounds cercosporin and phleichrome) was investigated by integrating measurements of helical twisting power with a conformational analysis by DFT calculations and with the prediction of their twisting ability by the surface-chirality method. The two *quasi*-enantiomeric derivatives induce oppositely handed cholesteric phases when introduced as dopants in nematic solvents. We evaluated the role of the different conformations of the chiral hydroxyalkyl side chains in determining the helical twisting power: They were found to affect the strength of the chirality transfer, although the handedness of the induced cholesteric phase is essentially determined by the axial chirality (helicity) of the core of the perylenequinones.

Introduction

The phenomenon of chiral induction in nematic mesophases has been known for a long time [1]. By addition of a chiral nonracemic compound, a nematic liquid crystal is transformed into a chiral nematic (or cholesteric) phase. Here the director, i.e., the local alignment direction, rotates in space in helical way, along a perpendicular axis [2,3]. The handedness of this helix reflects the configuration of the dopant: Enantiomers induce oppositely handed cholesterics. Only in the last few decades has the generation of cholesteric liquid crystals and the amplification of the molecular chirality observed upon doping

nematic phases with chiral derivatives attracted great interest in the field of material science [3,4]. In this context, one of the major research lines focuses on the investigation of the chirality transfer between "shape persistent" dopants and nematic solvents [2,5-11]. Thus, the chirality amplification from the molecular to mesophase level can be exploited for the determination of the absolute configuration [2,3,5,6,12-24]. In fact, this technique has been fruitfully applied to different classes of systems, possessing either stereogenic centers or axial chirality.

In this work, chirality induction in liquid crystals has been used for a structural study of helical perylenequinones. This is an important family of natural products, characterized by the presence of a helical chiral conjugated pentacyclic core [25]. These systems have attracted considerable attention due to their photosensitizing properties and their phytotoxic activity. Another reason for the interest in perylenequinones is their peculiar structural properties, which require special strategies for the complete structural determination. In particular we have focused on the two helical perylenequinones, cercosporin (**1**), [26] and phleichrome (**2**) [27], shown in Figure 1. They have the same stereochemical features: Two bulky methoxy groups or a strained seven-membered ring in positions 6 and 7, two side chains in positions 1 and 12 and a nonplanar helical shape. The helicity generates axial chirality, which, when associated with the presence of asymmetrically substituted carbon atoms in the side chains, gives rise to diastereoisomerism. Cercosporin and phleichrome are characterized by a special coupling between conformation and configuration: The conformational preferences of the side chains in the "1–12 bay region" are critical for the generation of the helical structure. X-ray crystallography established the *R*,*R* configuration at C14 and C17 of cercosporin (**1**) and the sign of the axial chirality as *M* [26,28]. Phleichrome (**2**) features opposite chirality, having *P* axial chirality and *S*,*S* configuration at C14 and C17 [27].

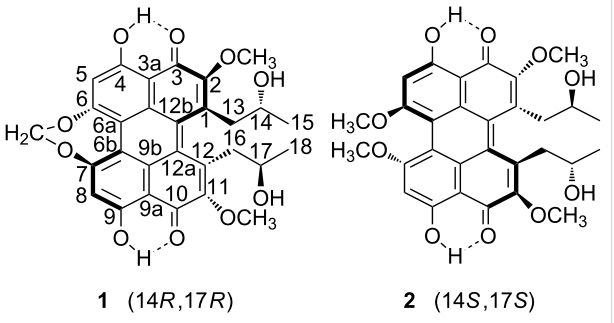

1 (14*R*,17*R*) **2** (14*S*,17*S*)

Figure 1: Chemical structure of the helical perylenequinones under investigation: Cercosporin (**1**) and phleichrome (**2**).

The ring substituents give **1** and **2** a limited, though non-negligible conformational freedom. To understand the relation between molecular structure and chiral induction in liquid crystals, we integrated measurements of helical twisting power (HTP) with a conformational analysis, performed by density functional theory (DFT) calculations, and with the prediction of the twisting ability of conformers, by the surface chirality (SC) method [29].

Results and Discussion

HTP measurement

The propensity of a dopant to induce a helical organization in the liquid-crystalline matrix is measured by its helical twisting power, which is defined as

$$\mathrm{HTP} = \lim_{c\to 0} \left(p\ c\ r \right)^{-1}$$

where p is the helical pitch (in μm) of the cholesteric phase, and c and r are the concentration (molar fraction) and the enantiomeric excess of the dopant, respectively. The sign of HTP is taken as positive or negative if the induced cholesteric is right- or left-handed, respectively. The HTP of **1** and **2** was measured in the liquid-crystal mixture E7 [30] at a temperature of 298 K. The values −12 μm^{-1} and +54 μm^{-1} were obtained for **1** and **2**, respectively. The opposite sign observed for the two compounds clearly reflects their opposite configuration. The handedness of the induced cholesterics is that which is expected for helicoidal disc-like dopants, as binaphthyl derivatives [20] and helicene-like molecules [22,24], i.e., left-handed for the *M* and right-handed for the *P* molecular helicity. In view of the similar molecular shape of **1** and **2**, the difference between the absolute values of their HTP is somewhat surprising. As a possible explanation for this difference we can devise a different conformation of the aromatic core in the two compounds or a different arrangement of the substituents, in particular of the chiral hydroxyalkyl side chains (henceforth "the side chains"). To explore this issue we performed a computational study at different levels: Single-molecule DFT calculations were carried out to evaluate energy and geometry of all the conformers of **1** and **2**, and the SC method was used to estimate their twisting ability.

Conformational analysis by DFT

For each of the side chains in position 1 and 12 of cercosporin and phleichrome, three conformational states are possible, which are shown in Figure 2, where the same notation as in [31] is used. This makes a total of six conformers for each molecule, which are labeled according to the state of each side chain; thus, for instance, $g^+\ t$ is a conformer with one chain in the *gauche*$^+$ and the other in the *trans* state. The conformers with side chains in different states are two-fold degenerate: $g^+\ t$ (= $t\ g^+$), $g^+\ g^-$ (= $g^-\ g^+$) and $g^-\ t$ (= $t\ g^-$).

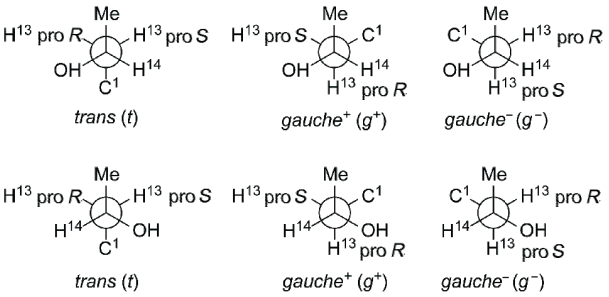

Figure 2: Newman projections of the conformational states of the side chain linked at C1 of cercosporin (**1**), with 14*R* configuration (top), and of phleichrome (**2**), with 14*S* configuration (bottom). Analogous states exist for the other chain, linked at C12.

For the conformational study, we used DFT calculations in vacuum as implemented in the Gaussian suite of programs [32,33]. We selected the hybrid functional B3LYP [34] with the 6-31g(d,p) basis set, which is a standard choice and is relatively inexpensive from the computational point of view. Then, considering that dispersive interactions between the side chains and the aromatic ring could be crucial for the systems under investigation**,** further calculations were carried out with the functional M06-2X [35], which was developed recently to provide a better description of nonlocal electronic correlation with respect to standard functionals. In this case the more demanding 6-31g+(d,p) basis set was used. Geometry optimization of all the conformers of **1** and **2** was carried out. In the starting configurations, the methoxy substituents were taken always in the same orientation, which was found to be only slightly modified in the optimized geometry. The C–O–C bonds of the methoxy groups in the "6,7-bay region" of **2** lie in the plane of the adjacent aromatic ring, in agreement with the torsional potential of anisole [36]. For steric reasons, a planar arrangement is not possible for the methoxy substituents at the 2 and 11 positions. In general, two orientations are allowed for each methoxy group, with torsional angles in the ranges +(110°–145°) (*p* states) and −(110°–145°) (*m* states). Thus, we can distinguish four different states of the methoxy groups, labelled as (*m*,*m*), (*m*,*p*), (*p*,*m*) and (*p*,*p*). To limit the computational cost, we only considered the (*p*,*p*) states. This is the state found in one of the available X-ray structures of cercosporin [26], whereas the other structure has the methoxy groups in the (*m*,*p*) state [28].

Our calculations confirm that the "propeller" form, found in X-ray structures of **1** [26,28], is significantly more stable than the other, called "double butterfly" by Falk and co-workers [37]. The two geometries, as obtained for the g^+ g^+ conformer of **1,** are shown in Figure 3. Table 1 reports the twist angles χ_1 [C(1)–C(12b)–C(12a)–C(12)] and χ_2 [C(6)–C(6a)–C(6b)–C(7)], which characterize the helical shape of the core of **1** and **2**. Not surprisingly, in view of the opposite configuration, the twist angles of the propeller form of **1** and **2** have opposite signs. We have found that χ_1 and χ_2 have a weak dependence on the side chain conformation. Our results are in good agreement with X-ray data for cercosporin [26,28], whereas for phleichrome no structural data are available. However, the prediction that $\chi_1 \sim \chi_2 \sim 30°$ appears reasonable for **2**, considering that the narrower

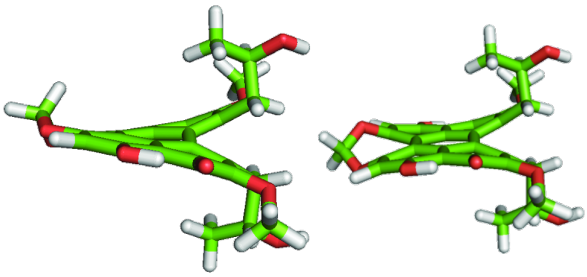

Figure 3: "Propeller" (left) and "double butterfly" geometry (right) of the g^+ g^+ conformer of **1**, as obtained by geometry optimization by DFT at the M06-2X/6-31+g(d,p) level [33].

Table 1: Twist angles for **1** and **2**, as obtained by DFT geometry optimization and by crystallography. The "propeller" form is considered, unless otherwise specified (the symbol *db* denotes the "double butterfly" geometry).

compound	method	χ_1 (°)	χ_2 (°)
1[a]	DFT-B3LYP/6-31g(d,p)	−30.0 to −30.9	−11.8 to −12.6
	DFT/M06-2X/6-31+g(d,p)	−29.0 to −29.7	−13.1 to −12.0
1 (*db*)[b]	DFT/M06-2X/6-31+g(d,p)	−26.4	18.1
1[a]	X-ray [28]	−29.8	−9.2
	X-ray [26]	−27.4	−9.9
2[b]	DFT-B3LYP/6-31g(d,p)	32.4 to 34.0	30.8 to 31.6
	DFT/M06-2X/6-31+g(d,p)	32.0 to 33.1	29.6 to 30.3

[a]range of angles for six side-chain conformers; [b]g^+g^+ conformer.

χ_1 angle in cercosporin is a consequence of the constraints imposed by the bridge in the "6,7-bay region".

In view of their higher stability, only conformers in the propeller form were considered in our systematic analysis of the effects of side-chain conformations. Very similar structures were obtained by geometry optimization at the B3LYP/6-31g(d,p) and at the M06-2X/6-31+g(d,p) level; the latter are shown in Figure 4. On the contrary, the conformer energies were found to depend strongly on the level of calculation, as shown in Table 2. Significant differences between conformers were predicted at the B3LYP/6-31g(d,p) level: The *t t* was strongly preferred and either g^- or g^+ states were found to have a highly destabilizing effect for **1** and **2**, respectively. Much smaller differences in conformer stability were obtained at the M06-2X level. To check whether the discrepancies between the two kinds of calculations were mainly due to the functional or due to the basis set, we also performed a few calculations for **2** at the B3LYP/6-31+g(d,p) level. With the new basis we found a significant decrease of the energy differences between conformers, which points to an important role of diffuse functions.

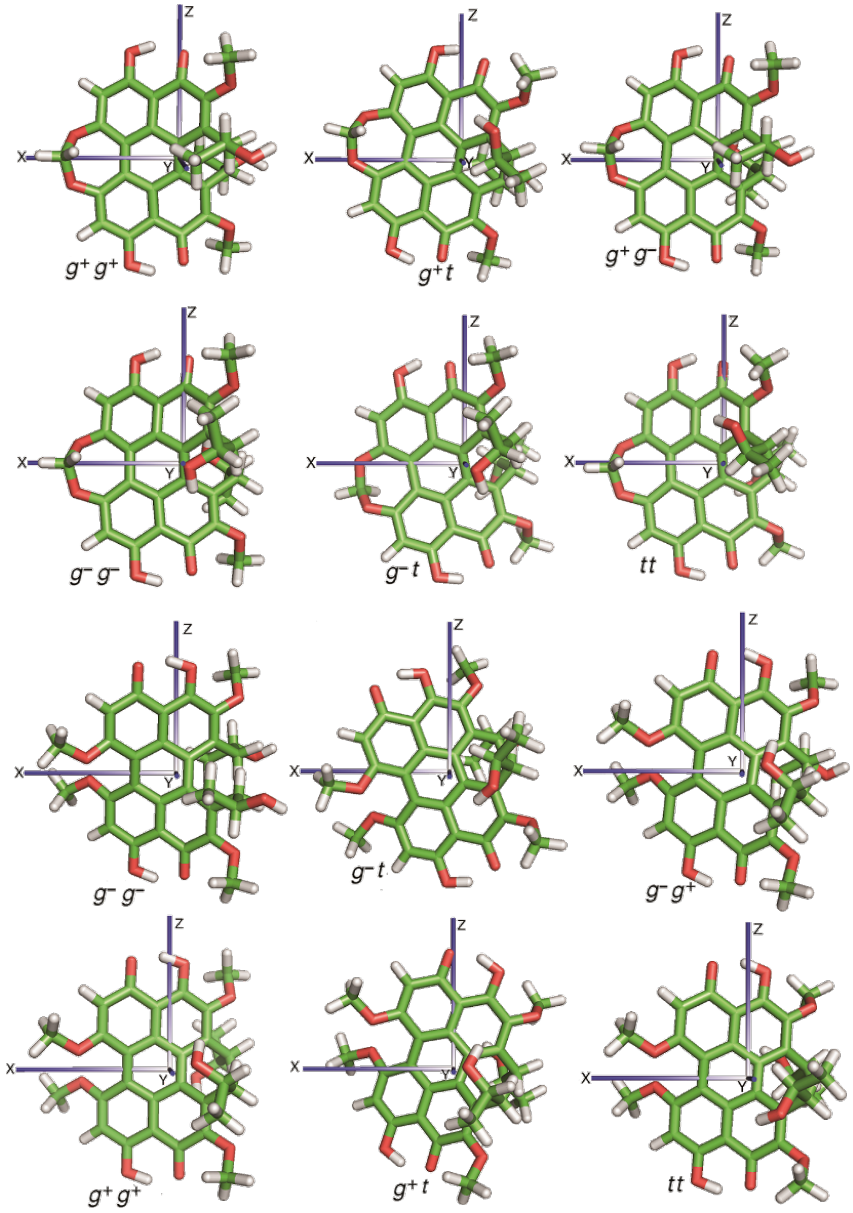

Figure 4: Optimized geometry of all conformers of **1** (upper half) and **2** (lower half), obtained at the DFT/M06-2X/6-31+g(d,p) level [33]. Superimposed on each structure, the principal axes (*x*,*y*,*z*) of the Saupe matrix calculated by the SC method [29] are shown. The reference frame is defined in such a way that the *z* and *y* axes have the highest tendency to lie parallel and perpendicular to the director, respectively.

Table 2: Energy of the conformers of **1** and **2**, obtained by geometry optimization by DFT at the (a) B3LYP/6-31g(d,p) and (b) M06-2X/6-31+g(d,p) level of the theory. Within each set, the most stable conformer is taken as the reference (E = 0).

conformer	E **1** (a) [kJ/mol]	E **1** (b) [kJ/mol]	conformer	E **2** (a) [kJ/mol]	E **2** (b) [kJ/mol]
$g^+ g^+$	7.7	0.3	$g^- g^-$	9.8	0
$g^+ t$	4.7	0.8	$g^- t$	5.3	1.4
$t\ t$	0	0	$t\ t$	0	0.1
$g^+ g^-$	13.3	3.2	$g^- g^+$	16.4	3.6
$g^- t$	9.6	2.5	$g^+ t$	10.8	1.8
$g^- g^-$	18.2	3.4	$g^+ g^+$	22.5	6.8

Table 3: Probability of the three conformational states around bonds C(13)–C(14) and C(16)–C(17) for compounds **1** and **2**, as obtained by our DFT calculations and by NOE experiments [31].

compound	method	probability		
		trans	*gauche*$^+$	*gauche*$^-$
1	B3LYP/6-31g(d,p)	0.84	0.14	0.02
1	M06-2X/6-31+g(d,p)	0.37	0.40	0.23
1	NOE [19]	0.35	0.53	0.15
2	B3LYP/6-31g(d,p)	0.87	0.01	0.12
2	M06-2X/6-31+g(d,p)	0.42	0.23	0.35
2	NOE [31]	0.34	0.13	0.58

Although the conformer population is not directly accessible, we can try to analyze our results in the light of experimental data. Of the two X-ray structures of cercosporin reported in the literature, one has the side chains in the $g^+ g^+$ [28] and the other in the $g^- g^-$ conformation [26]. These do not appear to be compatible with the strong preference for the *trans* state predicted by B3LYP calculations, but the conformational preferences in crystals might be biased by the environment. More suitable information on the molecular conformation in solution can be obtained from NMR-NOE experiments [31]; however, these do not provide the population of each single conformer but only the overall probability of t, g^+ and g^- states around bonds C(13)–C(14) and C(16)-C(17). For ease of comparison, we have collected these probabilities for compounds **1** and **2** in Table 3, together with estimates based on our DFT calculations. Experimentally, a preference for *gauche*$^+$ (for **1**) and *gauche*$^-$ (for **2**) was inferred. This is in strong contrast with our B3LYP predictions. The M06-2X results are closer to the experimental data, although non-negligible differences appear: For **1** the contribution of *gauche*$^+$ states is underestimated, mainly at the expense of the *gauche*$^-$ states, and the discrepancies are even larger for **2**, which is predicted to have a prevalence of *trans* states, whereas experimentally a net prevalence of *gauche*$^-$ states was found. A possible reason for the lack of agreement between theory and experiment is the fact that calculations were performed in vacuum, whereas experiments were carried out in acetone. According to our calculations, the conformers of phleichrome (**2**) would have higher dipole moment than those of cercosporin (**1**), therefore **2** should be more sensitive to solvent polarity (acetone has a dielectric constant of about 20 at room temperature).

HTP predictions by the SC method

Within the SC approach, the HTP of a chiral dopant in a nematic solvent is proportional to the so-called chirality parameter Q, which is defined in terms of the helicity of the molecular surface and the orientational order of the dopant [29]. The proportionality factor between HTP and Q depends on the macroscopic properties of the host. Therefore, it is the same for different dopants in the same host; typical values of this factor are about 2–3 [2].

We calculated the chirality parameter Q of the conformers of **1** and **2**, using the molecular geometries obtained by DFT, with either the B3LYP or the M06-2X functional. The results are shown in Figure 5, together with the probability distribution of conformers. We can see in the figure that the side-chain conformation can significantly affect the chirality parameter. For the sake of comparison, we calculated also the chirality parameter of the bare cores, obtaining $Q = -7{\cdot}10^{-3}$ nm^3 for **1** and $Q = +9{\cdot}10^{-3}$ nm^3 for **2**. These opposite values are in line with the fact that the two cores are almost the mirror image of each other. In fact, we can see in Figure 5 that the same relation remains for the whole molecules: The Q value predicted for a given conformer of **1** is close in magnitude to the Q value for the conformer of **2** that is nearly its mirror image, but opposite in sign. The magnitude of Q for the cores lies within the values obtained for the various conformers of the whole molecule: Depending on their orientation, side chains were found to either enhance or weaken the twisting ability of the core. The sign of the chirality parameter Q can be easily explained on the basis of the chirality and the orientational behavior of the two perylenequinones. All conformers are predicted to preferentially orient with the normal to the aromatic rings lying perpendicular to the nematic director, and with some preference for aligning to the director their z axis, whose direction in the molecule slightly depends on the chain conformation (Figure 4). Thus they convey to the phase the molecular helicity along the molecular y axis (perpendicular to the aromatic rings), which is left-handed for cercosporin (**1**) and right-handed for phleichrome (**2**).

It is worth remarking that the results shown in Figure 5 were obtained for the six structures, differing in the conformation of the side chains at positions 1 and 12, and all having the

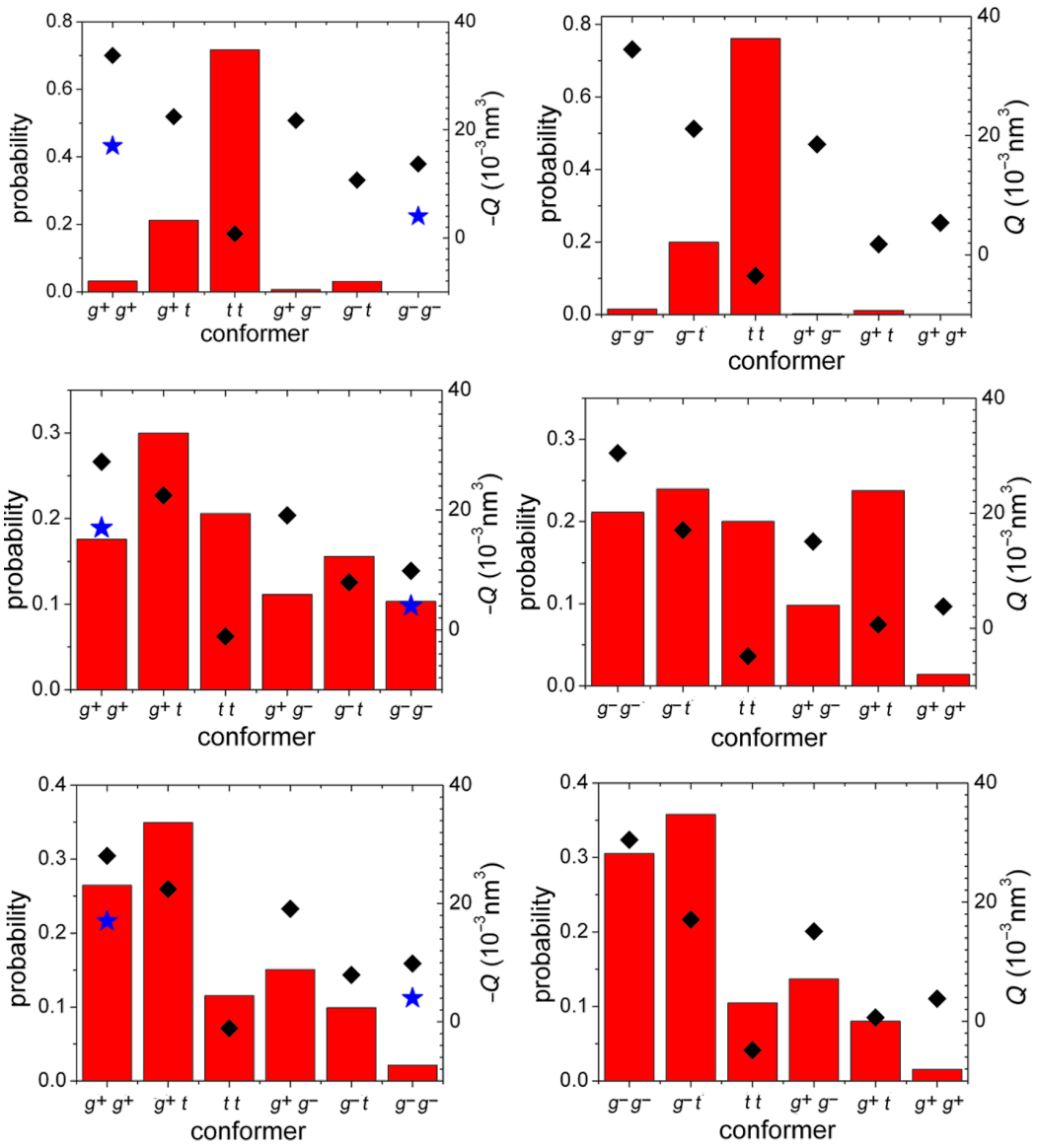

Figure 5: Chirality parameter *Q* (diamonds) and probability distribution (bars), calculated for all conformers of **1**, on the left, and **2**, on the right. Conformer geometry and energy were obtained by DFT calculations at the B3LYP/6-31g(d,p) (top) and the M06-2X/6-31+g(d,p) level (middle). The plots on the bottom report the *Q* values obtained with the geometry calculated at the M06-2X/6-31+g(d,p) level, along with conformer probability distributions inferred from NOE measurements [31]. Stars represent the *Q* values calculated for the X-ray structures of **1** [26,28]. For ease of comparison, the values are reported as the negative of *Q* for **1**.

methoxy substituents in the (*p*,*p*) state. Explorative calculations, at the M06-2X/6-31+g(d,p) level, were performed for selected conformers of **2**, with the methoxy substituents in (*m*,*m*), (*m*,*p*) and (*p*,*m*) states. It was found that the state of the methoxy groups can affect the relative energy (up to a couple of kJ/mol) and, to a lesser extent, the *Q* parameter differences between conformers; however, it does not dramatically modify the trend reported in Figure 5 (middle).

We have also shown in Figure 5 (left) the *Q* values calculated for the available X-ray structures of cercosporin [26,28]. The differences from the results reported for structures obtained by DFT, with the same conformation of the side chains, derive from relatively small changes in the molecular geometry.

Table 4 reports the HTP values measured for **1** and **2**, along with the *Q* values, calculated for the two compounds by averaging over all conformers (see Experimental). Negative and positive helical twisting power are predicted for **1** and for **2**, respectively, in agreement with experiments. However, the *Q* parameters do not scale with the measured HTPs: Whereas the absolute value of the HTP of phleichrome is about four times as

big as that of cercosporin, the Q value calculated for **2** is smaller than that of **1**. We supposed that the main reason for these differences could be the unsatisfactory conformer distributions, which were used to calculate the average chirality parameters. Thus, on moving from the distributions derived from B3LYP to those from M06-2X calculations, the ratio between the absolute values of Q for **1** and **2** decreases, and a further decrease can be seen when the NOE probabilities are used. However, this ratio remains far from the experimental value, due to an overestimate of the magnitude of the chirality parameter Q for cercosporin (**1**).

Table 4: Chirality parameter Q, calculated for compounds **1** and **2** by averaging over conformers. Conformer geometry and probabilities obtained by DFT calculations were used, unless otherwise specified. In the last column the HTPs measured in the nematic phase E7 are reported.

compound	method	$Q/10^{-3}$ nm^3	HTP/μm^{-1}
1	B3LYP/6-31g(d,p)	−7	
1	M06-2X/6-31+g(d,p)	−15	−12
1	NOE[a] [31]	−19	
2	B3LYP/6-31g(d,p)	2	
2	M06-2X/6-31+g(d,p)	11	+54
2	NOE[a] [19]	17	

[a]Conformer geometries obtained by DFT/M06-2X/6-31+g(d,p) calculations and distribution derived from NOE experiments.

A possible origin of the lower twisting ability of **1** in comparison to **2**, found in experiments, could be atropisomerization. As a consequence of this process, the sample would contain both cercosporin and its atropisomer. Whereas the former induces a left-handed twist of the nematic director, the latter, having P axial chirality, is expected to induce a twist in the opposite sense, with the net effect of lowering the HTP of this dopant. Although atropisomerization is known as a very slow process, our hypothesis is supported by the finding that its rate is significantly higher for cercosporin than for phleichrome [31].

Conclusion

We have performed HTP measurements, showing that the natural products cercosporin (**1**) and phleichrome (**2**) induce a left-handed and right-handed twist of the nematic director, respectively. This is exactly what is expected for molecules with fused aromatic rings arranged in a helical fashion, having M and P helicity, respectively. Thus chirality induction in liquid crystals appears to be a suitable technique to determine the axial configuration of perylenequinones.

The integration of experiments with the results of calculations at different levels has allowed us to gain an insight into the conformational preferences of the systems under investigation and into the role of configuration and conformation in determining their twisting ability. We have evaluated the contribution of molecular structures, differing in the conformation of the chiral hydroxyalkyl chains, to the twisting ability of compounds **1** and **2**. Comparing the behavior of these molecules to that of their bare aromatic cores, we have shown that the substituents, although they do not change the sign of the HTP, affect its magnitude.

Our study has evidenced the difficulty of obtaining reliable estimates of the conformational distribution of the perilenequinones by DFT calculations in vacuum and the extreme sensitivity of the results to the choice of the functional and the basis set. In particular, the B3LYP/6-31g(d,p) level was found to be fully inadequate to account for the relative stability of the conformers. Better results were obtained by using M06-2X, a recently developed functional that is more suitable for the treatment of dispersion interactions, and by augmenting the basis set with diffuse functions.

Experimental

Helical twisting power measurement

Cholesteric pitch and handedness were obtained at $T = 298$ K by using the lens version of the Grandjean–Cano method [38,39]. The commercially available (Merck) nematic solvent E7 (nematic–isotropic transition temperature $T_{NI} \sim 330$ K) is composed of a eutectic mixture of cyanobiphenyl and terphenyl compounds [30].

DFT calculations

Atomic coordinates and energy of the conformers of **1** and **2** were obtained by geometry optimization in vacuum, by using DFT at the B3LYP/6-31g(d,p) [32] and M06-2X/6-31+g(d,p) levels [33]. In each case, the starting geometry was defined by suitably adjusting the conformation of the methoxy groups and of the hydroxyalkyl side chains.

SC calculations

The chirality parameter Q of a given conformer is defined as

$$Q = -\sqrt{2/3}(Q_{xx}S_{xx} + Q_{yy}S_{yy} + Q_{zz}S_{zz})$$

where S_{ii} is the ith cartesian component of the Saupe ordering matrix, which specifies the degree of alignment of the ith molecular axis to the local director, and Q_{ii} quantifies the helicity of the molecular surface, as viewed along the same axis. The Saupe matrix $\boldsymbol{S}$ and the surface chirality tensor $\boldsymbol{Q}$ of single conformers were calculated as explained in [40], giving the parameter ξ, which quantifies the orienting strength of the medium, the value 2.5 nm^{-2}.

The molecular surface, needed to calculate the ***S*** and ***Q*** tensors, was generated on the basis of atomic coordinates by using the program MSMS [41]. We assumed the following set of van der Waals radii: r_H = 0.1 nm, r_O = 0.15 nm and r_C = 0.185 nm [42], along with a rolling sphere radius equal to 0.3 nm [40] and a density of vertices equal to 500 nm^{-2}.

The chirality parameter of a given compound Q, was calculated as

$$Q = \sum_j g_j w_j Q^{(j)}$$

where the sum is over all the conformers and g_j, w_j are the degeneracy and the probability of each of them, respectively. The probability is defined as

$$w_j = \frac{e^{-E_j/k_BT} Z_j}{\sum_m g_m e^{-E_m/k_BT} Z_m}$$

where k_B is the Boltzmann constant, T is the temperature, E_j is the potential energy of the jth conformer, obtained by DFT calculations in vacuum, and Z_j is its orientational partition function. This accounts for the stabilization of the conformer in the nematic environment and is defined as

$$Z_j = \int e^{-U_j(\Omega)/k_BT} d\Omega$$

where $U_j(\Omega)$ is the orientational potential experienced by a dopant, in the orientation defined by the Euler angles Ω, inside the liquid-crystal phase [29,40].

Acknowledgements

The authors are grateful to Professor G. Nasini (A. Quilico CNR Center, Politecnico di Milano) for providing samples of **1** and **2**. AF and EF acknowledge financial support from the University of Padova (ex 60% grants). GPS and SP acknowledge financial support from MIUR through the National Interest Research Programme (PRIN 2009, grant 2009N5JH4F_002 "Stimuli responsive liquid crystalline phases and supramolecular systems"). Computational resources and assistance were provided by the "Laboratorio Interdipartimentale di Chimica Computazionale" (LICC) at the Dipartimento di Scienze Chimiche of the University of Padova.

References

1. Friedel, M. G. *Ann. Phys.* **1922,** *18,* 273–474.
2. Pieraccini, S.; Ferrarini, A.; Spada, G. P. *Chirality* **2008,** *20,* 749–759. doi:10.1002/chir.20482
3. Pieraccini, S.; Masiero, S.; Ferrarini, A.; Spada, G. P. *Chem. Soc. Rev.* **2011,** *40,* 258–271. doi:10.1039/b924962c
4. Eelkema, R.; Feringa, B. L. *Org. Biomol. Chem.* **2006,** *4,* 3729–3745. doi:10.1039/b608749c
5. Spada, G. P.; Proni, G. *Enantiomer* **1998,** *3,* 301–314.
6. Gottarelli, G.; Spada, G. P. *Top. Stereochem.* **2003,** *24,* 425–455. doi:10.1002/0471471895.ch7
7. Furuno, Y.; Sato, H.; Yoshida, J.; Hoshino, N.; Fukuda, Y.; Yamagishi, A. *J. Phys. Chem. B* **2007,** *111,* 521–526. doi:10.1021/jp065586b
8. Yoshizawa, A.; Kobayashi, K.; Sato, M. *Chem. Commun.* **2007,** 257–259. doi:10.1039/b611538a
9. Thompson, M. P.; Lemieux, R. P. *J. Mater. Chem.* **2007,** *17,* 5068–5076. doi:10.1039/b712253e
10. Goh, M.; Akagi, K. *Liq. Cryst.* **2008,** *35,* 953–965. doi:10.1080/02678290802305098
11. Raynes, P.; Cowling, S. J.; Goodby, J. W. *Anal. Methods* **2009,** *1,* 88–92. doi:10.1039/b9ay00126c
12. Gottarelli, G.; Samorĭ, B.; Marzocchi, S.; Stremmenos, C. *Tetrahedron Lett.* **1975,** *16,* 1981–1984. doi:10.1016/S0040-4039(00)72340-9
13. Eelkema, R.; Feringa, B. L. *Org. Lett.* **2006,** *8,* 1331–1334. doi:10.1021/ol060076l
14. Eelkema, R.; Feringa, B. L. *J. Am. Chem. Soc.* **2005,** *127,* 13480–13481. doi:10.1021/ja054352n
15. Rinaldi, P. L.; Wilk, M. *J. Org. Chem.* **1983,** *48,* 2141–2146. doi:10.1021/jo00161a005
16. van Delden, R. A.; Feringa, B. L. *Chem. Commun.* **2002,** 174–175. doi:10.1039/b110721f
17. van Delden, R. A.; Feringa, B. L. *Angew. Chem., Int. Ed.* **2001,** *40,* 3198–3200. doi:10.1002/1521-3773(20010903)40:17<3198::AID-ANIE3198>3.0.CO;2-I
18. Rosini, C.; Spada, G. P.; Proni, G.; Masiero, S.; Scamuzzi, S. *J. Am. Chem. Soc.* **1997,** *119,* 506–512. doi:10.1021/ja962445m
19. Superchi, S.; Donnoli, M. I.; Proni, G.; Spada, G. P.; Rosini, C. *J. Org. Chem.* **1999,** *64,* 4762–4767. doi:10.1021/jo990038y
20. Gottarelli, G.; Hibert, M.; Samorì, B.; Solladié, G.; Spada, G. P.; Zimmermann, R. *J. Am. Chem. Soc.* **1983,** *105,* 7318–7321. doi:10.1021/ja00363a019
21. Gottarelli, G.; Proni, G.; Spada, G. P.; Fabbri, D.; Gladiali, S.; Rosini, C. *J. Org. Chem.* **1996,** *61,* 2013–2019. doi:10.1021/jo951823n
22. Ferrarini, A.; Gottarelli, G.; Nordio, P. L.; Spada, G. P. *J. Chem. Soc., Perkin Trans. 2* **1999,** 411–418. doi:10.1039/a809593k
23. Pieraccini, S.; Donnoli, M. I.; Ferrarini, A.; Gottarelli, G.; Licini, G.; Rosini, C.; Superchi, S.; Spada, G. P. *J. Org. Chem.* **2003,** *68,* 519–526. doi:10.1021/jo020427j
24. Ferrarini, A.; Pieraccini, S.; Masiero, S.; Spada, G. P. *Beilstein J. Org. Chem.* **2009,** *5,* No. 50. doi:10.3762/bjoc.5.50
25. Weiss, U.; Merlini, L.; Nasini, G. *Prog. Chem. Org. Nat. Prod.* **1987,** *52,* 1–71.
26. Nasini, G.; Merlini, L.; Andreetti, G. D.; Bocelli, G.; Sgarabotto, P. *Tetrahedron* **1982,** *38,* 2787–2796. doi:10.1016/0040-4020(82)85005-9
27. Arnone, A.; Camarda, L.; Nasini, G.; Merlini, L. *J. Chem. Soc., Perkin Trans. 1* **1985,** 1387–1392. doi:10.1039/P19850001387
28. Mentzafos, D.; Terzis, A.; Philippakis, S. E. *Cryst. Struct. Commun.* **1982,** *11,* 71–74.
29. Ferrarini, A.; Moro, G. J.; Nordio, P. L. *Phys. Rev. E* **1996,** *53,* 681–688. doi:10.1103/PhysRevE.53.681
30. Raynes, E. P.; Tough, R. J. A.; Davies, K. A. *Mol. Cryst. Liq. Cryst.* **1979,** *56,* 63–68. doi:10.1080/01406567908071968

31. Scaglioni, L.; Mazzini, S.; Mondelli, R.; Merlini, L.; Ragg, E.; Nasini, G. *J. Chem. Soc., Perkin Trans. 2* **2001,** 2276–2286. doi:10.1039/b107071c
32. *Gaussian 03,* Revision C.02; Gaussian, Inc.: Wallingford CT, 2004.
33. *Gaussian 09,* Revision A.1; Gaussian Inc.: Wallingford CT, 2009.
34. Becke, A. D. *J. Chem. Phys.* **1993,** *98,* 5648–5652. doi:10.1063/1.464913
35. Zhao, Y.; Truhlar, D. G. *Theor. Chem. Acc.* **2008,** *120,* 215–241. doi:10.1007/s00214-007-0310-x
36. Bossa, M.; Morpurgo, S.; Stranges, S. *J. Mol. Struct. Theochem.* **2002,** *618,* 155–164. doi:10.1016/S0166-1280(02)00469-4
37. Etzlstorfer, C.; Falk, H.; Müller, N. *Monatsh. Chem.* **1993,** *124,* 431–439. doi:10.1007/BF00814139
38. Heppke, G.; Oestreicher, F. *Z. Naturforsch., A* **1977,** *32,* 899–901.
39. Gottarelli, G.; Samorí, B.; Stremmenos, C.; Torre, G. *Tetrahedron* **1981,** *37,* 395–399. doi:10.1016/S0040-4020(01)92027-7
40. Ferrarini, A. *Liq. Cryst.* **1999,** *26,* 201–210. doi:10.1080/026782999205335
41. Sanner, M. F.; Olson, A. J.; Spehner, J. C. *Biopolymers* **1996,** *38,* 305–320. doi:10.1002/(SICI)1097-0282(199603)38:3<305::AID-BIP4>3.0.CO;2-Y
42. Bondi, A. *J. Phys. Chem.* **1964,** *68,* 441–451. doi:10.1021/j100785a001

License and Terms

Beilstein Journal of Organic Chemistry

Synthesis of oleophilic electron-rich phenylhydrazines

Aleksandra Jankowiak[1] and Piotr Kaszyński*[1,2]

Full Research Paper

Open Access

Address:
[1]Organic Materials Research Group, Department of Chemistry, Vanderbilt University, Nashville, TN 37235 and [2]Faculty of Chemistry, University of Lódź, Tamka 12, 91403 Lódź, Poland

Email:
Piotr Kaszyński* - piotr.kaszynski@vanderbilt.edu

* Corresponding author

Keywords:
arylhydrazines; methodology; synthesis

Beilstein J. Org. Chem. **2012,** *8,* 275–282.
doi:10.3762/bjoc.8.29

Received: 14 November 2011
Accepted: 06 February 2012
Published: 20 February 2012

This article is part of the Thematic Series "Progress in liquid crystal chemistry II".

Guest Editor: S. Laschat

Abstract

Phenylhydrazines **1** substituted with two or three long-chain alkyl, alkoxy or alkylsulfanyl groups were successfully prepared by acid-induced removal of the Boc group in hydrazides **2**. The reaction is carried out with 5 equivalents of TfOH in CF_3CH_2OH/CH_2Cl_2 at −40 °C for 1.5 min. Under these conditions, the deprotected hydrazine **1** is fully protonated, which increases its stability in the reaction medium. The hydrazines were isolated in 60–86% yields and purities >90%. The hydrazides **2** were obtained in 43–71% yields from aryl bromides **5**, which were lithiated with *t*-BuLi and subsequently reacted with di-*tert*-butyl azodicarboxylate (DTBAD).

Introduction

Mono-arylhydrazines **I** are important intermediates in the synthesis of a number of heterocycles, including indoles [1] and some azoles (for example [2,3]), many of which exhibit biological activity and are used in drug development [4-6]. Arylhydrazines are also key intermediates in the preparation of stable radicals such as verdazyl [7-9] and benzo[1,2,4]triazinyls [10-12].

The parent phenylhydrazine and many of its electron-deficient derivatives, such as *p*-nitrophenylhydrazine, are stable under ambient conditions and are conveniently obtained by using classical methods, such as the reduction of diazonium salts [13-15]. In contrast, electron-rich arylhydrazines are far less numerous and their preparation is complicated by oxidative instability.

To access functionalized and sensitive arylhydrazines several methods involving the deprotection of hydrazides **II** have been developed (Figure 1). Hydrazides **II** are efficiently obtained by the addition of organometallic reagents **III**, prepared from aryl halide **IV**, to azodicarboxylate diesters (**AD**) [16,17]. Alternatively, **II** can be obtained in the Pd(0)- or Cu^{2+}-catalyzed reaction of arylboronic acid **V** to **AD** [18-20]. The latter method is especially suited for arylhydrazides substituted with sensitive functional groups. Protected electron-rich arylhydrazines,

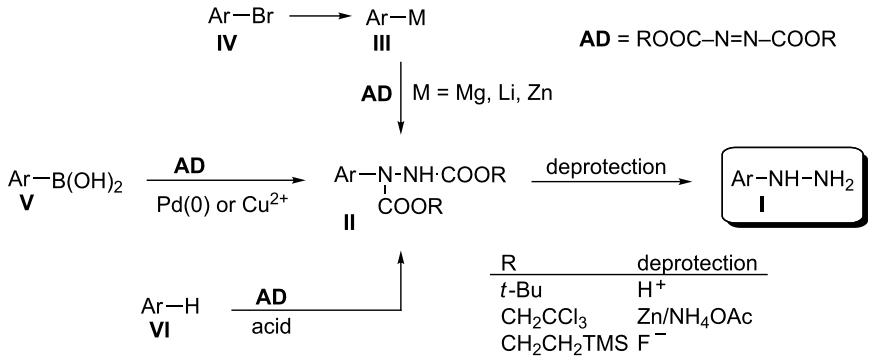

Figure 1: Selected methods for the preparation of arylhydrazines **I** through hydrazides **II**.

hydrazides **II**, containing the 2,2,2-trichloroethyl group (R = CH_2CCl_3) are conveniently prepared by direct electrophilic amination of arenes **VI** with bis(2,2,2-trichloroethyl) azodicarboxylate (BTCEAD) under Lewis [21,22] or Brønsted [23] acid conditions.

By judicious choice of the substituent R, the removal of the protecting group in **II** and formation of arylhydrazines **I** can be accomplished under acidic (R = *t*-Bu) [16], reductive (R = CH_2CCl_3) [24], or nearly neutral (R = CH_2CH_2TMS) conditions [22,25]. Among the three methods, the most straightforward is the removal of the Boc group under acidic conditions. Unfortunately, the literature method for deprotection (HCl in isopropanol, 70 °C) has limited scope, and electron-rich 3,4-dimethoxyphenylhydrazine could not be obtained under these conditions, although 4-pentyloxyphenylhydrazine hydrochloride was isolated in 60% yield [16]. The controlled reduction of 2,2,2-trichloroethyl esters (**II**, R = CH_2CCl_3) with Zn in aqueous MeOH containing NH_4OAc gave access to a number of small, electron-rich phenylhydrazines, including 3,4-dimethoxyphenylhydrazine isolated in 76% yield as hydrochloride [24].

In the context of our research program in liquid-crystalline verdazyl derivatives [26], we needed phenylhydrazines **1** (Figure 2) substituted with multiple long-chain alkyl, alkoxy and alkylsulfanyl groups. Here we demonstrate an efficient method for the preparation of several hydrophobic di- and trisubstituted phenylhydrazines in purities sufficient for further chemical transformations. Finally, we demonstrate the application of one of the phenylhydrazines for the preparation of a discotic liquid crystal.

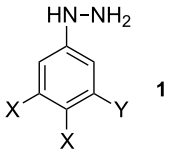

1

a: X = OC_8H_{17}, Y = H
b: X = $C_{10}H_{21}$, Y = H
c: X = Y = SC_6H_{13}
d: X = Y = SC_8H_{17}
e: X = Y = $SC_{10}H_{21}$
f: X = Y = $SC_{12}H_{25}$
g: X = Y = OC_8H_{17}
h: X = Y = $OC_{10}H_{21}$

Figure 2: The structures for hydrazines **1a**–**1h**.

Results and Discussion

Our initial attempts at the preparation of 3,4-dioctyloxyphenylhydrazine (**1a**) focused on deprotection of the trichloroethyl ester **3a** under buffered reductive conditions, according to the general literature procedure [24]. In aqueous MeOH hydrazide **3a** was practically insoluble, and the reaction mixture was triphasic. Under these conditions no formation of hydrazine **1a** was observed. Changing MeOH to EtOH and increasing its volume by two-fold gave homogenous solutions within which the desired hydrazine **1a** was formed along with significant quantities of **4** as the major products (Scheme 1). The deamination product **4** was isolated and identified by comparison with the authentic sample. The yield and proportions of the two products, **1a** and **4**, varied from run to run, according to the ^{1}H NMR spectra. Therefore, we focused on the acid-catalyzed deprotection of Boc-substituted hydrazines (Scheme 2), hydrazides **2**, expecting that the reaction could be performed under fully homogenous conditions.

Analysis of the reaction mechanism for the deprotection of **2** under acidic conditions shows that removal of the Boc group generates *t*-Bu^+, which reacts with the solvent, or alternatively it can alkylate the benzene ring of arylhydrazine (Scheme 2). For less reactive arylhydrazines the former process is faster, $k_1 << k_2$, and deprotection with HCl in iPrOH is effective [16]. For dialkoxyphenylhydrazines apparently $k_1 >> k_2$ and the desired hydrazine is not obtained [16].

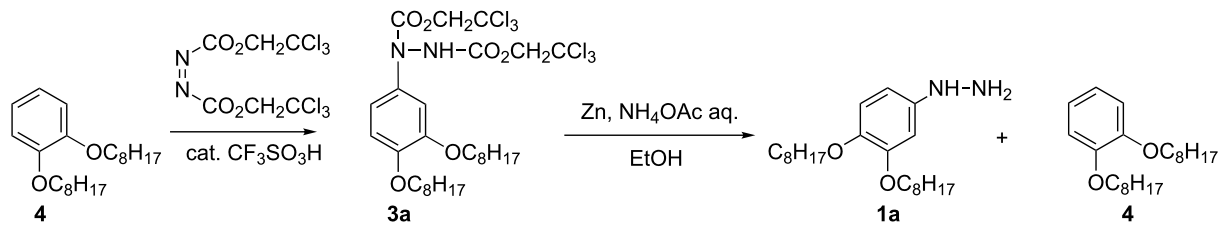

Scheme 1: Formation and deprotection of **3a** under reductive conditions.

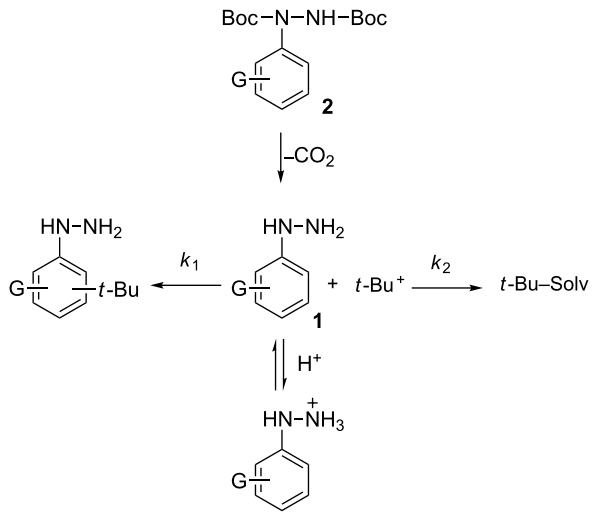

Scheme 2: General mechanism for the deprotection of arylhydrazides. G represents a substituent.

The nucleophilicity of the hydrazine can be suppressed by its fast and complete protonation with a strong acid (Scheme 2). In this situation, the transient *t*-Bu^+ is trapped with the solvent, forming volatile products, which simplifies isolation of the hydrazine as a crude product. We have focused on this approach to arylhydrazines employing trifluoromethanesulfonic acid (TfOH), which was used as an effective catalyst in the deprotection of *tert*-butyl aryl ethers [27].

Addition of catalytic amounts of the TfOH acid (10 mol %) to solutions of hydrazide **2a** (Figure 3) in a mixture of CF_3CH_2OH/CH_2Cl_2 at −40 °C gave little conversion to hydrazine **1a**. With 1.5 equiv of TfOH, hydrazide **2a** was only partially converted to hydrazine **1a**. With 5 equiv of TfOH the reaction was complete in less than 2 min and the crude hydrazine **1a** was isolated as the sole product. Reaction times under 2 min appear to be optimum; the purity of the hydrazine decreased with increasing reaction times.

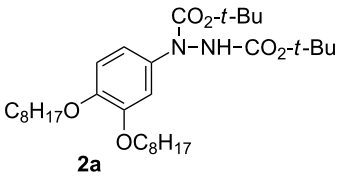

Figure 3: Structure of hydrazide **2a**.

By using this protocol, hydrazines **1** were isolated as viscous oils in purities >90% and yields of 60–86%, according to ^{1}H NMR analysis with 1,4-dimethoxybenzene as the internal standard (Scheme 3). Attempts at the preparation of crystalline hydrochlorides of **1** were unsuccessful and the viscous salts rapidly darkened and decomposed.

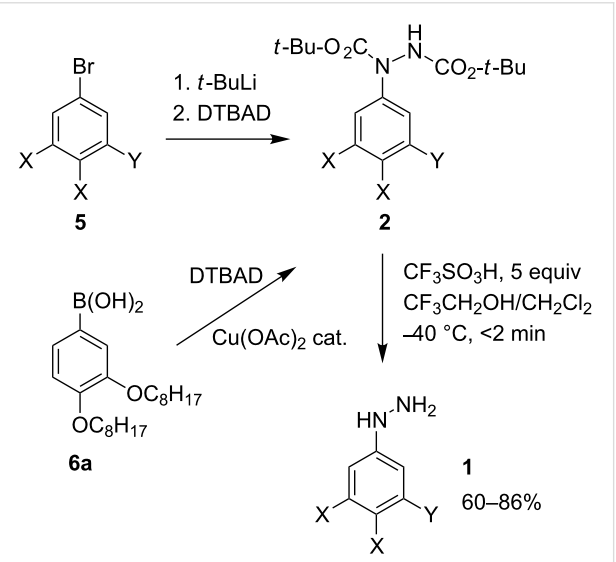

Scheme 3: Synthesis of arylhydrazines **1**. Substituents X and Y are defined in Figure 2.

The Boc-protected arylhydrazines, hydrazides **2**, were conveniently obtained by direct addition of aryllithium to di-*tert*-butyl azodicarboxylate (DTBAD, Scheme 3). The latter was prepared by lithiation of aryl bromides **5** with *t*-BuLi to avoid the formation of *n*-BuBr with *n*-BuLi and N-butylation of hydrazide **2**. Hydrazide **2a** was also obtained by the Cu^{2+}-catalyzed addition [18] of arylboronic acid **6a** [28] to DTBAD. The yields of both syntheses of **2a** were comparable.

The trichloroethyl hydrazide **3a** was prepared by acid-catalyzed amination of 1,2-dioctyloxybenzene (**4**) with BTCEAD in the presence of catalytic amounts of TfOH, according to a general literature procedure [23] (Scheme 1).

The requisite bromobenzene **5a** was prepared by bromination of 1,2-dioctyloxybenzene (**4**) [29] with $CuBr_2$ in MeCN according to a literature method [30] (Scheme 4). This method is a convenient alternative to the alkylation of the less readily accessible 4-bromocatechol (**7**) [28].

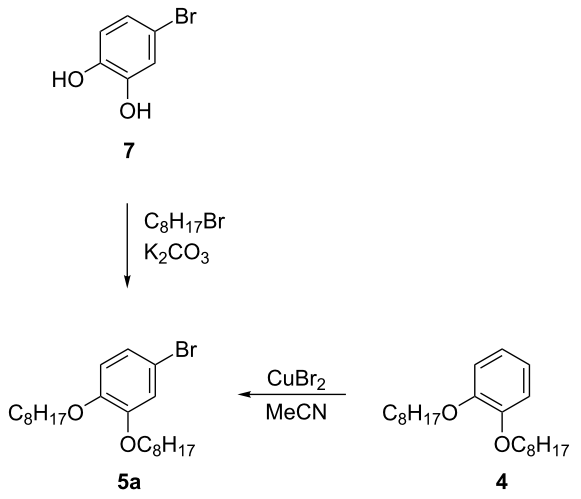

Scheme 4: Preparation of bromide **5a**.

1-Bromo-3,4-didecylbenzene (**5b**) was obtained by bromination of 1,2-didecylbenzene (**8**) [31], obtained by the Kumada method [32], with Br_2 in acetic anhydride (Scheme 5). Typically, the electrophilic bromination of 1,2-dialkylbenzenes results in 4,5-dibromo derivatives as the major products [33,34]. In contrast, the present method permits selective monobromination, although the bromo derivative **5b** was isolated only in about 85% purity. The product could not be purified rigorously from several unidentified contaminants either by chromatography or by distillation due to the lack of separation or partial decomposition. Therefore, crude **5b** was used for the preparation of hydrazide **2b**, which was easily purified by chromatographic methods.

The attempted monoiodination of **8** with BTMA·ICl_2 by using a general literature method [35] gave only traces of the product and nearly all of the starting material was recovered. Iodination under the Kern conditions [36,37] (HIO_3/I_2) gave a mixture of mono- and diiodo derivatives, which were difficult to separate. Manipulation of the reaction time and temperature failed to give the desired monoiodo derivative as the major product.

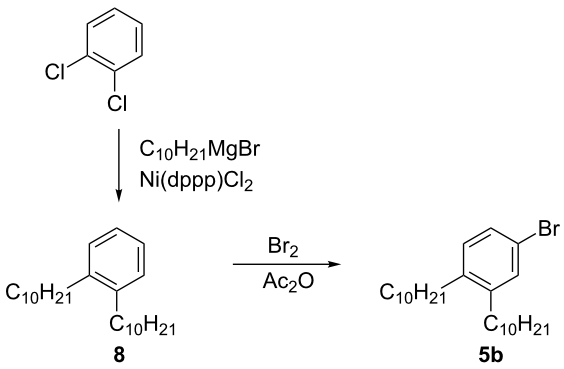

Scheme 5: Preparation of **5b**.

The preparation of bromobenzenes substituted with alkylsulfanyl groups, **5c**–**5f**, is described elsewhere [38]. Bromides **5g** [39,40] and **5h** [41] were obtained according to the respective literature procedures by alkylation of 5-bromopyrogallol.

The 3,4,5-trialkylsulfanylphenylhydrazines **1c**–**1f** have been used in the preparation of 6-oxoverdazyl derivatives that exhibit liquid-crystalline properties [26]. For instance, radical **9**, prepared from **1d** (Figure 4), exhibits a monotropic columnar rectangular phase (Cr 62 (Col_r 60) I), a broad absorption band in the visible region, and redox potentials $E^{0/+1}{}_{1/2}$ = +0.99 V and $E^{0/-1}{}_{1/2}$ = −0.45 V versus SCE. Photovoltaic studies of **9** demonstrated hole mobility $\mu_h = 1.52 \times 10^{-3}$ cm^2 $V^{-1}s^{-1}$ in the mesophase with an activation energy E_a = 0.06 ± 0.01 eV.

Conclusion

We have developed a synthetic protocol for the efficient preparation of electron-rich phenylhydrazines **1** substituted with alkylsulfanyl, alkyl and alkoxy groups from Boc hydrazides **2**. Experiments demonstrate that the addition of hydrazides **2** to a large excess of TfOH (5 equiv) at −40 °C gives hydrazines **1** in yields ranging from 60–86% and with purity >90%, which is sufficient for subsequent chemical transformations. The optimum reaction time is less than 2 min, typically 90 sec, and longer times lead to a lower purity of the product.

The presented method for the preparation of phenylhydrazines is an attractive alternative to Leblanc's method, which relies on the reductive deprotection of trichloroethyl hydrazide **3** under heterogenous conditions. Our method involves homogenous solutions, low temperatures and short reaction times, and is particularly suited to oleophilic ("greasy") arylhydrazines such as **1**, which are important intermediates for the preparation of verdazyls and other heterocycles that may exhibit, e.g., liquid-crystalline properties (e.g., **9**). In comparison with Leblanc's protocol, our method is also a regiocontrolled hydrazinylation

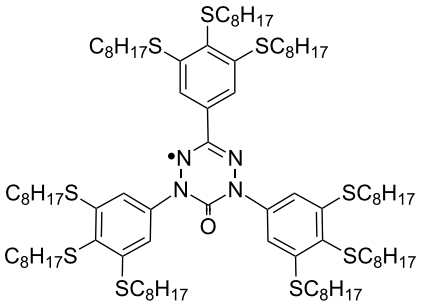

9

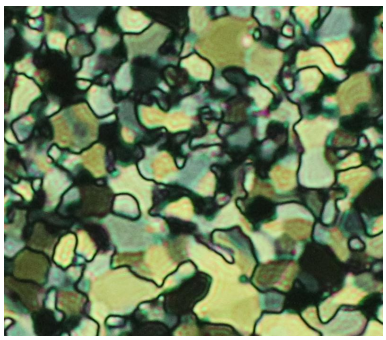

Figure 4: The structure of verdazyl radical **9** and a texture of the Col_r phase.

of the aromatics with the more accessible DTBAD through the organolithium. Although we focus on long-chain-substituted phenylhydrazines, we believe that this method can be used for other electron-rich arylhydrazines.

Experimental

Reagents and solvents were obtained commercially. Reactions were carried out under Ar. ^{1}H NMR spectra were obtained at 400 MHz in $CDCl_3$ and referenced to the solvent, unless specified otherwise.

Arylhydrazines **1**

General procedure

A solution of hydrazide **2** (1 mmol) in a mixture of CH_2Cl_2 (3 mL)/CF_3CH_2OH (1 mL) was rapidly added to a solution of TfOH (0.750 g, 0.44 mL, 5 mmol) in CF_3CH_2OH (1 mL) at −40 °C under Ar. The mixture was stirred for 1.5 min, and CH_2Cl_2 (5 mL) followed by sat. $NaHCO_3$ (10 mL) were added under very vigorous stirring. The organic layer was separated and the aqueous layer extracted (3 × CH_2Cl_2). Then the extracts were dried (Na_2SO_4) and the solvents were evaporated to give crude arylhydrazine **1** in purities typically >90% as a viscous, yellow to orange oil that darkened upon standing. The quantitative analysis of the deprotection reaction was conducted with 0.2 mmol of **2** as described above. The yield of the hydrazines was established by adding known quantities of 1,4-dimethoxybenzene (2.0 mL of 25 mM solution in CH_2Cl_2, 0.05 mmol) to the CH_2Cl_2 extract, evaporation of the resulting solution, and integration of the low-field ^{1}H NMR signals.

3,4-Dioctyloxyphenylhydrazine (1a): ^{1}H NMR (400 MHz, $CDCl_3$) δ 0.88 (t, *J* = 6.8 Hz, 6H), 1.26–1.36 (m, 16H), 1.37–1.47 (m, 4H), 1.70–1.85 (m, 4H), 3.92 (t, *J* = 6.7 Hz, 2H), 3.96 (t, *J* = 6.7 Hz, 2H), 6.34 (dd, J_1 = 8.5 Hz, J_2 = 2.6 Hz, 1H), 6.46 (d, *J* = 2.6 Hz, 1H), 6.82 (d, *J* = 8.5 Hz, 1H); ^{1}H NMR (500 MHz, DMSO-d_6) δ 0.86 (t, *J* = 6.7 Hz, 6H), 1.20–1.36 (m, 16H), 1.37–1.46 (m, 4H), 1.61 (quint, *J* = 7.0 Hz, 2H), 1.68 (quint, *J* = 6.9 Hz, 2H), 3.78 (t, *J* = 6.4 Hz, 2H), 3.87 (t, *J* = 6.3 Hz, 2H), 6.24 (dd, J_1 = 8.5 Hz, J_2 = 2.3 Hz, 1H), 6.47 (d, *J* = 2.3 Hz, 1H), 6.71 (d, *J* = 8.6 Hz, 1H).

3,4-Didecylphenylhydrazine (1b): ^{1}H NMR (500 MHz, $CDCl_3$) δ 0.88 (t, *J* = 6.9 Hz, 6H), 1.22–1.40 (m, 28H), 1.47–1.58 (m, 4H), 2.51 (t, *J* = 7.0 Hz, 2H), 2.53 (t, *J* = 7.1 Hz, 2H), 2.6 (brs, 3H), 6.59–6.65 (m, 2H), 7.01 (d, *J* = 8.0 Hz, 1H).

3,4,5-Trihexylsulfanylphenylhydrazine (1c): ^{1}H NMR (400 MHz, $CDCl_3$) δ 0.87 (t, *J* = 6.9 Hz, 3H), 0.89 (t, *J* = 6.8 Hz, 6H), 1.20–1.35 (m, 12H), 1.36–1.52 (m, 6H), 1.59 (quint, *J* = 7.5 Hz, 2H), 1.71 (quint, *J* = 7.4 Hz, 4H), 2.77 (t, *J* = 7.4 Hz, 2H), 2.83 (t, *J* = 7.3 Hz, 4H), 3.2 (brs, 3H), 6.41 (s, 2H).

3,4,5-Trioctylsulfanylphenylhydrazine (1d): ^{1}H NMR (500 MHz, $CDCl_3$) δ 0.87 (t, *J* = 6.9 Hz, 3H), 0.88 (t, *J* = 6.6 Hz, 6H), 1.20–1.34 (m, 24H), 1.38–1.43 (m, 2H), 1.44–1.53 (m, 4H), 1.59 (quint, *J* = 7.5 Hz, 2H), 1.72 (quint, *J* = 7.5 Hz, 4H), 2.77 (t, *J* = 7.5 Hz, 2H), 2.84 (t, *J* = 7.4 Hz, 4H), 6.40 (s, 2H).

3,4,5-Tridecylsulfanylphenylhydrazine (1e): ^{1}H NMR (400 MHz, $CDCl_3$) δ 0.87 (t, *J* = 6.8 Hz, 3H), 0.88 (t, *J* = 6.8 Hz, 6H), 1.20–1.35 (m, 36H), 1.36–1.52 (m, 6H), 1.59 (quint, *J* = 7.6 Hz, 2H), 1.71 (quint, *J* = 7.3 Hz, 4H), 2.76 (t, *J* = 7.5 Hz, 2H), 2.83 (t, *J* = 7.3 Hz, 4H), 6.40 (s, 2H).

3,4,5-Tridodecylsulfanylphenylhydrazine (1f): ^{1}H NMR (500 MHz, $CDCl_3$) δ 0.88 (t, *J* = 6.8 Hz, 9H), 1.20–1.35 (m, 48H), 1.36–1.51 (m, 6H), 1.59 (quint, *J* = 7.5 Hz, 2H), 1.71 (quint, *J* = 7.4 Hz, 4H), 2.77 (t, *J* = 7.4 Hz, 2H), 2.84 (t, *J* = 7.1 Hz, 4H), 6.40 (s, 2H).

3,4,5-Trioctyloxyphenylhydrazine (1g): Soft yellow solid; ^{1}H NMR (400 MHz, $CDCl_3$) δ 0.88 (t, *J* = 6.7 Hz, 9H),

1.22–1.38 (m, 24H), 1.42–1.53 (m, 6H), 1.72 (quint, *J* = 7.1 Hz, 2H), 1.79 (quint, *J* = 7.1 Hz, 4H), 3.86 (t, *J* = 6.6 Hz, 2H), 3.95 (t, *J* = 6.6 Hz, 4H), 6.06 (s, 2H).

3,4,5-Tridecyloxyphenylhydrazine (1h): ^{1}H NMR (400 MHz, $CDCl_3$) δ 0.88 (t, *J* = 6.8 Hz, 9H), 1.21–1.38 (m, 36H), 1.39–1.64 (m, 6H), 1.65–1.84 (m, 6H), 3.86 (t, *J* = 6.6 Hz, 2H), 3.95 (t, *J* = 6.6 Hz, 4H), 6.06 (s, 2H); ^{1}H NMR (400 MHz, C_6D_6) δ 0.92 (t, *J* = 6.8 Hz, 9H), 1.22–1.58 (m, 38H), 1.63–1.73 (m, 4H), 1.78 (quint, *J* = 7.1 Hz, 4H), 1.97 (quint, *J* = 8.3 Hz, 2H), 3.89 (t, *J* = 6.4 Hz, 4H), 4.23 (t, *J* = 6.5 Hz, 2H), 6.03 (s, 2H).

Preparation of hydrazides **2**

General procedure

To a solution of the substituted bromobenzene **5** (1.0 mmol) in dry THF (10 mL), *t*-BuLi (1.7 M in pentane, 2.2 mmol) was added under Ar at −78 °C. After 1.5 h a THF (1 mL) solution of di-*tert*-butyl azodicarboxylate (DTBAD, 345 mg, 1.5 mmol) was added dropwise. The mixture was stirred at −78 °C for 0.5 h, then 1 h at rt, and quenched with 5% HCl. The organic products were extracted (Et_2O), the extracts dried (Na_2SO_4), the solvents evaporated, and the residue was passed through a short silica-gel column (hexane/CH_2Cl_2 then CH_2Cl_2) to give hydrazides **2** as white solids.

1,2-Bis(*tert*-butoxycarbonyl)-1-(3,4-dioctyloxyphenyl)-hydrazine (2a): Yield 71%; mp 55–57 °C; ^{1}H NMR (500 MHz, $CDCl_3$) δ 0.88 (t, *J* = 6.9 Hz, 6H), 1.22–1.38 (m, 16H), 1.39–1.51 (m, 4H), 1.49 (s, 18H), 1.73–1.84 (m, 4H), 3.96 (t, *J* = 6.6 Hz, 2H), 3.97 (t, *J* = 6.6 Hz, 2H), 6.71 (brs, 1H), 6.80 (d, *J* = 8.6 Hz, 1H), 6.86–6.92 (m, 1H), 6.93–7.02 (m, 1H); Anal. calcd for $C_{32}H_{56}N_2O_6$: C, 68.05; H, 9.99; N, 4.96; found: C, 68.35; H, 9.82; N, 5.02.

Method B: To a solution of 3,4-dioctyloxyphenylboronic acid (**6a**, 50 mg, 0.13 mmol) in THF (2 mL), di-*tert*-butyl azodicarboxylate (DTBAD, 30 mg, 0.13 mmol) was added followed by $Cu(OAc)_2$ (cat) under an Ar atmosphere. The mixture was stirred at rt overnight, the solvent was evaporated and the residue was purified on a short silica-gel column (CH_2Cl_2) to give 50 mg (68% of yield) of hydrazide **2a**.

1,2-Bis(*tert*-butoxycarbonyl)-1-(3,4-didecylphenyl)hydrazine (2b): Yield 63%; mp 37–38 °C; ^{1}H NMR (500 MHz, $CDCl_3$) δ 0.88 (t, *J* = 6.8 Hz, 6H), 1.23–1.40 (m, 28H), 1.49 (s, 18H), 1.48–1.59 (m, 4H), 2.52–2.59 (m, 4H), 6.70 (brs, 1H), 7.06 (d, *J* = 8.2 Hz, 1H), 7.08–7.21 (br m, 2H); Anal. calcd for $C_{36}H_{64}N_2O_4$: C, 73.42; H, 10.95; N, 4.76; found: C, 73.06; H, 10.88; N, 4.74.

1,2-Bis(*tert*-butoxycarbonyl)-1-(3,4,5-trihexylsulfanyl-phenyl)hydrazine (2c): Yield 43%; mp 74–75 °C; ^{1}H NMR (400 MHz, $CDCl_3$) δ 0.87 (t, *J* = 6.9 Hz, 3H), 0.88 (t, *J* = 6.9 Hz, 6H), 1.23–1.37 (m, 12H), 1.38–1.52 (m, 6H), 1.51 (s, 18H), 1.60 (quint, *J* = 7.4 Hz, 2H), 1.72 (quint, *J* = 7.2 Hz, 4H), 2.81 (t, *J* = 7.5 Hz, 2H), 2.84 (t, *J* = 7.4 Hz, 4H), 6.69 (brs, 1H), 6.99 (brs, 2H); Anal. calcd for $C_{34}H_{60}N_2O_4S_3$: C, 62.15; H, 9.20; N, 4.26; found: C, 62.35; H, 9.34; N, 4.22.

1,2-Bis(*tert*-butoxycarbonyl)-1-(3,4,5-trioctylsulfanyl-phenyl)hydrazine (2d): Yield 55% yield; mp 51–52 °C; ^{1}H NMR (400 MHz, $CDCl_3$) δ 0.84–0.91 (m, 9H), 1.21–1.35 (m, 24H), 1.36–1.50 (m, 6H), 1.51 (s, 18H), 1.60 (quint, *J* = 7.4 Hz, 2H), 1.72 (quint, *J* = 7.5 Hz, 4H), 2.81 (t, *J* = 7.5 Hz, 4H), 2.83 (t, *J* = 7.4 Hz, 2H), 6.69 (brs, 1H), 6.98 (brs, 2H); the analytically pure sample was obtained by recrystallization (MeCN); Anal. calcd for $C_{40}H_{72}N_2O_4S_3$: C, 64.82; H, 9.79; N, 3.78; found: C, 64.92; H, 9.56; N, 3.91.

1,2-Bis(*tert*-butoxycarbonyl)-1-(3,4,5-tridecylsulfanyl-phenyl)hydrazine (2e): Yield 56%; mp 50–51 °C; ^{1}H NMR (500 MHz, $CDCl_3$) δ 0.87 (t, *J* = 6.8 Hz, 3H), 0.88 (t, *J* = 7.0 Hz, 6H), 1.21–1.36 (m, 38H), 1.37–1.51 (m, 6H), 1.51 (s, 18H), 1.60 (quint, *J* = 7.4 Hz, 2H), 1.71 (quint, *J* = 7.4 Hz, 4H), 2.81 (t, *J* = 7.6 Hz, 2H), 2.83 (t, *J* = 7.4 Hz, 4H), 6.70 (brs, 1H), 6.98 (brs, 2H); Anal. calcd for $C_{46}H_{86}N_2O_4S_3$: C, 66.78; H, 10.48; N, 3.39; found: C, 66.75; H, 10.07; N, 3.43.

1,2-Bis(*tert*-butoxycarbonyl)-1-(3,4,5-tridodecylsulfanyl-phenyl)hydrazine (2f): Yield 50%; mp 49–51 °C; ^{1}H NMR (500 MHz, $CDCl_3$) δ 0.88 (t, *J* = 6.7 Hz, 9H), 1.22–1.36 (m, 50H), 1.35–1.51 (m, 6H), 1.51 (s, 18H), 1.60 (quint, *J* = 7.4 Hz, 2H), 1.71 (quint, *J* = 7.2 Hz, 4H), 2.81 (t, *J* = 7.4 Hz, 2H), 2.83 (t, *J* = 7.2 Hz, 4H), 6.69 (brs, 1H), 6.98 (brs, 2H); Anal. calcd for $C_{52}H_{98}N_2O_4S_3$: C, 68.52; H, 10.84; N, 3.07; found: C, 68.82; H, 10.83; N, 3.06.

1,2-Bis(*tert*-butoxycarbonyl)-1-(3,4,5-trioctyloxy-phenyl)hydrazine (2g): Yield 45%; white crystals (MeCN/EtOAc); mp 73–74 °C; ^{1}H NMR (400 MHz, $CDCl_3$) δ 0.88 (t, *J* = 6.8 Hz, 9H), 1.23–1.38 (m, 24H), 1.38–1.52 (m, 6H), 1.50 (s, 18H), 1.73 (quint, *J* = 7.4 Hz, 2H), 1.77 (quint, *J* = 6.9 Hz, 4H), 3.92 (t, *J* = 6.8 Hz, 2H), 3.93 (t, *J* = 6.6 Hz, 4H), 6.64 (brs, 2H), 6.68 (brs, 1H); Anal. calcd for $C_{40}H_{72}N_2O_7$: C, 69.32; H, 10.47; N, 4.04; found: C, 69.61; H, 10.43; N, 3.91.

1,2-Bis(*tert*-butoxycarbonyl)-1-(3,4,5-tridecyloxy-phenyl)hydrazine (2h): Yield 64%; mp 55–57 °C; ^{1}H NMR (400 MHz, $CDCl_3$) δ 0.88 (t, *J* = 6.8 Hz, 9H), 1.21–1.38 (m, 38H), 1.41–1.54 (m, 6H), 1.50 (s, 18H), 1.67–1.82 (m, 6H), 3.91 (t, *J* = 6.8 Hz, 2H), 3.93 (t, *J* = 6.6 Hz, 4H), 6.64 (brs, 2H),

6.68 (brs, 1H); Anal. calcd for $C_{46}H_{86}N_2O_7$: C, 70.91; H, 11.12; N, 3.60; found: C, 71.31; H, 11.08; N, 3.65.

1,2-Bis(2,2,2-trichloroethoxycarbonyl)-1-(3,4-dioctyloxyphenyl)hydrazine (3a): To the solution of 1,2-dioctyloxybenzene (**4**, 1.10 g, 3.31 mmol) in dry CH_2Cl_2 (20 mL), one drop of CF_3SO_3H was added under Ar at −78 °C followed by a solution of bis(2,2,2-trichloroethyl) azodicarboxylate (BTCEAD, 1.50 g, 3.97 mmol) in CH_2Cl_2 (3 mL). The reaction mixture was stirred for 20 min, warmed up to rt, stirred for 10 min, and quenched with 25% NH_4OAc. The organic products were extracted (CH_2Cl_2), the extracts dried (Na_2SO_4), and the solvent evaporated. The viscous residue was passed through a silica-gel plug (hexane/CH_2Cl_2 then CH_2Cl_2) to give 1.03 g (36% yield) of the hydrazide **3a** as a viscous oil: ^{1}H NMR (400 MHz, $CDCl_3$) δ 0.88 (t, J = 6.7 Hz, 3H), 0.89 (t, J = 7.2 Hz, 3H), 1.24–1.39 (m, 16H), 1.41–1.50 (m, 4H), 1.80 (quint, J = 7.0 Hz, 4H), 3.96 (t, J = 6.6 Hz, 2H), 3.99 (t, J = 6.6 Hz, 2H), 4.82 (s, 4H), 6.83 (d, J = 8.6 Hz, 1H), 6.97 (d, J = 8.2 Hz, 1H), 7.02 (brs, 1H), 7.39 (brs, 1H); Anal. calcd for $C_{28}H_{42}Cl_6N_2O_6$: C, 47.01; H, 5.92; N, 3.92; found: C, 46.27; H, 5.72; N, 3.92.

1-Bromo-3,4-didecylbenzene (5b): To a solution of 1,2-didecylbenzene (**8**, 1.00 g, 2.8 mmol) in a mixture of Ac_2O (3 mL) and CH_2Cl_2 (3 mL), Br_2 (0.30 mL, 5.6 mmol) and catalytic amounts of I_2 were added. The reaction mixture was stirred overnight at rt, water was added, the organic products were extracted (hexane), the extracts dried (Na_2SO_4), and the solvents evaporated. The residue was passed through a silica-gel plug (hexane) to give 1.20 g (~85% yield, based on NMR, contained ~15% of at least two impurities) of 4-bromo-1,2-didecylbenzene (**5b**) as a colorless oil: ^{1}H NMR (500 MHz, $CDCl_3$) major signals δ 0.88 (t, J = 6.8 Hz, 6H), 1.20–1.40 (m, 28H), 1.49–1.58 (m, 4H), 2.53 (t, J = 7.4 Hz, 2H), 2.55 (t, J = 7.5 Hz, 2H), 6.98 (d, J = 8.2 Hz, 1H), 7.22 (dd, J_1 = 8.2 Hz, J_2 = 1.8 Hz, 1H), 7.25–7.27 (m, 1H); ^{1}H NMR (400 MHz, CD_2Cl_2) major signals δ 0.86 (t, J = 6.8 Hz, 6H), 1.20–1.40 (m, 28H), 1.49–1.58 (m, 4H), 2.52 (t, J = 7.4 Hz, 2H), 2.55 (t, J = 7.5 Hz, 2H), 6.99 (d, J = 8.2 Hz, 1H), 7.19 (dd, J_1 = 8.1 Hz, J_2 = 2.2 Hz, 1H), 7.25 (d, J = 2.1 Hz, 1H); HRMS-EI (m/z): $[M]^+$ calcd for $C_{26}H_{45}Br$, 436.2705; found, 436.2726; since **5b** undergoes partial decomposition during attempted short-path distillation (>260 °C/0.2 mmHg), it was used without further purification for the preparation of **2b**.

1,2-Didecylbenzene (8): Following a general procedure [31], a solution of 1,2-dichlorobenzene (10.0 g, 68.0 mmol), Ni(dppp)Cl_2 (370 mg, 0.68 mmol), and *n*-decylmagnesium bromide (272 mmol) in a dry THF (100 mL) was heated under reflux overnight. The crude product was passed through a silica-gel plug (hexane) and short-path distilled (220–230 °C/0.3 mmHg) to collect 11.4 g (48% yield) of 1,2-didecylbenzene (**8**) as a colorless oil: ^{1}H NMR (400 MHz, $CDCl_3$) δ 0.88 (t, J = 6.8 Hz, 6H), 1.20–1.43 (m, 28H), 1.57 (quint, J = 7.7 Hz, 4H), 2.59 (t, J = 8.0 Hz, 4H), 7.06–7.16 (m, 4H); HRMS–EI (m/z): $[M]^+$ calcd for $C_{26}H_{46}$, 358.3600; found, 358.3583.

Acknowledgements

This project was supported by a Vanderbilt University Discovery Grant.

References

1. Robinson, B. *The Fisher Indole Synthesis;* Wiley & Sons: New York, 1982.
2. Elguero, J. Pyrazoles. In *Comprehensive Heterocyclic Chemistry II;* Katritzky, A. R.; Rees, C. W.; Scriven, E. F. V., Eds.; Pergamon, 1996; Vol. 3, pp 1–75. doi:10.1016/B978-008096518-5.00059-9
3. Garratt, P. J. 1,2,4-Triazoles. In *Comprehensive Heterocyclic Chemistry II;* Katritzky, A. R.; Rees, C. W.; Scriven, E. F. V., Eds.; Pergamon, 1996; Vol. 4, pp 127–163. doi:10.1016/B978-008096518-5.00080-0
4. Duffy, K. J.; Darcy, M. G.; Delorme, E.; Dillon, S. B.; Eppley, D. F.; Erickson-Miller, C.; Giampa, L.; Hopson, C. B.; Huang, Y.; Keenan, R. M.; Lamb, P.; Leong, L.; Liu, N.; Miller, S. G.; Price, A. T.; Rosen, J.; Shah, R.; Shaw, T. N.; Smith, H.; Stark, K. C.; Tian, S.-S.; Tyree, C.; Wiggall, K. J.; Zhang, L.; Luengo, J. I. *J. Med. Chem.* **2001,** *44,* 3730. doi:10.1021/jm010283l
5. He, L.; Chang, H.-X.; Chou, T.-C.; Savaraj, N.; Cheng, C. C. *Eur. J. Med. Chem.* **2003,** *38,* 101. doi:10.1016/S0223-5234(02)01420-4
6. Sugimoto, A.; Tanaka, H.; Eguchi, Y.; Ito, S.; Takashima, Y.; Ishikawa, M. *J. Med. Chem.* **1984,** *27,* 1300. doi:10.1021/jm00376a013
7. Wiley, P. F. Verdazyls. *Chemistry of 1,2,3-Triazines and 1,2,4-Triazines, Tetrazines and Pentazines;* The Chemistry of Heterocyclic Compounds; Willey & Sons: New York , 1978; pp 1225–1246.
8. Koivisto, B. D.; Hicks, R. G. *Coord. Chem. Rev.* **2005,** *249,* 2612. doi:10.1016/j.ccr.2005.03.012
9. Hicks, R. G. Verdazyls and Related Radicals Containing the Hydrazyl [R_2N-NR] Group. In *Stable Radicals: Fundamentals and Applied Aspects of Odd-Electron Compounds;* Hicks, R. G., Ed.; Wiley & Sons, 2010; pp 245–280. And references therein.
10. Neugebauer, F. A.; Umminger, I. *Chem. Ber.* **1980,** *113,* 1205. doi:10.1002/cber.19801130402
11. Constantinides, C. P.; Koutentis, P. A.; Krassos, H.; Rawson, J. M.; Tasiopoulos, A. J. *J. Org. Chem.* **2011,** *76,* 2798. doi:10.1021/jo200210s
12. Koutentis, P. A.; Lo Re, D. *Synthesis* **2010,** 2075. doi:10.1055/s-0029-1218782
13. Hunsberger, I. M.; Shaw, E. R.; Fugger, J.; Ketcham, R.; Lednicer, D. *J. Org. Chem.* **1956,** *21,* 394. doi:10.1021/jo01110a004
14. Bandgar, B. P.; Thite, C. S. *Synth. Commun.* **1997,** *27,* 635. doi:10.1080/00397919708003336
15. Browne, D. L.; Baxendale, I. R.; Ley, S. V. *Tetrahedron* **2011,** *67,* 10296. doi:10.1016/j.tet.2011.09.146
16. Demers, J. P.; Klaubert, D. H. *Tetrahedron Lett.* **1987,** *28,* 4933. doi:10.1016/S0040-4039(00)96662-0

17. Velarde-Ortiz, R.; Guijarro, A.; Rieke, R. D. *Tetrahedron Lett.* **1998,** *39,* 9157. doi:10.1016/S0040-4039(98)02108-X
18. Kabalka, G. W.; Guchhait, S. K. *Org. Lett.* **2003,** *5,* 4129. doi:10.1021/ol035544v
19. Uemura, T.; Chatani, N. *J. Org. Chem.* **2005,** *70,* 8631. doi:10.1021/jo051387x
20. Muñiz, K.; Iglesias, A. *Angew. Chem., Int. Ed.* **2007,** *46,* 6350. doi:10.1002/anie.200700288
21. Zaltsgendler, I.; Leblanc, Y.; Bernstein, M. A. *Tetrahedron Lett.* **1993,** *34,* 2441. doi:10.1016/S0040-4039(00)60436-7
22. Mitchell, H.; Leblanc, Y. *J. Org. Chem.* **1994,** *59,* 682. doi:10.1021/jo00082a035
23. Leblanc, Y.; Boudreault, N. *J. Org. Chem.* **1995,** *60,* 4268. doi:10.1021/jo00118a052
24. Dufresne, C.; Leblanc, Y.; Berthelette, C.; McCooeye, C. *Synth. Commun.* **1997,** *27,* 3613. doi:10.1080/00397919708007084
25. Hudlicky, T.; Seoane, G.; Pettus, T. *J. Org. Chem.* **1989,** *54,* 4239. doi:10.1021/jo00278a052
26. Jankowiak, A.; Pociecha, D.; Szczytko, J.; Monobe, H.; Kaszyński, P. *J. Am. Chem. Soc.* **2012,** *134,* 2465. doi:10.1021/ja209467h
27. Holcombe, J. L.; Livinghouse, T. *J. Org. Chem.* **1986,** *51,* 111. doi:10.1021/jo00351a028
28. Sienkowska, M. J.; Farrar, J. M.; Zhang, F.; Kusuma, S.; Heiney, P. A.; Kaszynski, P. *J. Mater. Chem.* **2007,** *17,* 1399. doi:10.1039/b615545f
29. Collins, R. F.; Davis, M. *J. Chem. Soc. C* **1966,** 366. doi:10.1039/J39660000366
30. Bhatt, S.; Nayak, S. K. *Synth. Commun.* **2007,** *37,* 1381. doi:10.1080/00908320701230026
31. Mohr, B.; Enkelmann, V.; Wegner, G. *J. Org. Chem.* **1994,** *59,* 635. doi:10.1021/jo00082a022
32. Tamao, K.; Sumitani, K.; Kiso, Y.; Zembayashi, M.; Fujioka, A.; Kodama, S.-i.; Nakajima, I.; Minato, A.; Kumada, M. *Bull. Chem. Soc. Jpn.* **1976,** *49,* 1958. doi:10.1246/bcsj.49.1958
33. Sonoda, M.; Sakai, Y.; Yoshimura, T.; Tobe, Y.; Kamada, K. *Chem. Lett.* **2004,** *33,* 972. doi:10.1246/cl.2004.972
34. Hanack, M.; Haisch, P.; Lehmann, H.; Subramanian, L. R. *Synthesis* **1993,** 387. doi:10.1055/s-1993-25869
35. Kajigaeshi, S.; Kakinami, T.; Moriwaki, M.; Tanaka, T.; Fujisaki, S.; Okamoto, T. *Bull. Chem. Soc. Jpn.* **1989,** *62,* 439. doi:10.1246/bcsj.62.439
36. Wirth, H. O.; Königstein, O.; Kern, W. *Justus Liebigs Ann. Chem.* **1960,** *634,* 84. doi:10.1002/jlac.19606340109
37. Jasiński, M.; Jankowiak, A.; Januszko, A.; Bremer, M.; Pauluth, D.; Kaszyński, P. *Liq. Cryst.* **2008,** *35,* 343. doi:10.1080/02678290701817318
38. Jankowiak, A.; Dębska, Z.; Romański, J.; Kaszyński, P. *J. Sulfur Chem.* **2012,** *33*. doi:10.1080/17415993.2011.644554
39. Maeda, H.; Haketa, Y.; Nakanishi, T. *J. Am. Chem. Soc.* **2007,** *129,* 13661. doi:10.1021/ja074435z
40. Yasuda, T.; Shimizu, T.; Liu, F.; Ungar, G.; Kato, T. *J. Am. Chem. Soc.* **2011,** *133,* 13437. doi:10.1021/ja2035255
41. Ma, C.-Q.; Pisula, W.; Weber, C.; Feng, X.-L.; Müllen, K.; Bäuerle, P. *Chem.–Eur. J.* **2011,** *17,* 1507. doi:10.1002/chem.201002198

License and Terms

Beilstein Journal of Organic Chemistry

Liquid-crystalline nanoparticles: Hybrid design and mesophase structures

Gareth L. Nealon*, Romain Greget, Cristina Dominguez, Zsuzsanna T. Nagy, Daniel Guillon, Jean-Louis Gallani and Bertrand Donnio*

Review

Open Access

Address:
Institut de Physique et Chimie des Matériaux de Strasbourg (IPCMS), CNRS-Université de Strasbourg (UMR 7504), 23 rue du Loess, BP 43, 67034 Strasbourg Cedex 2, France

Email:
Gareth L. Nealon* - gareth.nealon@ipcms.u-strasbg.fr;
Bertrand Donnio* - bdonnio@ipcms.u-strasbg.fr

* Corresponding author

Keywords:
hybrid; liquid crystal; mesogen; mesomorphism; mesophase; nanoparticle; self-organisation; supramolecule

Beilstein J. Org. Chem. **2012,** *8,* 349–370.
doi:10.3762/bjoc.8.39

Received: 09 November 2011
Accepted: 09 February 2012
Published: 08 March 2012

This article is part of the Thematic Series "Progress in liquid crystal chemistry II".

Guest Editor: S. Laschat

Abstract

Liquid-crystalline nanoparticles represent an exciting class of new materials for a variety of potential applications. By combining supramolecular ordering with the fluid properties of the liquid-crystalline state, these materials offer the possibility to organise nanoparticles into addressable 2-D and 3-D arrangements exhibiting high processability and self-healing properties. Herein, we review the developments in the field of discrete thermotropic liquid-crystalline nanoparticle hybrids, with special emphasis on the relationship between the nanoparticle morphology and the nature of the organic ligand coating and their resulting phase behaviour. Mechanisms proposed to explain the supramolecular organisation of the mesogens within the liquid-crystalline phases are discussed.

Introduction

The term "nanotechnology" has gone far beyond the realms of universities and research laboratories and is understood by scientist and layman alike to be synonymous with "high-tech" and "futuristic", promising to bring about tremendous advances in our quality of life. By utilising a "bottom-up" approach, whereby atomic and molecular components are assembled in a controlled fashion [1], scientists hope to greatly expand the scope of accessible technologies and tackle the existing and future challenges in novel ways. Perhaps the most ambitious goal of this field of endeavour is the creation of molecular machines and devices, with dimensions on the order of atoms and molecules, capable of performing specific predetermined tasks [2]. At the core of this nanotechnology revolution lies the nanoparticle (NP), the most common of which being metallic particles (including alloys and oxides) with at least one dimension smaller than 100 nm. These species can exhibit physical

and chemical properties that differ tremendously from their bulk counterparts, and which depend not only on their composition but also on their shape and size [3].

Nanoparticle science is ever expanding with its interest derived from the desire to understand the synthesis and fundamental properties [4-9] and the myriad of potential applications of these unique species [10]. Fields as diverse as biology and medicine [11,12], optics and electro-optics [13,14], catalysis [12,15], and environmental remediation [16] are expected to benefit from the unique properties and promises offered by nanoparticles. Of course, in order to exploit the exciting properties of NPs, it is almost always necessary to incorporate them into a more complex structure, often through the use of a suitable organic coating, which not only imparts stability against aggregation but also other important features such as solubility, modularity, and optical and self-organisation properties.

The organisation of NPs into ordered systems is of crucial importance for their use in high-technology applications and devices, and a wide variety of "top-down" and "bottom-up" methods have been proposed and are continuously under development [17-20]. Central to these efforts is a consideration of the forces acting upon the NPs [21,22], which are determined by their composition (surface chemistry, magnetic/electrostatic properties) and morphology (size, shape and roughness) and can be manipulated by coating with suitable structure-directing agents. Amongst the techniques used to assemble NPs, self-assembly methods show immense promise towards achieving the ambitious results expected from the field of nanotechnology research [23]. Liquid-crystalline (LC) materials offer unique opportunities in the field of NP organisation due to the intrinsic order and fluid properties that they possess, allowing for complex architectures to be established with high processability and defect tolerance. The properties of LCs can also be influenced by external factors, such as applied magnetic and electric fields and surface effects, all of which lend these materials towards their use in stimuli-responsive advanced materials [24]. What follows is a brief introduction to some of the salient points in LC science, but a thorough introduction to the theory and background of liquid crystals is beyond the scope of this review, and the interested reader is directed to numerous texts on the subject [25-29].

The liquid-crystalline state is intermediate between that of a perfectly ordered crystal and a disordered isotropic liquid. The moieties within a liquid crystal possess intrinsic directional order, often accompanied by various degrees of positional order, whilst remaining in a fluid state. A material that exhibits a liquid-crystalline state as a function of temperature is referred to as *thermotropic*, whereas those that exhibit a LC phase in the presence of a solvent are known as *lyotropic*. A material that exhibits LC properties is referred to as a *mesogen* and is said to exhibit *mesomorphism*; although something that is *mesogenic* (e.g., proto-mesogens) is not necessarily *mesomorphic*.

Thermotropic liquid crystals are usually formed by molecules that contain at least two sections with contrasting chemical or structural character (*amphipathic*), most often in the form of a rigid anisotropic moiety appended with flexible segments. It is this amphipathic nature of the molecular structure that brings about the multi-step melting process that is characteristic of the liquid-crystalline state, due to the phase separation of the incompatible components [24,30-33]. Since the anisotropy of the molecular structure plays such an important role in the formation and properties of liquid-crystalline phases, the types of ligands involved are often classified according to their general shape characteristics. Thus, rodlike or calamitic molecules, for example, possess one axis much longer than the others, whereas discotic molecules exhibit one axis much shorter than the other two (Figure 1).

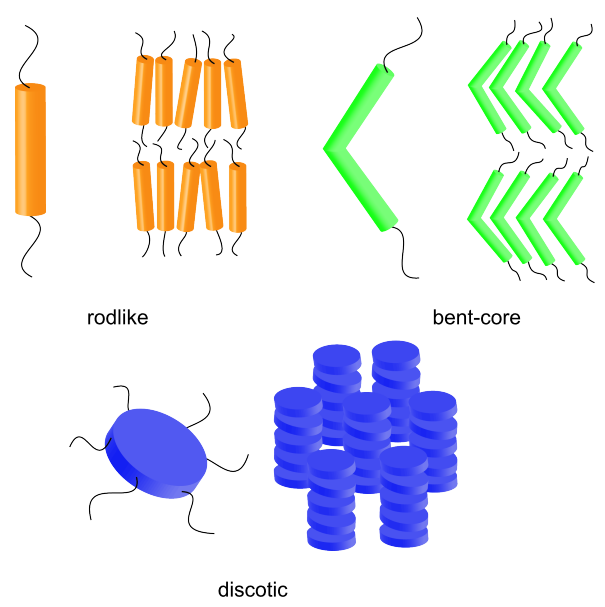

Figure 1: Three of the common molecular and supramolecular structural motifs in liquid crystal chemistry: rodlike, bent-core and discotic mesogens.

There are a variety of liquid-crystalline phases possible, based on the shape and chemical characteristics of the mesogen under investigation. The simplest is the nematic phase, whereby the mesogenic moieties exhibit an average alignment along a common direction (or *director*), whereas the smectic phases also display a degree of positional ordering (i.e., the mesogens with essentially calamitic structures are arranged into layers). Columnar phases arise from the stacking of disclike mesogenic

moieties into columns, which are in turn often arranged in a parallel manner into 2-D ordered lattices. Other mesophases include those possessing 3-D symmetry (cubic or tetragonal), and the so-called banana phases formed by bent-core mesogens [30,34,35].

This review will focus on publications that describe the preparation and characterisation of discrete thermotropic liquid-crystalline nanoparticle hybrids. Thus topics such as micellar [36] or lyotropic NPs [37,38], polymer coated/embedded NP mesogens [39-41] and the expansive field of NP-doped LC systems (including labile hybrid/ligand mixtures [42] and direct synthesis of NPs in LC matrices [43-46]) of interest for various high-technology applications [47], will not be discussed here, but the interested reader is directed to other publications in the field [48,49].

This review is structured in such a way as to highlight the various methods that have been successfully, and unsuccessfully, utilised in the quest for the preparation of nanoparticulate thermotropic liquid-crystalline materials. The various materials are classified according to the type of ligand coating used to impart mesogenic behaviour to the hybrid, highlighting their pivotal role in the design process. It is hoped that the reader will gain an understanding of the various factors that influence the mesophase behaviour of these new materials, and to appreciate some of the early trends that are appearing in this relatively young and exciting field of endeavour.

Review

Design considerations

In order for a nanoparticle sample to exhibit a thermotropic liquid-crystalline phase, it is necessary to first coat the NPs with a suitable material that allows, at the very least, the particles to form a fluid phase at relatively moderate temperatures (i.e., ideally <250 °C). From here, it becomes apparent that if one considers the two most commonly encountered NP morphologies, that is, pseudospherical polyhedra and anisotropic rod-/needlelike and platelike shapes, different strategies may be possible for inducing mesophase behaviour in these hybrids.

In the case of rod-/needlelike NPs with high aspect ratios, their inherent shape lends itself to the formation of LC phases such as nematics and smectics, subject to the reduction of interparticle interactions. This can be achieved by "dilution" with a solvent, and numerous examples of self-assembled structures of these types have been reported for rodlike [50] and disclike nanoparticles [51]. An alternative method for reducing interparticle interactions and to increase fluidity in the system is to coat the nanoparticle with a suitable organic sheath, and attempts of this type are discussed below.

In the case of pseudospherical polyhedral NPs, their lack of a naturally preferred orientation becomes a hurdle for their arrangement into LC phases, although regular 2-D arrangement into hexagonal lattices has been observed for simple monolayer-protected NPs on surfaces [52]. Whilst theoretical treatments predict that Au NPs coated with simple linear thiols should exhibit spontaneous asymmetry at low temperatures or in solution [53-55], simple NP-hybrids of this type are yet to exhibit LC phases. Therefore, it is clear that the ligands must impart sufficient anisotropy into the hybrid system to force the pseudospherical particles to form ordered self-assembled structures whilst maintaining a fluid state. Thus, parameters such as the orientational flexibility and mobility of the ligands on the NP surface are just as important as their chemical structure, or in other words, their mesogenic character.

Synthesis of liquid-crystal–nanoparticle hybrids

The synthesis of NP hybrids is of course largely determined by the nature of the nanoparticle, and is affected by factors such as the synthetic method used to prepare the inorganic species, the presence of coligands (stabilisers) and the surface chemistry of the particular material under investigation. Furthermore, the relative ease and flexibility of synthesis of the organic ligand(s) means that their design is tailored to the particular surface chemistry and morphology characteristics of the NP under investigation, ensuring a suitable anchoring group and structure-directing groups are present in the molecular structure.

In the case of Au NPs, which are by far the most extensively investigated, there are two main methods used for the preparation of hybrids; the first being direct synthesis of the NPs in the presence of the ligand of interest by using a modified Brust–Schiffrin procedure [56], and the other being a two-step process in which the NPs are first synthesised with a protective layer (e.g., a simple alkanethiol), followed by solvent-mediated ligand exchange to give the desired product (Figure 2) [12]. The first method gives a NP surface coated with exclusively (but not necessarily completely) the ligand of interest, whereas the second method invariably gives products with mixed ligand coatings. For NPs other than gold, the typical method is to prepare the NPs and then to add the ligand of interest (especially for metal oxides), or to perform a solvent-mediated ligand exchange in a similar manner to that described for the Au NPs above.

Regardless of the method of synthesis used, the purity of the final isolated sample is of course of utmost importance, since the presence of excess LC or non-mesogenic coligands could interfere with LC determination and give spurious results. Purification of the hybrids is typically undertaken through repeated

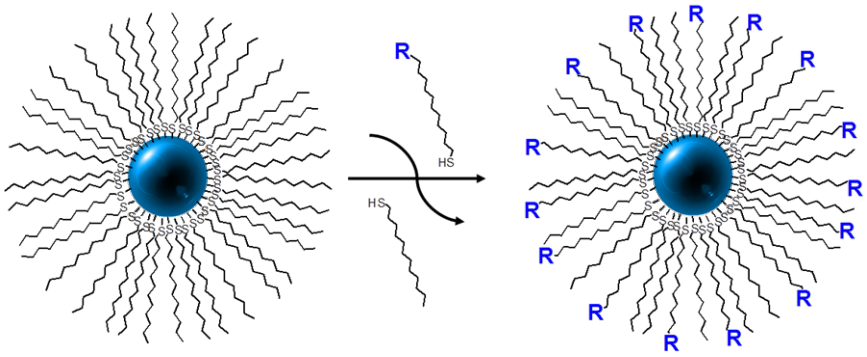

Figure 2: Schematic representation of the solvent-mediated ligand exchange process, illustrated for the partial exchange of thiols at the surface of a noble-metal nanoparticle; R represents a proto-mesogenic moiety.

precipitation, through centrifugation steps, or through chromatography techniques such as gel-permeation chromatography (GPC), or through a combination of these methods. Product purity and ligand-grafting rates and ratios can be determined through the use of techniques such as NMR spectroscopy, thermal analysis (DSC/TGA), elemental analysis, and other spectroscopic techniques (e.g., UV–vis).

At this point, it is worth making a note of the nomenclature used in this review. Ligand families are assigned a unique number, followed, where necessary, by numerals indicating the length of any alkyl chains appended to the molecule, which can be cross-referenced with the ligand charts shown throughout the text. Hybrids are represented by the general chemical formula of the NP followed by the ligand involved, separated by an "@" symbol. So, for example, an Au NP coated with ligand **1** is represented as "**Au@1**". If an alkylthiol of chain length *x* is present as a coligand on the surface of the nanoparticle, then nomenclature of the form "**Au@C$_x$/1**" is used when necessary.

Nanoparticles coated by rodlike proto-mesogenic ligands: End-on attachment

The most common and perhaps the most obvious method for inducing LC phases in NP hybrids is to introduce a suitably functionalised LC ligand onto the surface of the particle of interest. In so doing, it is hoped that the self-assembling and mesogenic potential of the ligand will be transferred to the hybrid product. Therefore, given their importance in liquid-crystal science, it is not surprising that rodlike or calamitic mesogenic molecules are the most commonly employed ligands to date in the preparation of liquid-crystalline nanoparticles. Importantly, all of the ligands chosen to date have a flexible spacer between the rigid rodlike segment of the molecule and the functional group used to attach the ligand to the NP surface, and in the case of pseudospherical NPs, the ligands usually display sizes commensurate with the size of the inorganic centre. Flexibility is an important characteristic that allows the ligands to deform easily, which is particularly true in the case of pseudospherical NPs since they allow the hybrid particles to develop anisotropic shapes, which is crucial for their arrangement into liquid-crystalline phases (except cubic structures).

Despite their apparently ideal shape characteristics, publications reporting on the thermotropic mesophases of suitably functionalised anisotropic NPs are relatively uncommon, even though they were some of the first in the field. These types of materials are of interest for the applications mentioned above, but their added advantage is the possibility to possess anisotropic magnetic, optical and electronic properties [57].

One of the earliest claims for the preparation of discrete nanoparticles exhibiting thermotropic liquid-crystalline phases involved the synthesis and functionalisation of anisotropic TiO_2 particles [58]. These nanoparticles were synthesised by using a sol–gel method in a variety of shapes and sizes, and subsequently functionalised by mixing them directly with an equal mass of amino-functionalised mesogenic ligands **1** and **2** (Figure 3).

Interestingly, highly anisotropic **TiO$_2$@1** hybrids several hundred nanometres in length and up to ~30 nm in width melted at 48 °C to give a series of optical textures up to 250 °C. X-ray analysis of the mesophase at 70, 90 and 100 °C indicated the existence of periodic particle interactions at an interval of 33.2 nm, which corresponded to the width of the NPs plus the surrounding organic sheath, and the authors concluded that the mesophase possessed a quasi-nematic 1-D order in the direction of the long axis of the acicular particles. The mesophase behaviour was lost for hybrids prepared with **1** and NPs with lower aspect ratios and a deliberately prepared polydisperse sample, and furthermore, none of the hybrids prepared with the cyanobiphenyl based amine **2** exhibited any mesophases.

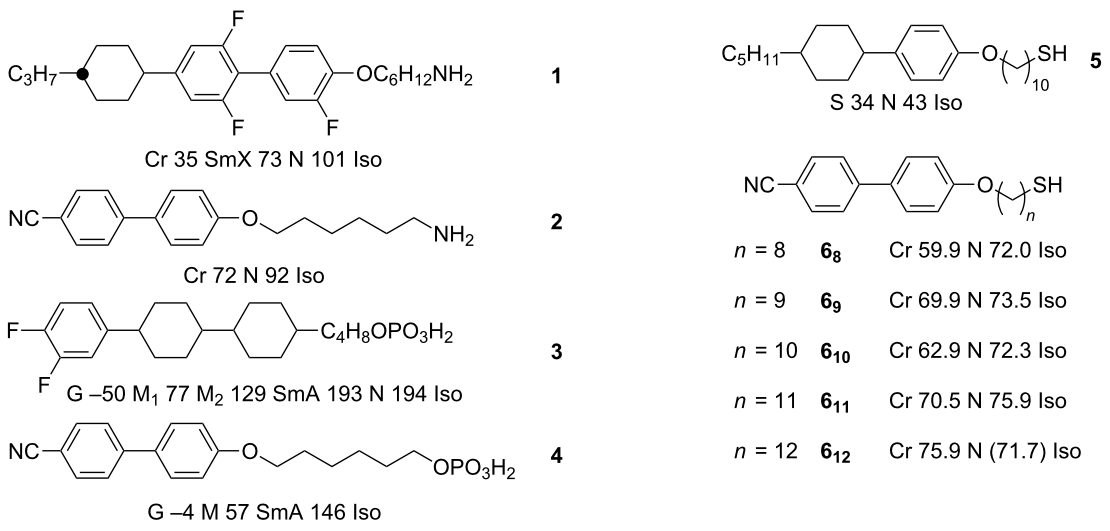

Figure 3: Chemical structures and LC properties of the rodlike ligands discussed in the text.

In an extension of this work, mesophase behaviour was reported for systems involving α-Fe_2O_3 NPs coated with mesogenic ligands containing a phosphonic acid anchoring group [59]. The NPs were prepared by using a sol–gel method, and grafting of the ligands was undertaken with 1:1 and 1:2 ligand/NP mass ratios. Mesogenic behaviour was observed for spindle-shaped **α-Fe_2O_3@3** 1:2 hybrids, with those prepared with NPs ~300 nm long and ~50 nm wide at 90 °C displaying a marbled texture under polarised optical microscopy (POM). SAXS experiments indicated the existence of periodic particle interactions at intervals of 49.7 and 46.5 nm respectively, which corresponded to the width of the NPs with a layer of ligand molecules on the surface. As was observed for **TiO_2@1**, these results indicated that the hybrids of **α-Fe_2O_3@3** exhibited a quasi-nematic one dimensional order in the direction of the long axis of the spindlelike NPs, which was lost upon the use of a polydisperse **α-Fe_2O_3** sample. Importantly, 1:2 and 1:1 **α-Fe_2O_3@3** cuboidal hybrids of ~90 nm size exhibited optically isotropic fluidic phases, and X-ray analysis at 170 °C indicated the presence of a superlattice with a simple cubic LC structure. Thus it was clear that the spindlelike NPs preferred nematic and the cuboidal NPs preferred cubic LC arrangements, respectively, which is an intuitive result highlighting the structure-directing influence of the NP morphology on the resulting mesophase.

Pseudospherical NPs are the most common inorganic core used to date in the field of LCNPs, and the first such report involved the direct synthesis of 3 nm Au NPs in the presence of a calamitic (cyclohexyl)phenoxy thiol (**5**, Figure 3) to give a densely packed surface coating (Figure 4a) [60]. The ligand showed both smectic and nematic phases, and the authors claimed that

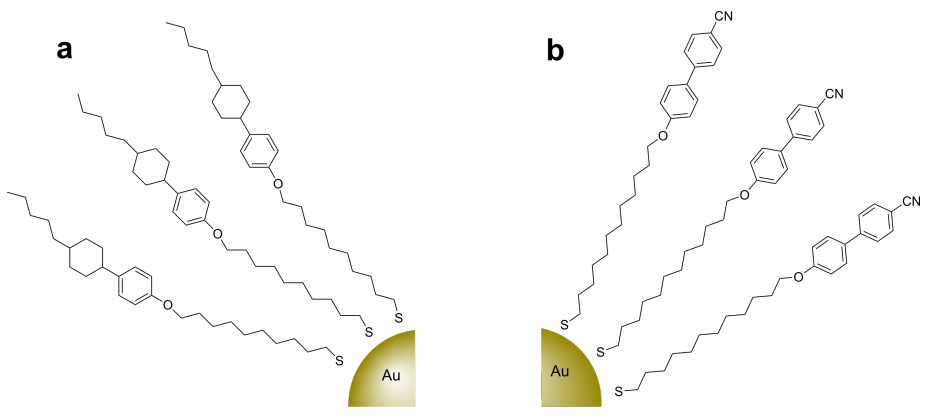

Figure 4: Schematic representation of pseudospherical Au NPs coated exclusively with mesogenic rodlike ligands (a) **Au@5** and (b) **Au@6_{12}**.

the **Au@5** hybrid displayed higher transition temperatures and a wider mesophase range than the free ligand, as determined from DSC and POM experiments. Unfortunately, no phase assignments were made by diffraction methods, precluding the determination of either the supramolecular interactions of the ligands or the positional arrangement of the NP cores, but this work was important in stimulating further research in the field by a variety of groups.

Subsequently, a similar procedure was reported in which Au NPs of diameter 2.7 ± 0.5 nm were directly synthesised in the presence of a cyanobiphenyl group appended with an alkylthiol moiety (**6_{12}**, Figure 4b) [61]. The thiol ligand exhibited a nematic phase, and the hybrids displayed a mesophase between 110 °C and 130 °C, but no distinct texture could be observed with POM (Table 1). Interestingly, direct observation of the possible arrangement of the NPs was obtained through annealing of a sample in the mesophase range on a TEM grid, followed by quenching to RT (Figure 5). Imaging of the material by TEM revealed 13–60 nm long strings of NPs, with an interstring distance of approximately 5.8 nm (i.e., roughly twice the length of the organic ligands) and an interparticle distance within the strings of 2 nm. These results were corroborated by SAXS analysis, indicating *d* spacings of 6.3 and 2.9 nm.

The authors argued that the ligands were acting like smectogens in between the strings, but that the distance between NPs within the strings was too small to be caused by end-to-end alignment of the organic moieties, and thus they must be tilted and/or overlapped. This was the first attempt at understanding the phase behaviour of these hybrids by postulating that the ligands were not uniformly disposed about the NP surface, but it was to become a common model used to explain the observed mesophase behaviour of hybrid pseudospherical NPs.

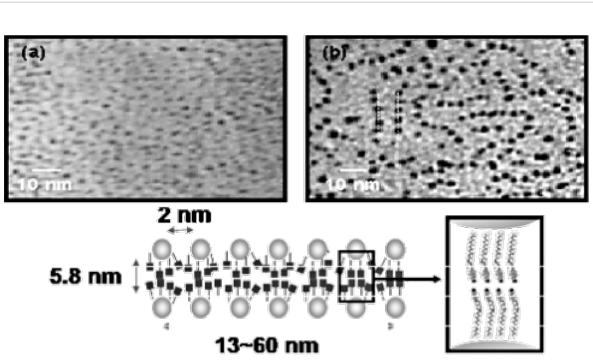

Figure 5: TEM images of **Au@6_{12}** (a) before and (b) after thermal treatment. Below: Proposed model of the nanoparticle arrangement within the strings. Reproduced by permission of The Royal Society of Chemistry [61].

Another detailed investigation into the disposition of the ligands about mesogenic Au NPs was reported based on hybrid particles prepared in a two-step process by using a wider suite of mesogenic cyanobiphenyl based thiols [62]. Gold NPs of ~2.4 nm diameter were first synthesised and isolated with a triphenylphosphine protective layer, followed by the addition of thiols **$6_{8–12}$** (Figure 3). The authors estimated the number of

Table 1: Summary of the phase behaviour of the hybrid NPs with rodlike ligands discussed in the text.[a]

NP type	NP size (nm)	Ligand	Phase assignments (Temp. °C)	Ref.
Au	3	**5**	Cr 74 LC 114 Iso	[60]
Au	2.7 ± 0.5	**6_{12}**	Cr 110 LC 130 Iso	[61]
Au	2.4	**6_8**	Meta.: Sm/N (89.7, 106.6; 149.9)	[62]
Au	2.4	**6_9**	Meta.: Sm/N (85.3; 100.8; 151.6)	[62]
Au	2.4	**6_{10}**	Meta.: Sm/N (82.1; 99.2; 151.9)	[62]
Au	2.4	**6_{11}**	Meta.: Sm/N (79.8; 92.1; 149.7)	[62]
Au	2.4	**6_{12}**	Meta.: Sm/N (85.1; 100.8; 150.5)	[62]
Au	2.0 ± 0.2	**$7_{9,9}$**	Sm 110 Iso	[63]
Au	2.0 ± 0.2	**$7_{4,4}$**	Col Crystal superlattice melts at 150	[63]
Au	2.0 ± 0.2	**$7_{1,6}$**	C_6:Sm; C_8: ModSm; C_{10}: Col; C_{12}:Col; C_{18}:NA	[63,64]
Au	2 ± 0.4	**$7_{2,5}$**	C_6:Sm; C_8: Sm; C_{12}:Col; C_{18}:NA	[64]
Au	2 ± 0.4	**$8_{12,12,12}$**	short-range positional order	[64]
Au	2 ± 0.4	**$8_{0,12,12}$**	short-range positional order	[64]
Au	2 ± 0.4	**$8_{0,8,0}$**	C_6:Sm; C_8: Sm; C_{12}:Sm; C_{18}:Sm	[64]
Au	2 ± 0.4	**9**	C_6:Sm; C_8: Sm; C_{12}:Sm; C_{18}:Sm	[64]

[a]LC = unidentified mesophase; Cr = crystal; Sm = smectic; ModSm = modified smectic; N = nematic; Cub = cubic; Col = columnar; Iso = isotropic liquid, Meta = metastable mixture.

ligands attached to the NPs after the exchange process to be ~150–215, which indicated a very dense packing on the surface. Thermal analysis indicated three thermal events for hybrids **Au@6$_{8–12}$** at ~85 °C, ~100 °C and ~150 °C (Table 1), with arguments based on thermochemical values suggesting that the first corresponded well to a melting transition, whereas the third event was reminiscent of a nematic-to-isotropic phase change due to the low enthalpy involved. The X-ray results indicated that the hybrid systems displayed complicated metastable behaviour, with the possible coexistence of more than one phase. In order to rationalise the results, the authors proposed a tactoidal geometry of the NPs, whereby the ligands formed two extended "hard" poles on the nanoparticles and a "soft" equator around the middle, which can be seen as an elaboration of the mechanism proposed previously [61] (Figure 6).

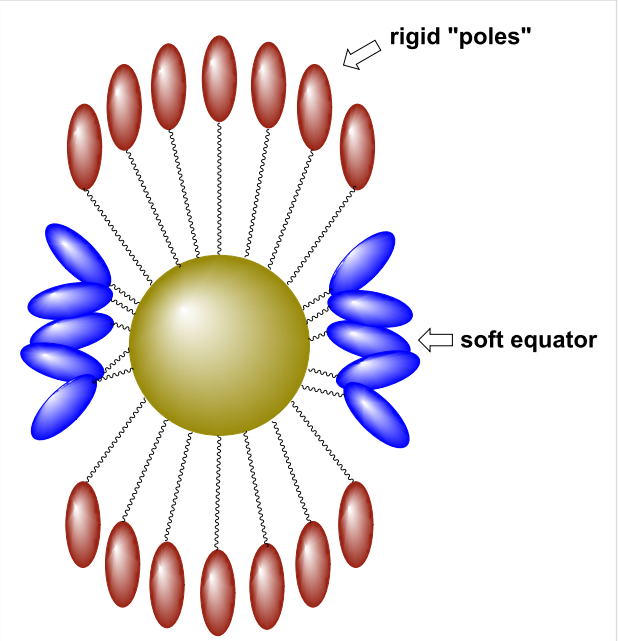

Figure 6: Ligand deformation at the surface of the gold NPs giving rigid "poles" and a soft equator. Such deformations impart the necessary anistropy to the system to impart LC behaviour. Adapted from [62].

Thus a tentative structural model was proposed whereby the NPs exhibit a local rectangular (or hexagonal) arrangement, with a local smectic A_2 order for the head-to-tail regions, and local smectic A_d order for the equators (Figure 7).

In a departure from cyanobiphenyl based ligands, smectic and columnar structures were observed in a large and systematic study for systems involving swallow-tailed rodlike mesogenic thiols **7$_{9,9}$**, **7$_{4,4}$**, **7$_{1,6}$** and **7$_{2,5}$** [63,64] (Figure 8) grafted onto 2.0 ± (0.2–0.4) nm Au NPs in two-step, solvent-mediated exchange processes. The authors noted that, for **Au@C$_{10}$/7$_{9,9}$**, **Au@C$_{10}$/7$_{4,4}$** and **Au@C$_{10}$/7$_{1,6}$** within the experimentally investigated limits of 1:2 and 1:1 mesogen/alkylthiol surface ratios, no differences in phase behaviour were observed [63]. Interesting results were reported for hybrids of ligand **7$_{9,9}$**, a rod-shaped ligand devoid of LC phases, whereby X-ray analysis of **Au@C$_{10}$/7$_{9,9}$** indicated the formation of a smectic A phase (Table 1). An explanation as to how nominally spherical particles could form a smectic A phase was derived from the observation that the thickness of the organic sheath between the layers was greater than the distance between NPs within the layers. This implied that there was some redistribution of the mesogenic groups on the surface towards opposite “poles” of the NPs to give cylinder-shaped hybrids (Figure 9). This mechanism of mesophase induction differs from those discussed previously [61,62] due to the presence of a mixed ligand shell about the metal centre, and thus the importance of ligand migration about the surface in the production of anisotropic hybrids is far more pronounced. It was noted, however, that the organic sublayer was less than twice the length of two rodlike ligands placed end-to-end, and thus the authors concluded that the rodlike ligands remained orientationally and positionally disordered and probably partially interdigitated. The liquidlike nature of the organic sublayer was confirmed by X-ray experiments, and the lack of observable birefringence in the sample was taken as further evidence of the orientational disorder of the molecules inside the organic layer of the smectic materials.

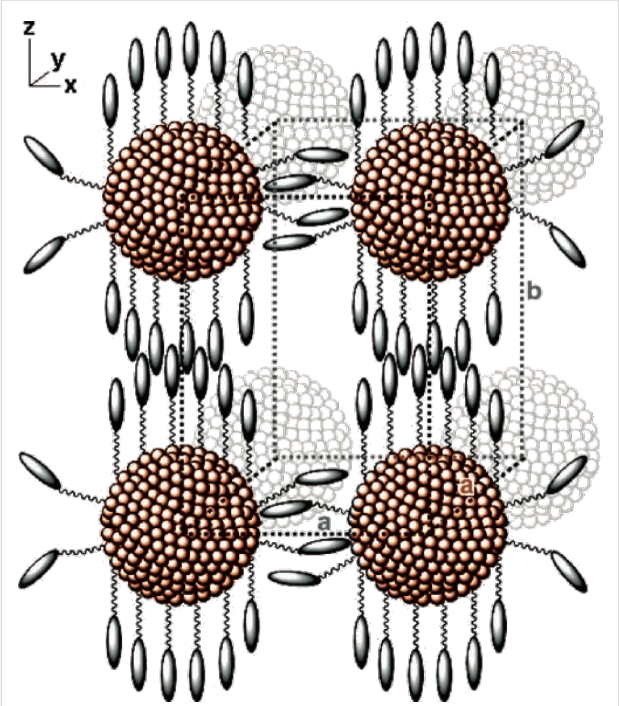

Figure 7: A simplified illustration of the local rectangular arrangement of nanoparticles in a condensed mixed phase. Reprinted with permission from [62]. Copyright 2011 Wiley-VCH Publishers.

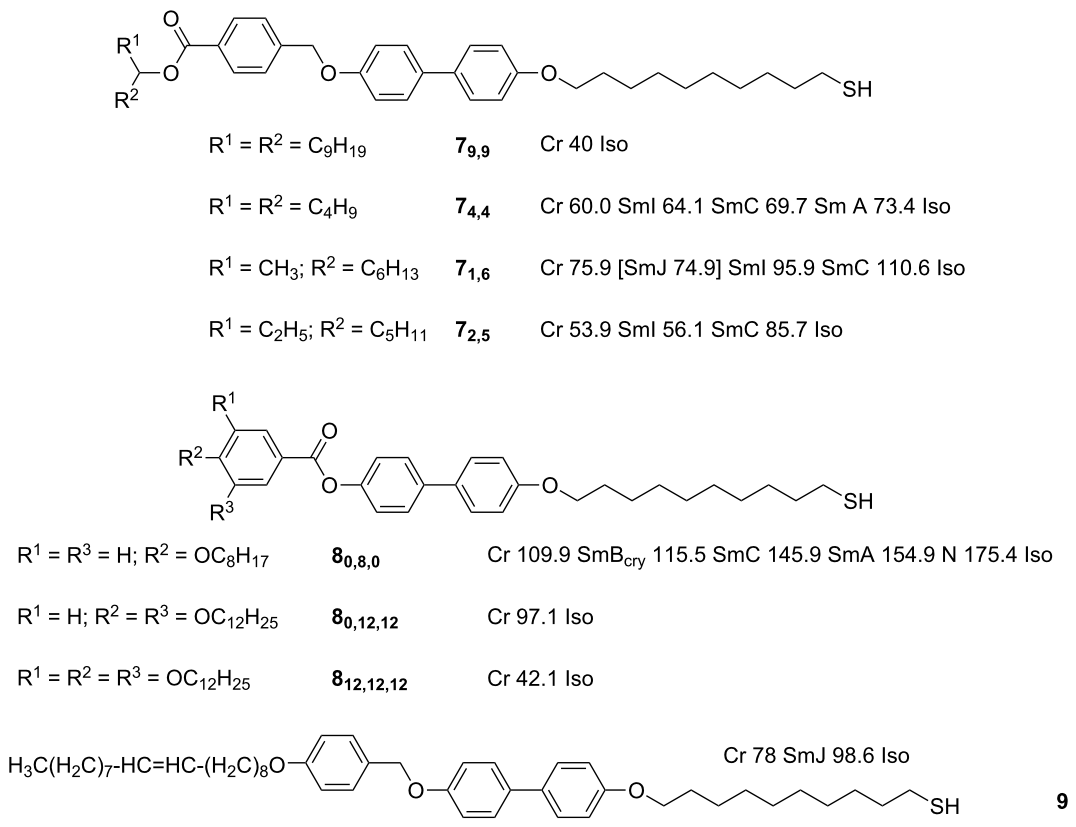

Figure 8: Chemical structures and LC properties of the rodlike ligands discussed in the text.

The role of subtle changes to the mesogenic ligand in determining the LC phase of the hybrids was highlighted by the results observed for the mesogenic thiols $\mathbf{7_{4,4}}$, and $\mathbf{7_{1,6}}$, which differ from $\mathbf{7_{9,9}}$ only in the length of the alkyl chains on the periphery of the molecule. In the case of **Au@C$_{10}$/7$_{4,4}$** and **Au@C$_{10}$/7$_{1,6}$**, the smectic arrangement observed for **Au@C$_{10}$/7$_{9,9}$** was replaced by columnar structures (Table 1), with the columns organised into body-centred orthorhombic unit cells, and an arrangement very close to being hexagonal. This arrangement is possible by shifting of the particles by *c*/2 along the column axis, which can be readily changed into the smectic phase through another shift of *c*/2, followed by positional decoupling of the layers along the *c* axis (Figure 9).

Interestingly, the important role of the alkylthiol coligand (referred to as the "primary grafting layer") in determining the LC behaviour of these swallow-tailed hybrids was also demonstrated [64] (the effect of the primary grafting layer had been investigated previously for NPs coated with laterally substituted mesogens [65], see below). It was found that the superstructures of the NPs coated with ligands $\mathbf{7_{1,6}}$ and $\mathbf{7_{2,5}}$ were affected by the length of the *n*-alkylthiols in the primary grafting layer. In these cases, particles that were grafted with short hexanethiols in the primary layer (**Au@C$_6$/7$_{1,6}$** and **Au@C$_6$/7$_{2,5}$**) exhibited smectic phases, whilst increasing the length of the *n*-alkylthiols invoked the formation of modulated smectic and columnar phases (Figure 10). The ligand migration model fits these results well as it explains the formation of the phases based on a geometrical shift from a cylindrical shape for the shorter primary grafting layers, to a more ellipsoidal (or "tricylindrical") shape for those particles with a primary grafting layer composed of longer *n*-alkylthiols (i.e., a "bulge" at the equator of the cylinders).

More pronounced changes in the structure of the grafted (proto-)mesogenic ligands produced rather significant changes in the phase behaviour of the resulting hybrids in the case of **Au@8$_{0,8,0}$**, **Au@8$_{0,12,12}$** and **Au@8$_{12,12,12}$** (Table 1). Whilst the particles coated with proto-mesogenic hemi-phasmidic ligands $\mathbf{8_{12,12,12}}$ and $\mathbf{8_{0,12,12}}$ (Figure 8) displayed only short-range positional order, particles coated with the single-chain mesogenic ligand $\mathbf{8_{0,8,0}}$ (Figure 8) displayed smectic phases, irrespective of the length of the primary grafting layer [64]. These latter results were mirrored for the structurally similar single-chained ligand **9** (Figure 8), which displayed an increase in the interparticle distance within the smectic layers upon an

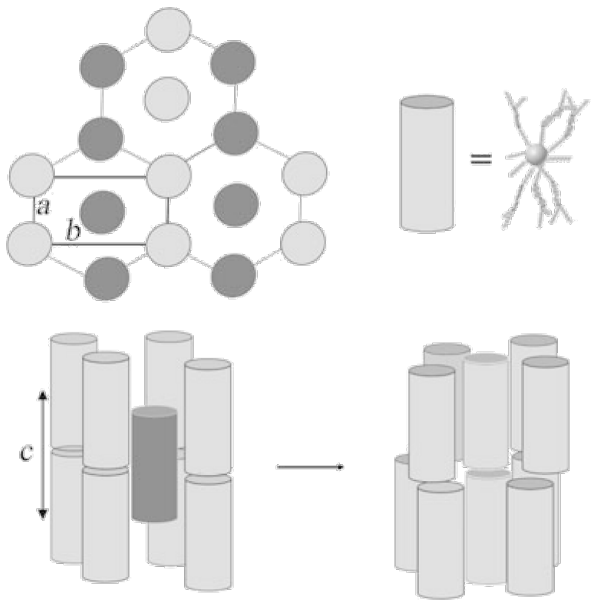

Figure 9: Schematic drawing of the arrangement of nanoparticles in the columnar phase, as viewed from above (top left) and from the side (bottom). The rearrangement of the ligands about the gold NP to form a cylinder is shown (top right). The smectic structure for **Au@C$_{10}$/7$_{9,9}$** (bottom right) can be obtained from the columnar phase for **Au@C$_{10}$/7$_{4,4}$** and **Au@C$_{10}$/7$_{1,6}$** (bottom left) through movement of the particles from the intermediate layer along the column axis and decoupling of the layers. Reprinted with permission from [63]. Copyright 2009 Wiley-VCH Publishers.

increase in the length of the primary grafting layer. Once again, the orientational disorder of the organic layers was also confirmed by the lack of birefringence in the samples, and the ligand-migration model was used to explain the smectic phases arising from the formation of cylindrical hybrid moieties. This behaviour is reversible upon further heating to the isotropic state, whereby the ligands rearrange to give pseudospherical particles again (Figure 11). The authors argued that the lack of mesogenic behaviour observed for hybrids **Au@8$_{0,12,12}$** and **Au@8$_{12,12,12}$** was due to the large volume required to accommodate the polycatenar ligands at the poles of the NPs, which would create cylinders "pinched" in the middle, and thus unable to arrange themselves into a suitable mesophase structure.

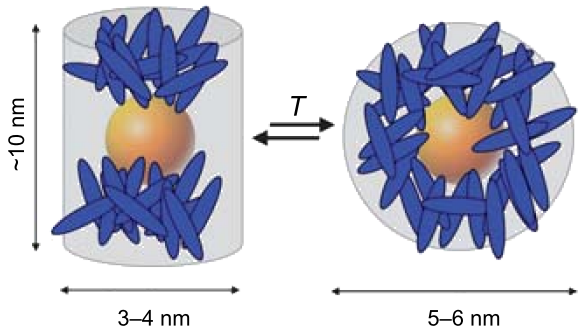

Figure 11: Reversible migration of the surface ligands as a function of temperature (and phase). Only the blue mesogenic ligands are depicted in this image. Reprinted with permission from [64]. Copyright 2010 Wiley-VCH Publishers.

It is also worth briefly mentioning a couple of examples in which rodlike mesogenic or proto-mesogenic ligands have been grafted to NPs for studies focused on properties other than liquid crystallinity, in order to emphasise the wider applicability of this approach to nanohybrid science. Fundamental studies into the photochemical activity of lipophilic azobenzene- and stilbene thiols (**10**, Figure 12) on Au NPs surfaces were reported [66], which indicated a chromophore-to-NP distance dependence of the photoisomerisation and photodimerisation efficiency in these systems. Interesting examples of the potential application of this type of approach were shown by the grafting of similar azobenzene ligands **11** (Figure 12) to the surfaces of γ-Fe_2O_3 [67] and FePt [68] NPs, which exhibited a photoswitchable change in magnetisation, and which the authors attributed to a change in the electric polarisation at the

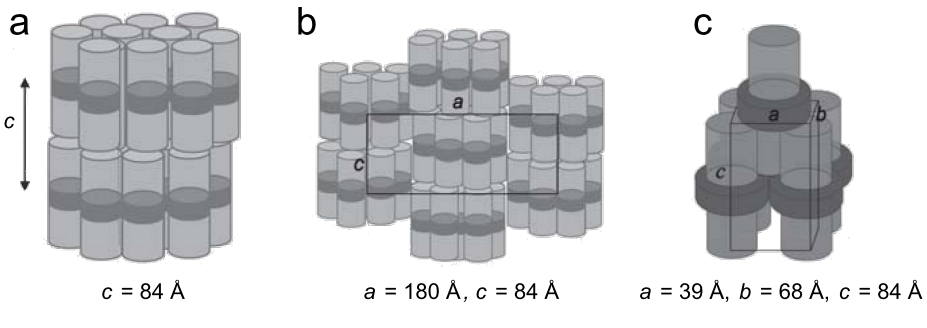

Figure 10: The proposed structural models resulting from ligand migration at the NP surface: (a) Smectic (**Au@C$_6$/7$_{1,6}$**) (b) modulated smectic **Au@C$_8$/7$_{1,6}$**, (c) columnar (**Au@C$_{12}$/7$_{1,6}$**). Light grey and dark grey indicate the disposition and form of the mesogenic groups and alkylthiols respectively. Reprinted with permission from [64]. Copyright 2010 Wiley-VCH Publishers.

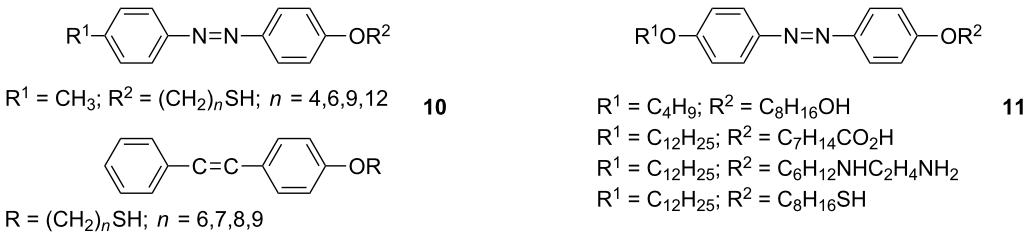

Figure 12: Photochromic and photo-mesogenic rodlike ligands.

surface induced by the *cis–trans* isomerisation of the azo moiety upon irradiation, although no indication was given as to whether the hybrids displayed any mesophase behaviour.

Nanoparticles coated with rodlike proto-mesogenic ligands: Side-on attachment

The first assignment of a nematic phase for a pseudospherical NP was realised through the use of a laterally substituted rodlike mesogenic thiol (**12**, Figure 13) [69]. In this study, Au-NPs of diameters 1.6 ± 0.4 nm were targeted because of their small size and low polydispersity, such that the size variations in the NPs were lower than the maximum size of the mesogenic thiol used. The final hybrids were prepared according to the two-step process, through solvent-mediated ligand exchange of hexanethiol coated NPs with **12**, to give a final surface coverage of 1:1 as determined by ^{1}H NMR analysis. Through thermal analysis, POM and miscibility experiments, the existence of the nematic phase was deduced (Table 2), as evidenced by the *Schlieren* and marbled textures observed under crossed polarisers (Figure 14).

The success of this approach prompted further work involving a slightly longer rodlike side-on nematogenic ligand (**13**, Figure 13), which was grafted in a solvent-mediated exchange process onto hexane- or dodecanethiol protected Au NPs of 1.7–2.0 nm diameter [70]. NMR spectroscopic analysis of the products indicated that the final alkylthiol:mesogen surface concentrations were ~2:1. Partial coverage of the surface led to

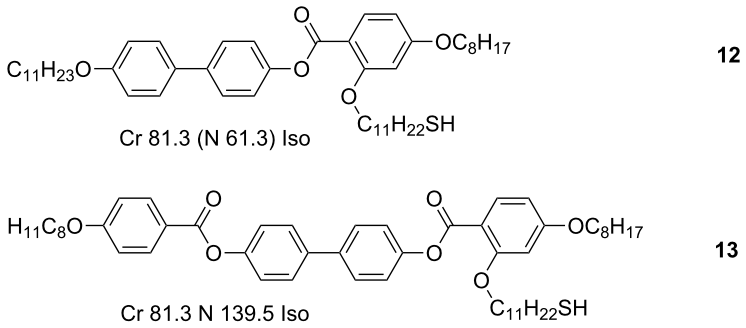

Figure 13: Chemical structures and LC properties of side-on mesogens used to coat NPs.

Table 2: Summary of the phase behaviour of the hybrid NPs with laterally substituted ligands discussed in the text.[a]

NP type	NP size (nm)	Ligand	Phase assignments (Temp. °C)	Ref.
Au	1.6 ± 0.4	**12**	g −3 N 43.8 Iso	[69]
Au	1.7 ± 0.4	**C_6/13**	Cr 73.1 N[b] 118.7 Iso	[70]
Au	2.0 ± 0.4	**C_{12}/13**	Cr 45.7 N[b] 126 Iso	[70]
Au	1.7 ± 0.4	**C_6/13**	Col_r 80 Col_h 118.7 Iso	[65]
Au	2.0 ± 0.4	**C_{12}/13**	$R\bar{3}m$ 126 Iso	[65]

[a]Cr = crystal; N = nematic; Col_r = columnar rectangular; Col_h = columnar hexagonal; g = glass; Iso = isotropic liquid. [b]Provisional nematic assignment, although subsequent experiments indicated a columnar structure.

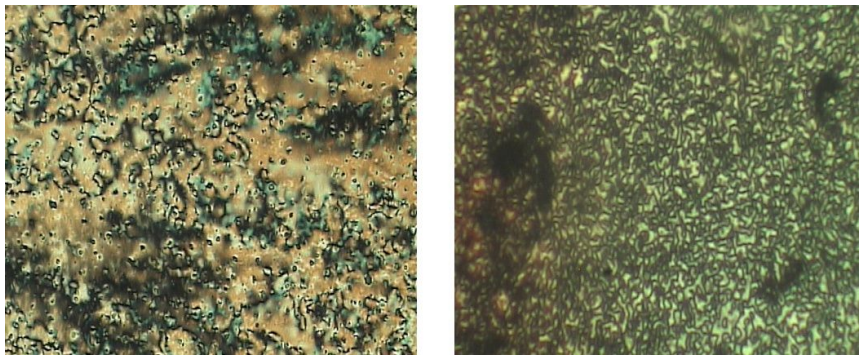

Figure 14: Left: POM image of ligand **12**. Right: POM image of *Schlieren* texture of the hybrid **Au@12**. Reprinted with permission from [69]. Copyright 2006 American Chemical Society.

thermally unstable hybrids, due to delamination and/or surface reorganisation of the ligands. As reported for the related system above [69], both the hexane- and dodecanethiol coated hybrids **Au@C$_6$/13** and **Au@C$_{12}$/13** exhibited mesogenic behaviour, attributed to the formation of an enantiotropic nematic phase, which displayed typical marbled or *Schlieren* textures by POM. Furthermore, the hybrids showed complete miscibility with the neat ligand and its olefinic precursor, which was interpreted as providing further evidence of the existence of a nematic phase. It was noted that the defect textures were formed more easily in the shorter chain hexanethiol system, possibly as a result of greater freedom of movement for the mesogenic groups at the surface. The chain lengths also played a role in the different melting temperatures (45.7 °C for **Au@C$_{12}$/13** versus 73.1 °C for **Au@C$_6$/13**, Table 2), with the potential plastifying effect of the longer chains being invoked as a possible explanation. Particles coated exclusively with **13** showed only a glass transition, and this was attributed to the lack of orientational mobility of the mesogenic groups at the surface of the NPs.

In a subsequent report, a more detailed investigation into the hybrids obtained from ligand **13** and Au NPs was undertaken [65]. Roughly 40% of the protective hexane- or dodecanethiol ligands were exchanged with **13** by using the two-step process, and the hybrids were examined by POM, X-ray and TEM techniques. The hybrids coated with primary dodecane- and hexanethiol layers (**Au@C$_{12}$/13** and **Au@C$_6$/13**) displayed optically isotropic phases above 126 °C and 119 °C, respectively (Table 2), but a birefringent threaded texture typical of a nematic phase below these temperatures (Figure 15).

Interestingly, X-ray analysis of **Au@C$_{12}$/13** (Figure 16a) and **Au@C$_6$/13** (Figure 16b) indicated that the particles were arranged into columns in both cases. In the case of **Au@C$_{12}$/13** the GISAXS pattern indicated a rhombohedral lattice ($R\bar{3}m$ space group), the columns being arranged in a triangular lattice,

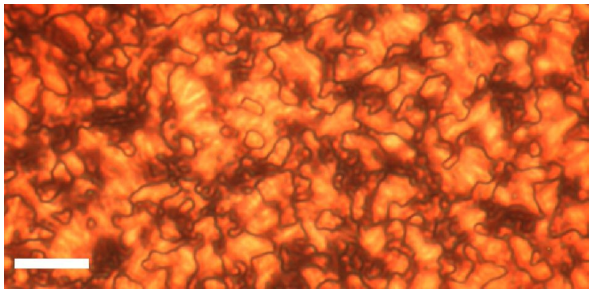

Figure 15: Threaded nematic texture of **Au@ C$_{12}$/13** as observed by POM at RT. Scale bar = 10 µm. Reprinted with permission from [65]. Copyright 2009 Wiley-VCH Publishers.

with the three columns displaced along the *z*-axis by 0, *c*/3 and 2*c*/3 (Figure 16a). The $R\bar{3}m$ structure of the LC phase was also confirmed by TEM observation, whereby a triangular lattice is observed when viewing the phase down the [001] axis, and stripes are observed when the sample is viewed perpendicular to the $[1\,\bar{1}\,1]$ direction (Figure 17).

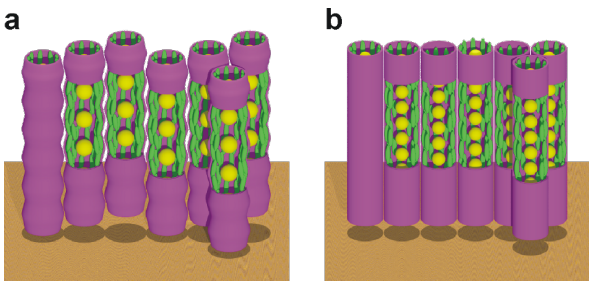

Figure 16: Schematic representation of the gold NP columnar structures. (a) Rhombohedral phase in **Au@C$_{12}$/13** and (b) hexagonal columnar phase in **Au@C$_6$/13**. Gold NPs = yellow, ligands = green. Reprinted with permission from [65]. Copyright 2009 Wiley-VCH Publishers.

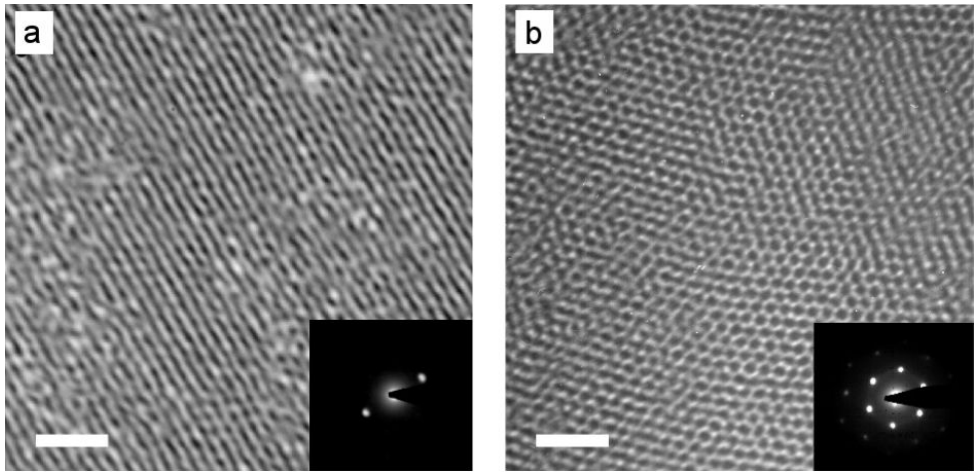

Figure 17: TEM images of thin films of the $R\bar{3}m$ phase of **Au@C$_{12}$/13** recorded with the beam (a) parallel to the $(1\bar{1}1)$ plane and (b) parallel to the [001] axis. Scale bar = 20 nm. Insets show the corresponding electron-diffraction patterns. Reprinted with permission from [65]. Copyright 2009 Wiley-VCH Publishers.

Between 30 and 80 °C, **Au@C$_6$/13** exhibited a 2-D rectangular lattice with a plane group of *c*2*mm*, whereas above 90 °C the lattice was 2-D hexagonal, *p*6*mm*, with the transition arising from shrinking in the *a* direction. Thus, there was 2-D lateral long-range ordering of the columns in the case of **Au@C$_6$/13**, whereas **Au@C$_{12}$/13** displayed evidence of 3-D long-range ordering. The structural model indicated that both **Au@C$_{12}$/13** and **Au@C$_6$/13** were comprised of NP columns, with the surrounding mesogens axially aligned in the column direction. Despite these results, however, the optical textures and defects observed with POM were distinctly characteristic of a nematic phase, and thus implied the absence of any positional order.

This study clearly highlighted the important role of the connectivity and morphology of the ligands in orienting the pseudospherical NPs [71] into the columnar structures observed. Columnar ordering of pseudospherical cores functionalised with laterally substituted mesogens has been observed previously for liquid-crystalline silsesquioxanes [72-74], indicating that this self-assembly motif may prove to be quite general. Importantly, this work demonstrated that the interparticle spacings within the columns could be modulated not only by the combined effects of the mesogenic and alkylthiol coligands (16.5 Å for **Au@C$_{12}$/13**, and 4.8 Å for **Au@C$_6$/13**), but also during the rectangular to hexagonal phase change for **Au@C$_6$/13**. These results are of interest due to the fact that, by controlling and modulating the interparticle distances through ligand design and thermally induced phase changes, one can also anticipate the possibility of controlling the electronic and magnetic properties of nanoparticle assemblies that depend on interparticle separations [7,14].

Nanoparticles coated with bent-core ligands

Bent-core mesogens display a bend in their molecular structure (Figure 18), which leads to new packing motifs and provides the possibility of forming mesophases exhibiting polar order and chiral superstructures, even in the absence of any intrinsic chirality. These interesting and unique properties have made them attractive targets in research and development, both academically and for potential applications such as electro- and nonlinear optical devices and photonics [34,75]. This interest has extended to the new field of liquid-crystalline nanoparticles, and some preliminary investigations into the integration of bent-core mesogens into new NP hybrids have been reported.

An early report investigated the grafting of bent-core ligands **14$_{10,10}$** and **14$_{12,11}$** (Figure 18) to hexanethiol coated Au NPs with diameters of 2.8 ± 0.6 and 2.5 ± 0.5 nm by TEM (3.9 ± 1.5 nm and 2.4 ± 0.8 nm by XRD), respectively, in a two-step process to give a 1:1 mixed monolayer coverage [76]. Bent-core ligand **14$_{10,10}$** displayed a monotropic LC phase whilst **14$_{12,11}$** was not mesomorphic. Unfortunately, the hybrids did not display any LC phases, though they could be dispersed into some selected bent-core LC hosts, which showed evidence of a reduction in the electro-optical response time, τ, but a relatively unaffected spontaneous polarisation, *P*. The lack of mesophase behaviour for the pure hybrids was attributed, at least in part, to the high transition temperatures of the bent-core ligands essentially preventing any mesophase development before the onset of sample decomposition through thiol desorption. In another report, despite the success in producing mesophases with Au NPs with a variety of rodlike mesogens, side-on grafting of polycatenar bent-core mesogen **15** (Figure 18) onto

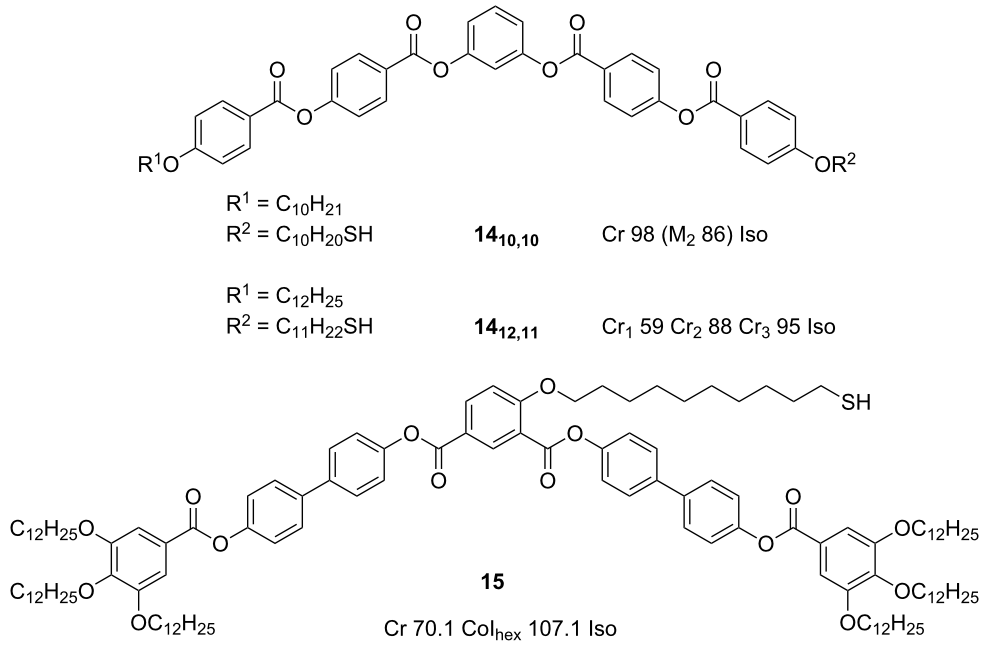

Figure 18: Chemical structures and mesogenic properties of bent-core proto-mesogenic ligands used to coat NPs.

decanethiol protected 2.0 ± 0.2 nm Au NPs also failed to produce any LC phases, although X-ray analysis indicated that the hybrid may exhibit some short range fcc or distorted icosahedral structure arising from the presence of cybotactic groups up to 200 °C [63].

Nanoparticles coated with proto-dendritic ligands

One of the major design factors that must be considered when preparing hybrid NPs for potential LC applications is the relative sizes of the core and the organic shell. It stands to reason that as the thickness ratio between the ligand and the NP increases, the shape-directing properties of the deformable organic shell become more dominant, and thus this parameter could be a powerful tool in the preparation of LCNPs. Increasing the size ratio of the organic component can be achieved by either decreasing the size of the core particle, and/or increasing the thickness of the surrounding molecules, with the latter approach finding success for example in the case of polymer-coated NP hybrids [38-41]. Dendrimers and dendrons offer some advantages in this context, due to the ability to exert a high degree of control over their structure and composition, with their size readily increased through additional generational growth. These properties have led to their exploitation in a number of applications, from catalysis and molecular electronics to nanomedicine [77], and their use in liquid crystal applications is relatively well established [31,78]. Recognising this potential, a study was reported [79] in which a series of liquid-crystalline and non-liquid-crystalline dendrons were prepared containing thiol or disulfide groups within their structures. Hybrid Au NP materials were prepared with cyanobiphenyl terminated dendron **16** (Figure 19) by using both direct and solvent-mediated ligand exchange methods. The direct method produced very small Au NPs of diameter 1.2 ± 0.4 nm coated exclusively with dendron **16**. Using the two-step method, hybrid Au NPs with diameters of 1.7 ± 0.4 nm were prepared, with a surface concentration of approximately 40% of the mesogenic dendron on the surface, as determined by ^{1}H NMR spectroscopy. Unfortunately, both of the hybrids with 100 and 40% loading of **16** failed to display any mesomorphic properties, although the fully covered hybrids were able to form highly ordered structures on carbon-coated copper grids (Figure 20). Interestingly, the NPs organised themselves into stripes or rows, with a gap of 6.5 nm between the rows (i.e., 1.3 times the length of compound **16**), but smaller than 1 nm within any given row. This organisation was far less pronounced in the sample containing 40% of **16** on the NP surface. Whilst these compounds did not exhibit any LC phases, the results of the surface arrangement of these hybrids are useful for considering how the ligands are disposed about the metallic centre, and how they interact with each other. The authors proposed that the cyanobiphenyl groups must be interdigitated between the rows, giving a smectic-type arrangement on the surface, with the extremely short interparticle distance within the rows implying

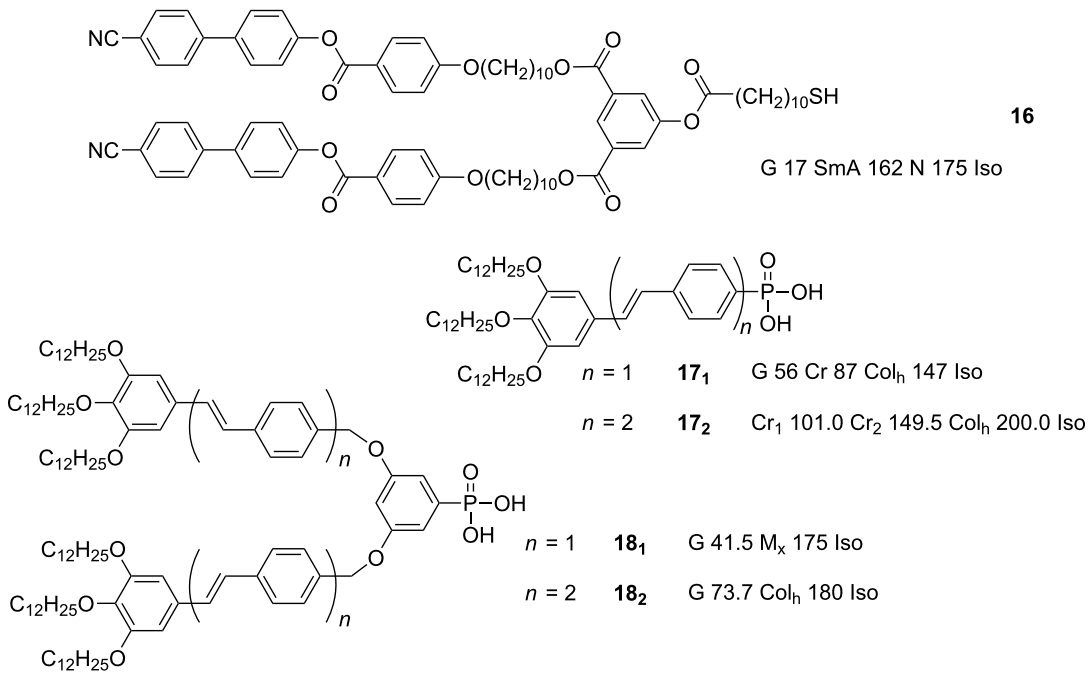

Figure 19: Chemical structures and mesogenic properties of dendritic and proto-dendritic ligands used to coat NPs.

that the hybrids are highly anisotropic in shape, either from ligand migration on the surface to the poles of the NPs, and/or through a significant orientational bias of the ligands away from the particle equators towards the poles.

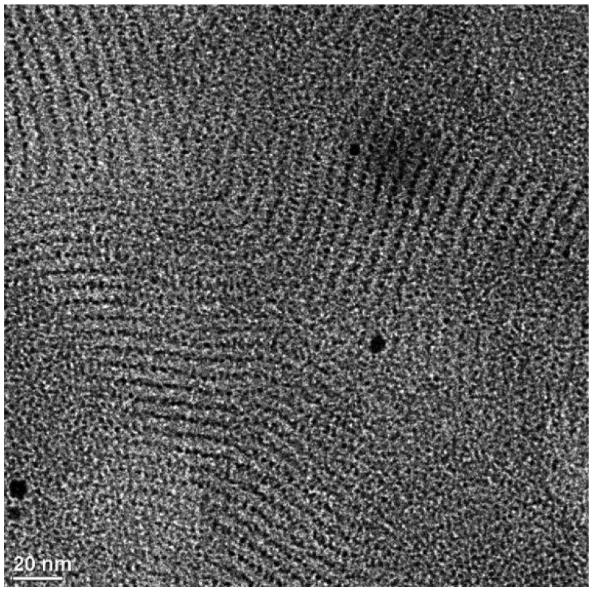

Figure 20: TEM image showing the arrangement of the hybrid NPs **Au@16** into regularly spaced rows. Reprinted with permission from [79]. Copyright 2008 Wiley-VCH Publishers.

In a departure from the work on gold NPs, an investigation into the functionalisation of pseudospherical ferrite NPs with luminescent prodendritic ligands was undertaken in order to investigate the thermal, magnetic and luminescent properties of the resulting hybrids [80]. The protodendritic oligo(phenylene vinylene) derived ligands included phosphonic acid functional groups (**17** and **18**, Figure 19) for anchoring onto the surface of the NPs. The ferrite nanoparticles were prepared by using a coprecipitation method, followed by a hydrothermal growth process to give cuboidal NPs of 39 ± 5 nm width. These particles were then functionalised with the OPV ligands by direct grafting in solution, followed by purification by magnetic separation or centrifugation, to give surface coverages of 100% for the polycatenar G0 ligands $\mathbf{17_1}$ and $\mathbf{18_1}$ and 67% and 88% for the G1 ligands $\mathbf{17_2}$ and $\mathbf{18_2}$, respectively, as determined by TGA and UV–vis spectral analyses. Whilst the dendronised NPs maintained their intrinsic magnetic properties, none of them displayed any mesophases, and the simplest explanation for this begins with the large size discrepancy between the ligands and the NPs, combined with the potentially unfavourable morphology of the cuboidal NPs (although large size discrepancies between ligand and NP did not appear to inhibit LC formation in the case of large anisotropic, including cuboidal, NPs previously [58,59], see above). In this case, the rigidity of the ligands coupled to the lack of a flexible spacer between the ligand and NP surface probably also played a role

in inhibiting LC-phase formation, although similar systems involving the direct attachment of rigid rodlike ligands without a flexible spacer to Au NPs allowed their incorporation into a nematic LC host [81]. Ligands **17** and **18** would be unable to distort to any significant extent, and furthermore, they would not have been of sufficient bulk to induce anisotropy to the hybrids, serving merely as potential "lubricants" to reduce interparticle interactions through their long terminal alkyl chains.

At this point, it is worth noting that much of the work reported on liquid-crystalline NPs has involved the use of mesogenic ligands grafted to the NP of choice in order to induce mesophases in the resulting hybrids. An alternative holistic approach, whereby none of the constituent parts are mesomorphic in isolation, but which display mesomorphic phases upon their combination into one hybrid system has also been reported [82]. This publication was the first to report on dendrimer-functionalised gold NPs that exhibited a thermotropic cubic phase and 2-D hexagonal arrangement on a surface.

Dodecanethiol coated Au NPs of diameter 2.1 ± 0.5 nm were partially coated with dendron **19** (Figure 21) by solvent-mediated ligand exchange to give a final surface coverage of ~4:5 dendron to dodecanethiol. This represents a rather dense surface coverage, corresponding to an average chain cross-sectional area of A_{Chain} = 18.1 ± 0.5 Å^2, which is below the value of 21.4 Å^2 expected for alkanethiols on flat gold surfaces. This discrepancy was rationalised as being due to the ability of the thiols to adsorb also at the edges between the flat polyhedral faces of the nanoparticle surface, thus increasing the effective loading relative to a macroscopic planar system.

The dendritic part was decoupled from the NP surface by a dodecyl chain spacer to allow flexibility and to maintain the conical dendron structure at a distance from the NP. This was thought to be advantageous for enhancing the interparticle interactions and to aid in the stabilisation of the mesophase, with the peripheral alkyl chains included to ensure that the system was fluid. The overall design of the hybrid resembled that of spherical micellar structures, which are good candidates for the formation of cubic arrangements in the mesophase.

Differential scanning calorimetric and SAXS analysis of the hybrid indicated a melting transition at −12.2 °C (heating)/−16.5 °C (cooling), and that the particles possessed liquidlike order between −10 °C and 60 °C (Table 3), which changed to a cubic-lattice arrangement of space group $Im\bar{3}m$ at higher temperatures (i.e., the packing arrangement of the material involved the cubic arrangement of a single type of pseudospherical (truncated octahedral) hybrid particle, one at

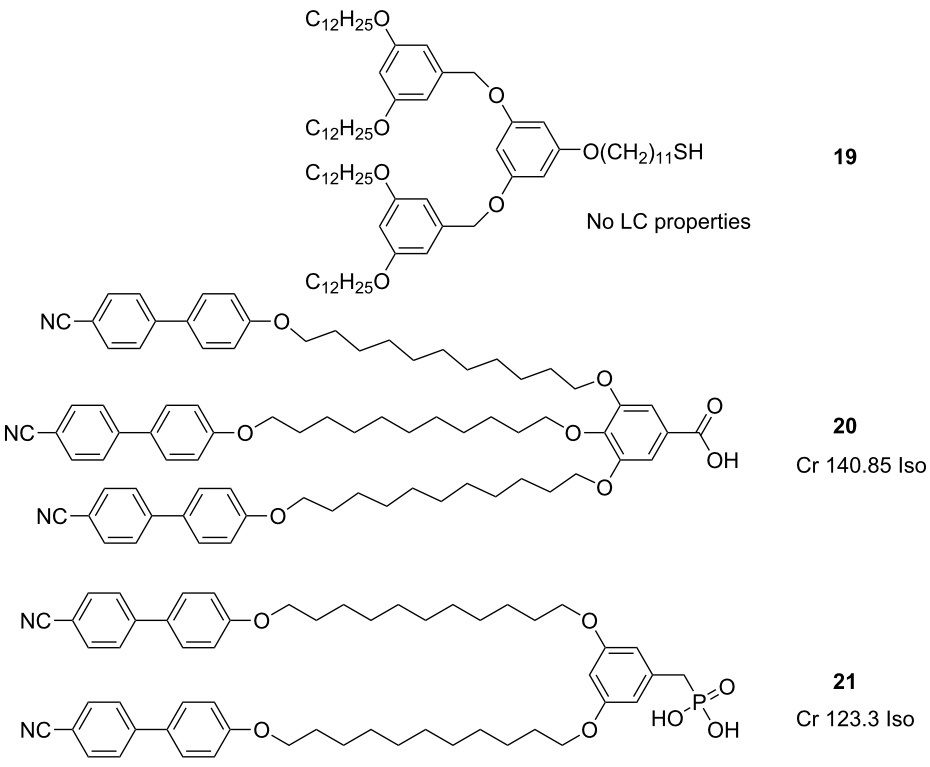

Figure 21: Chemical structures and mesogenic properties of dendritic and proto-dendritic ligands used to coat NPs.

Table 3: Summary of the phase behaviour of the hybrid NPs with dendritic and proto-dendritic ligands discussed in the text.

NP type	NP size (nm)	Ligand	Phase assignments (Temp. °C)[a]	Ref.
Au	2.1 ± 0.5	**19**	Cr −12.2 Iso 70–80 Cub 180 Dec	[82]
Fe_2O_3	3.3 ± 0.7	**20**	g 40–60 N 180.2 Iso	[85]
Fe_2O_3	3.3 ± 0.7	**21**	g 30–50 N 174.2 Iso	[85]

[a]Cr = crystal; N = nematic; Cub = cubic; g = glass; Iso = isotropic liquid; Dec = decomposition.

the corners and one at the centre of the unit cell; Figure 22). This "inverse-melting" thermal behaviour is a relatively uncommon phenomenon, but it has been observed in various chemical systems [83] and is known as "re-entrance" [84].

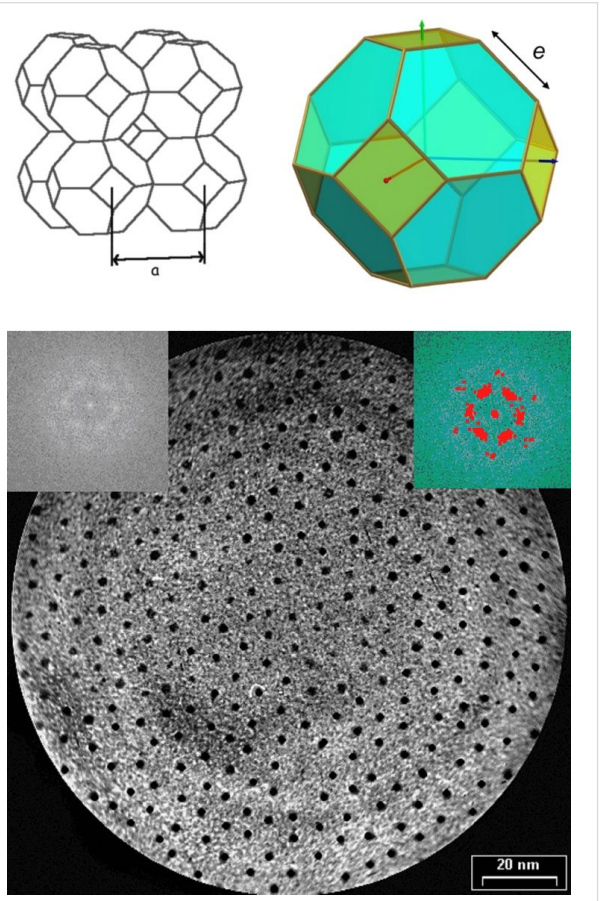

Figure 22: Top left: Body-centred (I) cubic lattice of $Im\bar{3}m$ symmetry composed of truncated octahedrons. Top right: The truncated octahedron—a semiregular Archimedean tetradecahedron. Bottom: Self-organisation in a hexagonal lattice as observed by TEM. Reprinted with permission from [82]. Copyright 2007 Wiley-VCH Publishers.

The dendronised nanoparticles spontaneously self-assembled into a hexagonal lattice on the TEM grid: The mean distances between first and second neighbours were about 7.6 and 13.7 nm, respectively, in very good agreement with the NP diameter and the dendritic shell (Figure 22). This system also displayed ferromagnetism between 1.8 K and 400 K, and an unusually slow magnetic relaxation, which reaches a maximum at around the transition temperature between the isotropic liquid and the cubic phase [86]. These results are of interest from the standpoint of information storage applications, and could lead to the development of new materials with novel magnetic properties.

In another report in which a similar approach was utilised [85] the synthesis and functionalisation of pseudospherical magnetic ferrite NPs [87] with pro-mesogenic ligands was described. The NPs were synthesised by the thermal decomposition of iron oleate complexes at high temperature in high-boiling-point solvent to give products of 3.3 ± 0.7 nm diameter. The cyanobiphenyl terminated ligands **20** and **21** (Figure 21) with carboxylic acid and phosphonic acid anchoring groups, respectively, were grafted onto the surface of the NPs by means of a ligand-exchange process to displace some of the adsorbed oleate protective layer. Thermogravimetric analysis was used as a means of determining the surface loading of the ligands, and the results indicated that the phosphonic acid derivative (100 ± 10 **21** : 50 ± 10 OA) was three times more efficient at adsorbing to the surface than the carboxylic acid derivative (30 ± 10 **20** : 95 ± 10 OA). Ligands **20** and **21** were both non-mesogenic, directly melting into isotropic liquids at 140.5 °C and 123.2 °C respectively, whereas the hybrids exhibited higher clearing temperatures of ~180 °C (**Fe_2O_3@20**) and 174 °C (**Fe_2O_3@21**) (Table 3). Upon heating, the samples developed a low birefringent and fluid texture, which could not be assigned to any specific mesophase, and below 50–60 °C these mesophases froze into a glassy state.

X-ray analysis of the materials upon heating indicated average interparticle periodicities of 7.5 ± 0.5 nm (**Fe_2O_3@20**) and 6.9 ± 0.1 nm (**Fe_2O_3@21**), which corresponded well with the sizes of the NPs with their organic coatings. The correlation length for **Fe_2O_3@21** was found to be about three times that of **Fe_2O_3@20**, which the authors argued was caused by the increased cohesion between the hybrid NPs due to more efficient interdigitation of the cyanobiphenyl groups. The observation of a second, weak diffusion occurring at around 1.5 nm (**NP@20**) and 1.8 nm (**NP@21**) was assigned to weakly correl-

ated cybotactic clusters, as in classical nematic phases. Thus, the mesophase was assigned as a quasi-nematic phase consisting of a quasi-regular isotropic distribution of the NP nuclei within the organic matrix characterised by a local nematic order (Figure 23). This view of the packing was also confirmed by TEM imaging.

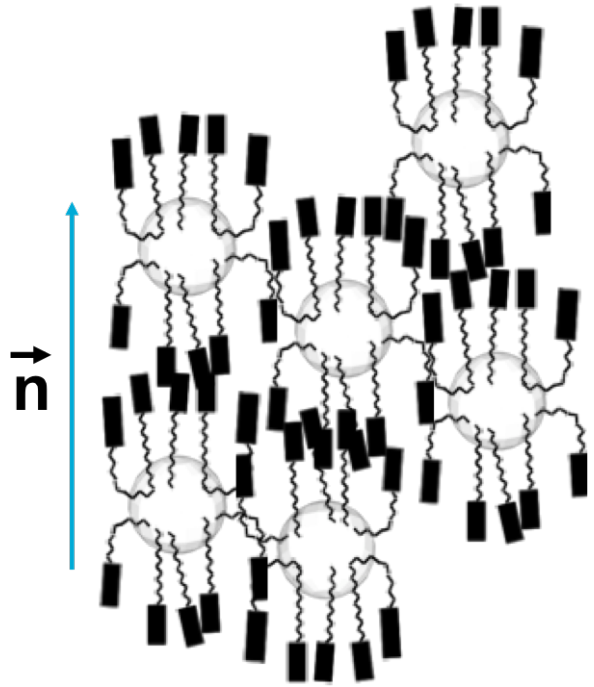

Figure 23: Model proposed for the organisation of the hybrids within the quasi-nematic mesophase. Reprinted with permission from [85]. Copyright 2010 Wiley-VCH Publishers.

A recent report [88] describes the grafting of dendrons $\mathbf{22_{1–3}}$ (Figure 24) to carboxylic acid functionalised Au NPs of diameters 5.9 ± 0.6, 6.8 ± 0.7 and 6.8 ± 0.8 nm through a surface amidation reaction. Interestingly, the hybrids only displayed 2-D hexagonal organisation (TEM) when coated with the second generation dendron $\mathbf{22_2}$, with a random arrangement observed for NPs coated with $\mathbf{22_1}$ and $\mathbf{22_3}$. This ordering behaviour was broadly consistent in 3-D as well, whereby hybrids coated with $\mathbf{22_1}$ and $\mathbf{22_3}$ showed no order, but the hybrid of $\mathbf{22_2}$ with Au NPs of 6.8 ± 0.7 nm diameter exhibited a primitive cubic phase after annealing of the sample.

Nanoparticles coated with discotic proto-mesogenic ligands

Discotic mesogens are those which display one molecular axis considerably shorter than the other two, and they are extensively investigated [89,90] due to their potential use in a variety of high-technology applications [89], perhaps most notably for opto-electronic devices [91] and organic electronics [92]. The basis for much of this interest lies in their inherent ability to self-organise into columnar structures, which exhibit directional properties, such as electrical conduction along the column axis.

Au NPs of 2.4 nm average diameter coated with triphenylene based mesogenic thiols $\mathbf{23_{6,6}}$ (Figure 25) were prepared by using the direct method to give a surface exclusively coated with the discotic ligands [93]. These materials did not display mesomorphism in the neat state, but were readily dispersed into the columnar phase of triphenylene discotic liquid crystals without disruption of the nature of the mesophase. Furthermore, thin films of $\mathbf{Au@23_{6,6}}$ displayed 2-D hexagonal ordering on

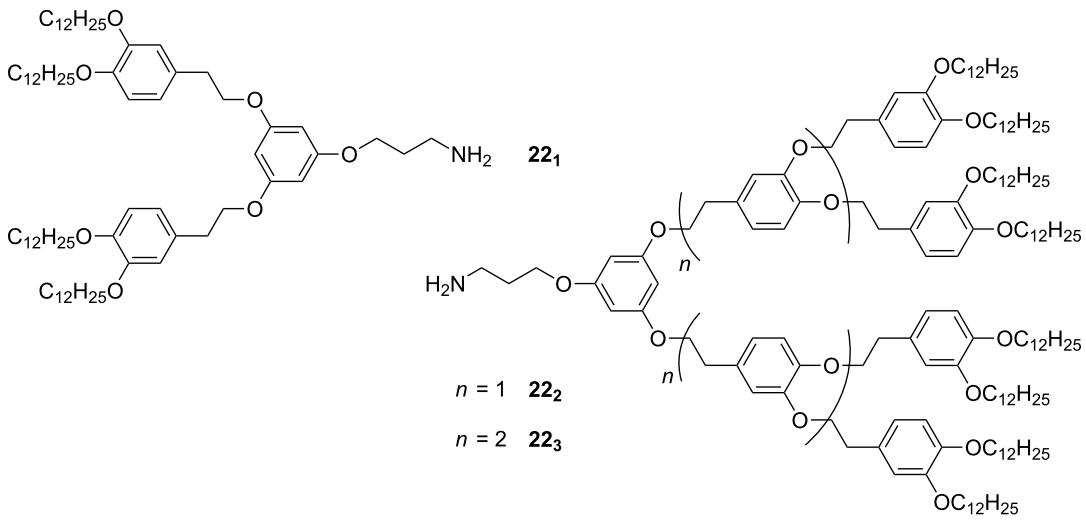

Figure 24: Mesogenic dendrons used to coat Au NPs.

TEM grids, with interparticle distances less than twice the length of the organic moieties suggesting that the ligands at the surface were intercalated to some extent.

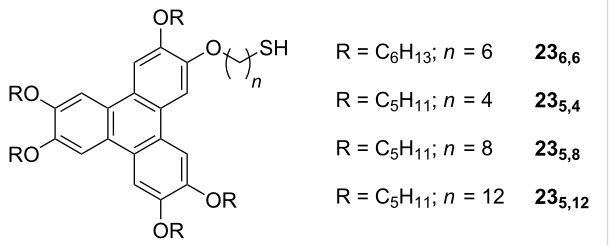

Figure 25: Chemical structures of the discotic mesogenic ligands used to coat NPs.

In another investigation into ligands of this type [94], although no mention was made of their liquid-crystalline properties, it was shown that NPs coated with triphenylenes **23$_{5,4}$**, **23$_{5,8}$** and **23$_{5,12}$** (Figure 25) were able to self-assemble into beautiful 2-D structures with hexagonal, squarelike and stripelike arrangements as a function of both the length of the tethering group and the solvent polarity (Figure 26). These results bode well for the use of these discotic materials in NP self-organisation, and it appears only a matter of time before LC phases are observed for discrete hybrids of this type.

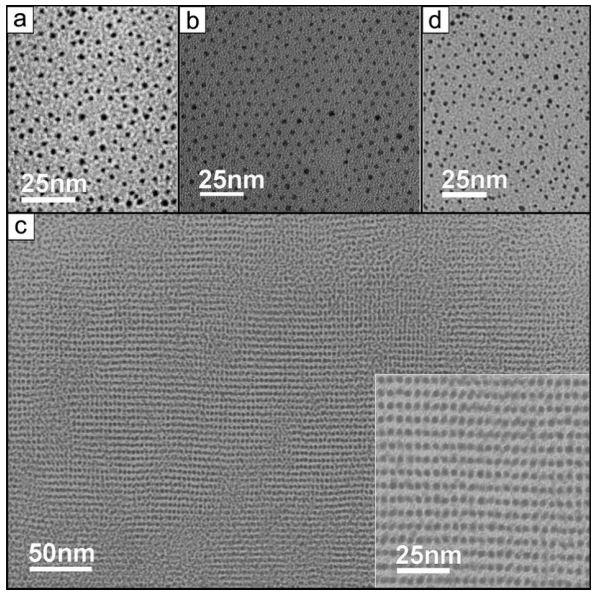

Figure 26: TEM images of **Au@23$_{5,12}$** prepared from aged solutions stood for 10 days in solutions of (a) 1:1 MeOH/toluene (disordered), (b) 2:1 MeOH/toluene (hcp), (c) 3:1 MeOH/toluene (stripelike; inset is an expansion), (d) 4:1 MeOH toluene (disordered). Reprinted with permission from [94]. Copyright 2007 American Chemical Society.

Conclusion

Whilst it is clear that the field of liquid-crystalline nanoparticles is still in its infancy, the exciting results reported to date indicate that these new materials are viable, with a few early trends emerging from the literature. By coating NPs with suitably designed ligands it is possible to soften the interparticle potentials and introduce sufficient anisotropy to allow the hybrids to self-organise into ordered fluid phases. From this starting point, it is unsurprising to find that the mesogenic properties of these hybrid NP systems depend on a synergy between the nature of the grafted ligand and the size and shape of the NP under investigation.

Starting with the core of the hybrid, one observes that the morphology of the nanoparticle is of supreme importance in determining the mesomorphic properties of the systems reported to date, though further investigation is warranted in order to clarify as to what effect the chemical composition of the NP could have on the phase behaviour of the materials. The size and shape are critical parameters as expected, with the results reported also indicating that highly polydisperse samples display no discernable mesophase behaviour, which is consistent with theoretical treatments [95,96]. This is particularly apparent for systems in which the organic ligand is small relative to the size of the NP, the clearest examples of this are seen for highly anisotropic NPs, which form nematic phases upon suitable functionalisation, whereas cuboidal NPs form simple cubic phases. Nevertheless, the presence of an anisotropic NP functionalised with a mesogenic ligand is not sufficient to guarantee the formation of a mesophase, as it has been shown that the aspect ratio may play an important role in determining the ability of the hybrid materials to self-assemble. This can be understood by considering the packing constraints acting upon these hard particles, whereby LC ordering would be impeded by the void volumes that are present between particles due to their local curvature. Approaches involving the use of thick, deformable organic coatings may provide an avenue towards the realisation of mesophase behaviour in these systems, with dendrons and polymers being the most likely candidates for this role.

Of course, design arguments based solely on the shape and size of the hybrid components do not allow one to gain a clear overall picture of the dynamic nature of LCNPs. It is also necessary to consider the nature of the ligand itself, be it mesogenic or otherwise, in the context of its shape, anisotropy, flexibility, mobility and its surface concentration. Based on the limited results available, it is not possible to state definitively whether coating of a nanoparticle exclusively with the mesogenic ligand of interest promotes or inhibits mesophase formation, as examples are available showing both behaviours. Neither is it

possible to guarantee LC-phase formation in the presence of a mixture of mesogenic and non-mesogenic coligands. However, what does become clear, at least in the case of pseudospherical NPs, is that the surface species must have sufficient flexibility and mobility in order to either migrate about the surface of the NP, and/or orientationally distort themselves such that the overall hybrid can obtain the anisotropic shape necessary for the formation of mesophases. Ligand reorganisation akin to the formation of separate surface domains [97] appears to be a dominant mechanism in the case of mixed-ligand systems, whereas ligand deformation into hard poles and a soft equatorial region has been proposed for systems involving a single mesogenic ligand on the surface. These mechanisms highlight the pivotal role of the ligand in influencing the structure of the mesophase, allowing the pseudospherical nanoparticles to be arranged into a variety of phases, such as nematics, smectics, columnar and cubics (Figure 27). Importantly, it is apparent that mesogenic ligands are not always necessary for inducing mesogenic properties in the NP hybrids. The LC phases reported for systems involving non-mesogenic ligand precursors indicate that it should be possible to consider the design of these LC hybrid materials in a more holistic manner, whereby the whole is more than simply just the sum of its parts.

At this point, it is worth mentioning a word of caution regarding the characterisation of these new materials. The phase behaviour of typical "simple" organic LCs can often be characterised with a certain degree of confidence using a mixture of thermal analysis and POM, and with mixing tests with compounds exhibiting the same phase used as a confirmation. Early results have indicated that such a strategy could be quite misleading in some NP hybrid systems, with the POM textures (or lack thereof) observed for the hybrids bearing no relation to those observed for simple organic LCs exhibiting the same phase (e.g., nematic, smectic etc.). Similarly, phase assignments made through mixing experiments should also be treated with caution. It therefore becomes imperative that researchers in this field endeavour to characterise their materials fully using diffraction techniques, complemented by the array of other traditional methods (e.g., TEM, POM).

Encouragingly, it is clear that the field of LCNPs is wide open for chemists to design and synthesise new hybrids, and it only seems a matter of time before we will see not only a wider variety of phases observed, but also new applications for these novel materials. By controlling the spatial assembly of NPs into ordered structures and combining the processability and defect tolerance of the LC state, the structural and functional versatility of the organic coating, and the unique magnetic, optical and electrical properties (including synergistic collective behaviours and the emergence of new physical properties [98-100]) of NPs, liquid-crystalline nanoparticles are poised to address some of the exciting challenges of this century. The future looks bright for the preparation of addressable assemblies of multifunctional hybrids, including high-density recording media [101,102], single-electron microelectronic [103] and charge-transport devices [4], nanoscale plasmon waveguides [104] and metamaterials [62,105]. The field of nanotechnology will only advance whilst scientists have a variety of methods available to them for the production of the nanostructures that they desire, and LCNPs show tremendous promise in adding an important tool for the fabrication of exciting new materials.

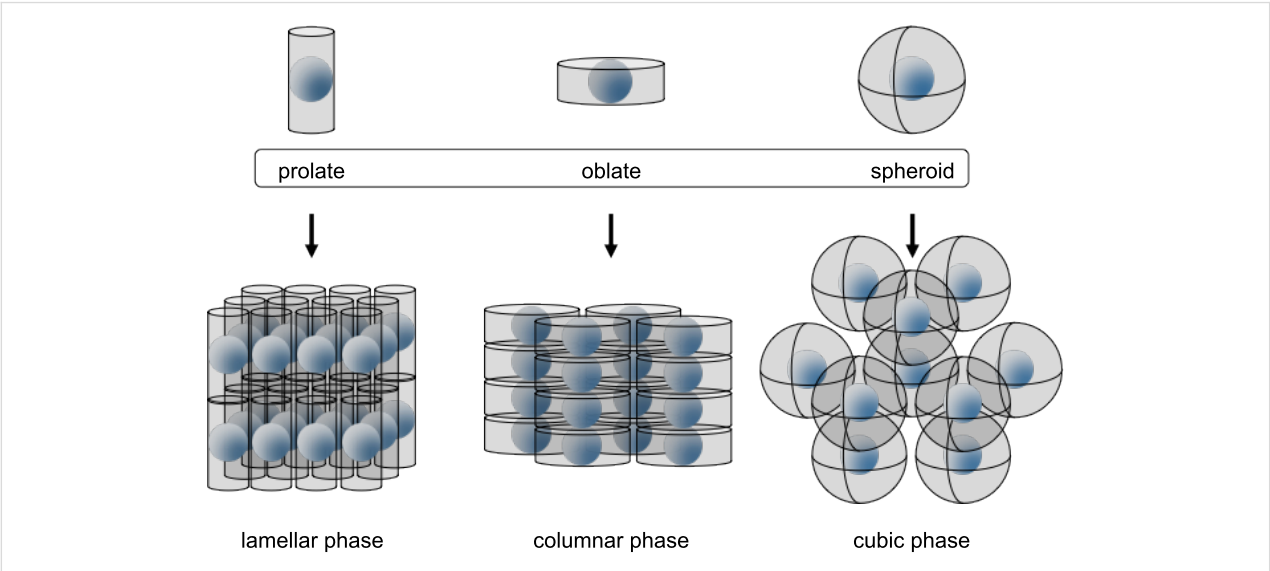

Figure 27: Some of the various hybrid geometries and packing motifs possible upon ligand grafting to the surface of a pseudospherical NP. The role of the ligand(s) in migrating and deforming at the surface is crucial in providing these structures.

Acknowledgements

Part of this work has been supported by the EU "Dendreamers" project (7th FP—THE PEOPLE PROGRAMME. The Marie Curie Actions—ITN, No. 215884-2) and the CNRS.

References

1. Claridge, S. A.; Castleman, A. W., Jr.; Khanna, S. N.; Murray, C. B.; Sen, A.; Weiss, P. S. *ACS Nano* **2009,** *3,* 244–255. doi:10.1021/nn800820e
2. Balzani, V.; Credi, A.; Venturi, M. *Molecular Devices and Machines - A Journey into the Nano World;* Wiley-VCH: Weinheim, Germany, 2003. doi:10.1002/3527601600
3. Baletto, F.; Ferrando, R. *Rev. Mod. Phys.* **2005,** *77,* 371–423. doi:10.1103/RevModPhys.77.371
4. Zabet-Khosousi, A.; Dhirani, A.-A. *Chem. Rev.* **2008,** *108,* 4072–4124. doi:10.1021/cr0680134
5. Jun, Y.-w.; Choi, J.-s.; Cheon, J. *Angew. Chem., Int. Ed.* **2006,** *45,* 3414–3439. doi:10.1002/anie.200503821
6. Lu, A.-H.; Salabas, E. L.; Schüth, F. *Angew. Chem., Int. Ed.* **2007,** *46,* 1222–1244. doi:10.1002/anie.200602866
7. Murray, C. B.; Kagan, C. R.; Bawendi, M. G. *Annu. Rev. Mater. Sci.* **2000,** *30,* 545–610. doi:10.1146/annurev.matsci.30.1.545
8. Park, J.; Joo, J.; Kwon, S. G.; Jang, Y.; Hyeon, T. *Angew. Chem., Int. Ed.* **2007,** *46,* 4630–4660. doi:10.1002/anie.200603148
9. Burda, C.; Chen, X.; Narayanan, R.; El-Sayed, M. A. *Chem. Rev.* **2005,** *105,* 1025–1102. doi:10.1021/cr030063a
10. Goesmann, H.; Feldmann, C. *Angew. Chem., Int. Ed.* **2010,** *49,* 1362–1395. doi:10.1002/anie.200903053
11. Kennedy, L. C.; Bickford, L. R.; Lewinski, N. A.; Coughlin, A. J.; Hu, Y.; Day, E. S.; West, J. L.; Drezek, R. A. *Small* **2011,** *7,* 169–183. doi:10.1002/smll.201000134
12. Daniel, M.-C.; Astruc, D. *Chem. Rev.* **2004,** *104,* 293–346. doi:10.1021/cr030698+
13. Haase, M.; Schäfer, H. *Angew. Chem., Int. Ed.* **2011,** *50,* 5808–5829. doi:10.1002/anie.201005159
14. Talapin, D. V.; Lee, J.-S.; Kovalenko, M. V.; Shevchenko, E. V. *Chem. Rev.* **2010,** *110,* 389–458. doi:10.1021/cr900137k
15. Schlögl, R.; Hamid, S. B. A. *Angew. Chem., Int. Ed.* **2004,** *43,* 1628–1637. doi:10.1002/anie.200301684
16. Kaur, A.; Gupta, U. *J. Mater. Chem.* **2009,** *19,* 8279–8289. doi:10.1039/b901933b
17. Tang, Z.; Kotov, N. A. *Adv. Mater.* **2005,** *17,* 951–962. doi:10.1002/adma.200401593
18. Curri, M. L.; Comparelli, R.; Striccoli, M.; Agostiano, A. *Phys. Chem. Chem. Phys.* **2010,** *12,* 11197–11207. doi:10.1039/b926146j
19. Stebe, K. J.; Lewandowski, E.; Ghosh, M. *Science* **2009,** *325,* 159–160. doi:10.1126/science.1174401
20. Bishop, K. J. M.; Wilmer, C. E.; Soh, S.; Grzybowski, B. A. *Small* **2009,** *5,* 1600–1630. doi:10.1002/smll.200900358
21. Min, Y.; Akbulut, M.; Kristiansen, K.; Golan, Y.; Israelachvili, J. *Nat. Mater.* **2008,** *7,* 527–538. doi:10.1038/nmat2206
22. Wang, Z. L. *Adv. Mater.* **1998,** *10,* 13–30. doi:10.1002/(SICI)1521-4095(199801)10:1<13::AID-ADMA13>3.0.CO;2-W
23. Grzelczak, M.; Vermant, J.; Furst, E. M.; Liz-Marzán, L. M. *ACS Nano* **2010,** *4,* 3591–3605. doi:10.1021/nn100869j
24. Bisoyi, H. K.; Kumar, S. *Chem. Soc. Rev.* **2011,** *40,* 306–319. doi:10.1039/b901793n
25. Chandrasekhar, S. *Liquid Crystals,* 2nd ed.; Cambridge University Press: Cambridge, 1994.
26. Kumar, S. *Liquid Crystals: Experimental Study of Physicla Properties and Phase Transitions;* Cambridge University Press: Cambridge, 2001.
27. Demus, D.; Goodby, J.; Gray, G. W.; Spiess, H.-W.; Vill, V., Eds. *Handbook of Liquid Crystals;* Wiley-VCH: Weinheim, Germany, 1998.
28. Goodby, J. W.; Saez, I. M.; Cowling, S. J.; Görtz, V.; Draper, M.; Hall, A. W.; Sia, S.; Cosquer, G.; Lee, S.-E.; Raynes, E. P. *Angew. Chem., Int. Ed.* **2008,** *47,* 2754–2787. doi:10.1002/anie.200701111
29. Kato, T.; Mizoshita, N.; Kishimoto, K. *Angew. Chem., Int. Ed.* **2006,** *45,* 38–68. doi:10.1002/anie.200501384
30. Tschierske, C. *J. Mater. Chem.* **1998,** *8,* 1485–1508. doi:10.1039/a800946e
31. Donnio, B.; Buathong, S.; Bury, I.; Guillon, D. *Chem. Soc. Rev.* **2007,** *36,* 1495–1513. doi:10.1039/b605531c
32. Skoulios, A.; Guillon, D. *Mol. Cryst. Liq. Cryst.* **1988,** *165,* 317–332. doi:10.1080/00268948808082205
33. Tschierske, C. *Annu. Rep. Prog. Chem., Sect. C: Phys. Chem.* **2001,** *97,* 191–267. doi:10.1039/b101114f
34. Reddy, R. A.; Tschierske, C. *J. Mater. Chem.* **2006,** *16,* 907–961. doi:10.1039/b504400f
35. Tschierske, C. *J. Mater. Chem.* **2001,** *11,* 2647–2671. doi:10.1039/b102914m
36. Herrikhuyzen, J. v.; Portale, G.; Gielen, J. C.; Christianen, P. C. M.; Sommerdiyk, N. A. J. M.; Meskers, S. C. J.; Schenning, A. P. H. J. *Chem. Commun.* **2008,** 697–699. doi:10.1039/b715820c
37. Davidson, P.; Gabriel, J.-C. P. *Curr. Opin. Colloid Interface Sci.* **2005,** *9,* 377–383. doi:10.1016/j.cocis.2004.12.001
38. Gabriel, J.-C. P.; Davidson, P. *Top. Curr. Chem.* **2003,** *226,* 119–172. doi:10.1007/3-540-36408-0_5
39. Barmatov, E. B.; Pebalk, D. A.; Barmatova, M. V. *Langmuir* **2004,** *20,* 10868–10871. doi:10.1021/la048601h
40. Shandryuk, G. A.; Matukhina, E. V.; Vasil'ev, R. B.; Rebrov, A.; Bondarenko, G. N.; Merekalov, A. S.; Gas'kov, A. M.; Talroze, R. V. *Macromolecules* **2008,** *41,* 2178–2185. doi:10.1021/ma701983y
41. Garcia-Márquez, A.; Demortière, A.; Heinrich, B.; Guillon, D.; Bégin-Colin, S.; Donnio, B. *J. Mater. Chem.* **2011,** *21,* 8994–8996. doi:10.1039/c1jm11381j
42. Saliba, S.; Coppel, Y.; Davidson, P.; Mingotaud, C.; Chaudret, B.; Kahn, M. L.; Marty, J.-D. *J. Mater. Chem.* **2011,** *21,* 6821–6823. doi:10.1039/c1jm10525f
43. Vemula, P. K.; Aslam, U.; Mallia, V. A.; John, G. *Chem. Mater.* **2007,** *19,* 138–140. doi:10.1021/cm062464n
44. Vemula, P. K.; Mallia, V. A.; Bizati, K.; John, G. *Chem. Mater.* **2007,** *19,* 5203–5206. doi:10.1021/cm071359q
45. Antharjanam, P. K. S.; Prasad, E. *New J. Chem.* **2010,** *34,* 420–425. doi:10.1039/b909428h
46. Zadoina, L.; Soulantica, K.; Ferrere, S.; Lonetti, B.; Respaud, M.; Mingotaud, A.-F.; Falqui, A.; Genovese, A.; Chaudret, B.; Mauzac, M. *J. Mater. Chem.* **2011,** *21,* 6988–6994. doi:10.1039/c0jm03872e
47. Qi, H.; Hegmann, T. *J. Mater. Chem.* **2008,** *18,* 3288–3294. doi:10.1039/b718920f
48. Hegmann, T.; Qi, H.; Marx, V. M. *J. Inorg. Organomet. Polym. Mater.* **2007,** *17,* 483–508. doi:10.1007/s10904-007-9140-5

49. Akimoto, M.; Kundu, S.; Isomura, K.; Hirayama, I.; Kobayashi, S.; Takatoh, K. *Mol. Cryst. Liq. Cryst.* **2009,** *508,* 1–13. doi:10.1080/15421400903058130
50. Li, L.-s.; Walda, J.; Manna, L.; Alivisatos, A. P. *Nano Lett.* **2002,** *2,* 557–560. doi:10.1021/nl0255146
51. Saunders, A. E.; Ghezelbash, A.; Smilgies, D.-M.; Sigman, M. B., Jr.; Korgel, B. A. *Nano Lett.* **2006,** *6,* 2959–2963. doi:10.1021/nl062419e
52. Lin, X. M.; Jaeger, H. M.; Sorensen, C. M.; Klabunde, K. J. *J. Phys. Chem. B* **2001,** *105,* 3353–3357. doi:10.1021/jp0102062
53. Lane, J. M. D.; Grest, G. S. *Phys. Rev. Lett.* **2010,** *104,* 235501. doi:10.1103/PhysRevLett.104.235501
54. Luedtke, W. D.; Landman, U. *J. Phys. Chem.* **1996,** *100,* 13323–13329. doi:10.1021/jp961721g
55. Luedtke, W. D.; Landman, U. *J. Phys. Chem. B* **1998,** *102,* 6566–6572. doi:10.1021/jp981745i
56. Brust, M.; Walker, M.; Bethell, D.; Schiffrin, D. J.; Whyman, R. *J. Chem. Soc., Chem. Commun.* **1994,** 801–802. doi:10.1039/C39940000801
57. Polarz, S. *Adv. Funct. Mater.* **2011,** *21,* 3214–3230. doi:10.1002/adfm.201101205
58. Kanie, K.; Sugimoto, T. *J. Am. Chem. Soc.* **2003,** *125,* 10518–10519. doi:10.1021/ja0357691
59. Kanie, K.; Muramatsu, A. *J. Am. Chem. Soc.* **2005,** *127,* 11578–11579. doi:10.1021/ja054232f
60. Kanayama, N.; Tsutsumi, O.; Kanazawa, A.; Ikeda, T. *Chem. Commun.* **2001,** 2640–2641. doi:10.1039/b108909a
61. In, I.; Jun, Y.-W.; Kim, Y. J.; Kim, S. Y. *Chem. Commun.* **2005,** 800–801. doi:10.1039/b413510e
62. Draper, M.; Saez, I. M.; Cowling, S. J.; Gai, P.; Heinrich, B.; Donnio, B.; Guillon, D.; Goodby, J. W. *Adv. Funct. Mater.* **2011,** *21,* 1260–1278. doi:10.1002/adfm.201001606
63. Wojcik, M.; Lewandowski, W.; Matraszek, J.; Mieczkowski, J.; Borysiuk, J.; Pociecha, D.; Gorecka, E. *Angew. Chem., Int. Ed.* **2009,** *48,* 5167–5169. doi:10.1002/anie.200901206
64. Wojcik, M.; Kolpaczynska, M.; Pociecha, D.; Mieczkowski, J.; Gorecka, E. *Soft Matter* **2010,** *6,* 5397–5400. doi:10.1039/c0sm00539h
65. Zeng, X.; Liu, F.; Fowler, A. G.; Ungar, G.; Cseh, L.; Mehl, G. H.; Macdonald, J. E. *Adv. Mater.* **2009,** *21,* 1746–1750. doi:10.1002/adma.200803403
66. Zhang, J.; Whitesell, J. K.; Fox, M. A. *Chem. Mater.* **2001,** *13,* 2323–2331. doi:10.1021/cm000752s
67. Mikami, R.; Taguchi, M.; Yamada, K.; Suzuki, K.; Sato, O.; Einaga, Y. *Angew. Chem., Int. Ed.* **2004,** *43,* 6135–6139. doi:10.1002/anie.200460964
68. Suda, M.; Nakagawa, M.; Iyoda, T.; Einaga, Y. *J. Am. Chem. Soc.* **2007,** *129,* 5538–5543. doi:10.1021/ja0682374
69. Cseh, L.; Mehl, G. H. *J. Am. Chem. Soc.* **2006,** *128,* 13376–13377. doi:10.1021/ja066099c
70. Cseh, L.; Mehl, G. H. *J. Mater. Chem.* **2007,** *17,* 311–315. doi:10.1039/b614046g
71. Goodby, J. W.; Saez, I. M.; Cowling, S. J.; Gasowska, J. S.; MacDonald, R. A.; Sia, S.; Watson, P.; Toyne, K. J.; Hird, M.; Lewis, R. A.; Lee, S.-E.; Vaschenko, V. *Liq. Cryst.* **2009,** *36,* 567–605. doi:10.1080/02678290903146060
72. Karahaliou, P. K.; Kouwer, P. H. J.; Meyer, T.; Mehl, G. H.; Photinos, D. J. *Soft Matter* **2007,** *3,* 857–865. doi:10.1039/b617696h
73. Kaneko, K.; Mandai, A.; Heinrich, B.; Donnio, B.; Hanasaki, T. *ChemPhysChem* **2010,** *11,* 3596–3598. doi:10.1002/cphc.201000587
74. Saez, I. M.; Goodby, J. W.; Richardson, R. M. *Chem.–Eur. J.* **2001,** *7,* 2758–2764. doi:10.1002/1521-3765(20010702)7:13<2758::AID-CHEM2758>3.0.CO;2-T
75. Etxebarria, J.; Ros, M. B. *J. Mater. Chem.* **2008,** *18,* 2919–2926. doi:10.1039/b803507e
76. Marx, V. M.; Girgis, H.; Heiney, P. A.; Hegmann, T. *J. Mater. Chem.* **2008,** *18,* 2983–2994. doi:10.1039/b802554a
77. Astruc, D.; Boisselier, E.; Ornelas, C. *Chem. Rev.* **2010,** *110,* 1857–1959. doi:10.1021/cr900327d
78. Rosen, B. M.; Wilson, C. J.; Wilson, D. A.; Peterca, M.; Imam, M. R.; Percec, V. *Chem. Rev.* **2009,** *109,* 6275–6540. doi:10.1021/cr900157q
79. Frein, S.; Boudon, J.; Vonlanthen, M.; Scharf, T.; Barberá, J.; Süss-Fink, G.; Bürgi, T.; Deschenaux, R. *Helv. Chim. Acta* **2008,** *91,* 2321–2337. doi:10.1002/hlca.200890253
80. Buathong, S.; Ung, D.; Daou, T. J.; Ulhaq-Bouillet, C.; Pourroy, G.; Guillon, D.; Ivanova, L.; Bernhardt, I.; Bégin-Colin, S.; Donnio, B. *J. Phys. Chem. C* **2009,** *113,* 12201–12212. doi:10.1021/jp902046d
81. Khatua, S.; Manna, P.; Chang, W.-S.; Tcherniak, A.; Friedlander, E.; Zubarev, E. R.; Link, S. *J. Phys. Chem. C* **2010,** *114,* 7251–7257. doi:10.1021/jp907923v
82. Donnio, B.; García-Vázquez, P.; Gallani, J.-L.; Guillon, D.; Terazzi, E. *Adv. Mater.* **2007,** *19,* 3534–3539. doi:10.1002/adma.200701252
83. Crisanti, A.; Leuzzi, L. *Phys. Rev. Lett.* **2005,** *95,* 087201. doi:10.1103/PhysRevLett.95.087201
84. Terzis, A. F.; Vanakaras, A. G.; Photinos, D. J. *Mol. Cryst. Liq. Cryst.* **2000,** *352,* 265–274. doi:10.1080/10587250008023184
85. Demortière, A.; Buathong, S.; Pichon, B. P.; Panissod, P.; Guillon, D.; Bégin-Colin, S.; Donnio, B. *Small* **2010,** *6,* 1341–1346. doi:10.1002/smll.201000285
86. Donnio, B.; Derory, A.; Terazzi, E.; Drillon, M.; Guillon, D.; Gallani, J.-L. *Soft Matter* **2010,** *6,* 965–970. doi:10.1039/b918602f
87. Demortière, A.; Panissod, P.; Pichon, B. P.; Pourroy, G.; Guillon, D.; Donnio, B.; Bégin-Colin, S. *Nanoscale* **2011,** *3,* 225–232. doi:10.1039/c0nr00521e
88. Kanie, K.; Matsubara, M.; Zeng, X.; Liu, F.; Ungar, G.; Nakamura, H.; Muramatsu, A. *J. Am. Chem. Soc.* **2012,** *134,* 808–811. doi:10.1021/ja2095816
89. Laschat, S.; Baro, A.; Steinke, N.; Giesselmann, F.; Hägele, C.; Scalia, G.; Judele, R.; Kapatsina, E.; Sauer, S.; Schreivogel, A.; Tosoni, M. *Angew. Chem., Int. Ed.* **2007,** *46,* 4832–4887. doi:10.1002/anie.200604203
90. Kumar, S. *Chem. Soc. Rev.* **2006,** *35,* 83–109. doi:10.1039/b506619k
91. Kaafarani, B. R. *Chem. Mater.* **2011,** *23,* 378–396. doi:10.1021/cm102117c
92. Sergeyev, S.; Pisula, W.; Geerts, Y. H. *Chem. Soc. Rev.* **2007,** *36,* 1902–1929. doi:10.1039/b417320c
93. Kumar, S.; Pal, S. K.; Kumar, P. S.; Lakshminarayanan, V. *Soft Matter* **2007,** *3,* 896–900. doi:10.1039/b701380a
94. Shen, Z.; Yamada, M.; Miyake, M. *J. Am. Chem. Soc.* **2007,** *129,* 14271–14280. doi:10.1021/ja073518c
95. Onsager, L. *Ann. N. Y. Acad. Sci.* **1949,** *51,* 627–659. doi:10.1111/j.1749-6632.1949.tb27296.x
96. Vroege, G. J.; Lekkerkerker, H. N. W. *Rep. Prog. Phys.* **1992,** *55,* 1241–1309. doi:10.1088/0034-4885/55/8/003
97. Lattuada, M.; Hatton, T. A. *Nano Today* **2011,** *6,* 286–308. doi:10.1016/j.nantod.2011.04.008
98. Pileni, M. P. *J. Phys. Chem. B* **2001,** *105,* 3358–3371. doi:10.1021/jp0039520

99. Bedanta, S.; Kleemann, W. *J. Phys. D: Appl. Phys.* **2009,** *42,* 013001. doi:10.1088/0022-3727/42/1/013001
100. Dumestre, F.; Martinez, S.; Zitoun, D.; Fromen, M.-C.; Casanove, M.-J.; Lecante, P.; Respaud, M.; Serres, A.; Benfield, R. E.; Amiens, C.; Chaudret, B. *Faraday Discuss.* **2004,** *125,* 265–278. doi:10.1039/b303376g
101. Shi, J.; Gider, S.; Babcock, K.; Aweschalom, D. D. *Science* **1996,** *271,* 937–941. doi:10.1126/science.271.5251.937
102. Sun, S.; Murray, C. B.; Weller, D.; Folks, L.; Moser, A. *Science* **2000,** *287,* 1989–1992. doi:10.1126/science.287.5460.1989
103. Greshnykh, D.; Frömsdorf, A.; Weller, H.; Klinke, C. *Nano Lett.* **2009,** *9,* 473–478. doi:10.1021/nl803520r
104. Maier, S. A.; Brongersma, M. L.; Kik, P. G.; Meltzer, S.; Requicha, A. A. G.; Atwater, H. A. *Adv. Mater.* **2001,** *13,* 1501–1505. doi:10.1002/1521-4095(200110)13:19<1501::AID-ADMA1501>3.0.CO;2-Z
105. Shevchenko, E. V.; Talapin, D. V.; O'Brien, S.; Murray, C. B. *J. Am. Chem. Soc.* **2005,** *127,* 8741–8747. doi:10.1021/ja050510z

Beilstein Journal of Organic Chemistry

Synthesis and mesomorphic properties of calamitic malonates and cyanoacetates tethered to 4-cyanobiphenyls

Katharina C. Kress, Martin Kaller, Kirill V. Axenov, Stefan Tussetschläger and Sabine Laschat*

Full Research Paper

Open Access

Address:
Institut für Organische Chemie, Universität Stuttgart, Pfaffenwaldring 55, 70569 Stuttgart, Germany

Email:
Stefan Tussetschläger - stefan.tussetschlaeger@oc.uni-stuttgart.de;
Sabine Laschat* - Sabine.Laschat@oc.uni-stuttgart.de

* Corresponding author

Keywords:
cyanoacetates; 4-cyanobiphenyls; liquid crystals; malonates; nematic

Beilstein J. Org. Chem. **2012,** *8,* 371–378.
doi:10.3762/bjoc.8.40

Received: 08 November 2011
Accepted: 20 February 2012
Published: 09 March 2012

This article is part of the Thematic Series "Progress in liquid crystal chemistry II".

Associate Editor: P. J. Skabara

Abstract

4-Cyano-1,1'-biphenyl derivatives bearing ω-hydroxyalkyl substituents were reacted with methyl 3-chloro-3-oxopropionate or cyanoacetic acid, giving liquid-crystalline linear malonates and cyanoacetates. These compounds formed monotropic nematic phases at 62 °C down to ambient temperature upon cooling from the isotropic liquid. The mesomorphic properties were investigated by differential scanning calorimetry, polarizing optical microscopy and X-ray diffraction (WAXS).

Introduction

Nematic liquid crystals display mesophases in which the molecules are oriented along one vector defined by the director axis, but with the molecular arrangement in random positional order [1]. Nematic phases typically display low viscosity [2-4]. Due to the long-range orientational order they reveal anisotropic properties. These features make nematic liquid crystals very attractive materials for electronics [5-8], for the construction of liquid crystal displays [9-11], or as anisotropic conductors [12,13]. Over the past few decades, a huge variety of organic calamitic compounds, which form nematic liquid crystals, have been synthesized and investigated [1,14].

Bulkin et al. were the first to investigate the phase behaviour of metal β-diketonate complexes such as **1** [15] (Scheme 1). Although they were not able to detect any mesophases, their study motivated others to examine the mesomorphic properties of β-diketonates in more detail [16]. Among the first examples of a nematic β-diketonate is the Cu complex **2** described by Haase [17-21]. In contrast to the various diketonato metallomesogens only a little information is available about the mesomorphic properties of metal-free diketones. Among the few examples are the nematic compounds **3** [22] and **4** [23,24] (Scheme 1).

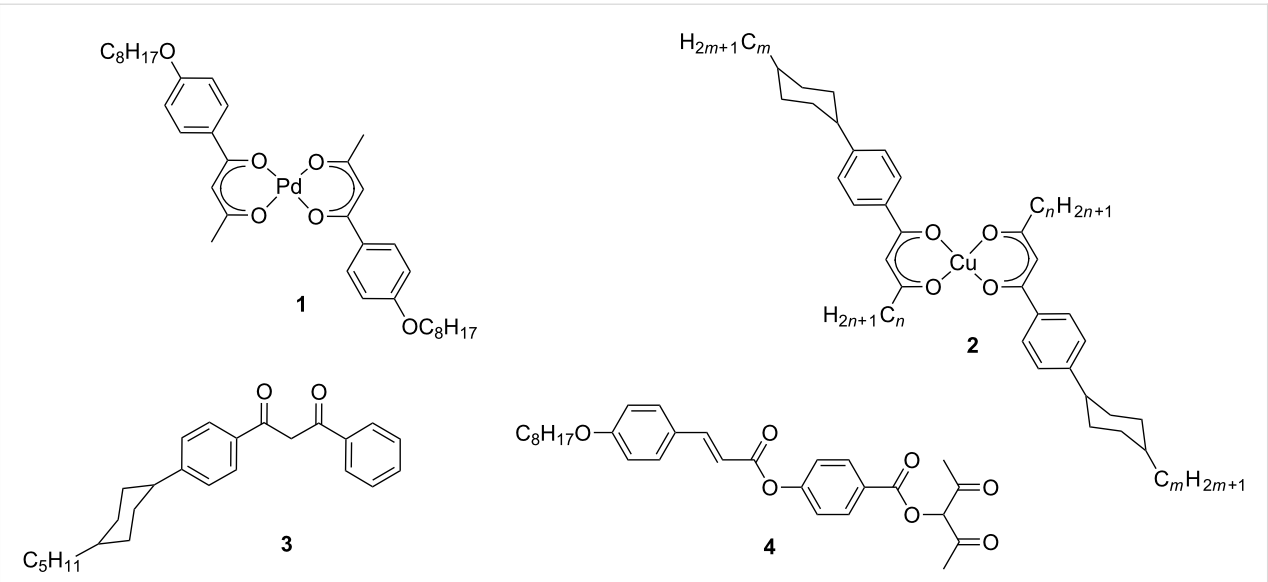

Scheme 1: Diketonato metallomesogens and diketones with mesomorphic properties.

The corresponding malonates and cyanoacetates are well known as suitable ligands for strong coordination of main-group and transition metals [25]. Benzylidene derivatives of malonic esters, so called swallow-tailed liquid crystals, were described as forming smectic phases [26]. However, most work on liquid-crystalline malonates has been devoted to C_{60} fullerene dendrimers [27-31]. Only a few liquid crystalline cyanoacetates have been described so far. The first example, a dihydrazide, was reported by Schubert [32]. Furthermore some calamitic and bent-core mesogens derived from α-cyanocinnamic acid were described in the literature [33,34]. Therefore, we decided to explore the synthesis and mesomorphic properties of malonates and cyanoacetates **5** tethered to calamitic 4-cyanobiphenyl units (Scheme 2).

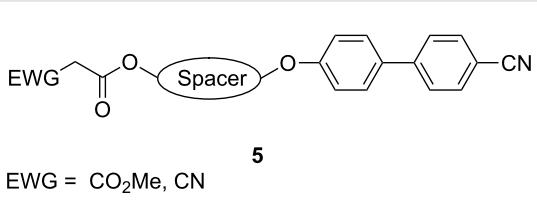

Scheme 2: Malonates and cyanoacetates tethered to calamitic 4-cyanobiphenyl units.

Results and Discussion

The syntheses of malonate and cyanoacetate derivatives **11**, **13** are shown in Scheme 3. Starting from the corresponding diols **6a**,**b**, 6-bromohexan-1-ol (**7a**) and 10-bromodecan-1-ol (**7b**) were obtained in moderate yields by bromination with aqueous HBr in toluene [35]. The bromides **7a**,**b** were reacted with 4-cyano-1,1'-biphenol (**8**) in acetone in the presence of K_2CO_3 giving compounds **9a**,**b**, bearing C_6- or C_{10}-spacers, in 68% and 60% yield, respectively [36-38] after recrystallization from methanol (Scheme 3).

The malonate unit was attached by treatment of the compounds **9a**,**b** with methyl 3-chloro-3-oxopropionate (**10**) in the presence of pyridine in CH_2Cl_2 to yield the malonates **11a**,**b** in 57% and 65%, respectively, after column chromatography. In a parallel approach, the precursors **9a**,**b** were converted to the corresponding cyanoacetates **13a**,**b** by esterification of cyanoacetic acid (**12**) in the presence of DMAP and dicyclohexylcarbodiimide in CH_2Cl_2. After chromatography the cyanoacetates **13a**,**b** were isolated as colourless solids in 59% and 41% yield.

The obtained malonate and cyanoacetic esters **11a,b** and **13a,b** were subjected to differential scanning calorimetry (DSC) studies (Figure 1, Figure 2, and Table 1).

During the first heating runs all compounds did not show the appearance of any liquid-crystalline phase, but melted without decomposition into isotropic liquids. It was observed that the melting points increased with an increase of the spacer length between 4-cyanobiphenyl and ester groups. Thus, melting points were recorded at 49.1 °C/63.4 °C for the series of **11a**/**11b** and at 89.0 °C/93.2 °C for the series of **13a**/**13b**, respectively (Table 1). The cyano group is a stronger electron-acceptor than the ester function, and thus the cyanoacetic ester molecules are more polarized than the corresponding malonates. Stronger dipole–dipole interactions for cyano esters **13** led to an increase of their clearing points compared with malonates **11**.

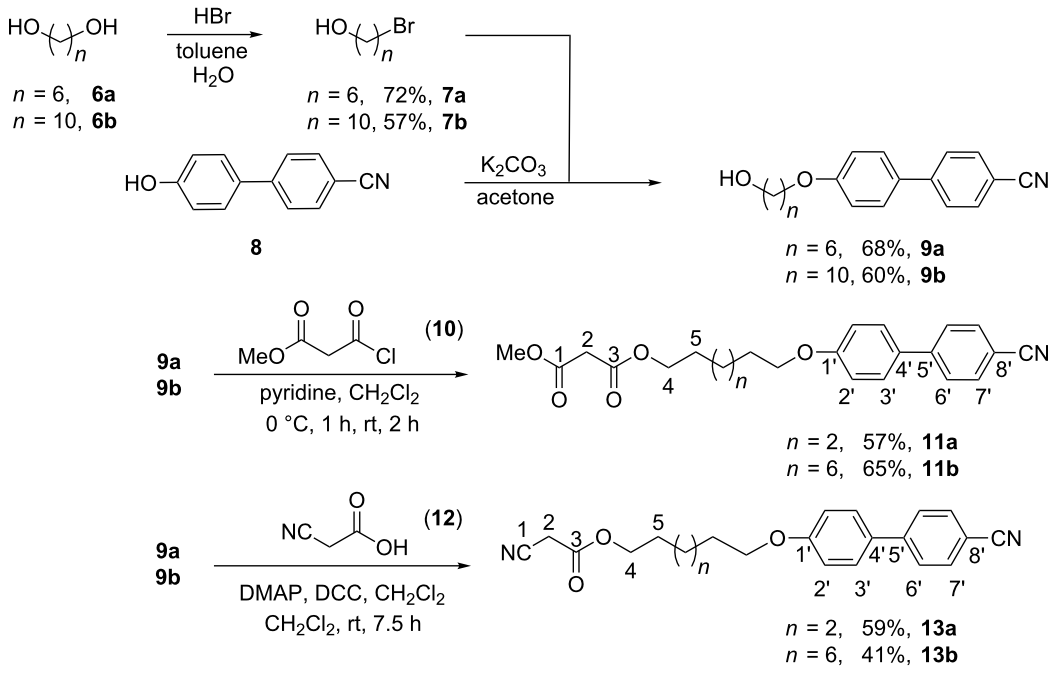

Scheme 3: Synthesis of malonate and cyanoacetates tethered to 4-cyano-biphenyl moieties.

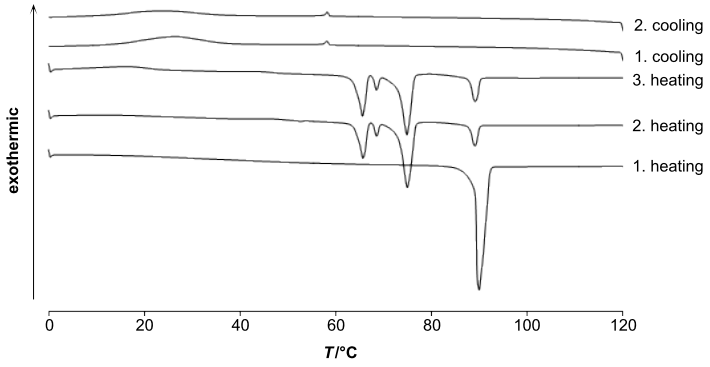

Figure 1: DSC traces of **13a** (heating/cooling rate 5 K/min).

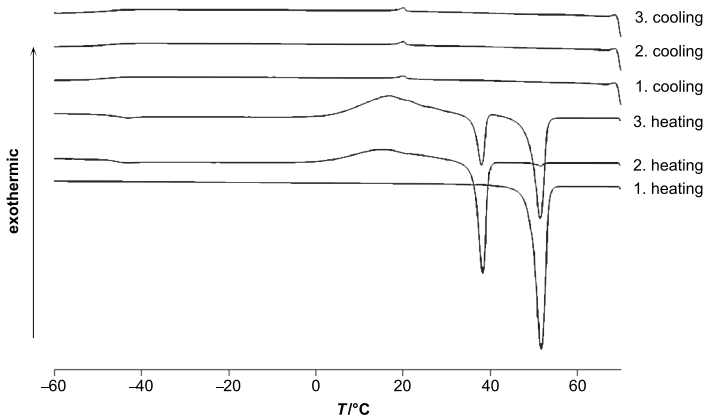

Figure 2: DSC traces of **11a** (heating/cooling rate 10 K/min).

Table 1: Phase-transition temperatures [°C] and enthalpies [kJ/mol] of **11** and **13**.[a]

	n	Cr_1	*T*	Δ*H*	Cr_2	*T*	Δ*H*	Cr_3/N	*T*	Δ*H*	I	
11a	6	●	49.1	32.4	–	–	–	–	–	–	●	1. heating[b]
		●	–	–	–	–	–	N	21.2	−0.32	●	1. cooling[b]
		●	4.1	−12.0	●	36.2	17.6	Cr_3	49.9	0.27	●	2. heating[b]
		●	–	–	–	–	–	N	20.9	−0.29	●	2. cooling[b]
		●	5.0	−18.2	●	35.9	7.72	Cr_3	48.8	20.7	●	3. heating[b]
11b	10	●	63.4	53.2	–	–	–	–	–	–	●	1. heating[c]
		●	10.0	−24.2	●	14.8	−3.45	N	35.6	−0.68	●	1. cooling[c,d]
		●	54.8	39.8	–	–	–	Cr_3	59.9	7.35	●	2. heating[c]
		●	14.8	−24.2	●	31.1	−0.33	N	35.4	−0.46	●	2. cooling[c]
13a	6	●	89.0	39.6	–	–	–	–	–	–	●	1. heating[c]
		●	–	–	–	–	–	N	58.7	−0.38	●	1. cooling[c]
		●	64.1	9.19	●	73.0	22.7	Cr_3	87.8	−4.34	●	2. heating[c,e]
		●	–	–	–	–	–	N	58.7	−0.41	●	2. cooling[c]
		●	63.9	11.6	●	72.9	19.8	Cr_3	87.8	5.48	●	3. heating[c,f]
13b	10	●	93.2	49.1	–	–	–	–	–	–	●	1. heating[c]
		●	52.7	−41.1	–	–	–	N	61.8	−0.71	●	1. cooling[c]
		●	74.7	13.5	●	86.3	−7.41	Cr_3	91.5	41.5	●	2. heating[c,g]
		●	52.7	−41.1	–	–	–	N	61.9	−0.98	●	2. cooling[c]

[a]Cr crystalline; N nematic; I isotropic; ● phase was observed; – phase was not observed. [b]Heating and cooling rate: 10 K/min. [c]Heating and cooling rate: 5 K/min. [d]Another crystal-to-crystal transition (31.2 °C, −0.24 kJ/mol) was observed. [e]Another crystal-to-crystal transition (67.7 °C, 1.62 kJ/mol) was observed. [f]Another crystal-to-crystal transition (67.6 °C, 1.86 kJ/mol) was observed. [g]Another crystal-to-crystal transition (78.1 °C, 21.0 kJ/mol) was observed.

The additional Cr→Cr transitions in the 2nd and 3rd heating curves (Figure 1 and Figure 2) are probably due to equilibration and the presence of keto-enol tautomers. Molecular geometry phase-behaviour relationships in keto-enamine/imino-enol tautomers of ferrocenophanes have been previously studied by Galyametdinov [39]. In the first cooling runs the appearance of nematic mesophases was observed for both series **11a**,**b** and **13a**,**b**. All compounds displayed small transition enthalpies in a range between −0.3 and −0.7 kJ/mol (Table 1) for the transition from the isotropic liquid to the corresponding mesophases. While C_6-linked compounds displayed monotropic nematic mesophases at temperatures of 21 °C for **11a** and 59 °C for **13a**, their longer and more flexible C_{10}-linked homologues showed higher transition temperatures at 36 °C for **11b** and 62 °C for **13b** upon cooling from the isotropic liquid. Due to supercooling, no crystallisation could be observed for compound **11a** and, therefore, no mesophase range could be determined. But the second and third heating runs of **11a** showed broad recrystallization peaks (Figure 2).

Polarizing optical microscope (POM) studies

POM observations of compounds **11a**,**b** and **13a**,**b** revealed textures typical for nematic phases, only upon cooling from the isotropic liquid (Figure 3 and Figure 4).

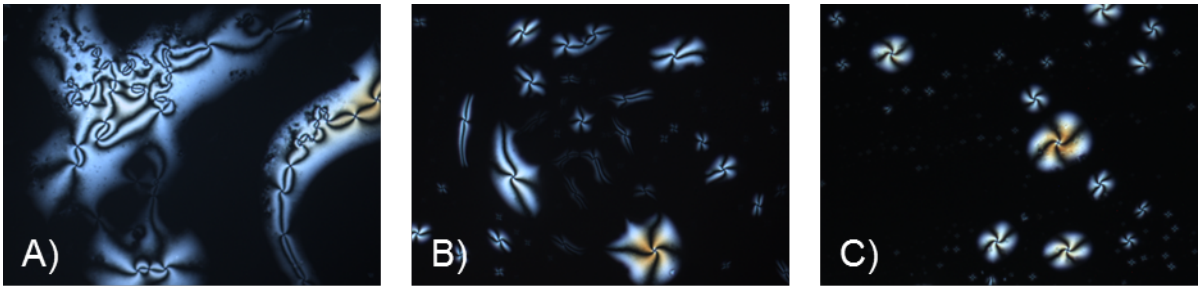

Figure 3: Schlieren textures of **11a** and **11b** under crossed polarizers, upon cooling (cooling rate 5 K/min) from the isotropic liquid (magnification 200×): (A) **11a** (20 °C), (B) **11a** (14 °C), (C) **11b** (29 °C).

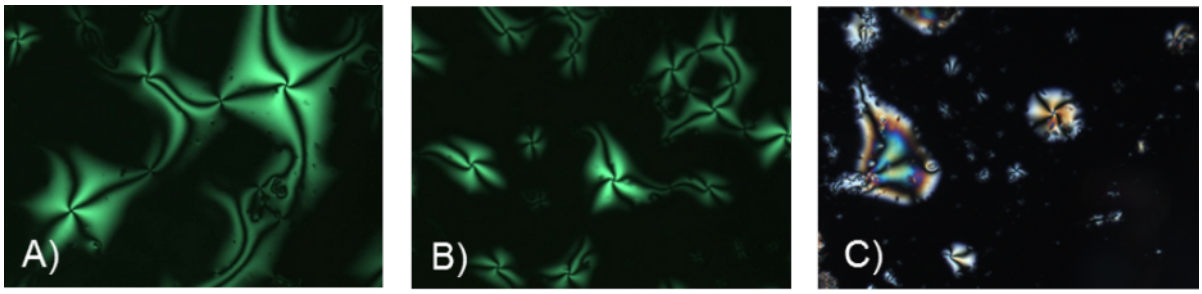

Figure 4: Schlieren textures of **13a** and **13b** under crossed polarizers upon cooling (cooling rate 5 K/min) from the isotropic liquid (magnification 200×): (A) **13b** (61 °C), (B) **13b** at 61 °C, different section, (C) **13a** (46 °C).

Schlieren textures with fourfold brushes were observed for compound **13b** at the transition from the isotropic liquid into the nematic phase. Quite similar textures were published by Dierking [40,41]. The areas without birefringence in Figure 3 and Figure 4 derive from homeotropic alignment of the molecules.

X-ray diffraction studies

The assignment of the nematic mesophases were exemplarily confirmed by wide-angle X-ray scattering (WAXS) experiments on compound **11a**. Representative 2D diffractograms of the crystalline phase, the isotropic phase and the nematic phase are shown in Figure 5.

In the isotropic phase (Figure 5, part B) only a diffuse symmetric halo is observed. The diffraction pattern of **11a** at 15 °C (Figure 5, part C) displays a halo split into two diffuse, crescent reflections, which is typical for nematic mesophases [42].

Conclusion

The mesogenic 4-cyano-1,1'-biphenyl group can be attached to either a malonate or a cyanoacetic ester scaffold by means of simple reaction sequences and with the aid of cheap chemical precursors. Linked ester molecules **11a**,**b** and **13a**,**b** have a distinct linear shape and easily form monotropic mesophases at ambient temperature upon cooling from the isotropic liquid. Following POM and X-ray studies, nematic mesophases could be assigned to all the described compounds **11a**,**b** and **13a**,**b**.

Experimental

General information

All reactions were carried out under a nitrogen atmosphere with Schlenk-type glassware. Solvents were dried and distilled under nitrogen prior to use. Flash chromatography was performed on silica gel, with grain size 40–63 μm (Macherey-Nagel).

The following instruments were used for physical characterization of the compounds. Elemental analyses: Carlo Erba Strumentazione Elemental Analyzer, Modell 1106. NMR: Bruker ARX-500 (^{1}H, 500 MHz; ^{13}C, 125 MHz). Assignments of the resonances are supported by 2D experiments and chemical shift calculations. ^{1}H and ^{13}C NMR spectra were referenced to an internal Me_4Si (TMS) standard. IR: Bruker 22 FT-IR spectrometer with a golden-gate single-reflection diamond ATR system. MS: Bruker Daltonics mikro-TOF-Q (ESIMS). Differ-

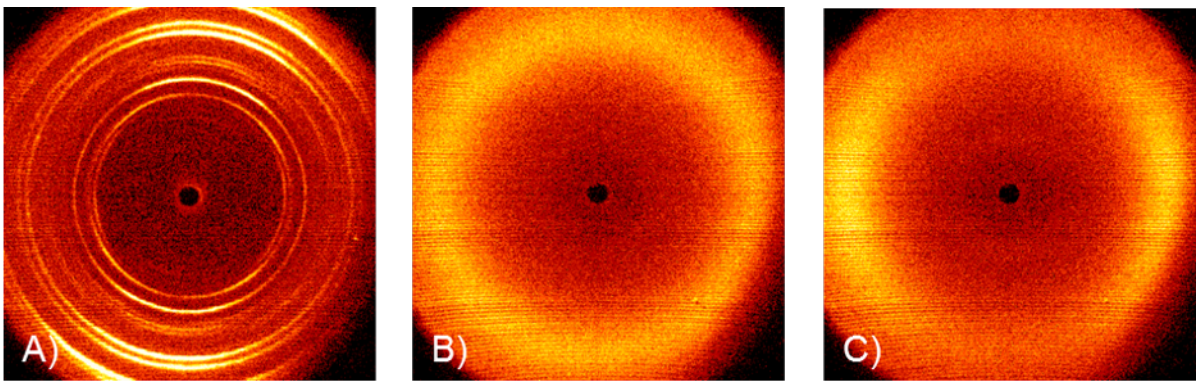

Figure 5: 2D X-ray scattering patterns of **11a**: (A) crystalline phase at 50 °C, (B) isotropic phase at 25 °C, and (C) nematic phase at 15 °C.

ential scanning calorimetry (DSC): Mettler-Toledo DSC 822e (heating/cooling rates were 5 or 10 K·min^{-1}). Polarizing optical microscopy: Olympus BX50 polarizing microscope combined with a Linkam TP93 central controller. X-ray diffraction (WAXS): Bruker AXS Nanostar C diffractometer employing Ni-filtered Cu Kα radiation (λ = 1.5418 Å).

6-[(4'-cyano-[1,1'-biphenyl]-4-yl)oxy]hexyl methyl malonate (**11a**)

Pyridine (150 mg, 1.69 mmol) and then methyl 3-chloro-3-oxopropionate (**10**) (114 mg, 0.84 mmol) were added over 10 min at 0 °C under a N_2 atmosphere to a solution of 4'-((6-hydroxyhexyl)oxy)-[1,1'-biphenyl]-4-carbonitrile (**9a**) (500 mg, 1.69 mmol) in abs. CH_2Cl_2 (5 mL). The reaction mixture was stirred at 0 °C for 1 h, then for 2 h at rt. The reaction was quenched with 1 N H_2SO_4 (3 mL). The aqueous layer was extracted with CH_2Cl_2 (3 × 5 mL). The combined organic layers were washed with brine (40 mL), dried over $MgSO_4$ and evaporated under reduced pressure. The crude product was purified by column chromatography on silica gel (hexanes/EtOAc 20:1) to give **11a** as a colourless solid (188 mg, 0.48 mmol, 57%). Mp 49.1 °C; ^{1}H NMR (500 MHz, $CDCl_3$) δ 1.41–1.47 (m, 2H, 6-H), 1.49–1.55 (m, 2H, 7-H), 1.67–1.73 (m, 2H, 5-H), 1.79–1.85 (m, 2H, 8-H), 3.39 (s, 2H, 2-H), 3.74 (s, 3H, OC*H*$_3$), 4.01 (t, *J* = 6.4 Hz, 2H, 9-H), 4.17 (t, *J* = 6.4 Hz, 2H, 4-H), 6.98 (d, *J* = 8.5 Hz, 2H, 2'-H), 7.52 (d, *J* = 8.5 Hz, 2H, 3'-H), 7.64 (d, *J* = 8.5 Hz, 2H, 6'-H), 7.69 (d, *J* = 8.5 Hz, 2H, 7'-H) ppm; ^{13}C NMR (125 MHz, $CDCl_3$) δ 25.6, 25.7 (C-6, C-7), 28.4 (C-5), 29.0 (C-8), 41.4 (C-2), 52.5 (O*C*H$_3$), 65.6 (C-4), 67.8 (C-9), 110.0 (C-8'), 115.0 (C-2'), 119.1 (*C*N), 127.0 (C-6'), 128.3 (C-3'), 131.3 (C-5'), 132.6 (C-7'), 145.3 (C-4'), 159.7 (C-1'), 166.6 (C-3), 167.0 (C-1) ppm; ATR–FTIR ṽ: 2936 (m), 2858 (w), 2224 (m), 1967 (w), 1730 (s), 1602 (m), 1494 (m), 1246 (s), 1014 (m), 822 (s); ESIMS (*m*/*z*): 343.1 [M + K]$^+$, 418.1 [M + Na]$^+$, 396.1 [M + H]$^+$, 278.15 [$C_{19}H_{20}NO$]$^+$; Anal. calcd for $C_{23}H_{25}NO_5$: C, 69.86; H, 6.37; N, 3.54; found: C, 69.47; H, 6.37; N, 3.47; R_f 0.56 (hexanes/EtOAc 2:1).

10-[(4'-cyano-[1,1'-biphenyl]-4-yl)oxy]decyl methyl malonate (**11b**)

The ester **11b** was obtained by the same procedure as described above for **11a** from 4'-((10-hydroxydecyl)oxy)-[1,1'-biphenyl]-4-carbonitrile (**9b**) (560 mg, 1.60 mmol), methyl 3-chloro-3-oxopropionate (**10**) (109 mg, 0.80 mmol) and pyridine (126 mg, 1.60 mmol) in abs. CH_2Cl_2 (5 mL). The crude product was purified by column chromatography on silica gel (gradient: hexanes/EtOAc, 20:1, then 15:1) to give **11b** as a colourless solid (240 mg, 0.53 mmol, 65%). Mp 63.4 °C; ^{1}H NMR (500 MHz, $CDCl_3$) δ 1.31–1.35 (m, 10H, 6-H, 7-H, 8-H, 9-H, 10-H), 1.44–1.50 (m, 2H, 11-H), 1.61–1.67 (m, 2H, 5-H), 1.77–1.83 (m, 2H, 12-H), 3.38 (s, 2H, 2-H), 3.75 (s, 3H, OC*H*$_3$), 4.00 (t, *J* = 6.5 Hz, 2H, 13-H), 4.14 (t, *J* = 6.8 Hz, 2H, 4-H), 6.98–6.99 (m, 2H, 2'-H), 7.51–7.53 (m, 2H, 3'-H), 7.63–7.64 (m, 2H, 6'-H), 7.68–7.69 (m, 2H, 7'-H) ppm; ^{13}C NMR (125 MHz, $CDCl_3$) δ 25.7 (C-6), 26.0 (C-11), 28.4 (C-5), 29.15 (C-12), 29.21, 29.33, 29.41, 29.45 (C-7, C-8, C-9, C-10), 41.4 (C-2), 52.4 (O*C*H$_3$), 65.7 (C-4), 68.1 (C-13), 110.0 (C-8'), 115.0 (C-2'), 119.1 (*C*N), 127.0 (C-6'), 128.3 (C-3'), 131.3 (C-5'), 132.6 (C-7'), 145.3 (C-4'), 159.8 (C-1'), 166.6 (C-3), 167.0 (C-1) ppm; ATR–FTIR ṽ: 2927 (m), 2854 (w), 2225 (m), 1735 (s), 1603 (m), 1494 (m), 1249 (s), 1180 (m), 903 (m), 823 (m); ESIMS (*m*/*z*): 474.2 [M + Na]$^+$, 452.2 [M + H]$^+$; Anal. calcd for $C_{27}H_{33}NO_5$: C, 71.82; H, 7.37; N, 3.10; found: C, 71.66; H, 7.34; N, 3.03; R_f 0.76 (hexanes/EtOAc 2:1).

6-[(4'-cyano-[1,1'-biphenyl]-4-yl)oxy]hexyl 2-cyanoacetate (**13a**)

To a solution of 4'-((6-hydroxyhexyl)oxy)-[1,1'-biphenyl]-4-carbonitrile (**9a**) (100 mg, 338 μmol) in abs. CH_2Cl_2 (2.5 mL) were added sequentially a solution of cyanoacetic acid (**12**) (32 mg, 376 μmol) in EtOAc (0.4 mL), a solution of DMAP (12 mg, 98 μmol) in abs. CH_2Cl_2 (0.8 mL) and then at 0 °C a solution of dicyclohexylcarbodiimide (77 mg, 376 μmol) in abs. CH_2Cl_2 (2.5 mL). The reaction mixture was stirred at rt for 7.5 h, then evaporated under vacuum. The crude product was purified by column chromatography on silica gel (hexanes/EtOAc 12:1) to give **13a** as a colourless solid (72 mg, 190 μmol, 59%). Mp 89.0 °C; ^{1}H NMR (500 MHz, $CDCl_3$) δ 1.43–1.49 (m, 2H, 6-H), 1.51–1.56 (m, 2H, 7-H), 1.71–1.76 (m, 2H, 5-H), 1.80–1.85 (m, 2H, 8-H), 3.45 (s, 2H, 2-H), 4.01 (t, *J* = 6.4 Hz, 2H, 9-H), 4.23 (t, *J* = 6.3 Hz, 2H, 4-H), 6.98–6.99 (m, 2H, 2'-H), 7.52–7.53 (m, 2H, 3'-H), 7.63–7.64 (m, 2H, 6'-H), 7.68–7.69 (m, 2H, 7'-H) ppm; ^{13}C NMR (125 MHz, $CDCl_3$) δ 24.7 (C-2), 25.5 (C-6), 25.6 (C-7), 28.3 (C-5), 29.0 (C-8), 66.9 (C-4), 67.8 (C-9), 110.0 (C-8'), 112.9 (C-1), 115.0 (C-2'), 119.1 (*C*N), 127.0 (C-6'), 128.3 (C-3'), 131.3 (C-5'), 132.5 (C-7'), 145.2 (C-4'), 159.6 (C-1'), 162.9 (C-3) ppm; ATR–FTIR ṽ: 2941 (m), 2866 (w), 2225 (w), 1746 (m), 1602 (m), 1494 (m), 1249 (m), 1180 (m), 903 (s), 723 (s); ESIMS (*m*/*z*): 385.1 [M + Na]$^+$, 363.1 [M + H]$^+$; Anal. calcd for $C_{22}H_{22}N_2O_3$: C, 71.91; H, 6.12; N, 7.57; found: C, 71.44; H, 6.06; N, 7.73; R_f 0.68 (hexanes/EtOAc 2:1).

10-[(4'-cyano-[1,1'-biphenyl]-4-yl)oxy]decyl 2-cyanoacetate (**13b**)

The cyanoacetic ester **13b** was obtained by the same procedure as described above for **13a** from 4'-((10-hydroxydecyl)oxy)-[1,1'-biphenyl]-4-carbonitrile (**9b**) (120 mg, 341 μmol), cyanoacetic acid (**12**) (32 mg, 376 μmol), DMAP (13 mg, 102 μmol), and dicyclohexylcarbodiimide (77 mg, 376 μmol) in abs. CH_2Cl_2 (6.5 mL). The crude product was purified by column chromatography on silica gel (hexanes/EtOAc 10:1) to give **13b**

as a colourless solid (57 mg, 140 μmol, 41%). Mp 93.2 °C; ^{1}H NMR (500 MHz, $CDCl_3$) δ 1.32–1.36 (m, 10H, 6-H, 7-H, 8-H, 9-H, 10-H), 1.44–1.50 (m, 2H, 11-H), 1.65–1.71 (m, 2H, 5-H), 1.78–1.83 (m, 2H, 12-H), 3.44 (s, 2H, 2-H), 4.00 (t, J = 6.5 Hz, 2H, 13-H), 4.20 (t, J = 6.9 Hz, 2H, 4-H), 6.98–6.99 (m, 2H, 2'-H), 7.51–7.53 (m, 2H, 3'-H), 7.63–7.64 (m, 2H, 6'-H), 7.68–7.69 (m, 2H, 7'-H) ppm; ^{13}C NMR (125 MHz, $CDCl_3$) δ 24.7 (C-2), 25.6 (C-6), 26.0 (C-11), 28.3 (C-5), 29.11 (C-12), 29.21, 29.32, 29.36, 29.40 (C-7, C-8, C-9, C-10), 67.1 (C-4), 68.1 (C-13), 110.0 (C-8'), 113.0 (C-1), 115.0 (C-2'), 119.1 (*C*N), 127.0 (C-6'), 128.3 (C-3'), 131.3 (C-5'), 132.5 (C-7'), 145.2 (C-4'), 159.7 (C-1'), 162.9 (C-3) ppm; ATR–FTIR $\tilde{\nu}$: 2928 (m), 2855 (w), 2225 (w), 1747 (m), 1603 (m), 1494 (m), 1250 (m), 1180 (m), 903 (s), 725 (s); ESIMS (*m*/*z*): 457.1 $[M + K]^+$, 441.2 $[M + Na]^+$, 436.2, 419.2 $[M + H]^+$; Anal. calcd for $C_{26}H_{30}N_2O_3$: C, 74.61; H, 7.22; N, 6.69; found: C, 74.04; H, 7.18; N, 6.54; R_f 0.58 (hexanes/EtOAc 2:1).

Supporting Information

Supporting Information File 1

Full experimental procedures and DSC traces of **11b** and **13b**.
[http://www.beilstein-journals.org/bjoc/content/supplementary/1860-5397-8-40-S1.pdf]

Acknowledgements

Generous financial support by the Bundesministerium für Bildung und Forschung, the Ministerium für Wissenschaft, Forschung und Kunst des Landes Baden-Württemberg and the Max-Planck-Gesellschaft (International Max Planck Research School for Advanced Materials fellowship for M.K.) is gratefully acknowledged. We would like to thank Ingo Dierking for helpful discussions and suggestions.

References

1. Goodby, J. W. In *Handbook of Liquid Crystals;* Demus, D.; Goodby, J.; Gray, G. W.; Spiess, H.-W.; Vill, V., Eds.; Wiley-VCH: Weinheim, Germany, 1998; Vol. 2A, pp 3–21.
2. Assanto, G.; Peccianti, M. *Mol. Cryst. Liq. Cryst.* **2008,** *488,* 163–178. doi:10.1080/15421400802240540
3. Eidenschink, R. *Mol. Cryst. Liq. Cryst.* **1983,** *94,* 119–125. doi:10.1080/00268948308084251
4. Raviol, A.; Stille, W.; Strobl, G. *J. Chem. Phys.* **1993,** *105,* 3788–3794. doi:10.1063/1.470057
5. O'Neill, M.; Kelly, S. M. *Adv. Mater.* **2003,** *15,* 1135–1146. doi:10.1002/adma.200300009
6. O'Neill, M.; Kelly, S. M. *Adv. Mater.* **2011,** *23,* 566–584. doi:10.1002/adma.201002884
7. Kopp, V. I.; Fan, B.; Vithana, H. K. M.; Genack, A. Z. *Opt. Lett.* **1998,** *23,* 1707–1709. doi:10.1364/OL.23.001707
8. Dąbrowski, R. *Mol. Cryst. Liq. Cryst.* **2004,** *421,* 1–21. doi:10.1080/15421400490501112
9. Kirsch, P.; Bremer, M. *Angew. Chem.* **2000,** *112,* 4384–4405. doi:10.1002/1521-3757(20001201)112:23<4384::AID-ANGE4384>3.0.CO;2-S
Angew. Chem., Int. Ed. **2000,** *39,* 4216–4235. doi:10.1002/1521-3773(20001201)39:23<4216::AID-ANIE4216>3.0.CO;2-K
10. Bisoyi, H. K.; Kumar, S. *Chem. Soc. Rev.* **2010,** *39,* 264–285. doi:10.1039/b901792p
11. Goodby, J. W. *Liq. Cryst.* **2011,** *38,* 1363–1387. doi:10.1080/02678292.2011.614700
12. Shimizu, Y.; Oikawa, K.; Nakayama, K.-i.; Guillon, D. *J. Mater. Chem.* **2007,** *17,* 4223–4229. doi:10.1039/b705534j
13. Yang, S. H.; Hsu, C.-S. *J. Polym. Sci., Part A: Polym. Chem.* **2009,** *47,* 2713–2733. doi:10.1002/pola.23342
14. Gray, G. W.; Kelly, S. M. *J. Mater. Chem.* **1999,** *9,* 2037–2050. doi:10.1039/a902682g
15. Bulkin, B. J.; Rose, R. K.; Santoro, A. *Mol. Cryst. Liq. Cryst.* **1977,** *43,* 53–58. doi:10.1080/00268947708084934
16. Giroud-Godquin, A. M. In *Handbook of Liquid Crystals;* Demus, D.; Goodby, J.; Gray, G. W.; Spiess, H.-W.; Vill, V., Eds.; Wiley-VCH: Weinheim, Germany, 1998; Vol. 2B, pp 901–932.
17. Mühlberger, B.; Haase, W. *Liq. Cryst.* **1989,** *5,* 251–263. doi:10.1080/02678298908026368
18. Dzhabarov, V. I.; Knyazev, A. A.; Strelkov, M. V.; Molostova, E. Y.; Schustov, V. A.; Haase, W.; Galyametdinov, Y. G. *Liq. Cryst.* **2010,** *37,* 285–291. doi:10.1080/02678290903506040
See for recent examples of liquid crystalline β-diketonate metal complexes.
19. Santoro, A.; Whitwood, A. C.; Williams, J. A. G.; Kozhevnikov, V. N.; Bruce, D. W. *Chem. Mater.* **2009,** *21,* 3871–3882. doi:10.1021/cm9012156
See for recent examples of liquid crystalline β-diketonate metal complexes.
20. Pucci, D.; Aiello, I.; Aprea, A.; Bellusci, A.; Crispini, A.; Ghedini, M. *Chem. Commun.* **2009,** 1550–1552. doi:10.1039/b818603k
See for recent examples of liquid crystalline β-diketonate metal complexes.
21. Yoshida, J.; Sato, H.; Hoshino, N.; Yamagishi, Y. *J. Phys. Chem. B* **2008,** *112,* 9677–9683. doi:10.1021/jp8011206
See for recent examples of liquid crystalline β-diketonate metal complexes.
22. Knyazev, A. A.; Dzhavarov, V. I.; Lapaev, D. V.; Lopkov, V. S.; Haase, W.; Galyametdinov, Y. G. *Russ. J. Gen. Chem.* **2010,** *80,* 756–760. doi:10.1134/S1070363210040122
23. Han, J.; Guo, H.; Wang, X.-G.; Pang, M.-L.; Meng, J.-B. *Chin. J. Chem.* **2007,** *25,* 129–131. doi:10.1002/cjoc.200790007
24. Han, J.; Zhang, L. F.; Wan, W. *Chin. Chem. Lett.* **2004,** *15,* 155–158.
25. Farago, M. E.; Amirhaeri, S. *Inorg. Chim. Acta* **1984,** *81,* 205–212. doi:10.1016/S0020-1693(00)88759-9
26. Lose, D.; Diele, S.; Pelzl, G.; Dietzmann, E.; Weissflog, W. *Liq. Cryst.* **1998,** *24,* 707–717. doi:10.1080/026782998206821
27. Maringa, N.; Lenoble, J.; Donnio, B.; Guillon, D.; Deschenaux, R. *J. Mater. Chem.* **2008,** *18,* 1524–1534. doi:10.1039/b717105f
28. Dardel, B.; Guillon, D.; Heinrich, B.; Deschenaux, R. *J. Mater. Chem.* **2001,** *11,* 2814–2831. doi:10.1039/b103798f
29. Chuard, T.; Dardel, B.; Deschenaux, R.; Even, M. *Carbon* **2000,** *38,* 1573–1576. doi:10.1016/S0008-6223(99)00286-9

30. Chuard, T.; Deschenaux, R.; Hirsch, A.; Schönberger, H. *Chem. Commun.* **1999,** 2103–2104. doi:10.1039/a905058b
31. Deschenaux, R.; Even, M.; Guillon, D. *Chem. Commun.* **1998,** 537–538. doi:10.1039/a709092g
32. Schubert, H.; Hoffmann, S.; Hauschild, J.; Marx, I. *Z. Chem.* **1977,** *17,* 414–415. doi:10.1002/zfch.19770171106
33. Kašpar, M.; Sverenyák, H.; Hamplová, V.; Pakhomov, S. A.; Glogarová, M. *Mol. Cryst. Liq. Cryst. Sci. Technol., Sect. A* **1995,** *260,* 241–246. doi:10.1080/10587259508038695
34. Pintre, I. C.; Serrano, J. L.; Blanca Ros, M.; Martínez-Perdiguero, J.; Alonso, I.; Ortega, J.; Folcia, C. L.; Etxebarria, J.; Alicante, R.; Villacampa, B. *J. Mater. Chem.* **2010,** *20,* 2965–2971. doi:10.1039/b923616c
35. Chong, J. M.; Heuft, M. A.; Rabbat, F. *J. Org. Chem.* **2000,** *65,* 5837–5838. doi:10.1021/jo000291u
36. Sahade, D. A. Polymerizable Liquid Crystal Compound, Polymerizable Liquid Crystal Composition, and Alignment Film. EP 2062882, May 27, 2009.
Chem. Abstr. **2008,** *149,* 91567.
37. Zugenmaier, P. *Liq. Cryst.* **2002,** *29,* 443–448. doi:10.1080/02678290110113522
38. Nakatsuji, S.; Ikemoto, H.; Akutsu, H.; Yamada, J.-i.; Mori, A. *J. Org. Chem.* **2003,** *68,* 1708–1714. doi:10.1021/jo0206972
39. Kadkin, O. N.; Han, H.; Galyametdinov, Y. G. *J. Organomet. Chem.* **2007,** *692,* 5571–5582. doi:10.1016/j.jorganchem.2007.09.010
40. Dierking, I. *Textures of Liquid Crystals;* Wiley-VCH: Weinheim, Germany, 2003. doi:10.1002/3527602054
41. Dierking, I. *Physik Journal* **2009**, *8* (4), 27–32.
42. Kuiper, S.; Norder, B.; Jager, W. F.; Dingemans, T. J.; van Turnhout, J.; Picken, S. J. *J. Phys. Chem. B* **2011,** *115,* 1416–1421. doi:10.1021/jp105643s

License and Terms

Beilstein Journal of Organic Chemistry

Perhydroazulene-based liquid-crystalline materials with smectic phases

Zakir Hussain*[1,2], Henning Hopf[1] and S. Holger Eichhorn[3]

Full Research Paper

Open Access

Address:
[1]Institut für Organische Chemie, Technische Universität Braunschweig, Hagenring 30, 38106 Braunschweig, Germany, Fax: +49(531)3915388, [2]Department of Chemistry, COMSATS Institute of Information Technology, University Road, Abbottabad, Pakistan and [3]Department of Chemistry and Biochemistry, University of Windsor, 401 Sunset Avenue, Essex Hall, Windsor, ON Canada N9B 3P4, Fax: +1 (519) 973-7064

Email:
Zakir Hussain* - chem63@yahoo.com; Henning Hopf - H.Hopf@tu-bs.de; S. Holger Eichhorn - eichhorn@uwindsor.ca

* Corresponding author

Keywords:
hydroazulenes; liquid crystals; nematic phases; smectic phases

Beilstein J. Org. Chem. **2012,** *8,* 403–410.
doi:10.3762/bjoc.8.44

Received: 05 December 2011
Accepted: 06 March 2012
Published: 16 March 2012

This article is part of the Thematic Series "Progress in liquid crystal chemistry II".

Guest Editor: S. Laschat

Abstract

New liquid-crystalline materials with a perhydroazulene core were synthesized and the stereochemistry of these compounds was investigated. The mesomorphic properties of the new LC compounds were investigated by differential scanning colorimetry, polarizing optical microscopy and X-ray diffraction. We report here on the LC properties of nonchiral materials, which predominantly exhibit smectic phases and display nematic phases only within narrow temperature ranges. The dependence of the mesogenic behavior of the new materials on the stereochemistry of the core system was also investigated. All newly synthesized compounds were fully characterized by the usual spectroscopic and analytical methods.

Introduction

Liquid crystals for display applications have to fulfill a complex, interdependent set of properties [1]. First of all, they must display a broad nematic phase, typically ranging from −30 °C to +80 °C. The absolute value for the dielectric anisotropy Δε should be large in order to decrease the operating voltage, since this will lower power consumption. The rotational viscosity γ_1 should be as low as possible to allow fast switching, and the birefringence Δn has to be adjusted to fit the precise display configuration, in particular the cell gap. In the molecular design of new liquid crystals, electro-optical properties can now be predicted quite precisely based on molecular modeling [1,2]. However, full evaluation of the value of a new structure is still only possible after synthesis. In the past few years many attempts have been made to improve the properties of calamitic liquid crystals [3-8]. However, there is still a growing need for more advanced materials to be synthesized and tested for the desired features of the displays. Moreover, the properties of the LC materials required for applications in LCDs are achieved by mixture formulation of various components, including about 15–20 individual LC molecules.

The nematic (N) liquid crystal phase, with its orientational order only, is the most important mesophase; it is used in almost all commercially available LC displays. On the other hand, the smectic (Sm) LC phases, with their orientational order, have found little commercially successful applications. So far, an enormous amount of experimental and theoretical work exists in the literature concerning the nematic liquid crystals [1-8], whereas smectic liquid crystals have not been studied to the same extent, although recently they have attracted considerable interest [9-12]. It has also been demonstrated that by modification of the basic structures a wide range of properties affecting the liquid crystal behavior of these materials can be changed. The core units presently used in most of the calamitic LCs are cyclohexane, phenylcyclohexane, etc. We previously introduced [13] a completely new core unit: the perhydroazulene ring system. This system provides a segment that may align in such a way that the long molecular axes are parallel, with the capability to induce anisotropy, whereas if we introduce terminal chains, they can provide flexibility to stabilize the molecular alignment within the mesophase. Such terminal chains can either be nonpolar straight alkyl chains or carry a polar substituent. Such molecules may form both nematic and smectic mesophases depending upon the type of substituents and their substituent combinations, as well as on the stereochemistry at their central junction and the relative orientation of the respective substituents.

Hydroazulene-based liquid-crystal molecules are expected to show mesogenic behavior if linearity exists in the system. Such linearity can be achieved by the introduction of terminal groups preferentially in *trans*- or *anti*-fashion. We previously employed a ring expansion strategy for the synthesis of the perhydroazulene core and were able to also purify several of our carbene adducts by way of HPLC [14]. If we start our synthesis by the introduction of relevant terminal groups into the isomer that can provide the material with *trans*-stereochemistry, the resulting derivatives could reveal mesogenic behavior as expected (Figure 1).

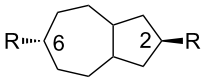

Figure 1: Overall molecular structure of the perhydroazulene core with *trans*-stereochemistry.

In the present contribution, we report on the synthesis and mesogenic properties of materials containing a perhydroazulene core system and discuss the dependence of the LC properties of these materials on the stereochemistry of this core. Resulting from our investigations, we describe here that the perhydroazulene core system, having substituents with only *trans* orientation, provides mesogenic properties. To the best of our knowledge, such studies are so far absent from the literature with regard to hydroazulene-based smectic liquid-crystalline materials.

Results and Discussion

The synthesis of *exo*-isomers **1a** and **1b** (Scheme 1) has already been reported [14]. Both isomers were purified through reversed-phase HPLC, obtained in >98% purity, and characterized by NMR spectroscopy as well as by their other analytical data [14]. The NMR data of **1a** and **1b** indicate that methylene groups in the five-membered ring carry pairwise enantiotopic and diastereotopic H-atoms; enantiotopic with respect to the internal mirror plane, diastereotopic with respect to above and below the plane of the molecules. A triplet at 1.40 ppm for **1a** and 1.34 ppm for **1b** with almost the same coupling constant (4.3 Hz) between the H-atoms at the cyclopropyl ring indicates an *anti*-relation between the ethoxycarbonyl group and the cyclohexene ring.

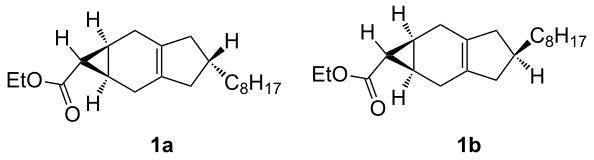

Scheme 1: Stereochemistry of carbene adducts **1a** and **1b**.

The isomers **1a** and **1b** were subsequently subjected to a ring-opening reaction to afford the cycloheptatrienes **4a** and **4b**. In a first step, the isomers **1** were first brominated in carbon tetrachloride [15], to produce the dibromides **2a** and **2b**. After the complete addition of bromine, triethylamine was added slowly, resulting in triethylamine hydrobromide and the formation of the norcaradiene intermediates **3a** and **3b** in situ. These were subsequently converted by overnight heating into the cycloheptatrienes **4a** and **4b** as slightly colored liquids, by an electrocyclic ring-opening mechanism and a subsequent base-catalyzed prototropic shift, as described for analogous compounds [13]. In principle, the double bonds in the seven-membered rings of these derivatives could be arranged in a different fashion through the so-called Berson–Willcott rearrangement [16] or by 1,5-H shift processes. The exclusive generation of the particular isomers shown is presumably associated with their greater thermodynamic stability. With a double bond at the ring junction, the resulting isomer possesses the most highly substituted double bond possible (Scheme 2).

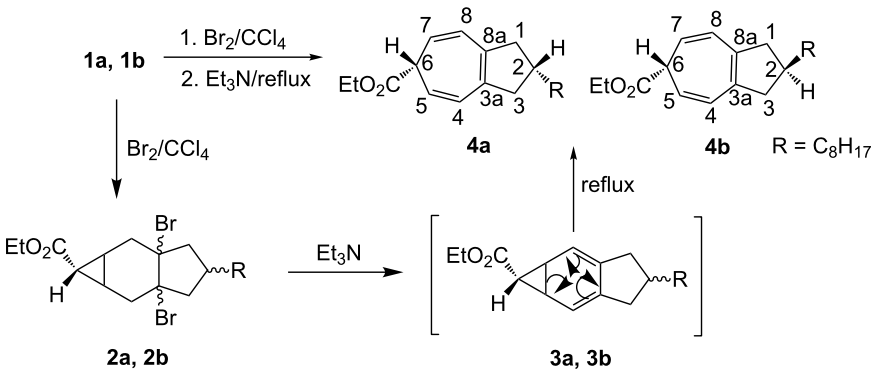

Scheme 2: Preparation of the tropylidenes **4a** and **4b**.

The two diastereomers **4a** and **4b** were separated and their structures were established by 1D and 2D NMR methods in addition to other analytical tools. The multiplet at 2.66 ppm in the ^{1}H NMR spectrum for 6-H, doublets at 6.15–6.19 ppm with the coupling constant 9.1 Hz for 4/8-H and a singlet at 141.79 ppm in the ^{13}C NMR spectrum for C-3a/8a indicated the formation of **4a** and **4b**. The orientation of the terminal groups and position of the double bonds in isomers similar to **4a** and **4b** was established by analysis of the X-ray structures of their corresponding acids [14].

Continuing the synthesis, the precursors **4a** and **4b** were hydrogenated in the presence of Pd/C, and ethyl acetate as solvent which resulted in the completely saturated perhydroazulene systems **5a** and **5b**. It is important to note that, in addition to **5a** and **5b**, we also observed the presence of one additional isomer (<5%) in both cases in the GC-chromatogram. The formation of such an isomer from pure **4a** or **4b** can only be rationalized if catalytic hydrogenation results in an isomer with a *trans*-ring junction at the 3a/8a-position, as described previously [13,14]. However, in the present investigation, we could not completely purify this minor isomer in order to establish its exact stereochemical structure. Based on the full characterization of **4a** and **4b** by spectroscopic, analytical and X-ray data, the structures of the perhydroazulene systems **5a** and **5b** were elucidated. The disappearance of doublets at 6.1 ppm with coupling constants of 9.1 Hz for the 4/8 protons in **4a** and **4b**, and the appearance of multiplets for these protons, indicated the formation of **5a** and **5b**. Complete NMR (1D, 2D) as well as other analytical data of the above isomers can be found separately in the experimental section. In order to gain additional insight into the structures of the above esters (**5a**, **5b**) and to confirm their stereochemistry, their hydrolysis [17] was carried out in the presence of NaOH and MeOH. Acids **6a** and **6b** were obtained in the form of colorless solids, which were recrystallized from hexane/dichloromethane. Although the single crystals obtained were not suitable for a high-quality X-ray analysis, we could compare the NMR data of the resulting acids with the data of similar acids [13]. Based on this comparison, we established that the protons at 3a and 8a point in the same direction leading to *cis*-fused systems. The cycloheptane rings display very similar conformations, with local mirror symmetry through C6 and the midpoint of the C3a–C8a bond. Hydrogen bonding between the acids produces the usual dimeric forms. The complete analytical and spectroscopic data of **6a** and **6b** (Scheme 3) can be found in the experimental section.

In a final step, esterification [18] of acids **6a** and **6b** was carried out in order to investigate the effect of stereochemistry on the liquid-crystalline properties in the resulting esters. We selected

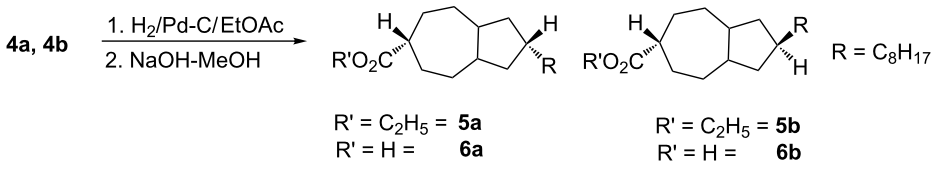

Scheme 3: Formation of esters **5a** and **5b** and the corresponding acids **6a** and **6b**.

two different phenols for this esterification step, one with a nonpolar end group, an alkyl chain, and the other with a polar end group, a cyano moiety. The newly synthesized derivatives **8a** and **8b** (Scheme 4) and **10a** and **10b** (Scheme 5) were carefully purified and characterized through 1D and 2D NMR as well as through their other analytical data.

Investigation of the mesogenic properties of the target compounds **8a**, **8b**, **10a** and **10b**

Investigation of the materials synthesized above for their phase-transition behavior showed that compounds **8a** and **10a**, with the ester and alkyl groups in 6- and 2-positions oriented *cis* to each other, do not display mesogenic behavior, and in both cases we see a clear crystal-to-isotropic transition (Table 1). However, compounds **8b** and **10b** with *trans*-orientations in the 6- and 2-positions showed several liquid-crystalline phases over a wide temperature range. Variable-temperature optical polarized microscopy (vt-OPM) and differential scanning calorimetry (DSC) measurements revealed that compound **8b** is converted into a SmC phase at ~28 °C and converts into a short-temperature-range SmA and N phase at ~101 °C and 107 °C, respectively. The conversion of the nematic phase to the isotropic phase in the case of **8b** was observed at 117 °C. Similar investigations on phase transitions of compound **10b** revealed that this material melts into a SmC phase at a much higher temperature, i.e., ~94 °C, compared to **8b**. This mesophase was stable up to 244 °C at which it converted into a short-range SmA phase followed by transitions into the nematic and isotropic phases at 253 °C and 266 °C, respectively. Appearance of transitions at much higher temperatures in case of **10b** compared to **8b** could be associated with the chemical structures of both compounds. In the case of **8b**, the presence of only one aromatic ring with a short alky chain at the ester side could result in a lower melting range, while the presence of cyanobiphenyl in the case of **10b** could cause its higher melting behavior.

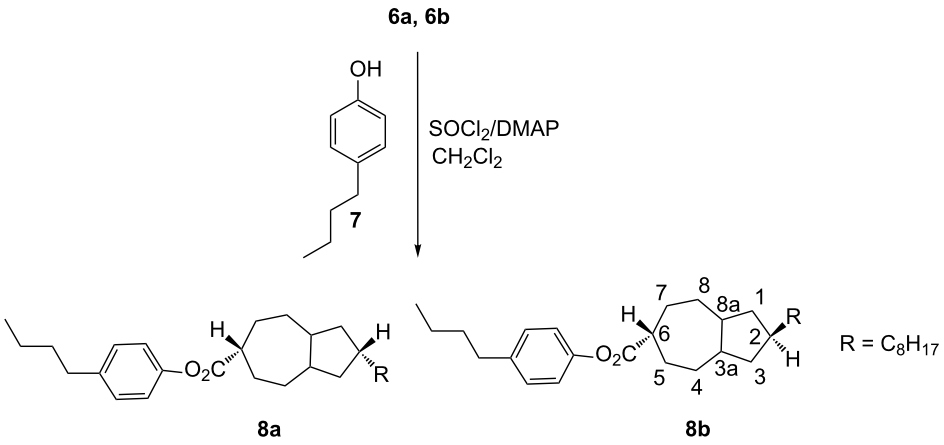

Scheme 4: Preparation of **8a** and **8b**.

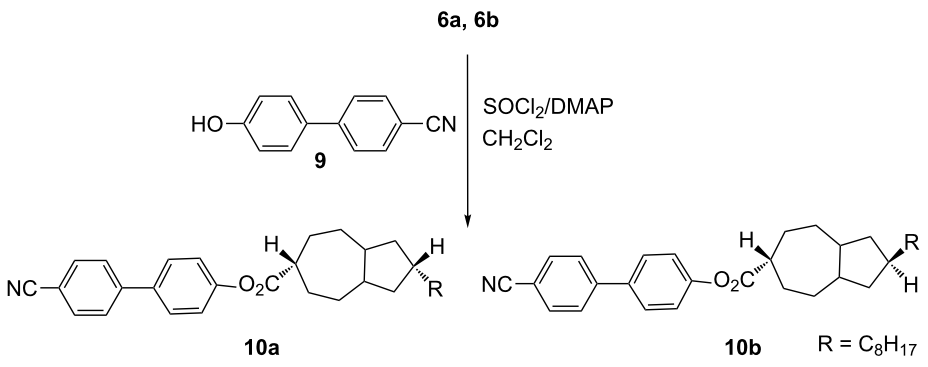

Scheme 5: Preparation of **10a** and **10b**.

Table 1: Liquid-crystal data of target materials **8a** and **8b** and **10a** and **10b**.

	Peak temperatures (enthalpies) of transitions on heating/cooling in °C (kJ/mol)					
	Cry→Cry	Cry→I	Cry→SmC	SmC→SmA	SmA→N	N→I
8a		41/30 (27.8/−27.4)				
8b	7.9[a]		28/7 (33.87/−24.28)	101/98 (1.63/−1.57)	107/104 (0.69/−0.92)	117/115 (0.48/−0.92)
10a		91/69 (19.72/−20.86)				
10b	77/58 (−5.87), 54 (−1.34), 52 (−0.72)		94/68 (13.54/−5.36)	244/222 (0.25/−0.005)	253/233 (0.15/−0.13)	266/263 (0.92/−0.52)

[a]Exothermic (cold crystallization) and endothermic transitions overlap (net enthalpic change is 5.04 kJ/mol).

Conclusion

We have synthesized new liquid-crystalline materials with a perhydroazulene core and investigated their stereochemistry by advanced NMR spectroscopic methods. On the basis of the concept that linearity in these molecules results in liquid-crystalline phases, we present data here on smectic as well as nematic phases that are observed in isomers with only *trans*-positioned terminal groups. We have also shown that by changing terminal group(s), a broad range of LC phases results, characterized by the transition temperatures of smectic phases in those isomers that carry a polar terminal group compared to those with a nonpolar terminal group. We have also fully described the synthesis of acid **6b**, which is the key intermediate, from the starting material **1b** in three steps with a total average yield of about 72%.

Experimental

TLC: Precoated plastic plates, PolyGram Sil G/UV_{254}. Column chromatography: Silica gel 60 (70–230 mesh) Merck (Darmstadt). Mp below 200 °C: Büchi 510 melting-point apparatus, above 200 °C: Kofler-Heiztischmikroskop, uncorrected. ^{1}H and ^{13}C NMR: Bruker DRX-400, ^{1}H NMR (400.1 MHz); ^{13}C NMR (100.6 MHz); chemical shifts (δ) are expressed in parts per million (ppm) downfield from tetramethylsilane or by using the residual nondeuterated solvent as internal standards ($CDCl_3$: ^{1}H: δ 7.26; ^{13}C: δ 77.00). IR: Nicolet 320 FT-IR and Bruker Tensor 27 spectrometer. Samples were prepared either as KBr pellets or as thin films. UV: In acetonitrile and methanol with a Beckman UV 5230 or a HP 8452A Diode Array spectrophotometer. MS: Finnigan MAT 8430 using the electron ionization method (EI, 70 eV). CH_2Cl_2 and Et_3N were distilled from CaH_2 under nitrogen, while all other chemicals were of reagent quality and used as obtained from the suppliers. Reactions were carried out under dried argon when necessary. The experimental procedures for the preparation of **4a, 4b**, **5a, 5b** as well as **6a, 6b** are essentially the same as described previously [13].

Ethyl 2-octyl-1,2,3,6-tetrahydro-6-azulenecarboxylate (4a, 4b): Ethyl 4-octyl-1,1a,2,3,4,5,6,6a-octahydrocyclopropa[*f*]indene-1-carboxylate (**1a**, 0.8 g, 2.51 mmol) was dissolved in CCl_4 (30 mL), and the solution was cooled in an ice bath. Bromine (0.41 g, 2.51 mmol) dissolved in CCl_4 (5 mL) was added dropwise under stirring. When the addition was complete, triethylamine (1.12 g, 11.18 mmol) was added. Triethylamine hydrobromide began to form immediately. The mixture was heated under reflux for 18 h. After being cooled, the hydrobromide was filtered off. The filtrate was evaporated and the resulting oil partitioned between benzene and dilute aqueous acid (HCl). The benzene layer was washed with water and dried with $MgSO_4$ and filtered to obtain the crude product. After solvent removal in vacuo, the product was purified by column chromatography on silica gel with dichloromethane and pentane (8:2) as eluents, to yield **4a** as light-bluish liquid (0.5 g, ~58%). Compound **4b,** also obtained as a light-bluish liquid (56% yield), was synthesized by the same procedure from **1b**.

Compound 4a: Bp 134–136 °C/5 Torr; ^{1}H NMR (400.1 MHz, $CDCl_3$) δ 0.86 (t, ^3J = 7.07 Hz, 3H, 19-H), 1.28 (t, ^3J = 7.14 Hz, 3H, 11-H), 1.22–1.26 (m, 14H, 12-H, 18-H), 2.21 (m, 1H, 2-H), 2.32–2.41/2.77–2.83 (m, 4H, 1-H, 3-H), 2.66 (m, 1H, 6-H), 4.25 (q, ^3J = 7.13 Hz, 2H, 10-H), 5.32–5.39 (m, 2H, 5-H, 7-H), 6.15–6.19 (2 × d, ^3J = 9.1 Hz, 2H, 4-H, 8-H); ^{13}C NMR (100.6 MHz, $CDCl_3$) δ 14.09/14.24 (2 × q, C-11, C-19), 22.67 (t, C-18), 28.34 (t, C-13), 29.32, 29.63, 29.80 (3 × t, C-14, C-16), 31.90 (t, C-17), 35.97 (t, C-12), 37.34 (d, C-2), 42.82 (2 × t, C-1, C-3), 45.22 (d, C-6), 60.92 (t, C-10), 115.99, 116.65 (2 × d, C-5, C-7), 125.31, 125.45 (2 × d, C-4, C-8), 141.79 (s, C-3a, C-8a), 173.24 (s, C-9); IR (film) $\tilde{\nu}$: 2956 (m, CH-stretch), 173 (s, C=O), 1612 (w) cm^{-1}; UV (CH_3CN) λ_{max} nm (log ε): 228 (3.77), 236 (3.68), 246 (3.66), 264 (3.50); MS (EI, 70 eV) *m*/*z* (%): 316 (9) [M^+], 243 (100) [$M^+ - C_3H_5O_2$], 129 (10) [243 − C_8H_{18}]; HRMS: calcd for $C_{21}H_{32}NaO_2$, 339.229999; found, 339.22998 ± 0.07 ppm.

Compound 4b: Bp 135–137 °C/5 Torr; ^{1}H NMR (400.1 MHz, $CDCl_3$) δ 0.86 (t, ^3J = 6.60 Hz, 3H, 19-H), 1.28 (t, ^3J = 7.13 Hz, 3H, 11-H), 1.25–1.26 (m, 14H, 12-H, 18-H), 2.21 (m, 1H, 2-H), 2.31–2.41/2.77–2.83 (m, 4H, 1-H, 3-H), 2.68 (m, 1H, 6-H), 4.22 (q, ^3J = 7.12 Hz, 2H, 10-H), 5.32–5.39 (m, 2H, 5-H, 7-H), 6.15–6.19 (2 × d, ^3J = 9.13 Hz, 2H, 4-H, 8-H); ^{13}C NMR (100.6 MHz, $CDCl_3$) δ 14.08/14.23 (2 × q, C-11, C-19), 22.65 (t, C-18), 28.20 (t, C-13), 29.30, 29.62, 29.79 (3 × t, C-14, C-16), 31.88 (t, C-17), 36.16 (t, C-12), 37.79 (d, C-2), 42.99 (2 × t, C-1, C-3), 45.21 (d, C-6), 60.91 (t, C-10), 115.96, 116.63 (2 × d, C-5, C-7), 125.29, 125.44 (2 × d, C-4, C-8), 141.68 (s, C-3a, C-8a), 173.24 (s, C-9); IR (film) $\tilde{\nu}$: 2958 (m, CH-stretch), 1738 (s, C=O), 1610 (w), 1465 (w) cm^{-1}; UV (CH_3CN) λ_{max} nm (log ε): 228 (3.77), 236 (3.68), 246 (3.66), 264 (3.50); MS (EI, 70 eV) *m*/*z* (%): 316 (9) [M^+], 243 (100) [$M^+ - C_3H_5O_2$], 129 (10) [243 − C_8H_{18}]; HRMS: calcd for $C_{21}H_{32}NaO_2$, 339.229999; found, 339.23009 ± 0.27 ppm.

Ethyl 2-octylperhydro-6-azulenecarboxylate (5a and **5b):** Ethyl 2-octyl-1,2,3,6-tetrahydro-6-azulenecarboxylate (**4a**, 1.3 g, 4.11 mmol) was dissolved in ethyl acetate (100 mL) in a 250 mL flask and Pd/C (0.33 g) was added to the mixture. A stream of H_2 was blown through the suspension after evacuation, and the flask was shaken for 2 h in a hydrogen atmosphere. The mixture was filtered to remove the catalyst and the solvent was evaporated to yield the product in quantitative yield as a colorless liquid. GC analysis indicated the presence of another isomer (about 15%), which could not be separated completely by column chromatography on silica gel, whereas the major isomer (>82%) was separated by elution with pentane, by increasing its polarity through the addition of dichloromethane (~50%). The major product was found to be the one with the *cis*-fused ring system, as expected (**5a**, 1.06 g, ~80%); this eluted first from the column followed by the isomer with the *trans*-fused system (always containing traces of the *cis*-fused derivative). Compound **5a:** Bp 145–150 °C/5 Torr; ^{1}H NMR (400.1 MHz, $CDCl_3$) δ 0.85 (t, ^3J = 6.84 Hz, 3H, 19-H), 1.23 (t, ^3J = 7.14 Hz, 3H, 14-H), 1.21–1.22 (m, 14H, side chain protons), 1.45–1.50 (m, 2H, 3a-H, 8a-H), 1.48–1.53 (m, 4H, 4-H, 8-H), 1.60–1.67 (m, 1H, 2-H), 0.82/1.81 (m, 4H, 1-H, 3-H), 2.00–2.09 (m, 4H, 5-H, 7-H), 2.57–2.62 (m, 1H, 6-H), 4.11 (q, ^3J = 7.12 Hz, 2H, 10-H); ^{13}C NMR (100.6 MHz, $CDCl_3$) δ 14.09, 14.28 (2 × q, C-11, C-19), 22.67 (t, C-18), 28.73 (t, C-13), 28.79 (2 × t, C-4, C-8), 29.82 (2 × d, C-5, C-7), 29.33, 29.65, 29.97 (3 × t, C-14, C-15, C-16), 31.91 (t, C-17), 35.52 (t, C-12), 40.23 (d, C-2), 41.69 (2 × t, C-1, C-3), 42.12 (2 × t, C-3a, C-8a), 43.46 (d, C-6), 59.98 (t, C-10), 176.12 (s, C=O); IR (film) $\tilde{\nu}$: 2932 (s, CH-stretch), 1732 (s, C=O), 1463, 1450 (w) cm^{-1}; UV (CH_3CN) λ_{max} nm (log ε): 204 (2.92), 216 (2.55), 234 (2.15), 284 (1.86); MS (EI, 70 eV) *m*/*z* (%): 322 (100) [M^+], 307 (17) [$M^+ - CH_3$], 293 (33) [$M^+ - C_2H_5$], 276 (20) [$M^+ - C_2H_6O$], 248 (16) [$M^+ - C_3H_6O_2$], 206 (55) [$M^+ - C_8H_{17}$], 135 (42) [209 − $C_3H_6O_2$]; HRMS: calcd for $C_{21}H_{38}O_2$, 322.287178; found, 322.287430 ± 0.78 ppm.

Compound 5b: Compound **5b** was obtained from **4b** by the same procedure as described for **5a** in 77% yield as a colorless liquid. bp 147–151 °C/5 Torr; ^{1}H NMR (400.1 MHz, $CDCl_3$) δ 0.86 (t, ^3J = 6.91 Hz, 3H, 19-H), 1.25 (t, ^3J = 7.12 Hz, 3H, 14-H), 1.21–1.24 (m, 14H, side chain protons), 1.45–1.55 (m, 2H, 3a-H, 8a-H), 1.49 (m, 4H, 4-H, 8-H), 1.68 (m, 1H, 2-H), 0.86/1.92 (m, 4H, 1-H, 3-H), 2.13 (m, 4H, 5-H, 7-H), 2.55 (m, 1H, 6-H), 4.12 (q, ^3J = 7.11 Hz, 2H, 10-H); ^{13}C NMR (100.6 MHz, $CDCl_3$) δ 14.11, 14.21 (2 × q, C-11, C-19), 22.67 (t, C-18), 28.73 (t, C-13), 28.86 (2 × t, C-4, C-8), 29.57 (2 × d, C-5, C-7), 29.33, 29.65, 29.97 (3 × t, C-14, C-15,C-16), 31.91 (t, C-17), 35.52 (t, C-12), 41.12 (d, C-2), 41.69 (2 × t, C-1, C-3), 41.90 (2 × t, C-3a, C-8a), 46.61 (d, C-6), 59.98 (t, C-10), 176.31 (s, C=O); IR (film) $\tilde{\nu}$: 2932 (s, CH-stretch), 1732 (s, C=O), 1463, 1450 (w) cm^{-1}; UV (CH_3CN) λ_{max} nm (log ε): 204 (2.92), 216 (2.55), 234 (2.15), 284 (1.86); MS (EI, 70 eV) *m*/*z* (%): 322 (100) [M^+], 307 (18) [$M^+ - CH_3$], 293 (35) [$M^+ - C_2H_5$], 276 (25) [$M^+ - C_2H_6O$], 248 (10) [$M^+ - C_3H_6O_2$], 206 (53) [$M^+ - C_8H_{17}$], 135 (45) [209 − $C_3H_6O_2$]; HRMS: calcd for $C_{21}H_{38}O_2$, 322.287176; found, 322.287435 ± 0.51 ppm.

2-Octylperhydro-6-azulenecarboxylic acid (6a): In a 250 mL round-bottomed flask EtOH (60 mL) and aqueous 1 M NaOH (36 mL) were placed. The solution was left to stir for a while and **5a** (300 mg, 0.93 mmol) was added slowly; the mixture was kept at room temperature and stirred for 4–6 h. When TLC analysis showed no more starting materials to be present, the mixture was acidified with 1 M HCl. The EtOH was evaporated and the residual aqueous solution was extracted twice with ethyl acetate and once with dichloromethane. The organic phases were combined, washed with water, and dried ($MgSO_4$). The solvent was evaporated and the residue purified by column chromatography on silica gel by first eluting the impurities with dichloromethane and finally washing the column with Et_2O to yield 240 mg (87%) of **6a** as a colorless solid. Acid **6b** was obtained from ester **5b** by the same procedure as for **6a** in 84% yield (230 mg), also as a colorless solid.

Compound 6a: Mp 102–104 °C; ^{1}H NMR (400.1 MHz, $CDCl_3$) δ 0.85 (t, ^3J = 6.91 Hz, 3H, 17-H), 1.23 (m, 14H, side chain protons), 1.55 (m, 2H, 3a-H, 8a-H), 1.58 (m, 4H, 4-H, 8-H), 1.71 (m, 1H, 2-H), 0.78/2.22 (m, 4H, 1-H, 3-H), 2.15–2.58 (m, 4H, 5-H, 7-H), 2.69 (m, 1H, 6-H); ^{13}C NMR (100.6 MHz, $CDCl_3$) δ 14.11 (q, C-17), 22.66 (t, C-16), 28.72 (t, C-11), 29.41 (2 × t, C-4, C-8), 29.68, 29.90, 29.99 (3 × t, C-12, C-13, C-14), 31.08 (t, C-15), 31.93 (2 × t, C-5, C-7), 32.07 (t, C-10), 37.67 (d, C-2), 41.21 (2 × d, C-3a, C-8a), 41.43

(2 × t, C-1, C-3), 43.54 (d, C-6), 182.23 (s, C=O); MS (EI, 70 eV) *m/z* (%): 294 (40) [M^+], 276 (18) [$M^+ - H_2O$], 265 (25) [$M^+ - C_2H_5$], 181 (51) [$M^+ - C_8H_{17}$], 179 (100) [181 − H_2], 133 (52) [179 − H_2CO_2].

Compound 6b: Mp 103–106 °C; ^{1}H NMR (400.1 MHz, $CDCl_3$) δ 0.80 (t, ^3J = 6.80 Hz, 3H, 17-H), 1.23 (m, 14H, side chain protons), 1.41–1.54 (m, 2H, 3a-H, 8a-H), 1.47–1.57 (m, 4H, 4-H, 8-H), 1.63–1.70 (m, 1H, 2-H), 0.67–0.70/1.83–2.10 (m, 4H, 1-H, 3-H), 2.15–2.58 (m, 4H, 5-H, 7-H), 2.67–2.69 (m, 1H, 6-H); ^{13}C NMR (100.6 MHz, $CDCl_3$) δ 14.09 (q, C-17), 22.67 (t, C-16), 28.72 (t, C-11), 29.35 (2 × t, C-4, C-8), 29.68, 29.90, 29.99 (3 × t, C-12, C-13, C-14), 31.08 (t, C-15), 31.93 (2 × t, C-5, C-7), 32.07 (t, C-10), 37.77 (d, C-2), 40.25 (2 × d, C-3a, C-8a), 42.48 (2 × t, C-1, C-3), 45.60 (d, C-6), 182.54 (s, C=O); MS (EI, 70 eV) *m/z* (%): 294 (36) [M^+], 276 (14) [$M^+ - H_2O$], 265 (26) [$M^+ - C_2H_5$], 181 (54) [$M^+ - C_8H_{17}$], 179 (100) [181 − H_2], 133 (52) [179 − H_2CO_2].

General procedure for esterification of 8a, 8b and 10a, 10b. Thionyl chloride (0.021 mL, 0.28 mmol) was added to a solution of 4-(*N*,*N*-dimethylamino)pyridine (DMAP, 34 mg, 0.27 mmol) in dichloromethane (5 mL) at −20 °C. Acid **6a** or **6b** (65 mg, 0.22 mmol) was added and the resulting solution was stirred for 1 h. Then, DMAP (34 mg, 0.27 mmol) and the phenol **7** (33.0 mg, 0.22 mmol) or **9** (43.0 mg, 0.22 mmol) were added and stirring was continued for another 1 h. The mixture was washed with water (5 mL) and the organic layer was separated and dried with sodium sulfate. The solvent was evaporated, and the remaining residue was separated by silica gel column chromatography, eluting with dichloromethane and pentane (1:1) to give the esters **8a**, **8b** or **10a**, **10b** as colorless solids.

Compound 8a: Mp 41–43 °C; ^{1}H NMR (400.1 MHz, $CDCl_3$) δ 0.86 (t, ^3J = 6.95 Hz, 3H, 27-H), 0.90 (t, ^3J = 7.35 Hz, 3H, 19-H), 1.24 (m, 14H, side chain protons), 1.30–1.35 (m, 2H, 17-H), 1.53–1.60 (m, 6H, 4-H, 8-H, 18-H), 1.63–1.66 (m, 1H, 2-H), 0.82/1.86 (m, 4H, 1-H, 3-H), 2.08–2.24 (m, 2H, 3a-H, 8a-H), 2.20–2.24 (m, 4H, 5-H, 7-H), 2.58 (t, ^3J = 7.72 Hz, 2H, 16-H), 2.87–2.90 (m, 1H, 6-H), 6.93 (d, ^3J = 11.10 Hz, 11-H, 15-H), 7.15 (d, ^3J = 11.06 Hz, 2H, 12-H, 14-H); ^{13}C NMR (100.6 MHz, $CDCl_3$) δ 13.67, 13.87 (2 × q, C-19, C-27), 22.03 (t, C-18), 22.44 (t, C-26), 28.50 (t, C-21), 28.53 (2 × t, C-4, C-8), 29.47 (2 × t, C-5, C-7), 29.10, 29.41, 29.74 (3 × t, C-22, C-23, C-24), 31.68 (t, C-25), 33.37 (t, C-20), 34.78 (t, C-16), 35.28 (t, C-17), 40.03 (d, C-2), 41.52 (2 × t, C-1, C-3), 41.80 (2 × d, C-3a, C-8a), 43.30 (d, C-6), 120.97 (2 × d, C-11, C-15), 128.94 (2 × d, C-12, C-14), 139.91 (s, C-13), 148.62 (s, C-10), 174.53 (s, C=O); IR (film) $\tilde{\nu}$: 2932 (s, CH-stretch), 1732 (s, C=O), 1463, 1450 (w), 1376, 1221 (w), 1183, 1143 (m), 1095, 1046, 1033 (w) cm^{-1}; UV (CH_3CN) λ_{max} nm (log ε): 204 (2.92), 216 (2.55), 234 (2.15), 284 (1.86), 312 (1.80), 342 (1.64), 374 (1.54); MS (EI, 70 eV) *m/z* (%): 426 (9) [M^+], 276 (100) [$M^+ - C_{10}H_{14}O$], 249 (17) [276 − CO], 163 (15) [276 − C_8H_{17}], 150 (85) [163 − CH]; HRMS: calcd for $C_{29}H_{46}NaO_2$, 449.338997; found, 449.338715 ± 0.63 ppm.

Compound 8b: ^{1}H NMR (400.1 MHz, $CDCl_3$) δ 0.86 (t, ^3J = 6.97 Hz, 3H, 27-H), 0.90 (t, ^3J = 7.35 Hz, 3H, 19-H), 1.24 (m, 14H, side chain protons), 1.31–1.36 (m, 2H, 17-H), 1.51–1.58/1.70–1.74 (m, 6H, 4-H, 8-H, 18-H), 1.64–1.67 (m, 1H, 2-H), 0.77/1.97 (m, 4H, 1-H, 3-H), 2.08–2.13 (m, 2H, 3a-H, 8a-H), 1.53/2.22 (m, 4H, 5-H, 7-H), 2.46–2.52 (m, 1H, 6-H), 2.57 (t, ^3J = 7.73 Hz, 2H, 16-H), 6.93 (d, ^3J = 8.48 Hz, 11-H, 15-H), 7.13 (d, ^3J = 8.50 Hz, 2H, 12-H, 14-H); ^{13}C NMR (100.6 MHz, $CDCl_3$) δ 13.69, 13.89 (2 × q, C-19, C-27), 22.07 (t, C-18), 22.46 (t, C-26), 28.50 (t, C-21), 29.12, 29.43, 29.76 (3 × t, C-22, C-23, C-24), 30.90 (2 × t, C-4, C-8), 31.70 (t, C-25), 32.02 (2 × t, C-5, C-7), 33.37 (t, C-20), 34.80 (t, C-17), 35.27 (t, C-16), 40.16 (d, C-2), 42.26 (2 × t, C-1, C-3), 42.86 (2 × d, C-3a, C-8a), 48.33 (d, C-6), 120.79 (2 × d, C-11, C-15), 128.84 (2 × d, C-12, C-14), 139.79 (s, C-13), 148.63 (s, C-10), 174.77 (s, C=O); IR (film) $\tilde{\nu}$: 2932 (s, CH-stretch), 1732 (s, C=O), 1463, 1450 (w), 1376, 1221 (w), 1183, 1143 (m), 1095, 1046, 1033 (w) cm^{-1}; UV (CH_3CN) λ_{max} nm (log ε): 204 (2.92), 216 (2.55), 234 (2.15), 284 (1.86), 312 (1.80), 342 (1.64), 374 (1.54); MS (EI, 70 eV) *m/z* (%): 426 (10) [M^+], 276 (100) [$M^+ - C_{10}H_{14}O$], 249 (21) [276 − CO], 163 (19) [276 − C_8H_{17}], 150 (85) [163 − CH]; HRMS: calcd for $C_{29}H_{46}NaO_2$, 449.339001; found, 449.339077 ± 0.17 ppm.

Compound 10a: Mp 91–93 °C; ^{1}H NMR (400.1 MHz, $CDCl_3$) δ 0.86 (t, ^3J = 6.97 Hz, 3H, 30-H), 1.24 (br m, 14H, side chain protons), 1.53 (br m, 4H, 4-H, 8-H), 1.66–1.69 (m, 1H, 2-H), 0.83/1.92 (m, 4H, 1-H, 3-H), 2.10–2.14 (m, 2H, 3a-H, 8a-H), 1.64/2.22 (m, 4H, 5-H, 7-H), 2.93–2.96 (m, 1H, 6-H), 7.17 (d, ^3J = 8.73 Hz, 2H, 12-H, 14-H), 7.56 (d, ^3J = 8.71 Hz, 2H, 11-H, 15-H), 7.64 (d, ^3J = 8.68 Hz, 2H, 17-H, 21-H), 7.70 (d, ^3J = 8.58 Hz, 2H, 18-H, 20-H); ^{13}C NMR (100.6 MHz, $CDCl_3$) δ 13.84 (q, C-30), 22.50 (t, C-29), 28.51 (t, C-24), 28.55 (2 × t, C-4, C-8), 29.12, 29.43, 29.75 (3 × t, C-25, C-26, C-27), 29.46 (2 × t, C-5, C-7), 31.70 (t, C-28), 35.30 (t, C-23), 40.06 (d, C-2), 41.54 (2 × t, C-1, C-3), 41.83 (2 × d, C-3a, C-8a), 43.45 (d, C-6), 110.44 (s, C-22), 118.70 (s, C-19), 122.16 (2 × d, C-11,C-15), 127.26 (2 × d, C-12, C-14), 128.00 (2 × d, C-17, C-21), 132.23 (2 × d, C-18, C-20), 136.48 (s, C-13), 144.65 (s, C-16), 151.16 (s, C-10), 174.29 (s, C=O); IR (film) $\tilde{\nu}$: 2932 (s, CH-stretch), 1732 (s, C=O), 1463, 1450 (w), 1376, 1221 (w), 1183, 1143 (m), 1095, 1046, 1033 (w) cm^{-1}; UV (CH_3CN) λ_{max} nm (log ε): 204 (2.92), 216 (2.55), 234 (2.15), 284 (1.86), 312 (1.80), 342 (1.64), 374 (1.54); MS (EI, 70 eV) *m/z* (%): 471

(5) [M^+], 276 (68) [$M^+ - C_{13}H_9NO$], 249 (38) [276 − CO], 135 (49) [249 − C_8H_{18}], 109 (55) [135 − C_2H_2], 95 (100) [109 − CH_2]; HRMS: calcd for $C_{32}H_{41}NO_2$, 471.313732; found, 471.313327 ± 0.86 ppm.

Compound 10b: ^{1}H NMR (400.1 MHz, $CDCl_3$) δ 0.87 (t, ^3J = 6.94 Hz, 3H, 30-H), 1.24 (br m, 14H, side chain protons), 1.33/1.77 (m, 4H, 4-H, 8-H), 1.65–1.69 (m, 1H, 2-H), 0.72/1.98 (m, 4H, 1-H, 3-H), 2.10–2.15 (m, 2H, 3a-H, 8a-H), 1.59/2.25 (m, 4H, 5-H, 7-H), 2.51–2.56 (m, 1H, 6-H), 7.14 (d, ^3J = 8.70 Hz, 2H, 12-H, 14-H), 7.55 (d, ^3J = 8.70 Hz, 2H, 11-H, 15-H), 7.63 (d, ^3J = 8.54 Hz, 2H, 17-H, 21-H), 7.70 (d, ^3J = 8.53 Hz, 2H, 18-H, 20-H); ^{13}C NMR (100.6 MHz, $CDCl_3$) δ 13.92 (q, C-30), 22.40 (t, C-29), 28.50 (t, C-24), 29.12, 29.43, 29.75 (3 × t, C-25, C-26, C-27), 30.90 (2 × t, C-4, C-8), 31.71 (t, C-28), 31.98 (2 × t, C-5, C-7), 35.27 (t, C-23), 40.01 (d, C-2), 42.32 (2 × t, C-1, C-3), 42.79 (2 × d, C-3a, C-8a), 48.31 (d, C-6), 110.66 (s, C-22), 118.62 (s, C-19), 122.03 (2 × d, C-11, C-15), 127.31 (2 × d, C-12, C-14), 127.96 (2 × d, C-17, C-21), 132.33 (2 × d, C-18, C-20), 136.55 (s, C-13), 144.55 (s, C-16), 151.16 (s, C-10), 174.54 (s, C=O); IR (film) $\tilde{\nu}$: 2932 (s, CH-stretch), 1732 (s, C=O), 1463, 1450 (w), 1376, 1221 (w), 1183, 1143 (m), 1095, 1046, 1033 (w) cm^{-1}; UV (CH_3CN) λ_{max} nm (log ε): 204 (2.92), 216 (2.55), 234 (2.15), 284 (1.86), 312 (1.80), 342 (1.64), 374 (1.54); MS (EI, 70 eV) *m*/*z* (%): 471 (6) [M^+], 276 (86) [$M^+ - C_{13}H_9NO$], 249 (50) [276 − CO], 135 (56) [249 − C_8H_{18}], 109 (57) [135 − C_2H_2], 95 (100) [109 − CH_2]; HRMS: calcd for $C_{32}H_{41}NO_2$, 471.313726; found, 471.313482 ± 0.52 ppm.

Supporting Information

Supporting Information File 1

Additional material.
[http://www.beilstein-journals.org/bjoc/content/supplementary/1860-5397-8-44-S1.pdf]

Acknowledgements

Z. H. thanks Prof. Dr. Wolfgang Gaertner at the Max-Planck Institute for Bioinorganic Chemistry, Muelheim (Germany), for his support to allow purification and characterization of all substances in the present study.

References

1. Kirsch, P.; Bremer, M. *Angew. Chem., Int. Ed.* **2000,** *112,* 4384–4405. doi:10.1002/1521-3757(20001201)112:23<4384::AID-ANGE4384>3.0.CO;2-S
*Angew. Chem., Int. Ed.***2000,** *39,* 4216–4235. doi:10.1002/1521-3773(20001201)39:23<4216::AID-ANIE4216>3.0.CO;2-K
2. Klasen, M.; Bremer, M.; Götz, A.; Manabe, A.; Naemura, S.; Tarumi, K. *Jpn. J. Appl. Phys.* **1998,** *37,* L945–L948. doi:10.1143/JJAP.37.L945
3. Kirsch, P.; Reiffenrath, V.; Bremer, M. *Synlett* **1999,** 389–396. doi:10.1055/s-1999-2619
4. Kelly, S. M. *Liq. Cryst.* **1991,** *10,* 261–272. doi:10.1080/02678299108036430
5. Gray, G. W.; Hird, M.; Lacey, D.; Toyne, K. J. *J. Chem. Soc., Perkin Trans. 2* **1989,** 2041–2053. doi:10.1039/P29890002041
6. Miyazawa, K.; Kato, T.; Itoh, M.; Ushioda, M. *Liq. Cryst.* **2002,** *29,* 1483–1490. doi:10.1080/02678290260372682
7. Miyazawa, K.; de Meijere, A. *Mol. Cryst. Liq. Cryst.* **2001,** *364,* 529–546. doi:10.1080/10587250108025023
8. Demus, D.; Goto, Y.; Sawada, S.; Nakagawa, E.; Saito, H.; Tarao, R. *Mol. Cryst. Liq. Cryst.* **1995,** *260,* 1–21. doi:10.1080/10587259508038680
9. Cordoyiannis, G.; Sánchez-Ferrer, A.; Finkelmann, H.; Rožič, B.; Žumer, S.; Kutnjak, Z. *Liq. Cryst.* **2010,** *37,* 349–353. doi:10.1080/02678290903548877
10. Ema, K.; Yao, H.; Takanishi, Y.; Takezoe, H.; Kusumoto, T.; Hiyama, T.; Yoshizawa, A. *Liq. Cryst.* **2002,** *29,* 221–225. doi:10.1080/02678290110099448
11. Cordoyiannis, G.; Pinto, L. F. V.; Godinho, M. H.; Glorieux, C.; Thoen, J. *Phase Transitions* **2009,** *82,* 280–289. doi:10.1080/01411590902858720
12. Gray, G. W. *Thermotropic Liquid Crystals,* 1st ed.; J. Wiley & Sons Inc.: New York, 1987; pp 1–22.
13. Hussain, H.; Hopf, H.; Pohl, L.; Oeser, T.; Fischer, A. K.; Jones, P. G. *Eur. J. Org. Chem.* **2006,** 5555–5569. doi:10.1002/ejoc.200500733
14. Hussain, Z.; Koley, D.; Hopf, H. *Helv. Chim. Acta* **2005,** *88,* 3263–3273. doi:10.1002/hlca.200590262
15. Luhowy, R.; Keehn, P. M. *J. Am. Chem. Soc.* **1977,** *99,* 3797–3805. doi:10.1021/ja00453a046
16. Berson, J. A.; Willcott, M. R., III. *J. Am. Chem. Soc.* **1966,** *88,* 2494–2502. doi:10.1021/ja00963a025
17. Luhowy, R.; Keehn, P. M. *Tetrahedron Lett.* **1976,** *17,* 1043–1046. doi:10.1016/S0040-4039(00)93746-8
18. Arrieta, A.; Garcia, T.; Palomo, C. *Synth. Commun.* **1982,** *12,* 1139–1146. doi:10.1080/00397918208065981

License and Terms

Beilstein Journal of Organic Chemistry

Liquid-crystalline heterodimesogens and ABA-heterotrimesogens comprising a bent 3,5-diphenyl-1,2,4-oxadiazole central unit

Govindaswamy Shanker, Marko Prehm and Carsten Tschierske*

Full Research Paper

Open Access

Address:
Institute of Chemistry, Organic Chemistry, Martin-Luther-University Halle-Wittenberg, Kurt Mothes Str. 2, D-06120 Halle/Saale, Germany, Tel: ++49 (0) 345 55 25664, Fax: ++49 (0) 345 55 27346

Email:
Carsten Tschierske* - carsten.tschierske@chemie.uni-halle.de

* Corresponding author

Keywords:
bent-core mesogens; cybotactic nematic phases; dimesogen; liquid crystals; 1,2,4-oxadiazoles; trimesogen

Beilstein J. Org. Chem. **2012,** *8,* 472–485.
doi:10.3762/bjoc.8.54

Received: 09 December 2011
Accepted: 07 March 2012
Published: 30 March 2012

This article is part of the Thematic Series "Progress in liquid crystal chemistry II".

Guest Editor: S. Laschat

Abstract

Three new types of terminally connected ABA-heterotrimesogens and heterodimesogens, composed of a bent 3,5-diphenyl-1,2,4-oxadiazole central unit and one or two rod-shaped 4-cyanobiphenyl cores or one 2-phenyl-1,3,4-thiadiazole core, connected by flexible spacers, have been synthesized, and their mesomorphic behavior was studied by optical polarizing microscopy (PM), differential scanning calorimetry (DSC) and X-ray diffraction (XRD). All dimesogens exhibit broad ranges of cybotactic nematic phases (N_{cybA} and N_{cybC}), in some cases accompanied by additional mesophases (CybA or SmC) at lower temperature. The combination of the 3,5-diphenyl-1,2,4-oxadiazole unit with one cyanobiphenyl core leads to the removal of tilted smectic and cybotactic nematic phases (SmC, N_{cybC}), which are replaced by the nontilted CybA phases and nematic phases composed of SmA-type clusters (N_{cybA}). The orthogonal cybotactic nematic phases of bent-core mesogens are of special interest for achieving biaxial nematic phases of the orthorhombic type. The orthogonal (N_{cybA}) and skewed (N_{cybC}) cybotactic nematic phases were distinguished by XRD and optical observations.

Introduction

Liquid-crystalline (LC) dimers of low-molar-mass compounds formed by the coupling of two mesogenic segments are of contemporary interest [1-4]. These compounds exhibit fascinating properties, often different from the single mesogens, and they can also be considered as model compounds for main-chain LC polymers [5-8]. Dimesogens can be categorized into mesogenic dimers (homodimesogens), composed of identical mesogenic units, and heterodimesogens combining different types of units, such as two distinct rod-like units [4], or combining rod-like with discotic [1,9,10], phasmidic or bent-core units, linked together through flexible chains [1]. These flexible chains, which in most cases represent linear alkyl

chains, connect the distinct mesogenic units, but depending on their length and degree of flexibility they can also decouple the segmental motions of the two interconnected mesogenic units, and hence these chains are also assigned as spacers. The properties of these dimesogens strongly depend on the topology of connection [11], the spacer length and spacer parity, resulting in linear and bent [1,3], T-shaped [12-14], Y-shaped [15] or H-shaped molecules [12,13,16-19]. Moreover, combinations of mesogenic units differing not only in shape [20-22], but also in polarity or compatibility of the mesogenic units [1-4,23], and dimesogens incorporating chiral [24-26] segments often result in unique interesting properties, which are fundamentally different from the individual mesogens.

Recent interest in dimesogens has been focused on combinations of two rod-like molecules through relatively short odd-numbered spacer units to obtain dimesogens with an overall bent shape [27-31] exhibiting properties that are characteristic for bent-core mesogens, such as polar ferroelectric or antiferroelectric switching LC phases [32-35] and spontaneous achiral symmetry breaking [34-36]. Also dimesogens combining two bent-core units terminally [37-43] or laterally [44], or combining a bent-core segment with a rod-shaped mesogen [40,45-54], and related end-to-end connected ABA-heterotrimesogens combining a bent-core segment with two rod-like units [55], or a rod-like core with two bent-core units [56], were synthesized and studied. These compounds are of interest with respect to the potential biaxiality of the nematic (N) [45,50,57] and nontilted smectic phases of these compounds [45]. Bent-core units have also been combined with disc-like units, but in this case the incompatibility and steric mismatch of the distinct units led to a loss of LC properties [58].

The 3,5-diphenyl-1,2,4-oxadiazole segment has recently attracted significant attention as a central building block for bent-core LC molecules (angle ~140°) [59-63], due to the ferroelectric-like polar switching observed in the nematic phases of some of these compounds under applied electric fields [64,65]. However, these nematic phases were only observed at high temperature, which makes their investigation difficult.

Herein, three types of compounds combining the bent 3,5-diphenyl-1,2,4-oxadiazole unit terminally with one or two rod-like mesogenic units through flexible spacers are reported (Scheme 1). The trimesogens **CB-Ox-CB/*n*** combine the 3,5-diphenyl-1,2,4-oxadiazole unit with two nematogenic cyanobiphenyl (CB) units (Scheme 2), in the dimesogens **CB-Ox/*n*** only one CB unit is incorporated, and in compounds **Thia-Ox/*n*** a 3-heptyl-5-phenyl-1,3,4-thiadiazole unit is incorporated (Scheme 3). All compounds form nematic phases over wide temperature ranges, in some cases accompanied by additional nontilted (CybA) or tilted (SmC) mesophases at lower temperatures.

Results and Discussion

Synthesis and characterization

The dimesogens and trimesogens were obtained by following the synthetic protocols described in Scheme 2 and Scheme 3 by DCC coupling of the ω-mesogen-functionalized alkanoic acids **2** [66] and **4** [66] with 4-[(4-hydroxyphenyl)-1,2,4-oxadiazol-5-yl]phenyl 4-hexylbenzoate (**3**) [67] and 3,5-bis(4-hydroxyphenyl)-1,2,4-oxadiazole (**1**) [65], respectively. The syntheses of the acids **2** and **4**, and the 1,2,4-oxadiazole substituted phenols **1** and **3** were reported previously in the cited references. The final compounds were purified by crystallization

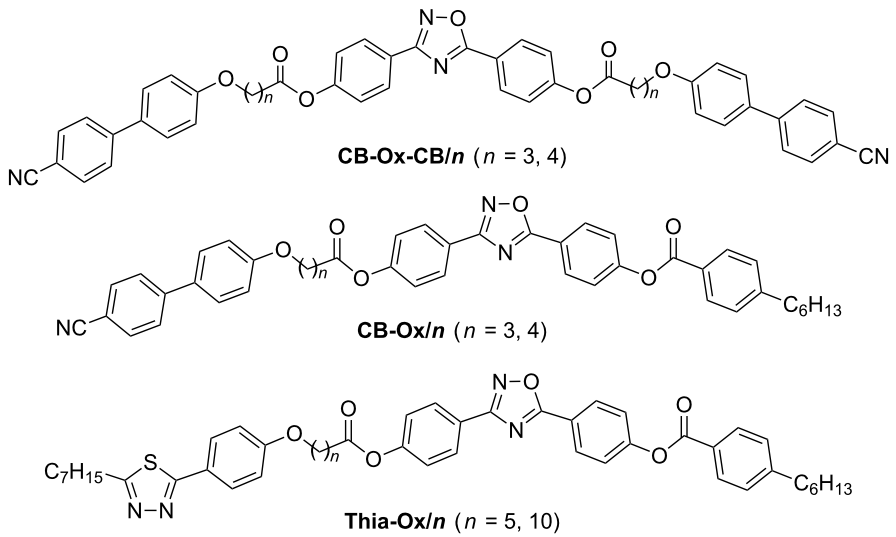

Scheme 1: Structures of the investigated ABA-heterotrimesogens **CB-Ox-CB/*n*** and heterodimesogens **CB-Ox/*n***, **Thia-Ox/*n***.

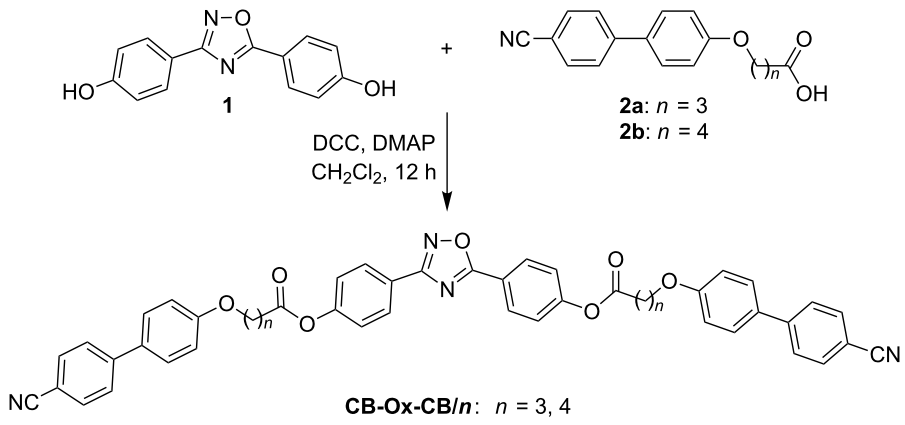

Scheme 2: Synthesis of the ABA-heterotrimesogens **CB-Ox-CB/*n***.

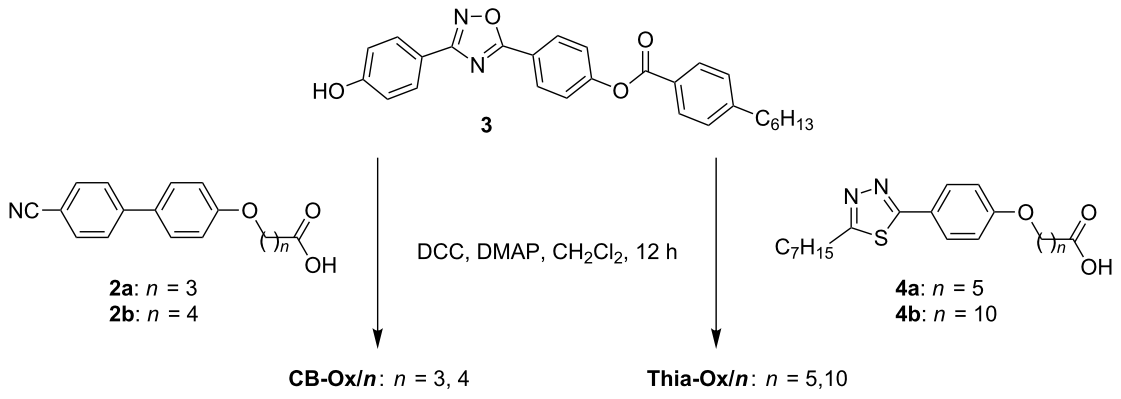

Scheme 3: Synthesis of the dimesogens **CB-Ox/*n*** and **Thia-Ox/*n***.

from ethyl acetate/ethanol mixtures. All compounds represent the first examples in their classes and their molecular structure was probed by ^{1}H-, ^{13}C NMR and microanalytic techniques (see Experimental).

Investigation of the liquid-crystalline behavior

Methods

The obtained di- and trimesogens were investigated by PM (Optiphot 2, Nikon) in conjunction with a heating stage (FP82HT, Mettler) and differential scanning calorimetry (DSC, DSC-7, Perkin-Elmer). The assignment of the mesophases is based on the combined results of optical textures and X-ray diffraction (XRD) studies. XRD investigations on aligned samples were performed by using a 2D wire detector (HI-Star, Siemens AG). Alignment was achieved either in thin capillaries under a magnetic field (B = 1 T) or by slow cooling of a small drop of the sample on a glass substrate; the incident X-ray beam was in this case nearly parallel to the glass plate. The transition temperatures, transition enthalpies and observed phase types are collated in Table 1. It is apparent from this table that all of the synthesized di- and trimesogens exhibit liquid-crystalline behavior.

Trimesogens **CB-Ox-CB/*n***

The trimesogens **CB-Ox-CB/*n*** comprising rod-shaped CB segments on either side of the 2,5-diphenyl-1,2,4-oxadiazole unit exhibit exclusively nematic phases (N). Upon cooling of these compounds from the isotropic liquid phase, Schlieren textures were observed, which are evidence of nematic phases [68,69]. These trimesogens have very high clearing temperatures at around T = 320 °C for compound **CB-Ox-CB/3** and at T = 245 °C for **CB-Ox-CB/4**. The major reason for the much higher nematic phase stability of **CB-Ox-CB/3** compared to the higher homologue may be the result of decreased chain decoupling of the mesogenic units by the shorter spacers and the fact that the spacers are even numbered (considering the ether oxygens and the COO groups as parts of the spacers), which gives a more linear coupling of the mesogenic units. XRD measurement of **CB-Ox-CB/4** confirms the N phase by the presence of two diffuse scattering peaks with maxima at

Table 1: Phase-transition temperature (T/°C) and associated enthalpy values (in square brackets, ΔH/kJ mol^{-1}) of the synthesized di- and trimesogens.[a]

Compound	Phase transition on heating							Phase transition on cooling						
CB-Ox-CB/3	Cr	187 [29.2]	N	320 (dec)	Iso			—[b]						
CB-Ox-CB/4	Cr	164 [38.1]	N	246 [4.2]	Iso			Iso	242 [−3.5]	N	123 [−25]	Cr		
CB-Ox/3	Cr	162 [40.1]	CybA	210 [<0.01]	N_{cybA}	302 (dec)	Iso	—[b]						
CB-Ox/4	Cr	130 [36.2]	CybA	148 [<0.01]	N_{cybA}	255 [1.7]	Iso	Iso	251 [−1.9]	N_{cybA}	146 [<0.01]	CybA	84 [−15.1]	Cr
Thia-Ox/5	Cr	144 [41.6]	SmC	173 [0.4]	N_{cybC}	224 [2.9]	Iso	Iso	223 [−2.1]	N_{cybC}	172 [−0.7]	SmC	114 [−37.2]	Cr
Thia-Ox/10	Cr_1	132 [84.7]	Cr_2	137 [33.6]	N_{cybC}	178 [0.9]	Iso	Iso	174 [−1.0]	N_{cybC}	123 [53.4]	Cr		

[a]Peak temperatures in the DSC thermograms obtained during the first heating and cooling cycles at 10 K/min; abbreviations: Cr = crystalline solid; Iso = isotropic liquid, N = nematic LC phase; N_{cybA} = cybotactic nematic phase formed by small SmA-type (nontilted) cybotactic clusters; N_{cybC} = cybotactic nematic phase formed by small SmC-type (tilted) cybotactic clusters; CybA = LC phase formed by extended SmA-type clusters; SmC = smectic C phase; dec = decomposition. [b]Due to decomposition at the N–Iso transition no cooling curve could be recorded.

d-values of 1.5 nm (very weak) and 0.46 nm, assigned to the average longitudinal distances and the average lateral distances between the molecules, respectively (Figure 1). The longitudinal distance is only about one third of the total molecular length in the most extended conformation, L_{max} = 4.6 nm, and hence it is most probably determined by the average length of the three individual aromatic cores. The absence of sufficiently long aliphatic segments and also the electrostatic interaction between the terminal CN groups and the aromatics seem to be responsible for the absence of any smectic phase and the complete mixing of the aromatics in the nematic phase. The low intensity of the diffuse small-angle scattering, due to the low electron-density contrast of these molecules with relatively short spacers does not, in this case, allow further conclusions about the details of the structure of these nematic phases to be drawn.

Dimesogens **CB-Ox/*n***

The dimesogens **CB-Ox/3** and **CB-Ox/4**, having a polar group at one end and an *n*-hexyl tail at the other, exhibit enantiotropic CybA–N phase sequences. Similar to the trimesogens **CB-Ox-CB/*n***, a strong influence of spacer length and spacer parity on the phase-transition temperatures for these dimesogens is also observed. The shorter compound **CB-Ox/3** with even-numbered spacer ($O(CH_2)_3COO$) has much higher temperatures of the CybA–N and N–Iso transitions. Upon cooling a sample of **CB-Ox/4** from the isotropic liquid, the nematic phase forms with a typical highly birefringent Schlieren texture (Figure 2b) [68]. This indicates a predominately homogeneous alignment (director ***n*** on average parallel to the substrate surface) of the sample. On reducing the temperature below 146 °C a change of the texture is observed upon which the Schlieren texture changes into a multidomain texture composed of small fan-like

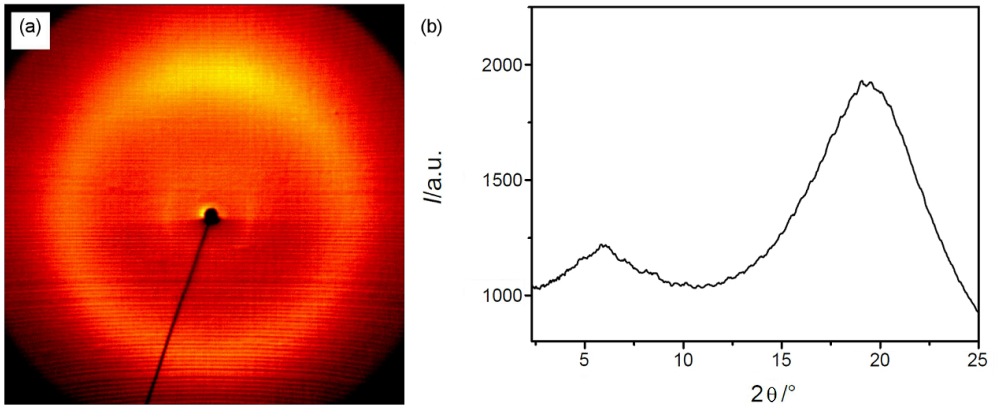

Figure 1: XRD pattern of a (partially) surface-aligned sample of the N phase of compound **CB-Ox-CB/4**: (a) diffraction pattern at 170 °C; (b) θ-scan at 170 °C.

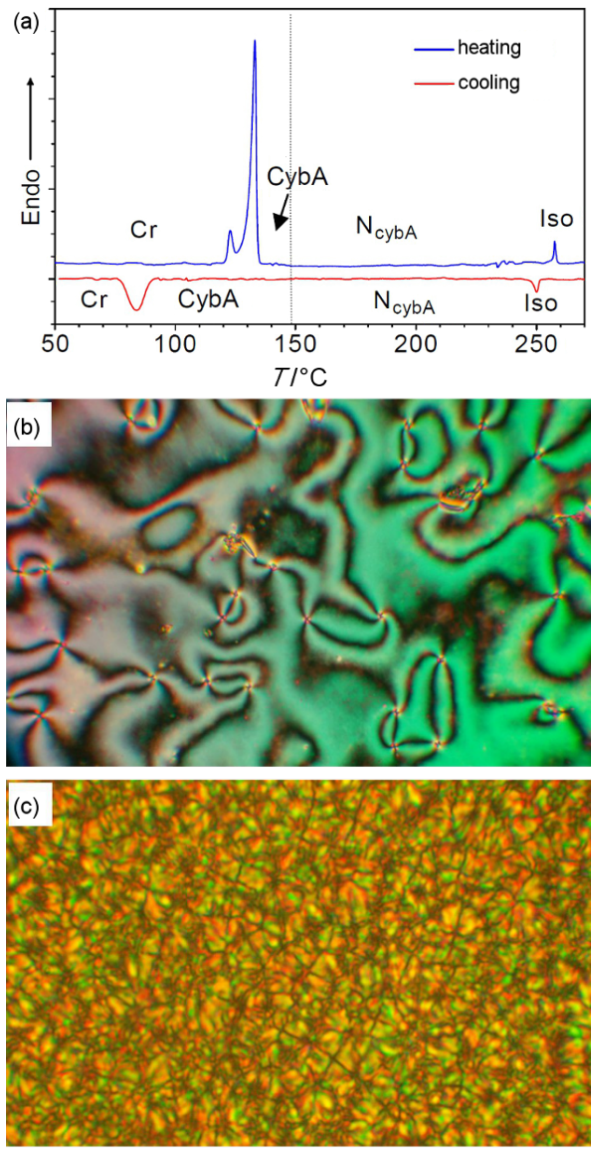

Figure 2: Dimesogen **CB-Ox/4**: (a) DSC traces obtained during initial heating and cooling cycles scanned at a rate of 10 K min^{-1}; (b,c) textures as seen between crossed polarizers for a homogenously aligned sample; (b) Schlieren texture of the N_{cybA} phase at T = 245 °C; (c) polydomain texture of the CybA phase at T = 135 °C.

domains (Figure 2c). This texture remains unaltered down to a temperature of 84 °C, below which crystallization takes place. Shearing the sample gives rise to reorganization with homeotropic alignment, which appears completely dark between crossed polarizers, and no birefringence occurs in this homeotropically aligned sample until crystallization sets in. This indicates the formation of a uniaxial mesophase, but surprisingly, no enthalpy change is associated with this transition as observed in the DSC traces (Figure 2a). Similar features can be observed for the shorter homologue **CB-Ox/3** (see Table 1).

XRD patterns of the nematic phase of compound **CB-Ox/4**, obtained with a magnetically aligned sample (B = 1 T), show diffuse scattering in the wide-angle region with two crescent-like maxima at d = 0.46 nm centered on the equator (Figure 3a). In the small-angle region a second diffuse scattering peak with a maximum at d = 4.23 nm (T = 150 °C) has clear maxima on the meridian of the diffraction pattern. This indicates an arrangement of the molecules with their long axes parallel to the magnetic field direction. The intensity of this small-angle scattering is higher than that of the wide-angle scattering (Figure 3c), which confirms the presence of cybotactic clusters with short-range smectic order [69-74]. Because the maxima of the diffuse peaks in the wide- and small-angle regions are perpendicular to each other the cybotactic clusters are of the nontilted SmA type (N_{cybA}) [57,75,76]. The transversal periodicity in these cybotactic clusters (d = 4.23 nm) is comparable to the molecular length L_{mol} = 4.5–4.6 nm in the most stretched conformation (determined with CPK models). This indicates a kind of monolayer organization of the molecules in the cybotactic clusters. In the SmA-like clusters the alkyl chains are segregated from the aromatic cores, and the aromatics are organized on average antiparallel to each other with complete intercalation of the aromatic units, i.e., the cyanobiphenyls and diphenyl-1,2,4-oxadiazole units appear not to be segregated (Figure 4a). In the aliphatic regions the alkyl chains are interdigitated and conformationally disordered. The size of the SmA type clusters can be estimated from the width of the small-angle scattering at the peak half maximum. The correlation length in the nematic phase at T = 150 °C, estimated according to $\xi_{\parallel,\perp} = 2/\Delta q$ from the full width at half maximum (Δq) [77], in the longitudinal direction is $\xi_{\parallel}$ = 5.3 nm and in the transversal direction is $\xi_{\perp}$ = 1.8 nm. Hence, the dimensions of the cybotactic clusters ($L_{\parallel,\perp}$) can be approximated to $L_{\parallel,\perp} = 3\xi_{\parallel,\perp}$ [78], leading to the values $L_{\parallel}$ = 16 nm and $L_{\perp}$ = 5 nm. Accordingly, the clusters are relatively large, composed on average of about 3–4 layers, and about 11 molecules are arranged in the cross section.

On reduction of the temperature further, there is a significant change in the XRD pattern, indicating a phase transition. The diffuse scattering on the meridian becomes sharper and strongly rises in intensity (Figure 3c). In addition, a weak second-order reflection becomes visible (Figure 3b). The maximum of the small-angle scattering is slightly shifted from d = 4.23 nm in the N_{cybA} phase at T = 150 °C to d = 4.31 nm in the low-temperature phase at T = 130 °C (Figure 3c). The diffuse outer scattering remains completely diffuse, confirming the absence of any in-plane order. As the maxima of the scattering peaks in the wide- and small-angle regions are perpendicular to each other, the molecules are on average nontilted. Because the position of the small-angle scattering is not significantly shifted, the orga-

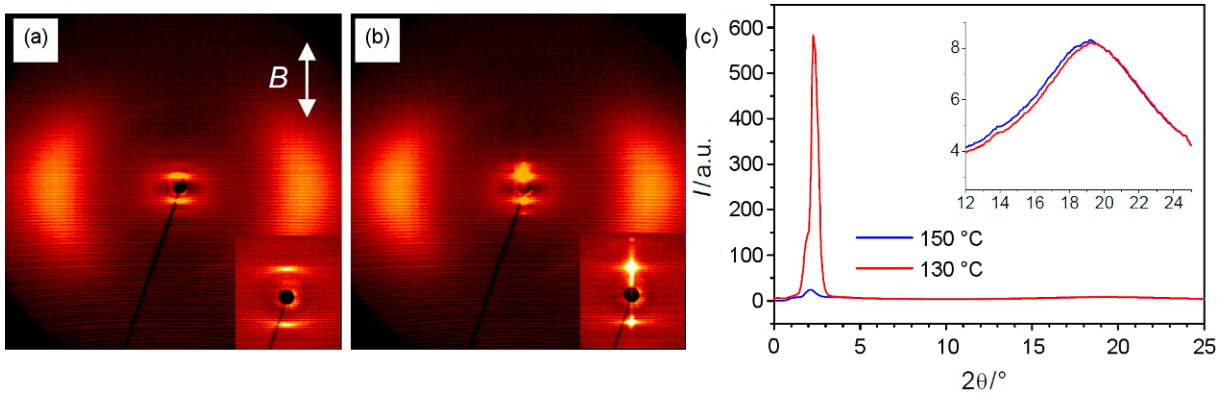

Figure 3: XRD data of the dimesogen **CB-Ox/4**: (a,b) diffraction patterns of a magnetic-field-aligned sample (the direction of the magnetic field is shown as a white arrow), the insets show the scattering in the small-angle region: (a) N_{cybA} at 150 °C; (b) CybA at 130 °C; (c) θ-scans at 150 °C and 130 °C in the small-angle regions of both the N_{cybA} and the CybA phase.

nization of the molecules should be identical to the model proposed for the SmA-type clusters forming the N_{cybA} phase (Figure 4a). This means that at this phase transition the molecular organization does not change fundamentally, but instead the short-range SmA-like clusters simply become fused to much larger clusters. The correlation length in this phase (T = 130 °C) was estimated to 27 nm in the longitudinal direction and 23 nm in the transversal direction. This is somewhat smaller than usually observed for typical SmA phases. Hence, although the correlation length is significantly increased, the smectic order seems not to be truly long-range. It appears that for this reason there is no measurable transition enthalpy for this phase transition (see DSC traces in Figure 2a) as would be expected for a transition to a SmA phase, and hence this phase is tentatively assigned as CybA. Related tilted [69] and nontilted phases [79] with structures intermediate between the N_{cyb} phases and undistorted smectic phases have been observed previously and seem to represent a typical phenomenon for molecules at the borderline between a bent-core and rod-like shape.

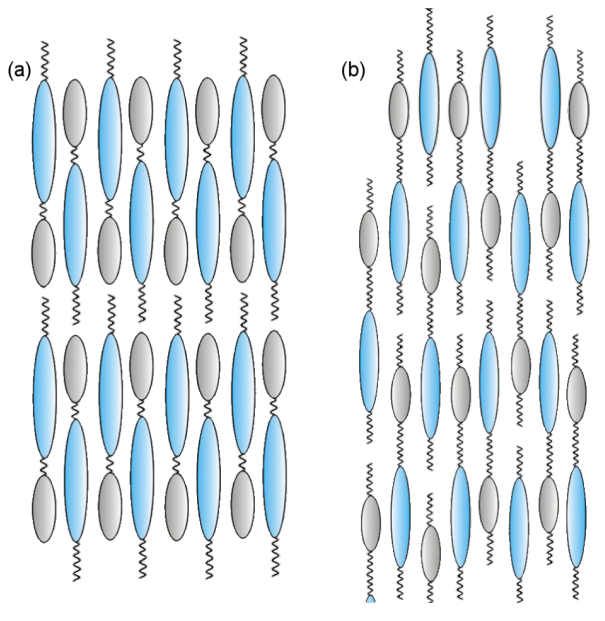

Figure 4: Models showing the suggested organizations of dimesogens in the smectic phases and in the preferred local structure in the cybotactic clusters of the related nematic phases: (a) monolayer structure ($d \sim L$); (b) intercalated structure ($d \sim ½ L$). The molecular tilt and the bent-shape of the mesogenic units are not considered.

Dimesogens **Thia-Ox/*n***

The dimesogens **Thia-Ox/5** and **Thia-Ox/10** have a molecular structure that is quite distinct from that of compounds **CB-Ox/*n***. Firstly, they have alkyl tails at both ends, and secondly, they incorporate a 1,3,4-thiadiazole unit, which is not strictly linear (bending angle 162°) [80] and within which the direction of the major dipole moment is perpendicular to the molecular long axis [80-82]. Finally, the spacer units of these thiadiazoles are also significantly longer (n = 5, 10) than those used for the related cyanobiphenyl-containing dimesogens (n = 3, 4). As a result, LC phases with a tilted organization of the molecules become dominant. The dimesogen **Thia-Ox/5**, with the shorter spacer, displays a SmC–N_{cybC} dimorphism and, remarkably, the SmC phase is removed for the longer homologue **Thia-Ox/10**.

A N-to-SmC transition is observed at T = 172–173 °C for the dimesogen **Thia-Ox/5** on reduction of the temperature (Figure 5) [68]. In contrast to the N_{cybA}–CybA-transition, for which no transition enthalpy could be detected (see Figure 2a), a small but clearly visible enthalpy change is observed for the N_{cybC}–SmC transition of **Thia-Ox/5** (Figure 5a). Under homeotropic boundary conditions (Figure 5c) the texture of the low-temperature phase is a Schlieren texture, indicating a

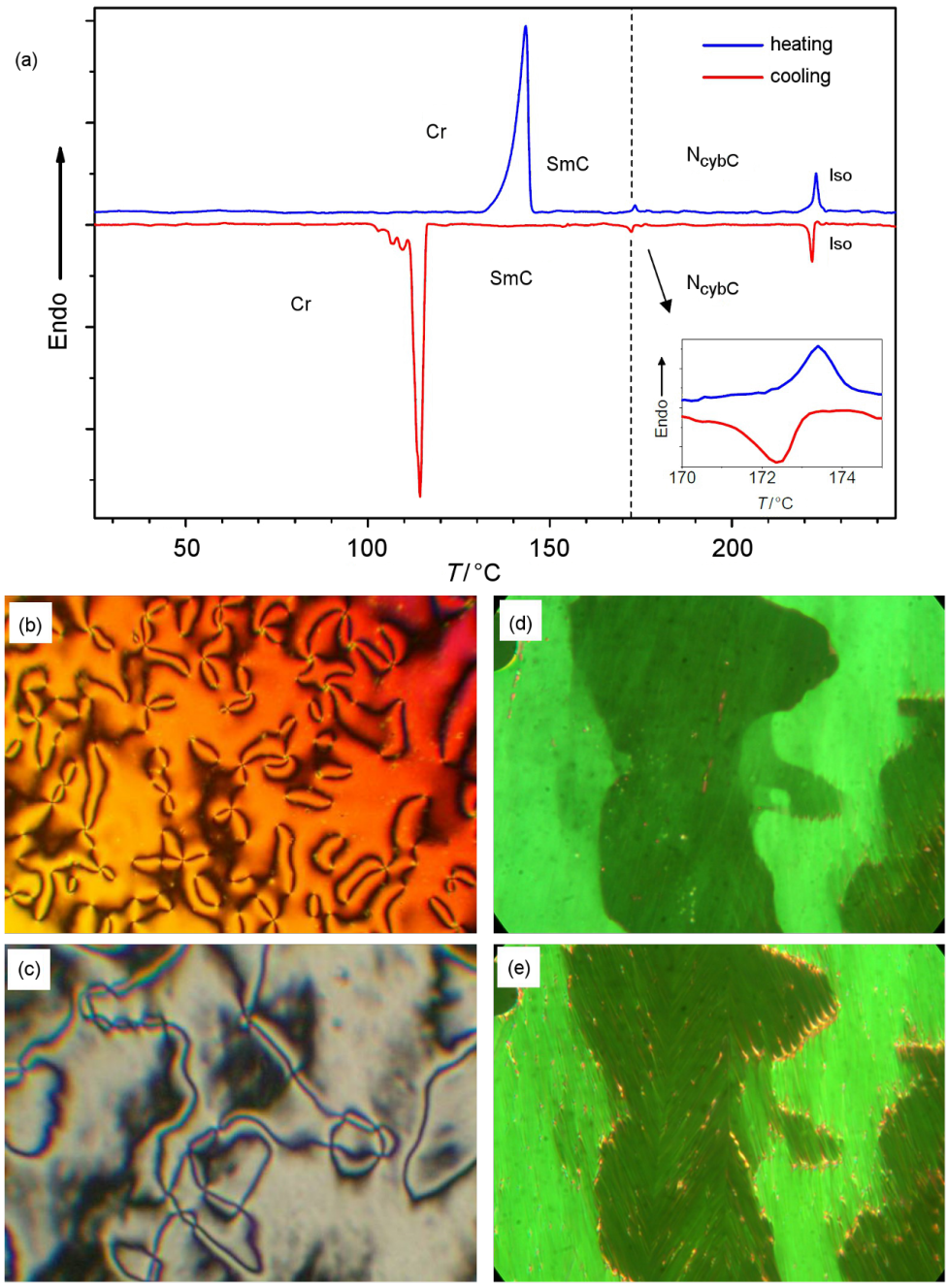

Figure 5: Dimesogen **Thia-Ox/5**: (a) DSC traces obtained during first heating and cooling cycles scanned at a rate of 10 K min^{-1}; (b,c) textures as observed between crossed polarizers, (b) N phase having a Schlieren texture at T = 220 °C and (c) SmC phase at T = 160 °C under homeotropic boundary condition; (d) N phase and (e) SmC phase under homogeneous boundary conditions; the same temperatures as (b,c), observed in polyimide-coated cells, 6 µm.

biaxial smectic phase. The smectic phase was investigated by XRD of a surface-aligned sample. The 2D XRD profile (Figure 6a) has a sharp Bragg peak (d = 4.4 nm) with its second-order reflection located on the meridian, confirming a well-defined layer-like organization. In the wide-angle region there is a diffuse scattering peak with a maximum at d = 0.46 nm providing evidence for a liquid-like ordered LC phase. It is split into maxima located beside the meridian, indicating a tilted organization of the molecules in the layers (Figure 6b). From the positions of the diffuse wide-angle scattering peaks a tilt angle of approximately 25° can be estimated. However, it is not possible to decide from the scattering pattern whether there is a synclinic or anticlinic arrangement of molecules in adjacent layers, but the relatively high birefringence of

the texture (Figure 5c) is more in line with a synclinic organization. Moreover, as is typical for synclinic tilted SmC phases, domains with different director orientation can be observed in homogeneously aligned samples (Figure 5d and Figure 5e), indicating an optical tilt corresponding to the XRD tilt.

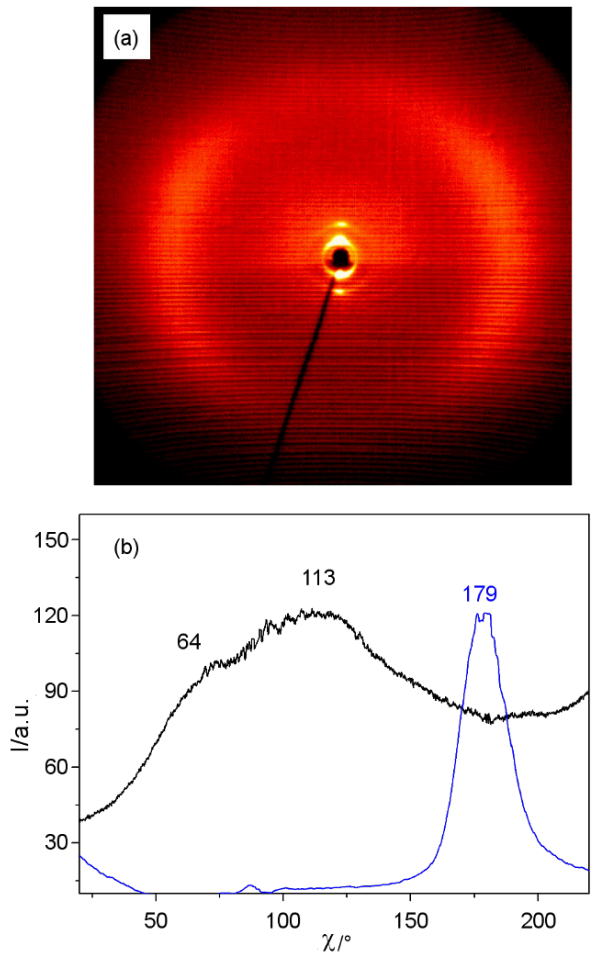

Figure 6: XRD data of the SmC phase of the dimesogen **Thia-Ox/5**: (a) diffraction pattern at T = 160 °C; (b) χ-scans over the diffuse scattering in the wide-angle region (black line: 2θ = 15–25°) and the 01 reflection (blue line: 2θ = 1–3°) at 160 °C; the lower part of the diffraction pattern is shaded by the heating stage, therefore, the intensity below the equator is diminished.

The nearly equal distribution of the diffuse scattering intensity on the left and the right of the XRD pattern (Figure 6a) can be explained with a multidomain structure of the sample with nearly equal contributions of the distinct tilt directions. The layer spacing of d = 4.4 nm is smaller than the length of the molecule (L_{mol} = 5.3 nm in the most stretched conformation). Considering the tilt, a calculated d-value of d_{cal} = 4.8 nm would be expected according to $d_{cal} = L_{mol} \cos \beta$ for the molecule in the most stretched conformation and a reduction to the experimental value of d = 4.4 nm is easily possible by conformational disorder. Hence, it is in line with a monolayer structure of the SmC phase in which the aromatic cores and the relatively short spacer units form one type of layer, which is separated by the layers formed by the aliphatic end-chains (Figure 4a). In the layers of the core units, the 3,5-diphenyl-1,2,4-oxadiazole-, 2-phenyl-1,3,4-thiadiazole and the relatively short C_5 spacer units are mixed, leading to an antiparallel organization of the molecules on average. In the N_{cybC} phases the fundamental structure should be retained but becomes a short-range local structure in the cybotactic clusters.

Compound **Thia-Ox/10**, with a much longer spacer unit than **Thia-Ox/5**, has exclusively a nematic phase and no transition to a SmC phase could be observed optically on cooling the sample down to 123 °C, at which point crystallization starts. The XRD pattern of a magnetically aligned sample (B = 1 T) of this nematic phase shows a crescent-like diffuse wide-angle scattering peak centered on the equator (Figure 7a). In the small-angle region a diffuse scattering peak with a maximum at d = 2.5 nm (T = 150 °C) is extended to a line parallel to the equator. The χ-scan over this scattering is split into two maxima located beside the meridian (Figure 7b). This indicates the presence of SmC-type cybotactic clusters with a tilt (β) of the molecules of about $\beta = \Delta\chi/2$ = 37–39°. The estimated cluster size is $L_{\parallel}$ = 5 nm and $L_{\perp}$ = 1.4 nm, corresponding to about two layers of aromatic cores and about 3 × 3 molecules in the transversal directions. Hence the size of these clusters is significantly smaller than for the N_{cybA} phase of compound **CB-Ox/4**. The d-value of the small-angle scattering maximum (d = 2.5 nm) is much smaller than the molecular length (L_{mol} = 5.9 nm) in the most stretched conformation. Considering the significant tilt the effective molecular length, calculated according to $L_{eff} = d/\cos \beta$ = 3.2 nm, corresponds to 0.54 L_{mol}. This small value, close to half the molecular length L_{mol}, suggests that in the cybotyctic clusters there is a mixed side-by-side packing of the individual aromatic units, separated by the aliphatic domains composed of the mixed terminal chains and C_{10} spacer units ("intercalated" structure, see Figure 4b) [3,4].

Hence, for the dimesogens **Thia-Ox/*n***, elongation of the spacers leads to a change of the molecular organization as indicated by a strong change of the d-spacing. Whereas in the case of **Thia-Ox/5** the rigid cores together with the C_5 spacers are organized side-by-side and separated from the alkyl chains in the monolayer smectic phases and in the cybotactic clusters of the nematic phase (Figure 4a), in the case of compound **Thia-Ox/10** the longer C_{10} spacers cannot be accommodated between the aromatic cores. These long spacers preferably mix with the terminal alkyl chains, and hence only the aromatics are organized side-by-side and the two distinct cores are mixed randomly (Figure 4b). Due to the significant mismatch of the

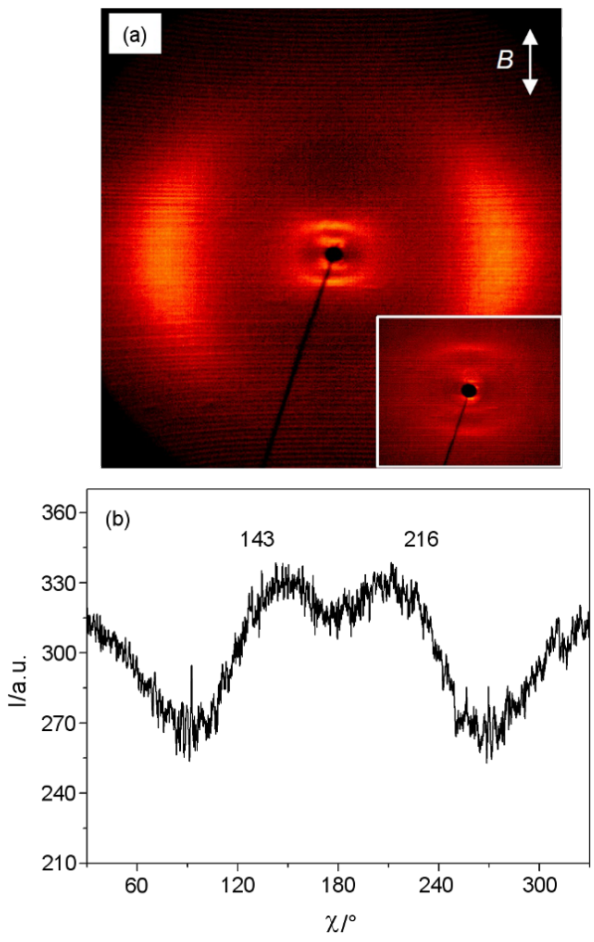

Figure 7: XRD pattern of a magnetic-field-aligned sample of the N_{cybC} phase of the dimesogen **Thia-Ox/10:** (a) diffraction pattern at T = 150 °C (inset = small-angle scattering); (b) χ-scan over the small-angle scattering (2θ = 2.5–5.0°). Besides the scattering at d = 2.5 nm there is a second very weak scattering with a maximum at a smaller θ-angle, corresponding to approximately twice the d-value. This would indicate a monolayer structure in the cybotactic clusters, similar to that described for **Thia-Ox/5**. It is unlikely that the much more intense scattering at a higher d-value represents the second order of the weak reflection. A possible explanation could therefore be a heterogeneous structure of the sample, probably provided by the interaction of the cybotactic clusters with the surface of the capillary, in which the majority represents the intercalated structure described in the text and the minority is formed by a monolayer structure as found for **Thia-Ox/5**. The proposed formation of a SmC surface layer is basically in line with texture observations made for compound **Thia-Ox/5** (see Figure 8c,d) in which no significant change of the texture is found at the N_{cybC}-to-SmC transition. It could be expected that the energetic difference between these two distinct types of layer structures is small, and hence variation of the cluster size under the influence of surface interactions could have an effect on the structure.

core length of the two mesogenic units, there is some unfavorable overlapping of alkyl chains and aromatics and therefore the layers are not well developed (see Figure 4b). Hence, a long-range smectic ordering cannot develop upon decreasing the temperature, and the molecules only retain an orientationally ordered organization in the SmC-type cybotactic clusters forming the N_{cybC} phase. Hence, for the thiadiazoles **Thia-Ox/*n***, elongation of the alkylene spacer unit connecting the two mesogenic cores removes the SmC phase, which is contrary to the usually observed effect that elongation of alkyl chains stabilizes smectic phases due to improved segregation. The promotion of nematic phases by elongation of an aliphatic spacer unit was previously observed for dimesogens combining two rod-like segments [3,4,83]. As a general rule, for this type of dimesogen the terminal chains must be longer than half the spacer length to form smectic phases [3,4]. According to this rule, the formation of smectic phases should in principle be possible for both compounds, **Thia-Ox/5** and **Thia-Ox/10**. It appears that the very different lengths of the two mesogenic units and probably also the bent shape of these units contribute additionally to destabilization of the smectic phase.

Although these two thiadiazole-containing dimesogens only form tilted LC phases (SmC, N_{cybC}), for **Thia-Ox/5** with a relatively short spacer the tilt is significantly reduced (25°) compared to the related 2,5-diphenyl-1,2,4-oxadiazoles without an attached rod-like unit (40–50°) [64,65]. In the dimesogen **Thia-Ox/10**, in which the two mesogenic units are more decoupled, the reduction of the tilt is much less (37–39° tilt). Hence, not only the type of rod-like mesogen, but also the degree of coupling of the rod-like units to the 3,5-diphenyl-1,2,4-oxadiazole core, seems to be important for the degree of tilt.

Distinguishing skewed and orthogonal cybotactic nematic phases

Usually the two distinct types of cybotactic nematic phases, N_{cybC} and N_{cybA}, can be distinguished by analyzing the shape of the diffuse small-angle X-ray scattering of magnetically aligned samples, which is split into two maxima beside the meridian for N_{cybC} phases (Figure 8a and Figure 8b) and is nonsplit and centered on the meridian for N_{cybA} phases (Figure 3a). During investigation of compounds **Thia-Ox/5** and **CB-Ox/4** we found that there are also some differences in the optical textures of N_{cybC} and N_{cybA} phases. On cooling from the isotropic liquid state, the textures occur as highly birefringent Schlieren textures (Figure 8a and Figure 8e) in both cases. On further cooling, the texture changes to a much less birefringent appearance for both compounds, attributed to an anchoring transition in which the direction of the molecules changes from parallel to the surface (homogeneous) to perpendicular or tilted with respect to the surface (homeotropic) (Figure 8b and Figure 8f) [52]. This anchoring transition, which depends on the LC material as well as on the properties of the surfaces, could be influenced by temperature-dependent changes of the dielectric anisotropies and steric surface–molecule interactions [52,84], but, as proposed previously, it is most probably also

related to the size of the cybotactic clusters forming the nematic phase [69]. At high temperature the clusters are small, and in a homogeneous cell the alignment is determined by the organization of the mesogenic cores parallel to the surface, giving highly birefringent (colorful) textures, as shown in Figure 8a and Figure 8e. As the cluster size grows with decreasing temperature the preferred orientation becomes that with the "layer planes" of the cybotactic smectic clusters being parallel to the

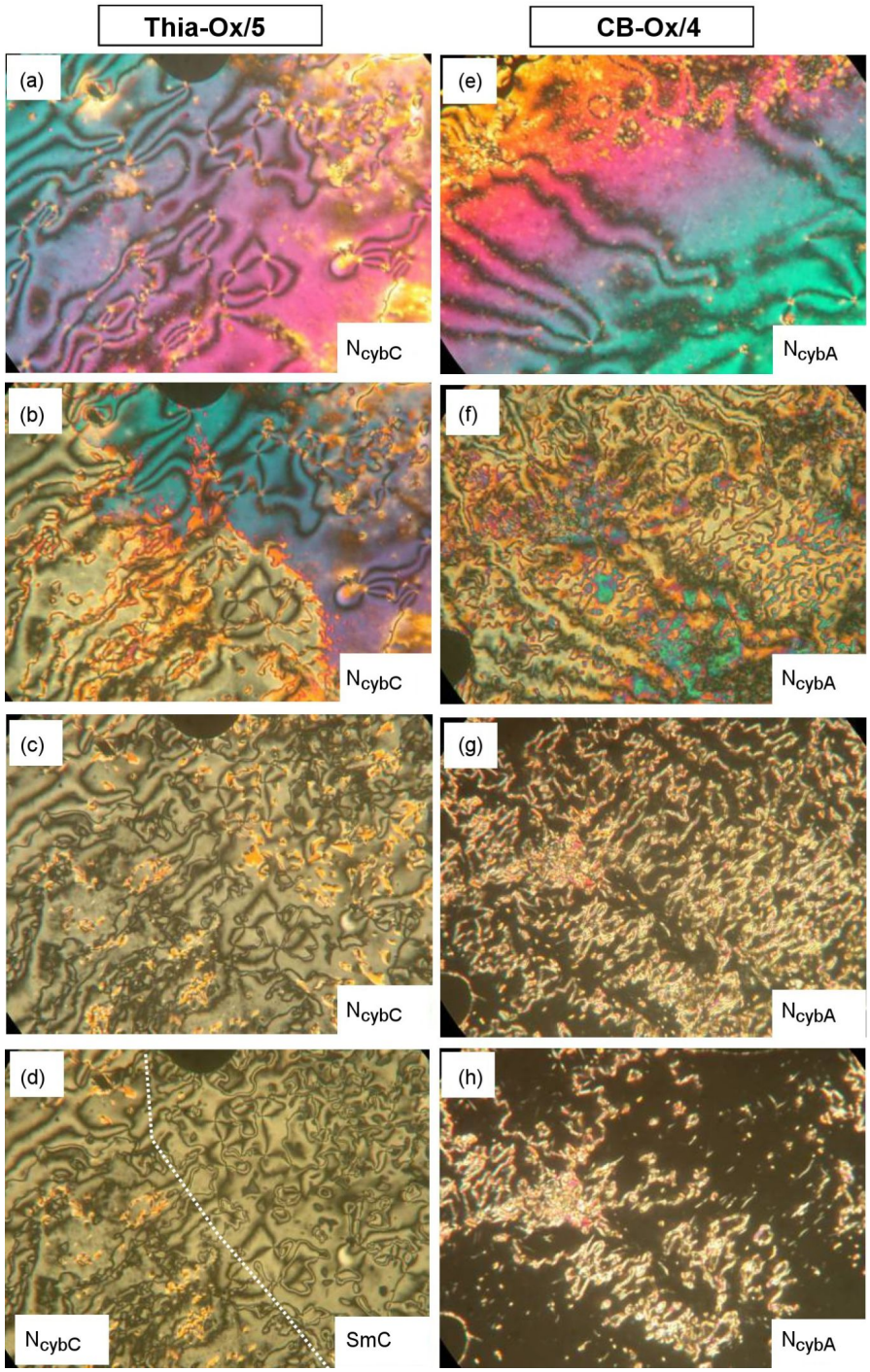

Figure 8: Comparison of the optical textures of distinct types of 1,2,4-oxadiazole based dimesogens as observed between nontreated glass plates (Menzel cover glasses, Menzel GmbH, Braunschweig) between crossed polarizers: (a–d) compound **Thia-Ox/5** at (a) T = 206 °C; (b) T = 197 °C; (c) T = 178 °C; (d) T = 173 °C N_{cybC}-to-SmC transition, the dotted line indicates the phase boundary; (e–h) compound **CN-Ox/4** at (e) T = 254 °C; (f) T = 232 °C; (g) T = 178 °C; (h) T = 150 °C (at T = 146 °C in the CybA phase all birefringence has disappeared).

cell-surface. In this homeotropic alignment the birefringence is significantly reduced and the textures appear either completely dark (molecules on average perpendicular to the surface, see Figure 8g and Figure 8h) or retain a low birefringence and then appear with gray Schlieren texture (molecules are tilted with respect to the surface, Figure 8c and Figure 8d). Due to surface interactions, the cybotactic clusters can in some cases become aligned at the surfaces even in the nematic phase by forming smectic surface layers, and these layers align the clusters of the bulk sample. In this way the surface anchoring determines the optical properties of the investigated samples. If the surface layer is nontilted (SmA-like) then the sample adopts a homeotropic alignment, which appears completely dark. Indeed for compounds **CB-Ox/*n*** with a N_{cybA}–CybA transition the birefringent Schlieren texture disappears upon approaching the transition to the CybA phase (Figure 8g and Figure 8h). In contrast, for compound **Thia-Ox/5**, with a N_{cybC}–SmC transition (and also for **Thia-Ox/10** without SmC phase), the birefringent texture, as typical for tilted smectic phases, is retained on cooling down to the transition to the SmC phase (Figure 8c and Figure 8d). In fact the N_{cybC}-to-SmC transition is hardly detected by polarizing microscopy (see Figure 8d), but it is clearly confirmed by the DSC peak (Figure 5a) and the XRD pattern (Figure 6a). However, the absence of birefringence in the homeotropically aligned sample does not prove the presence of a N_{cybA} phase, as in a N_{cybC} phase randomization of the tilt direction of the SmC clusters can also result in a completely dark appearance of the homeotropic samples, and in this case birefringence occurs only upon approaching the transition to the SmC phase. Hence, optical investigation can only be used as a first indication of N_{cybA} and N_{cybC} phases if the transition to a homeotropically aligned smectic phase is observed, but it usually requires additional confirmation by XRD of magnetically aligned samples.

Conclusion

The first examples of end-to-end connected bent-core–rod couples and rod–bent-core–rod trimesogens incorporating a bent 3,5-diphenyl-1,2,4-oxadiazole core have been synthesized and their LC phase behaviors were studied. All molecules show broad regions of nematic phases. The heterotrimesogens with two CB units (**CB-Ox-CB/*n***) form exclusively nematic phases, whereas related dimesogens with only one CB unit (**Ox-CB/*n***) show an additional CybA phase. The nematic phases of these dimesogens represent cybotactic nematic phases [68,71-73] composed of small SmA-like clusters. These cybotactic nematic phases composed of clusters with (on average) nontilted molecules are of significant interest, as restricted rotation around the long axes of the molecules would in this case lead to biaxial nematic phases of the orthorhombic type (N_{bo}) [57,73]. In contrast, biaxial nematic phases of the monoclinic type (N_{bm}) could be expected for cybotactic nematic phases composed of tilted SmC clusters in which the biaxiality is additionally influenced by the tilt of the molecules. Therefore, the rarely occurring N_{cybA} phases [75,76] are of significant interest in the search for biaxial nematic phases [57]. It is important to note here that the nematic phases of some 3,5-bis(4-hydroxyphenyl)-1,2,4-oxadiazole bis(4-alkyloxybenzoates) have been identified as ferroelectric-like switching cybotactic nematic phases (N_{cybCP}) [64,65], but in these N_{cybCP} phases the molecules are strongly tilted (40–50° tilt), such that the field-induced polar and biaxial nematic phases of these compounds represent subtypes of the monoclinic N_{bm} phases. It has been shown here that the combination of the 2,5-diphenyl-1,2,4-oxadiazole core with one CB unit in dimesogens leads to the removal of the tilt and promotes an orthogonal organization of the molecules (CybA, N_{cybA}). However, replacing the CB group by a 2-phenyl-1,3,4-thiadiazole core retains the tilted SmC-like organization of the simple 1,2,4-oxadiazole-based bent-core mesogens [81,82].

Experimental

Preparation of the trimesogens CB-Ox-CB/*n*

A mixture of 3,5-bis(4-hydroxyphenyl)-1,2,4-oxadiazole (**1**) [65] (0.39 mmol, 1 equiv), ω-(4'-cyanobiphenyl-4-yloxy)alkanoic acids (**2a**,**b**) [66] (0.78 mmol, 2 equiv) and a catalytic amount of DMAP were dissolved in dry CH_2Cl_2 and stirred for 5 min. To the above clear solution, *N*,*N*'-dicyclohexylcarbodiimide (DCC, 1.2 mmol, 3 equiv) was added and stirring was continued for 12 h at rt, followed by solvent evaporation and column chromatography with using EtOAc/*n*-hexane 2:8, to yield a solid, which was further purified by crystallization from EtOAc/EtOH 2:8.

CB-Ox-CB/3: 3,5-bis{4-[4-(4'-Cyanobiphenyl-4-yloxy)butanoyloxy]phenyl}-1,2,4-oxa-diazole; colorless solid; yield 71%; ^{1}H NMR (400 MHz, $CDCl_3$) δ 8.25 (d, J = 8.4 Hz, 2H, Ar), 8.16 (d, J = 8.0 Hz, 2H, Ar), 7.70 (dd, ^1J = 8.2 Hz, ^2J = 8.4 Hz, 8H, Ar), 7.56 (d, J = 8.4 Hz, 4H, Ar), 7.32 (d, J = 8.8 Hz, 2H, Ar), 7.27 (d, J = 8.0 Hz, 2H, Ar), 7.22 (d, J = 8.8 Hz, 4H, Ar), 4.17 (t, J = 5.8 Hz, 4H, 2 × OCH_2), 2.85 (m, 4H, 2× CH_2COO), 2.32 (m, 4H, 2 × CH_2); Analysis calcd for $C_{48}H_{36}N_4O_7$: C, 73.83; H, 4.65; N, 7.18; found: C, 73.76; H, 4.45; N, 6.91.

CB-Ox-CB/4: 3,5-bis{4-[5-(4'-Cyanobiphenyl-4-yloxy)pentanoyloxy]phenyl}-1,2,4-oxa-diazole; colorless solid; yield 75%; ^{1}H NMR (400 MHz, $CDCl_3$) δ 8.22 (d, J = 8.0 Hz, 2H, Ar), 8.17 (d, J = 8.0 Hz, 2H, Ar), 7.68 (dd, ^1J = 8.4 Hz, ^2J = 8.4 Hz, 8H, Ar), 7.52 (d, J = 8.8 Hz, 4H, Ar), 7.28 (d, J = 8.8 Hz, 2H, Ar), 7.21 (d, J = 8.0 Hz, 2H, Ar), 7.00 (d, J = 8.8 Hz, 4H, Ar), 4.09 (t, J = 5.2 Hz, 4H, 2 × OCH_2), 2.71 (m, 4H, 2 ×

CH_2COO), 1.97 (m, 8H, 4 × CH_2); ^{13}C NMR (125 MHz, $CDCl_3$) δ 175.01, 171.44, 171.21, 168.30, 159.50, 159.48, 154.13, 152.94, 145.19, 145.16, 132.55, 131.57, 131.54, 129.63, 128.84, 128.36, 127.08, 124.48, 122.43, 122.08, 121.76, 119.03, 115.08, 115.06, 110.15, 110.12, 67.46, 67.43, 33.96, 28.52, 21.60, 21.57; Anal. calcd for $C_{50}H_{40}N_4O_7$: C, 74.24; H, 4.98; N, 6.93; found: C, 73.94; H, 4.74; N, 6.62.

Preparation of the dimesogens **CB-Ox/*n*** and **Thia-Ox/*n***

A mixture of 4-[3-(4-hydroxyphenyl)-1,2,4-oxadiazol-5-yl]phenyl 4-hexylbenzoate (**3**) [67] (0.34 mmol, 1 equiv), ω-(4'-cyanobiphenyl-4'-yloxy)alkanoic acid (**2a**,**b**) [66] (0.34 mmol, 1 equiv) or ω-[4-(5-heptyl-1,2,4-thiadiazol-2yl)phenoxy]alkanoic acids (**4a**,**b**) [66] (0.34 mmol, 1 equiv) and a catalytic amount of DMAP were dissolved in dry CH_2Cl_2. To the above clear solution, *N*,*N*'-dicyclohexylcarbodiimide (DCC, 0.51 mmol, 1.1 equiv) was added and stirred for 12 h at rt, followed by solvent evaporation and column chromatography with EtOAc/*n*-hexane 2:8 to yield a solid, which was further purified by crystallization from EtOAc/EtOH 2:8.

CB-Ox/3: 4-(3-{4-[4-(4'-Cyanobiphenyl-4-yl)oxybutanoyloxy]phenyl}-1,2,4-oxadiazol-5-yl)phenyl 4-hexylbenzoate; colorless solid; yield 70%; ^1H NMR (400 MHz, $CDCl_3$) δ 8.24 (d, *J* = 8.8 Hz, 2H, Ar), 8.16 (d, *J* = 8.8 Hz, 2H, Ar), 8.07 (d, *J* = 8.4 Hz, 2H, Ar), 7.64 (dd, ^1J = 8.8 Hz, ^2J = 8.8 Hz, 4H, Ar), 7.49 (d, *J* = 8.4 Hz, 2H, Ar), 7.38 (d, *J* = 8.8 Hz, 2H, Ar), 7.28 (d, *J* = 8.4 Hz, 2H, Ar), 7.21 (d, *J* = 8.8 Hz, 2H, Ar), 6.96 (d, *J* = 8.8 Hz, 2H, Ar), 4.11 (t, *J* = 6.0 Hz, 2H, 1 × OCH_2), 2.81 (t, *J* = 7.2 Hz, 2H, 1 × CH_2), 2.67 (t, *J* = 7.6 Hz, 2H, CH_2COO), 2.23 (m, 2H, CH_2), 1.63–1.12 (m, 8H, 4× CH_2), 0.84 (t, *J* = 6.8 Hz, 3H, 1 × CH_3); ^{13}C NMR (125 MHz, $CDCl_3$) δ 175.13, 171.24, 168.29, 164.61, 159.36, 154.60, 152.88, 149.89, 145.15, 132.55, 131.74, 130.34, 129.67, 128.87, 128.77, 128.40, 127.11, 126.33, 124.60, 122.69, 122.06, 121.71, 119.03, 115.10, 110.18, 66.71, 36.09, 31.62, 31.04, 30.97, 28.88, 24.52, 22.54, 14.03; Anal. calcd for $C_{44}H_{39}N_3O_6$: C, 74.88; H, 5.57; N, 5.95; found: C, 74.58; H, 5.27; N, 5.69.

CB-Ox/4: 4-(3-{4-[5-(4'-Cyanobiphenyl-4-yloxy)pentanoyloxy]phenyl}-1,2,4-oxadiazol-5-yl)phenyl 4-hexylbenzoate; colorless solid; yield 74%; ^1H NMR (400 MHz, $CDCl_3$) δ 8.23 (d, *J* = 7.2 Hz, 2H, Ar), 8.14 (d, *J* = 6.8 Hz, 2H, Ar), 8.07 (d, *J* = 6.4 Hz, 2H, Ar), 7.63 (dd, ^1J = 6.8 Hz, ^2J = 6.8 Hz, 4H, Ar), 7.48 (d, *J* = 6.8 Hz, 2H, Ar), 7.38 (d, *J* = 6.8 Hz, 2H, Ar), 7.28 (d, *J* = 6.4 Hz, 2H, Ar), 7.20 (d, *J* = 7.2 Hz, 2H, Ar), 6.96 (d, *J* = 6.8 Hz, 2H, Ar), 4.04 (t, *J* = 4.4 Hz, 2H, 1 × OCH_2), 2.66 (t, *J* = 6.0 Hz, 4H, 2 × CH_2), 1.93–1.24 (m, 12H, 6× CH_2), 0.84 (t, *J* = 5.6 Hz, 3H, 1 × CH_3); Anal. calcd for $C_{45}H_{41}N_3O_6$: C, 75.09; H, 5.74; N, 5.84; found: C, 74.95; H, 5.61; N, 5.65.

Thia-Ox/5: 4-[3-(4-{6-[4-(5-Heptyl-1,3,4-thiadiazol-2-yl)phenoxy]hexanoyloxy}phenyl)-1,2,4-oxadiazol-5-yl]phenyl 4-hexylbenzoate; colorless solid; yield 69%; ^1H NMR (400 MHz, $CDCl_3$) δ 8.24 (d, *J* = 8.8 Hz, 2H, Ar), 8.15 (d, *J* = 8.8 Hz, 2H, Ar), 8.07 (d, *J* = 8.4 Hz, 2H, Ar), 7.80 (d, *J* = 8.8 Hz, 2H, Ar), 7.38 (d, *J* = 8.8 Hz, 2H, Ar), 7.28 (d, *J* = 8.8 Hz, 2H, Ar), 7.19 (d, *J* = 8.4 Hz, 2H, Ar), 6.91 (d, *J* = 8.8 Hz, 2H, Ar), 4.01 (t, *J* = 6.4 Hz, 2H, 1 × OCH_2), 3.05 (t, *J* = 7.6 Hz, 2H, 1 × CH_2), 2.66 (t, *J* = 7.2 Hz, 2H, 1 × CH_2), 2.60 (t, *J* = 7.2 Hz, 2H, CH_2COO), 1.80–0.82 (m, 30H, 12 × CH_2, 2 × CH_3); Anal. calcd for $C_{48}H_{54}N_4O_6S$: C, 70.74; H, 6.87; N, 5.87; found: C, 70.57; H, 6.54; N, 6.67.

Thia-Ox/10: 4-[3-(4-{11-[4-(5-Heptyl-1,3,4-thiadiazol-2-yl)phenoxy]undecanoyloxy}-phenyl)-1,2,4-oxadiazol-5-yl]phenyl 4-hexylbenzoate; colorless solid; yield 72%; ^1H NMR (400 MHz, $CDCl_3$) δ 8.23 (d, *J* = 8.8 Hz, 2H, Ar), 8.14 (d, *J* = 8.8 Hz, 2H, Ar), 8.07 (d, *J* = 8.4 Hz, 2H, Ar), 7.79 (d, *J* = 8.8 Hz, 2H, Ar), 7.37 (d, *J* = 8.8 Hz, 2H, Ar), 7.27 (d, *J* = 8.8 Hz, 2H, Ar), 7.18 (d, *J* = 8.4 Hz, 2H, Ar), 6.89 (d, *J* = 8.8 Hz, 2H, Ar), 3.96 (t, *J* = 6.4 Hz, 2H, 1 × OCH_2), 3.05 (t, *J* = 7.6 Hz, 2H, 1 × CH_2), 2.66 (t, *J* = 7.2 Hz, 2H, 1 × CH_2), 2.54 (t, *J* = 7.2 Hz, 2H, CH_2COO), 1.77–0.79 (m, 40H, 17 × CH_2, 2 × CH_3); ^{13}C NMR (125 MHz, $CDCl_3$) δ 175.09, 171.85, 169.47, 168.33, 168.11, 164.60, 161.27, 154.57, 153.03, 149.87, 130.34, 129.66, 129.27, 128.83, 128.76, 126.35, 124.43, 122.86, 122.67, 122.11, 121.73, 114.91, 68.18, 36.09, 34.38, 31.62, 31.61, 31.03, 30.17, 30.05, 29.43, 29.31, 29.30, 29.18, 29.12, 29.04, 28.94, 28.87, 28.86, 25.96, 24.84, 22.55, 22.54, 14.03, 14.02; Anal. calcd for $C_{53}H_{64}N_4O_6S$: C, 71.92; H, 7.29; N, 6.33; found: C, 71.65; H, 7.25; N, 6.29.

Acknowledgements

This work was supported by the EU within the FP7 funded Collaborative Project BIND (Grant No 216025) and the Cluster of Excellence "Nanostructured Materials".

References

1. Imrie, C. T.; Henderson, P. A.; Yeap, G.-Y. *Liq. Cryst.* **2009,** *36,* 755–777. doi:10.1080/02678290903157455
2. Goodby, J. W.; Saez, I. M.; Cowling, S. J.; Gasowska, J. S.; MacDonald, R. A.; Sia, S.; Watson, P.; Toyne, K. J.; Hird, M.; Lewis, R. A.; Lee, S.-E.; Vaschenko, V. *Liq. Cryst.* **2009,** *36,* 567–605. doi:10.1080/02678290903146060
3. Imrie, C. T. Liquid Crystal Dimers. In *Liquid Crystals II;* Mingos, D. M. P., Ed.; Structure and Bonding, Vol. 95; Springer: Berlin, Germany, 1999; pp 149–192.
4. Imrie, C. T.; Henderson, P. A. *Chem. Soc. Rev.* **2007,** *36,* 2096–2124. doi:10.1039/B714102E
5. Abe, A.; Furuya, H.; Zhou, Z.; Hiejima, T.; Kobayashi, Y. *Adv. Polym. Sci.* **2005,** *181,* 121–152. doi:10.1007/b107177
6. Ungar, G.; Percec, V.; Zuber, M. *Macromolecules* **1992,** *25,* 75–80. doi:10.1021/ma00027a013

7. Tokita, M.; Osada, K.; Watanabe, J. *Liq. Cryst.* **1998,** *24,* 477–480. doi:10.1080/026782998207325
8. Ober, C. K.; Jin, J.-I.; Zhou, Q.; Lenz, R. W. *Adv. Polym. Sci.* **1984,** *59,* 103–146. doi:10.1007/3-540-12818-2_8
9. Kumar, S. *Liq. Cryst.* **2009,** *36,* 607–638. doi:10.1080/02678290902755549
10. Kreuder, W.; Ringsdorf, H.; Herrmann-Schönherr, O.; Wendorff, J. H. *Angew. Chem., Int. Ed. Engl.* **1987,** *26,* 1249–1252. doi:10.1002/anie.198712491
11. Yoshizawa, A. *J. Mater. Chem.* **2008,** *18,* 2877–2889. doi:10.1039/B802712A
12. Andersch, J.; Tschierske, C. *Liq. Cryst.* **1996,** *21,* 51–63. doi:10.1080/02678299608033795
13. Weissflog, W.; Demus, D.; Diele, S.; Nitschke, P.; Wedler, W. *Liq. Cryst.* **1989,** *5,* 111–122. doi:10.1080/02678298908026354
14. Sato, M.; Yoshizawa, A.; Ogasawara, F. *Mol. Cryst. Liq. Cryst.* **2007,** *475,* 99–112. doi:10.1080/15421400701679939
15. Yamaguchi, A.; Nishiyama, I.; Yamamoto, J.; Yokoyama, H.; Yoshizawa, A. *J. Mater. Chem.* **2005,** *15,* 280–288. doi:10.1039/B406716A
16. Andersch, J.; Tschierske, C.; Diele, S.; Lose, D. *J. Mater. Chem.* **1996,** *6,* 1297–1307. doi:10.1039/JM9960601297
17. Prajapati, A. K.; Varia, M. C.; Sahoo, S. P. *Liq. Cryst.* **2011,** *38,* 861–869. doi:10.1080/02678292.2011.584636
18. Huh, S.-M.; Jin, J.-I.; Achard, M.-F.; Hardouin, F. *Liq. Cryst.* **1999,** *26,* 919–924. doi:10.1080/026782999204615
19. Zhang, Y.; Martinez-Perdiguero, J.; Baumeister, U.; Walker, C.; Etxebarria, J.; Prehm, M.; Ortega, J.; Tschierske, C.; O'Callaghan, M. J.; Harant, A.; Handschy, M. *J. Am. Chem. Soc.* **2009,** *131,* 18386–18392. doi:10.1021/ja9069166
20. Date, R. W.; Bruce, D. W. *J. Am. Chem. Soc.* **2003,** *125,* 9012–9013. doi:10.1021/ja0357947
21. Kouwer, P. H. J.; Mehl, G. H. *J. Am. Chem. Soc.* **2003,** *125,* 11172–11173. doi:10.1021/ja037075y
22. Apreutesei, D.; Mehl, G. H. *Chem. Commun.* **2006,** 609–611. doi:10.1039/B512120E
23. Attard, G. S.; Date, R. W.; Imrie, C. T.; Luckhurst, G. R.; Roskilly, S. J.; Seddon, J. M.; Taylor, L. *Liq. Cryst.* **1994,** *16,* 529–581. doi:10.1080/02678299408036531
24. Hardouin, F.; Achard, M. F.; Laguerre, M.; Jin, J.-I.; Ko, D.-H. *Liq. Cryst.* **1999,** *26,* 589–599. doi:10.1080/026782999205047
25. Yelamaggad, C. V.; Nagamani, S. A.; Hiremath, U. S.; Nair, G. G. *Liq. Cryst.* **2001,** *28,* 1009–1015. doi:10.1080/02678290110039499
26. Yelamaggad, C. V.; Shanker, G.; Hiremath, U. S.; Prasad, S. K. *J. Mater. Chem.* **2008,** *18,* 2927–2949. doi:10.1039/B804579H
27. Izumi, T.; Naitou, Y.; Shimbo, Y.; Takanishi, Y.; Takezoe, H.; Watanabe, J. *J. Phys. Chem. B* **2006,** *110,* 23911–23919. doi:10.1021/jp062208y
28. Takanishi, Y.; Toshimitsu, M.; Nakata, M.; Takada, N.; Izumi, T.; Ishikawa, K.; Takezoe, H.; Watanabe, J.; Takahashi, Y.; Iida, A. *Phys. Rev. E* **2006,** *74,* 051703. doi:10.1103/PhysRevE.74.051703
29. Henderson, P. A.; Imrie, C. T. *Liq. Cryst.* **2011,** *38,* 1407–1414. doi:10.1080/02678292.2011.624368
30. Panov, V. P.; Nagaraj, M.; Vij, J. K.; Panarin, Y. P.; Kohlmeier, A.; Tamba, M. G.; Lewis, R. A.; Mehl, G. H. *Phys. Rev. Lett.* **2010,** *105,* 167801. doi:10.1103/PhysRevLett.105.167801
31. Cestari, M.; Diez-Berart, S.; Dunmur, D. A.; Ferrarini, A.; de la Fuente, M. R.; Jackson, D. A.; Lopez, D. O.; Luckhurst, G. R.; Perez-Jubindo, M. A.; Richardson, R. M.; Salud, J.; Timimi, B. A.; Zimmermann, H. *Phys. Rev. E: Stat., Nonlinear, Soft Matter Phys.* **2011,** *84,* 031704. doi:10.1103/PhysRevE.84.031704
32. Niori, T.; Sekine, T.; Watanabe, J.; Furukawa, T.; Takezoe, H. *J. Mater. Chem.* **1996,** *6,* 1231–1233. doi:10.1039/JM9960601231
33. Link, D. R.; Natale, G.; Shao, R.; Maclennan, J. E.; Clark, N. A.; Körblova, E.; Walba, D. M. *Science* **1997,** *278,* 1924–1927. doi:10.1126/science.278.5345.1924
34. Reddy, R. A.; Tschierske, C. *J. Mater. Chem.* **2006,** *16,* 907–961. doi:10.1039/b504400f
35. Takezoe, H.; Takanishi, Y. *Jpn. J. Appl. Phys., Part 1* **2006,** *45,* 597–625. doi:10.1143/JJAP.45.597
36. Hough, L. E.; Spannuth, M.; Nakata, M.; Coleman, D. A.; Jones, C. D.; Dantlgraber, G.; Tschierske, C.; Watanabe, J.; Körblova, E.; Walba, D. M.; Maclennan, J. E.; Glaser, M. A.; Clark, N. A. *Science* **2009,** *325,* 452–456. doi:10.1126/science.1170028
37. Dantlgraber, G.; Diele, S.; Tschierske, C. *Chem. Commun.* **2002,** 2768–2769. doi:10.1039/b209106b
38. Keith, C.; Reddy, R. A.; Baumeister, U.; Hahn, H.; Lang, H.; Tschierske, C. *J. Mater. Chem.* **2006,** *16,* 3444–3447. doi:10.1039/B609555K
39. Keith, C.; Dantlgraber, G.; Reddy, R. A.; Baumeister, U.; Prehm, M.; Hahn, H.; Lang, H.; Tschierske, C. *J. Mater. Chem.* **2007,** *17,* 3796–3805. doi:10.1039/B706923E
40. Kosata, B.; Tamba, G.-M.; Baumeister, U.; Pelz, K.; Diele, S.; Pelzl, G.; Galli, G.; Samaritani, S.; Agina, E. V.; Boiko, N. I.; Shibaev, V. P.; Weissflog, W. *Chem. Mater.* **2006,** *18,* 691–701. doi:10.1021/cm051918y
41. Achten, R.; Koudijs, A.; Giesberg, M.; Marcelis, A. T. M.; Sudhölter, E. J. R.; Schröder, M. W.; Weissflog, W. *Liq. Cryst.* **2007,** *34,* 59–64. doi:10.1080/02678290601061330
42. Umadevi, S.; Sadashiva, B. K.; Murthy, H. N. S.; Raghunathan, V. A. *Soft Matter* **2006,** *2,* 210–214. doi:10.1039/B516638A
43. Umadevi, S.; Sadashiva, B. K. *Liq. Cryst.* **2007,** *34,* 673–681. doi:10.1080/02678290701343174
44. Shanker, G.; Prehm, M.; Tschierske, C. *J. Mater. Chem.* **2012,** *22,* 168–174. doi:10.1039/c1jm13649f
45. Yelamaggad, C. V.; Prasad, S. K.; Nair, G. G.; Shashikala, I. S.; Rao, D. S. S.; Lobo, C. V.; Chandrasekhar, S. *Angew. Chem., Int. Ed.* **2004,** *43,* 3429–3432. doi:10.1002/anie.200453908
46. Prasad, S. K.; Nair, G. G.; Rao, D. S. S.; Lobo, C. V.; Shashikala, I.; Yelamaggad, C. V. *Mol. Cryst. Liq. Cryst.* **2005,** *437,* 211–221. doi:10.1080/15421400590956612
47. Jákli, A.; Liao, G.; Shashikala, I.; Hiremath, U. S.; Yelamaggad, C. V. *Phys. Rev. E* **2006,** *74,* 041706. doi:10.1103/PhysRevE.74.041706
48. Tamba, M.-G.; Kosata, B.; Pelz, K.; Diele, S.; Pelzl, G.; Vakhovskaya, Z.; Kresse, H.; Weissflog, W. *Soft Matter* **2006,** *2,* 60–65. doi:10.1039/b511140d
49. Tamba, M.-G.; Weissflog, W.; Eremin, A.; Heuer, J.; Stannarius, R. *Eur. Phys. J. E* **2007,** *22,* 85–95. doi:10.1140/epje/e2007-00015-0
50. Stannarius, R.; Eremin, A.; Tamba, M.-G.; Pelzl, G.; Weissflog, W. *Phys. Rev. E* **2007,** *76,* 061704. doi:10.1103/PhysRevE.76.061704
51. Tamba, M.-G.; Baumeister, U.; Pelzl, G.; Weissflog, W. *Liq. Cryst.* **2010,** *37,* 853–874. doi:10.1080/02678291003798172
52. Lee, G.; Jeong, H.-C.; Araoka, F.; Ishikawa, K.; Lee, J. G.; Kang, K.-T.; Cepic, M.; Takezoe, H. *Liq. Cryst.* **2010,** *37,* 883–892. doi:10.1080/02678292.2010.481904

53. Yelamaggad, C. V.; Achalkumar, A. S.; Bonde, N. L.; Prajapati, A. K. *Chem. Mater.* **2006,** *18,* 1076–1078. doi:10.1021/cm052570
54. Yelamaggad, C. V.; Bonde, N. L.; Achalkumar, A. S.; Rao, D. S. S.; Prasad, S. K.; Prajapati, A. K. *Chem. Mater.* **2007,** *19,* 2463–2472. doi:10.1021/cm0625880
55. Yelamaggad, C. V.; Shashikala, I. S.; Li, Q. *Chem. Mater.* **2007,** *19,* 6561–6568. doi:10.1021/cm702698e
56. Tamba, M.-G.; Bobrovsky, A.; Shibaev, V.; Pelzl, G.; Baumeister, U.; Weissflog, W. *Liq. Cryst.* **2011,** *38,* 1531–1550. doi:10.1080/02678292.2011.626084
57. Tschierske, C.; Photinos, D. J. *J. Mater. Chem.* **2010,** *20,* 4263–4294. doi:10.1039/b924810b
58. Bisoyi, H. K.; Srinivasa, H. T.; Kumar, S. *Beilstein J. Org. Chem.* **2009,** *5,* No. 52. doi:10.3762/bjoc.5.52
59. Torgova, S. I.; Geivandova, S. A.; Francescangeli, O.; Strigazzi, A. *Pramana* **2003,** *61,* 239–248.
60. Torgova, S. I.; Karamysheva, L. A.; Geivandova, T. A.; Strigazzi, A. *Mol. Cryst. Liq. Cryst.* **2001,** *365,* 99–106. doi:10.1080/10587250108025286
61. Parra, M. L.; Hidalgo, P. I.; Elgueta, E. Y. *Liq. Cryst.* **2008,** *35,* 823–832. doi:10.1080/02678290802211114
62. Parra, M. L.; Hidalgo, P. I.; Soto-Bustamante, E. A.; Barberá, J.; Elgueta, E. Y.; Trujillo-Rojo, V. H. *Liq. Cryst.* **2008,** *35,* 1251–1262. doi:10.1080/02678290802513790
63. Gallardo, H.; Cristiano, R.; Vieira, A. A.; Filho, R. A. W. N.; Srivastava, R. M.; Bechtold, I. H. *Liq. Cryst.* **2008,** *35,* 857–863. doi:10.1080/02678290802243117
64. Francescangeli, O.; Stanic, V.; Torgova, S. I.; Strigazzi, A.; Scaramuzza, N.; Ferrero, C.; Dolbnya, I. P.; Weiss, T. M.; Berardi, R.; Muccioli, L.; Orlandi, S.; Zannoni, C. *Adv. Funct. Mater.* **2009,** *19,* 2592–2600. doi:10.1002/adfm.200801865
65. Shanker, G.; Nagaraj, M.; Vij, J. K.; Prehm, M.; Tschierske, C. *Adv. Funct. Mater.* **2012,** in press. doi:10.1002/adfm.201101770
66. Lunkwitz, R.; Tschierske, C.; Diele, S. *J. Mater. Chem.* **1997,** *7,* 2001–2011. doi:10.1039/A702034A
67. Shanker, G.; Tschierske, C. *Tetrahedron* **2011,** *67,* 8635–8638. doi:10.1016/j.tet.2011.09.039
68. Dierking, I. *Textures of Liquid Crystals;* Wiley-VCH Verlag GmBH and KGaA: Weinheim, 2003.
69. Keith, C.; Lehmann, A.; Baumeister, U.; Prehm, M.; Tschierske, C. *Soft Matter* **2010,** *6,* 1704–1721. doi:10.1039/b923262a
70. de Vries, A. *J. Mol. Liq.* **1986,** *31,* 193–202. doi:10.1016/0167-7322(86)80001-0
71. Francescangeli, O.; Vita, F.; Ferrero, C.; Dingemans, T. J.; Samulski, E. T. *Soft Matter* **2011,** *7,* 895–901. doi:10.1039/C0SM00745E
72. Francescangeli, O.; Samulski, E. T. *Soft Matter* **2010,** *6,* 2413–2420. doi:10.1039/C003310C
73. Peroukidis, S. D.; Karahaliou, P. K.; Vanakaras, A. G.; Photinos, D. J. *Liq. Cryst.* **2009,** *36,* 727–737. doi:10.1080/02678290902814700
74. Droulias, S.; Vanakaras, A. G.; Photinos, D. J. *Liq. Cryst.* **2010,** *37,* 969–976. doi:10.1080/02678292.2010.488819
75. Vaupotič, N.; Szydlowska, J.; Salamonczyk, M.; Kovarova, A.; Svoboda, J.; Osipov, M.; Pociecha, D.; Gorecka, E. *Phys. Rev. E* **2009,** *80,* 030701. doi:10.1103/PhysRevE.80.030701
76. Shanker, G.; Prehm, M.; Nagaraj, M.; Vij, J. K.; Tschierske, C. *J. Mater. Chem.* **2011,** *21,* 18711–18714. doi:10.1039/c1jm14653j
77. Guinier, A. *X-ray Diffraction;* Freeman and company: San Francisco, 1963.
78. Francescangeli, O.; Laus, M.; Galli, G. *Phys. Rev. E* **1997,** *55,* 481–487. doi:10.1103/PhysRevE.55.481
79. Nagaraj, M.; Lehmann, A.; Prehm, M.; Tschierske, C.; Vij, J. K. *J. Mater. Chem.* **2011,** *21,* 17098–17103. doi:10.1039/c1jm13140k
80. Seed, A. *Chem. Soc. Rev.* **2007,** *36,* 2046–2069. doi:10.1039/B612666A
81. Tschierske, C.; Joachimi, D.; Zaschke, H.; Kresse, H.; Linström, B.; Pelzl, G.; Demus, D.; Bak, G. Y. *Mol. Cryst. Liq. Cryst.* **1990,** *191,* 231–236. doi:10.1080/00268949008038599
82. Tschierske, C.; Zaschke, H.; Kresse, H.; Mädicke, A.; Demus, D.; Girdziunaite, D.; Bak, G. Y. *Mol. Cryst. Liq. Cryst.* **1990,** *191,* 223–230. doi:10.1080/00268949008038598
83. Date, R. W.; Imrie, C. T.; Luckhurst, G. R.; Seddon, J. M. *Liq. Cryst.* **1992,** *12,* 203–238. doi:10.1080/02678299208030393
84. Kumar, T. A.; Le, K. V.; Kim, J. K.; Takezoe, H.; Dhara, S. *Liq. Cryst.* **2011,** *38,* 917–924. doi:10.1080/02678292.2011.585522

License and Terms

Beilstein Journal of Organic Chemistry

Synthesis of 2,6-disubstituted tetrahydroazulene derivatives

Zakir Hussain*[1,2], Henning Hopf[1], Khurshid Ayub[2] and S. Holger Eichhorn[3]

Full Research Paper

Open Access

Address:
[1]Institut für Organische Chemie, Technische Universität Braunschweig, Hagenring 30, D-38106 Braunschweig, Germany; Fax: +49 5313915388, [2]Department of Chemistry, COMSATS Institute of Information Technology (CIIT), University Road, Abbottabad 22060, KPK, Pakistan; Fax: +92 (992) 383441 and [3]Department of Chemistry and Biochemistry, University of Windsor, 401 Sunset Avenue, Essex Hall, Windsor, ON Canada N9B 3P4, Fax: +1 (519) 973-7064

Email:
Zakir Hussain* - chem63@yahoo.com

* Corresponding author

Keywords:
carbene addition; hydroazulenes; liquid crystals; ring expansion

Beilstein J. Org. Chem. **2012,** *8,* 693–698.
doi:10.3762/bjoc.8.77

Received: 16 December 2011
Accepted: 17 April 2012
Published: 04 May 2012

This article is part of the Thematic Series "Progress in liquid crystal chemistry II".

Guest Editor: S. Laschat

Abstract

Synthesis of hydroazulene derivatives has been carried out through a ring-enlargement route by using carbene adduct intermediates. The protocol can be applied for the construction of functionalized hydroazulene skeletons as key components of many natural products as well as the core system of novel liquid-crystalline materials.

Introduction

Hydroazulene skeletons provide the basic ring systems of natural products, such as guaianolide sesquiterpenes [1,2] and the so-called furanether B series [3,4]. The stereoselective synthesis of *trans*-hydroazulene derivatives by a tandem Michael/intramolecular Wittig approach was reported previously [5]. Recently, a new synthetic method for the construction of a hydroazulene skeleton by a [5 + 2]cycloaddition reaction was also developed [6]. Additionally, there have been many reports on the synthesis of 2,6-disubstituted azulenes [7,8]. In 1951, the ring expansion of indanes was reported for the synthesis of such systems, but it delivered only very low yields [9]. We recently employed [10,11] the method reported by Keehn et al. [12] using Birch reduced indanes for the synthesis of 2,6-disubstituted perhydroazulene systems as core elements of novel liquid-crystalline (LC) materials.

As far as mesogenic compounds are concerned, there is still a growing need for more new derivatives to be synthesised and tested for features desirable for novel displays, which include, but are not limited to, lower driving voltages, lower power consumption and faster response times. In contrast to the core system presently used in most nematic LC materials, our new

core based on perhydroazulenes showed [13], e.g., improved properties regarding phase-transition temperatures. Therefore, due to its potential use as a subsystem of many natural products, as well as as the core moiety for novel LC materials, further investigation on perhydroazulene-based substrates and synthetic intermediates is desirable.

Results and Discussion

The synthesis of various intermediates and the final hydroazulene derivatives **9** and **10** is described in this section. 2-Indancarboxylic acid (**1**) [14] was reduced under Birch conditions [15] to 4,7-dihydro-2-indancarboxylic acid (**2**) as the kinetically controlled product. In order to carry out carbene additions to the obtained 1,4-cyclohexadiene system, esterification [16] of **2** was carried out in a one-pot procedure in DMF at 40 °C with 1,1'-carbonyldiimidazole, *tert*-butyl alcohol and DBU to afford ester **3** in quantitative yield. The ester **3** was then subjected to carbene addition by treatment with ethyl diazoacetate in the presence of a copper catalyst [17] in THF under reflux. The carbene adduct **4** was obtained as the major product, as a colorless oil in acceptable yields (55–60%, Scheme 1). In addition to **4**, we were able to isolate the side product **5** in ca. 10% yield. The formation of carbene adduct **4** from 2-indancarboxylic acid (**1**) can also be followed from the previous work [18]. Evidently, in the formation of the adduct, the carbene attacks the central double bond of the substrate.

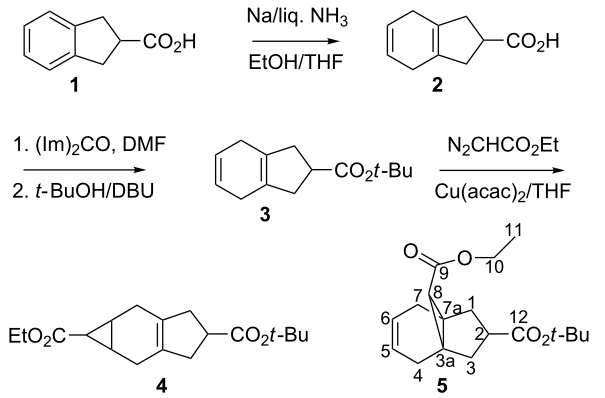

Scheme 1: Preparation of carbene adducts **4** [18] and **5**.

It is worth mentioning that in our earlier work on similar compounds [19], we isolated at least two isomers of **4** (with the methine hydrogen atom at the five-membered ring being present at either the α or β position). In our earlier work [10], carbene addition to similar compound(s) was found to give a mixture of stereoisomers. However, in the present case, we were only able to isolate **4** as a single stereoisomer. Furthermore, the procedure for the synthesis of compounds **4** and **5** is essentially the same as described previously for analogous compounds [10]. The complete characterization of intermediates **2** and **3** and carbene adduct **4** was carried out by NMR and related analytical techniques, similar to previous reports [18], while the 3D structure of **4** was further established based on the X-ray data of its derivative **6** [20].

It is important to note that the addition resulted in higher yields when the length of time used for the addition of the ethyl diazoacetate was extended, which was again similar to our earlier investigations [10]. The formation of only one major isomer (**4**) in this case could be due to the greater steric hindrance for carbene addition to the inner carbon–carbon double bond, in spite of the fact that the central olefinic double bond is more electron-rich and, hence, in principle more susceptible to such additions. In order to elucidate the configuration of **4**, ester cleavage with formic acid was carried out resulting in the acid **6** as a colorless solid, which was recrystallized from hexane and dichloromethane to afford single crystals suitable for X-ray analysis. The X-ray data [20] showed that the central, six-membered ring is almost planar but is slightly folded about the axis C(2)···C(6); the five-membered ring is essentially planar. The two larger rings are approximately coplanar, but the three- and six-membered rings form an interplanar angle of 78.4(1)°. The atoms of the ester side chain are coplanar and this plane forms a dihedral angle of 78.73(4)° with the central ring. In the crystal, the molecules form hydrogen-bonded dimers across inversion centers. Furthermore, a triplet in the ^{1}H NMR spectrum at δ = 1.54 ppm with a coupling constant of 4.2 Hz between the H-atoms at the cyclopropyl ring, indicates an *anti*-relation between the ethoxycarbonyl group and the cyclohexene ring.

The subsequent step comprised the ring opening of **4** to furnish the cycloheptatrienes **7** and **8**. The carbene adduct **4** was first treated with bromine leading to the formation of the corresponding dibromide, which was then followed by elimination with triethylamine to afford triethylamine hydrobromide alongside the formation of a norcaradiene intermediate in situ, which was transformed into the 2,6-disubstituted tetrahydroazulene **7** as a viscous oil. It is important to note that tetrahydroazulenes, in contrast to perhydroazulenes, are not very resistant towards dehydrogenation (oxidation) and, when kept at room temperature for a few days, form the corresponding azulenes (giving a bluish color).

Similar to our earlier investigations [10], various isomers could be formed through the rearrangement of double bonds in the seven-membered ring of **7**. However, through the NMR data of **7**, we saw the formation of an isomer with double bonds at the ring junction as a major isomer. Formation of one major isomer under the given conditions could be explained through the

hydrogen shifts of cycloheptatrienes by the so-called Berson–Willcott rearrangement [21]. We assume that bromination (Br_2) and dehydrobromination (Et_3N) of **4** resulted in the formation of an intermediate, which converted to **7** through thermal disrotatory electrocyclic ring opening and a base-catalyzed prototropic shift. The ester **7** underwent acid-catalyzed hydrolysis (formic acid) to afford **8** as a solid, which on recrystallization resulted in single crystals suitable for X-ray analysis (Scheme 2).

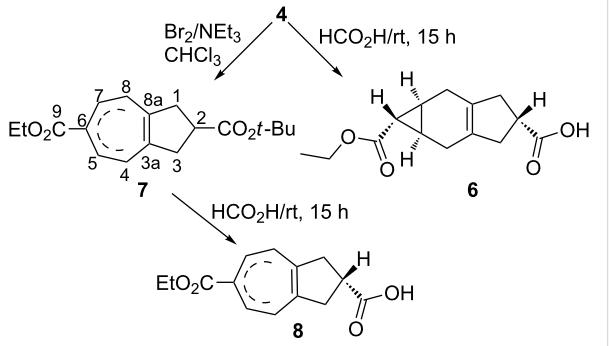

Scheme 2: Preparation of the cycloheptatrienes **7** and **8** [18,20].

The structural analysis of **8** revealed [22] an azulene framework that is partially hydrogenated to a cyclopentane subunit in places where molecules are slightly disordered in the lattice. These molecules represent the slightly torsionally distorted enantiomers of **8**. At this stage we did not find any hydrogen atom at position 6; however, additional H-atoms at C(4) and C(8), each with only 50% occupancy, were found. Acid **8** was further condensed [23] with *p*-cyanophenol in the presence of $SOCl_2$ and DMAP in dichloromethane to obtain the corresponding ester. The GC analysis of the product mixture indicated the presence of two isomers (ratio 3:1), which were later separated through reversed-phase HPLC (MeOH/H_2O 3:1) and characterized as derivatives **9** and **10** (Scheme 3).

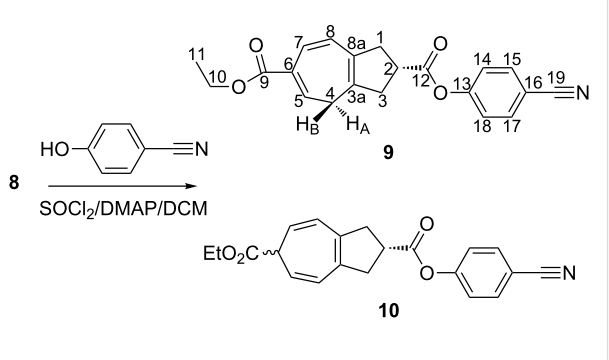

Scheme 3: Preparation of derivatives **9** and **10**.

The cycloheptatriene unit of **9** adopts, in sterically relaxed systems, a boat-like conformation, whereas its planar form represents the transition state of the thermal boat-inversion process. Additionally, since **8** and **9** possess a center of chirality at C(2), there are two different boat conformations of the cycloheptatriene unit possible, namely those in which C(4) is on the same or on the opposite side with respect to the substituent at C(2). The ^{1}H NMR spectrum (400 MHz, $CDCl_3$) of **9** displays diastereotopic (*syn* and *anti* to the ester group) H-atoms at C(4), indicating that the ring-inversion process is still slow at the temperature of the measurement, but the observed dd signals already show some line broadening.

Structure elucidation of compounds **9** and **10** was carried out by 1D and 2D NMR spectroscopy. Most ^{13}C-signals could be assigned through HMQC analysis. For quaternary carbons, analysis of HMBC data was sufficient to complete the assignment. In the ^{1}H NMR spectrum of compound **9**, the H-atom (H_A or H_α) at C(1) is located in the deshielding region of the carbonyl function and, hence, resonates slightly downfield (from its geminal H-atom, H_B) at δ = 2.94 ppm, together with the H-atoms at C(3), whereas H_B (H_β) itself resonates at δ = 2.92 ppm. Furthermore, the H-atom at C(2), being geminal to a strongly deshielding carboxylate group, gives a multiplet at δ = 3.49 ppm. Additionally, H-atoms at C(14) and C(18) show a doublet at δ = 7.22 ppm (J = 8.7 Hz), which is acceptable for such protons after considering the effect of cyano and carboxylate groups on the respective positions of the aromatic ring. The doublet at δ = 7.65 ppm (J = 8.7 Hz), integrated for two protons, was assigned to the H-atoms at C(15) and C(17). The most differentiated signals were identified for H-atoms at C(4) giving two distinct dd at δ = 2.50 ppm (J = 7.1, 13.4 Hz) and at δ = 2.65 ppm (J = 7.5, 13.5 Hz). These values seem very reasonable considering the envelope form of the seven-membered ring, in which C(4) extends out of the plane of the ring thereby allowing the remaining six carbon atoms to enhance the delocalization. This six-carbon system in turns generates a ring current similar to benzene, though less pronounced, allowing H_A to resonate in the deshielding region (δ = 2.65 ppm) and H_B in the shielding region (δ = 2.50 ppm). The H-atoms at positions C(5) and C(8) of the seven-membered ring (being almost in identical electronic environments), give a broad multiplet at δ = 6.52 ppm. However, a pronounced doublet at δ = 6.96 ppm (J = 11.2 Hz) is assigned for the hydrogen atom at position C(7) considering the effect of the nearby carboxylate group and several sp^2-hybridized carbon atoms in its immediate vicinity on both sides.

In the case of compound **10**, due to shifting of the double bonds, the single H-atom at C(4) becomes olefinic (conjugated) thereby resonating together with C(8); it displays a doublet at

δ = 5.47 ppm (J = 9.2 Hz). Similarly, the H-atoms at C(5) and C(7) give dd at δ = 6.22 ppm (J = 5.6, 9.1 Hz). The single proton at C(6) provides a triplet at δ = 2.73 ppm (J = 5.6 Hz). However, the exact stereochemistry at C(6) could not be established in the present case.

Finally, we investigated compounds **9** and **10** under a polarizing microscope for their textural features, and DSC experiments were carried out to determine the phase-transition temperatures. In the case of **9**, the first melting-point peak in the DSC never recovered, but a very broad transition at 5 °C was observed subsequently indicating the possibility of a very exothermic process on cooling to −40 °C. Furthermore, after the first melting the sample was an isotropic liquid down to 0 °C. The first melting showed complex behavior over a temperature range of 30 °C, and areas with Schlieren-like textures were present but were never recovered or reproduced. In the case of compound **10**, the same behavior was observed. As we mentioned earlier, tetrahydroazulenes, in contrast to perhydroazulenes, are not very resistant against dehydrogenation (oxidation), and when kept at room temperature for a few days, they form the corresponding azulenes. Such an unusual behavior of compounds **9** and **10** can easily be attributed to their oxidation. Additionally, our earlier investigations on similar compounds [10,13] showed that fully hydrogenated derivatives show pronounced mesogenic behavior.

Experimental

Thin-layer chromatography was performed by using precoated plastic plates, PolyGram Sil G/UV_{254}. Column chromatography was performed on silica gel 60 (70–230 mesh) from Merck (Darmstadt). HPLC analysis was carried out on a system consisting of Shimadzu (Duisburg, Germany), Gilson 305 pumps, a Shimadzu SPD-M10AV UV–vis detector, and a fraction collector. In the GC system, a Hewlett-Packard 6890 with a flame-ionization-detection (FID) system was used. All chromatograms were processed by ColaChrom software (Version 8.1) developed by MPI für Kohlenforschung, Mülheim, Germany. All organic solvents used in the study were HPLC grade and were purchased from Baker GmbH, Germany. The argon gas used was of high-purity grade. IR spectra were recorded using a Nicolet 320 FT-IR and a Bruker Tensor 27 spectrometer. Samples were prepared either as KBr pellets or as thin films. ^{1}H and ^{13}C NMR spectra were recorded on the following spectrometers: Bruker AC-200, ^{1}H NMR (200.1 MHz), ^{13}C NMR (50.3 MHz); Bruker DRX-400, ^{1}H NMR (400.1 MHz), ^{13}C NMR (100.6 MHz). Chemical shifts (δ) are expressed in parts per million (ppm) downfield from tetramethylsilane or by using the residual nondeuterated solvent as the internal standard ($CDCl_3$: ^{1}H, δ = 7.26 ppm; ^{13}C, δ = 77.00 ppm). Coupling constants are expressed in hertz. Mass spectra were recorded by using a Finnigan MAT 8430 spectrometer using the electron-ionization method (EI, 70 eV). Synthesis and analytical data of compounds **2**–**4** and **6** can be found in the literature [18].

Ethyl 2-*tert*-butoxycarbonyl-2,3,4,7-tetrahydro-1*H*-3a,7a-methanoinden-8-carboxylate (5): Compound **5** was obtained as a highly viscous, colorless oil in 10% yield during the synthesis of carbene adduct **4** as given in the literature [18]. R_f 0.41 (SiO_2; hexane/CH_2Cl_2 1:1); IR (film): 2900 (m, CH-stretch), 1695 and 1700 (s, C=O), 1340, 1250, 1133 (m) cm^{-1}; ^{1}H NMR (200.1 MHz, $CDCl_3$) δ 1.21 (t, ^3J = 7.1 Hz, H-C(11)), 1.31–1.40 (s, $C(CH_3)_3$), 1.55–1.68 (m, CH_2(1), CH_2(3)), 1.62 (br s, H-C(8)), 2.31 (br s, CH_2(4), CH_2(7)), 2.78–2.81 (m, H-C(2)), 4.08 (q, J = 7.1 Hz, CH_2(10)), 5.49 ppm (br s, H-C(5), H-C(6)); ^{13}C NMR (50.3 MHz, $CDCl_3$) δ 14.1 (q, C(11)), 27.80 (q, $C(CH_3)_3$), 29.41 (d, C(8)), 31.23 (t, C(4), C(7)), 34.31 (s, C(3a), C(7a)), 38.23 (d, C(2)), 42.68 (d, C(1), C(3)), 61.01 (t, C(10)), 80.12 (s, $C(CH_3)_3$), 125.60 (d, C(5), C(6)), 171.84, 172.01 (s, C(9), C(12)); EIMS m/z: 306 (8, M^+), 249 (57, $[M - C_4H_9]^+$), 205 (80, $[M - C_5H_9O_2]^+$), 132 (100, $[205 - C_3H_5O_2]^+$); HRMS (m/z): $[M]^+$ calcd for $C_{18}H_{26}O_4$, 306.183109; found, 306.183123 + 1.1 ppm.

6-Ethyl-tetrahydroazulene-2-carboxylate (8): To a stirred solution of **4** (3.06 g, 0.01 mol) in $CHCl_3$ (100 mL), a solution of Br_2 (0.6 mL, 0.01 mol) in $CHCl_3$ (5 mL) was added dropwise at 0 °C. When the addition was complete, triethylamine (6.91 mL, 49.71 mmol) was added. Triethylamine hydrobromide began to form immediately. The mixture was heated under reflux for 18 h. After cooling, the hydrobromide was filtered off. The filtrate was evaporated and the resulting oil partitioned between benzene and dilute aqueous acid (HCl). The benzene layer was washed with water, dried with $MgSO_4$ and filtered, and the solvent was removed. The reaction mixture was filtered through a small column of silica gel, eluting with pentane and dichloromethane (1:2). After evaporation of the solvent the crude product **7** was obtained as a viscous bluish oil (2.6 g, 85%). The preparation of compound **7** is analogous to that described in [10]. The crude intermediate **7** was not purified further and was subjected to hydrolysis directly: A solution of **7** (1.0 g, 3.29 mmol) in formic acid (100 mL) was stirred at rt for 15 h. The solvent was removed under reduced pressure and the crude product was recrystallized from hexane and dichloromethane to give 0.71 g (85%) of **8** as slightly bluish needles. R_f 0.35 (SiO_2; EtOAc/CH_2Cl_2 1:5); IR (film): 2913 (m, CH, stretch.), 1712, 1718 (s, C=O), 1320, 1150 (m) cm^{-1}; ^{1}H NMR (200.1 MHz, $CDCl_3$) δ 1.29 (t, ^3J = 7.1 Hz, CH_3(12)), 2.80–3.27 (m, CH_2(1), CH_2(3), H-C(2)), 4.18 (q, J = 7.1 Hz, CH_2(11)), 2.60–2.75/5.48–6.69 ppm (2 × m, 5 H, seven-membered ring-H); ^{13}C NMR (50.3 MHz, $CDCl_3$) δ 14.21 (q,

C(12)), 27.50 (t), 37.53 (t), 39.39 (t), 41.97 (d), 60.79 (d, C(11)), 117.87 (d), 124.60 (d), 126.61 (d), 130.61 (d), 133.99 (s), 132.70 (s), 166.81, 181.41 ppm (s, C(9), C(10)); EIMS *m*/*z*: 248 (19, M^+), 219 (59, $[M - C_2H_5]^+$), 203 (18, $[M - C_2H_5O]^+$), 175 (72, $[M - C_3H_5O_2]^+$), 129 (100, $[175 - HCO_2H]^+$); HRMS (*m*/*z*): $[M]^+$ calcd for $C_{14}H_{16}O_4$, 248.104859; found, 248.104835 + 0.96 ppm.

1,2,3,4-Tetrahydroazulene-2,6-dicarboxylic acid 2-(4-cyanophenyl) ester 6-ethyl ester (9): Thionyl chloride (0.021 mL, 0.28 mmol) was added to a solution of 4-(*N*,*N*-dimethylamino)pyridine (34 mg, 0.27 mmol) in dichloromethane (5 mL) at −20 °C. Acid **8** (70 mg, 0.28 mmol) was added and the resulting solution was stirred for 1 h. Then, 4-(*N*,*N*-dimethylamino)pyridine (34 mg, 0.27 mmol) and the *p*-cyanophenol (31 mg, 0.30 mmol) in dichloromethane were added and the stirring was continued for another 1 h. The mixture was washed with water (5 mL), and the organic layer was separated and dried with sodium sulfate to give a crude mixture of **9** and **10** (75 mg, 72%). The product mixture was filtered through a small column of silica gel, eluting with pentane and dichloromethane (1:2), to remove impurities, and was further separated through reversed-phase HPLC. The analytical HPLC indicated the presence of both isomers **9** and **10** in a 3:1 ratio. For preparative HPLC, the sample was dissolved in MeOH/CH_2Cl_2, and MeOH/H_2O 75:25 (v/v) was used as a mobile phase. Compound **9** was isolated in 97% purity (t_R 4.40 min), while **10** was obtained in 94% purity (t_R 4.98). R_f 0.32 (SiO_2; hexane/CH_2Cl_2 1:1); mp 83–84 °C; IR (film): 2931 (m CH, stretch), 1705 and 1714s (C=O), 1311, 1230, 1122 (m) cm^{-1}; ^{1}H NMR (400.1 MHz, $CDCl_3$) δ 1.29 (t, ^3J = 7.1 Hz, CH_3(11)), 2.50 (dd, *J* = 7.1, 13.4 Hz, H_β(4)), 2.65 (dd, *J* = 7.5, 13.5 Hz, H_α(4)), 2.92 (m, CH_2(3), H_β(1)), 2.94 (dd, *J* = 6.8, 17.4 Hz, H_α(1)), 3.49 (m, H-C(2)), 4.21 (q, *J* = 7.1 Hz, CH_2(10)), 6.52 (br. m, H-C(5), H-C(8)), 6.96 (d, *J* = 11.2 Hz, H-C(7)), 7.22 (d, *J* = 8.7 Hz, H-C(14), H-C(18)), 7.65 ppm (d, *J* = 8.7 Hz, H-C(15), H-C(17)); ^{13}C NMR (100.6 MHz, $CDCl_3$) δ 14.01 (q, C(11)), 27.26 (t, C(4)), 37.43 (t, C(3)), 39.63 (t, C(1)), 42.01 (d, C(5)), 60.63 (t, C(10)), 109.49 (s, C(19)), 117.94 (s, C(16)), 122.39 (d, C(2)), 126.74 (d, C(8)), 128.50 (2 × d, C(15), (17)), 130.47 (d, C(7)), 130.81 (s, C(3a), 132.27 (s, C(8a)), 133.50 (2 × d, C(14), C(18)), 133.61 (s, C(6)), 153.83 (s, C(13)), 166.52 (s, C(9)), 172.76 ppm (s, C(12)); EIMS *m*/*z*: 349 (27, $[M^+]$), 320 (100, $[M - C_2H_5]^+$), 304 (17, $[M - C_2H_5O]^+$), 276 (18, $[M - C_3H_5O_2]^+$), 203 (56, $[M - C_8H_4O_2N]^+$); HRMS (*m*/*z*): $[M + Na]^+$ calcd for $C_{21}H_{19}NO_4Na$, 372.120362; found, 372.120629 + 0.72 ppm.

1,2,3,6-Tetrahydroazulene-2,6-dicarboxylic acid 2-(4-cyanophenyl) ester 6-ethyl ester (10): R_f 0.29 (SiO_2; hexane/CH_2Cl_2 1:1); mp 80–82 °C; IR (film): 2927 (m, CH-stretch), 1703, 1712 (s, C=O), 1342, 1223, 1165 (m) cm^{-1}; ^{1}H NMR (400.1 MHz, $CDCl_3$) δ 1.29 (t, ^3J = 7.1 Hz, CH_3(11)), 2.73 (t, *J* = 5.6 Hz, H-C(6)), 3.16 (m, CH_2(1), CH_2(3)), 3.42 (m, H-C(2)), 4.25 (q, *J* = 7.1 Hz, CH_2(10)), 5.47 (d, *J* = 9.2 Hz, H-C(4), H-C(8)), 6.22 (dd, *J* = 5.6, 9.1 Hz, H-C(5), H-C(7)), 7.23 (d, *J* = 8.8 Hz, H-C(15), H-C(17)), 7.69 (d, *J* = 8.8 Hz, H-C(14), H-C(18)); ^{13}C NMR (100.6 MHz, $CDCl_3$) δ 14.0 (q, C(11)), 39.24 (t, C(1), C(3)), 40.95 (d, C(6)), 45.0 (d, C(2)), 60.9 (t, C(10)), 109.56 (s, C(19)), 117.94 (s, C(16)), 118.08 (2 × d, C(5), C(7)), 122.39 (2 × d, C(4), C(8)), 124.28 (2 × d, C(15), C(17)), 133.45 (2 × d, C(14), C(18)), 139.44 (2 × s, C(3a), C(8a)), 153.83 (s, C(13)), 172.50 (s, C(9)), 172.80 ppm (s, C(12)); EIMS 349 (26, $[M^+]$), 320 (100, $[M - C_2H_5]^+$), 304 (16, $[M - C_2H_5O]^+$), 276 (16, $[M - C_3H_5O_2]^+$), 203 (57, $[M - C_8H_4O_2N]^+$); HRMS (*m*/*z*): $[M + Na]^+$ calcd for $C_{21}H_{19}NO_4Na$, 372.120362; found, 372.120630 + 1.05 ppm.

Supporting Information

Supporting Information File 1

DSC-data of isomers **9** and **10**.
[http://www.beilstein-journals.org/bjoc/content/supplementary/1860-5397-8-77-S1.pdf]

Acknowledgements

Z. H. thanks Prof. Dr. Wolfgang Gärtner at the Max-Planck Institute for Bioinorganic Chemistry, Mülheim (Germany) for his support in purification and characterization all new substances in the present study.

References

1. Mehta, G.; Thomas, A. *Synth. Commun.* **1992,** *22,* 1831–1838.
2. Christie, J. J.; Varkey, T. E.; Whittle, J. A. *J. Org. Chem.* **1981,** *46,* 3590–3592. doi:10.1021/jo00331a002
3. Battaglia, R.; De Bernardi, M.; Fronza, G.; Mellerio, G.; Vidari, G.; Vita-Finsi, P. *J. Nat. Prod.* **1980,** *43,* 319–328. doi:10.1021/np50009a002
4. Price, M. E.; Schore, N. E. *J. Org. Chem.* **1989,** *54,* 5662–5667. doi:10.1021/jo00285a010
5. Fujimoto, T.; Uchiyama, Y.-k.; Kodama, Y.-i.; Ohta, K.; Yamamoto, I.; Kakehi, A. *J. Org. Chem.* **1993,** *58,* 7322–7323. doi:10.1021/jo00078a004
6. Mitachi, K.; Yamamoto, T.; Kondo, F.; Shimizu, T.; Miyashita, M.; Tanino, K. *Chem. Lett.* **2010,** *39,* 630–632. doi:10.1246/cl.2010.630
7. Ginsburg, D. *Non-Benzenoid Aromatic Compounds;* Interscience: New York, 1959.
8. Lloyd, D. *The Chemistry of Conjugated Cyclic Compounds;* Wiley: Chichester, 1989.
9. Plattner, P. A.; Fürst, A.; Müller, A.; Somerville, A. R. *Helv. Chim. Acta* **1951,** *34,* 971–988. doi:10.1002/hlca.19510340332
10. Hussain, Z.; Hopf, H.; Pohl, L.; Oeser, T.; Fischer, A. K.; Jones, P. G. *Eur. J. Org. Chem.* **2006,** 5555–5569. doi:10.1002/ejoc.200500733

11. Hussain, Z.; Hopf, H.; Eichhorn, H. S. *Beilstein J. Org. Chem.* **2012,** *8,* 403–410. doi:10.3762/bjoc.8.44
12. Luhowy, R.; Keehn, P. M. *J. Am. Chem. Soc.* **1977,** *99,* 3797–3805. doi:10.1021/ja00453a046
13. Hopf, H.; Hussain, Z.; Menon, R. S.; Raev, V.; Jones, P. G.; Pohl, L. M. *Synlett* **2011,** 1273–1276. doi:10.1055/s-0030-1260551
14. Carlson, G. L. B.; Quina, F. H.; Zarnegar, B. M.; Whitten, D. G. *J. Am. Chem. Soc.* **1975,** *97,* 347–354. doi:10.1021/ja00835a021
15. Sundeen, J. E.; Reid, J. A.; Osband, J. A.; Hauck, F. P. *J. Med. Chem.* **1977,** *20,* 1478–1485. doi:10.1021/jm00221a023
16. Ohta, S.; Shimabayashi, A.; Aono, M.; Okamoto, M. *Synthesis* **1982,** 833–834. doi:10.1055/s-1982-29961
17. Marchand, A. P.; Brockway, N. M. *Chem. Rev.* **1974,** *74,* 431–469. doi:10.1021/cr60290a002
18. Zindel, J.; Maitra, S.; Lightner, D. A. *Synthesis* **1996,** 1217–1222. doi:10.1055/s-1996-4370
19. Hussain, Z.; Koley, D.; Hopf, H. *Helv. Chim. Acta* **2005,** *88,* 3263–3272. doi:10.1002/hlca.200590262
20. Jones, P. G.; Hopf, H.; Hussain, Z. *Acta Crystallogr.* **2005,** *E61,* o3034–o3035. doi:10.1107/S1600536805026565
21. Berson, J. A.; Willcott, M. R., III. *J. Am. Chem. Soc.* **1966,** *88,* 2494–2502. doi:10.1021/ja00963a025
22. Hussain, Z.; Oeser, T.; Hopf, H. *Acta Crystallogr.* **2005,** *C61,* o652–o653. doi:10.1107/S0108270105029744
23. Arrieta, A.; Garcia, T.; Palomo, C. *Synth. Commun.* **1982,** *12,* 1139–1146. doi:10.1080/00397918208065981

License and Terms

Beilstein Journal of Organic Chemistry

Formation of smectic phases in binary liquid crystal mixtures with a huge length ratio

Nadia Kapernaum*[1], Friederike Knecht[1], C. Scott Hartley[2], Jeffrey C. Roberts[2], Robert P. Lemieux[2] and Frank Giesselmann[1]

Full Research Paper

Open Access

Address:
[1]Institut für Physikalische Chemie, Universität Stuttgart, D-70569 Stuttgart, Germany and [2]Department of Chemistry, Queen's University, Kingston, Ontario, Canada

Email:
Nadia Kapernaum* - n.kapernaum@ipc.uni-stuttgart.de

* Corresponding author

Keywords:
bidispersity; liquid crystals; phase diagrams; smectic phases; smectic F phase; structure and dynamics

Beilstein J. Org. Chem. **2012,** *8,* 1118–1125.
doi:10.3762/bjoc.8.124

Received: 05 April 2012
Accepted: 28 June 2012
Published: 19 July 2012

This article is part of the Thematic Series "Progress in liquid crystal chemistry II".

Guest Editor: S. Laschat

Abstract

A system of two liquid-crystalline phenylpyrimidines differing strongly in molecular length was studied. The phase diagram of these two chemically similar mesogens, with a length ratio of 2, was investigated, and detailed X-ray diffraction and electrooptical measurements were performed. The phase diagram revealed a destabilization of the nematic phase, which is present in the pure short compound, while the smectic state was stabilized. The short compound forms smectic A and smectic C phases, whereas the longer compound forms a broad smectic C phase and a narrow higher-ordered smectic phase. Nevertheless, in the mixtures, the smectic C phase is destabilized and disappears rapidly, whereas smectic A is the only stable phase observed over a broad concentration range. In addition, the smectic translational order parameters as well as the tilt angles of the mixtures are reduced. The higher-ordered smectic phase of the longer mesogen was identified as a smectic F phase.

Introduction

The mixing of different liquid crystals is a common technique to tailor their properties for specific applications. In particular, the mixing of two mesogens that are quite different from each other can strongly change the properties and the phase behavior of the mixtures compared to the pure compounds. We recently reported a systematic study of mixtures of mesogens differing in molecular length [1,2]. In these studies, chemically similar mesogens with length ratios ranging from 1 to 1.8 were investigated. In the systems with a large difference in length, strong changes in the phase diagram were observed. The nematic phase was destabilized while the smectic state was stabilized. The temperature range of the SmC phase, which was the dominant phase in most of the pure compounds, was reduced while the SmA phase became broader. In the systems with a length

ratio of 1.8, the smectic A phase was the only stable mesophase over a broad temperature and concentration range. Furthermore, a decrease of the tilt angle θ of the SmC phase, as well as a reduced smectic order parameter Σ in the SmA phase, were observed for these systems. We showed that the ordering of the bidisperse molecules in a SmA phase can be explained by extensive out-of-layer fluctuations (Figure 1) [1,2]. In a SmA phase of strongly bidisperse molecules, energetically unfavorable free volume remains between the layers in the absence of these fluctuations; this free volume is minimized in the "out-of-layer fluctuations" model by thermal translational fluctuations of the molecules along the layer normal. This model fits very well with the experimental data and reflects the molecular ordering in the smectic phases of bidisperse molecules best.

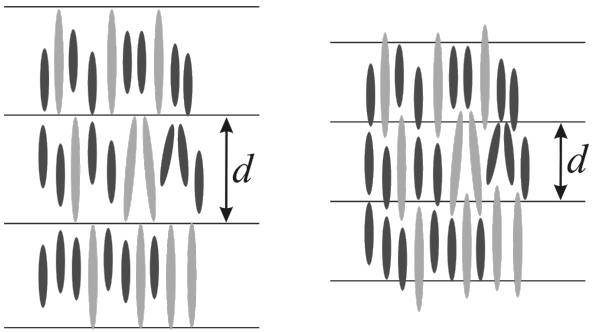

Figure 1: Smectic A phase of a mixture of two mesogens differing strongly in molecular length. Left: The layer spacing corresponds to the length of the long mesogen; no out-of-layer fluctuations occur. This leads to a lot of unfavorable free volume. Right: By reducing the smectic translational order the molecules are now densely packed. This leads to extensive out-of-layer fluctuations. Reproduced after [1].

The preference for the SmA over the SmC phase, which was observed for all systems with a large length ratio, may also be explained by extensive out-of-layer fluctuations [2]. The molecules in a nontilted SmA phase can easily propagate into the next layer, which is favorable for structures of bidisperse molecules in which such out-of-layer fluctuations are essential to fill the free volume between the molecules of quite different size. In the tilted SmC phase, the core of the molecules is more tilted than the alkyl chains, which leads to a zig-zag shape of the molecules [3]. Due to this zig-zag shape, the molecules are "locked" in their layers and the free volume between them is no longer compensated. This costs a lot of free energy, which destabilizes the SmC phase in these bidisperse systems. For more detailed information see [2]. In our earlier studies [1,2] we were able to show the influence of strongly differing molecular lengths up to a length ratio of 1.8. The effect of an even larger length difference has not been studied yet, and it is unclear whether a larger length difference might lead to demixing. Therefore a system of two chemically similar phenylpyrimidines with a length ratio of 2 was investigated in this study, to clarify whether the effects of a length difference of 1.8 can be enhanced by a bigger length difference. We report herein that this system shows similar effects as the system with a length ratio of 1.8, but also the first signs of reduced miscibility. The long compound used in this study, **PhP16** (see below in Scheme 1 and Figure 2), exhibits a heretofore unidentified higher-ordered smectic phase [4], which we have identified by detailed investigations reported herein as a smectic F (SmF) phase.

Results and Discussion

The liquid-crystalline materials used herein are shown in Scheme 1 and Figure 2. The component with long molecular length is the symmetric compound 2-(4-hexadecyloxyphenyl)-5-hexadecyloxypyrimidine (**PhP16**) [4]. It forms a broad SmC phase and a narrow higher-ordered smectic phase. Its molecular length was determined by molecular modelling as 50.6 Å. The component with short molecular length is the asymmetric compound 2-(4-butoxyphenyl)-5-octyloxypyrimidine (**2PhP**) [4]. It exhibits the typical liquid-crystalline phase sequence of nematic, smectic A and smectic C phases. Its molecular length is 25.6 Å, according to molecular modelling, which results in a **PhP16**/**2PhP** length ratio of almost 2.

First, the phase diagram of the system **PhP16**/**2PhP** was determined (Figure 3). This phase diagram is very similar to those reported in our earlier studies, with a length ratio of 1.8 [1,2]. Again, no destabilization of the smectic state was observed, and a eutectic point at approximately x_{16} = 0.015 was observed. However, the nematic phase disappears rapidly with increasing

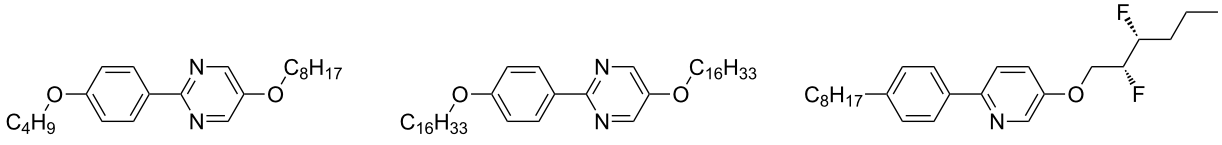

2PhP
Cr 59.4 SmC 87.6 SmA 96.8 N 98.6 I

PhP16
Cr 82 SmF 83 SmC 100 I

MDW510
Cr 85 I

Scheme 1: Chemical structures and phase-transition temperatures of the mesogens **2PhP** and **PhP16** and of the chiral dopant **MDW510**.

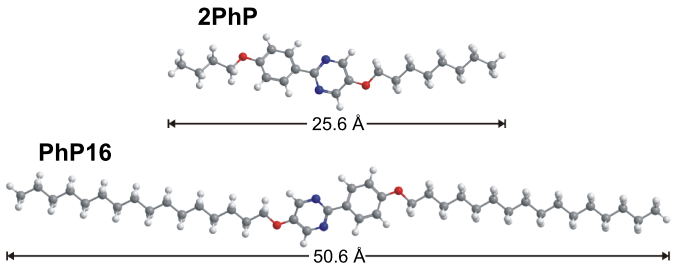

Figure 2: Molecular structures and molecular lengths of **2PhP** and **PhP16.** The longer mesogen **PhP16** is approximately twice the length of the shorter mesogen **2PhP**. The energy of each molecular structure was minimized by molecular modelling with the semiempirical method MOPAC/AM1 for the most extended conformers.

mole fraction x_{16} after a slight stabilization until $x_{16} = 0.1$, and it disappears at $x_{16} = 0.4$. In the smectic state, the SmA phase is much more stable than SmC. Although SmC is the dominant phase in both pure compounds, the SmC phase disappears after the addition of only 5 mol % of the long compound **PhP16**. On the other side of the phase diagram, the SmC phase is stable until a mole fraction of $x_{16} = 0.6$ is reached. Over a broad range of temperatures and concentrations, SmA is the dominant phase in the diagram.

Small-angle X-ray scattering (SAXS) measurements were performed for all mixtures. As shown in Figure 4, the layer spacing d measured at $T = T_c$ varies linearly with the mole fraction x_{16}. This linear dependence suggests that the Diele additivity rule [5] can be applied for the mixtures of **2PhP** and **PhP16**. The Diele additivity rule states that the layer spacing of a mixture depends linearly on the layer spacings of the pure compounds and the mole fraction. According to Diele, the layer spacing d of a mixture of two pure compounds A and B can be calculated as $d = d_A \cdot x_A + d_B \cdot x_B$. With this linearity of the smectic layer spacing, a value for the hypothetical SmA phase of pure **PhP16** is extrapolated to a value of $d = 50.2$ Å, which is in good agreement with the value of 50.6 Å calculated by using MOPAC/AM1 (Figure 2). For the short compound **2PhP**, there is also a good agreement between the calculated value of 25.6 Å for the extended length of the molecule and the experimentally determined d-value of 25.1 Å from SAXS.

Figure 5 shows the reduced layer spacings d/d_A (where d_A is the layer spacing of a hypothetical SmA phase in the temperature range of the SmC phase, calculated by extrapolation of the temperature-dependent layer spacing of the SmA phase) versus $T-T_c$ of the pure compound **2PhP** as well as for the mixtures with $x_{16} = 0.05$ and 0.7. Compound **2PhP** shows a substantial maximum layer shrinkage of 9.5%, whereas the mixture with $x_{16} = 0.05$ shows a narrow SmC phase and a maximum layer shrinkage of only 2% at $T-T_c = -5$ K, which is similar to the layer shrinkage of **2PhP** at the same reduced temperature. The mixture with $x_{16} = 0.7$ shows only a small maximum layer shrinkage of 1% at $T-T_c = -8$ K.

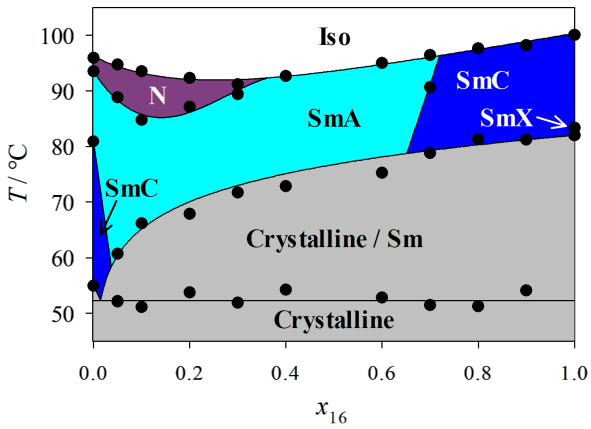

Figure 3: The phase diagram of the binary mixture system **PhP16**/**2PhP**.

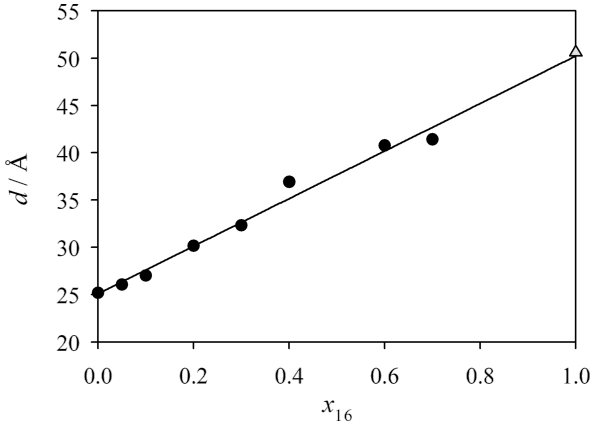

Figure 4: The layer spacing obtained by SAXS-measurements in the SmA phase at $T = T_c$ is plotted against the mole fraction x_{16} (closed circles) as well as the molecular length for pure **PhP16** calculated by molecular modelling (grey triangle).

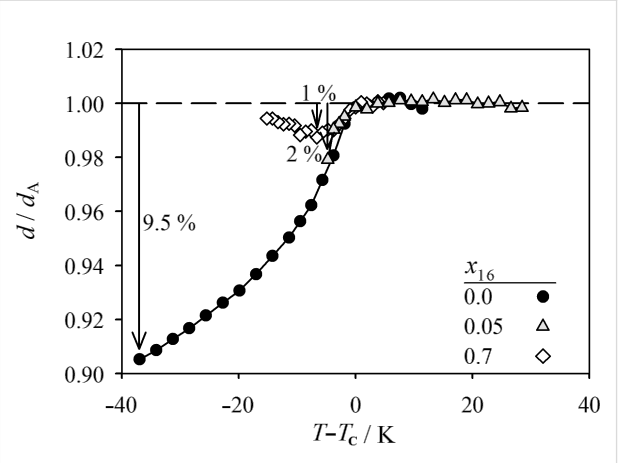

Figure 5: Reduced layer spacing d/d_A versus temperature difference to the phase-transition temperature $T-T_c$ for pure **2PhP** (closed circles) and the two mixtures that show SmA and SmC phases with x_{16} = 0.05 (grey triangles) and 0.7 (open squares).

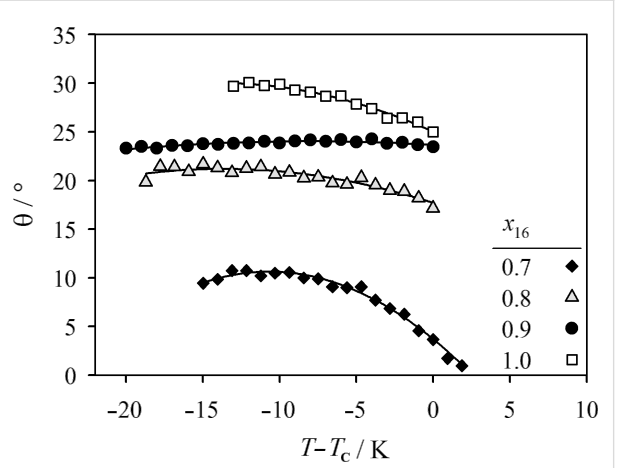

Figure 6: The tilt angle θ is plotted against the temperature difference to the phase-transition temperature $T-T_c$ for the mixtures with x_{16} = 0.7 (filled diamonds), 0.8 (grey triangles), 0.9 (filled circles) and the pure compound **PhP16** (open squares).

Figure 6 shows the optical tilt angles of the mixtures, which were determined in the ferroelectric SmC* phase [6,7] to gain a better understanding of the unusual behavior of the layer spacing. To obtain a chiral SmC* phase, 4 mol % of the chiral dopant (*R,R*)-2-(4-octylphenyl)-5-(2,3-difluorohexyloxy)pyridine (**MDW510**, Scheme 1) [8,9] was added. Optical tilt angles were measured for the mixtures with x_{16} = 1.0, 0.9, 0.8 and 0.7; the largest tilt angles were observed for the pure compound **PhP16**. The progressive addition of the short compound caused a reduction of the tilt angle from a value of ca. 25° for x_{16} = 0.9 to ca. 10° for x_{16} = 0.7. Further addition of the short compound caused the tilt angle to vanish completely, which corresponds to a concentration-induced phase transition from the SmC to the SmA phase. Optical tilt angles are compared with the tilt angles calculated from the X-ray layer shrinkage by using the expression $\theta = \cos^{-1}(d_C/d_A)$, and are in good agreement. This shows that the small layer shrinkage observed in the mixtures correlates to the small tilt angles, and that the mixtures do not exhibit so-called "de Vries-type" behavior [10].

The translational order parameter Σ [11,12] was measured in the SmA phase to give a measure of the degree of molecular ordering in the layers. Σ is defined as the amplitude of the density wave that originates from the 1-D periodic smectic layers [13]. In Figure 7, the smectic order parameters Σ for the pure compound **2PhP** and the mixtures with x_{16} = 0.05, 0.1, 0.2 and 0.4 are shown. The highest smectic order parameters were found for the pure compound **2PhP** in the range of 0.9. The addition of a small amount of **PhP16** reduced the smectic order to values around 0.85. Adding more **PhP16** caused further reduction in Σ to values around 0.8 for the x_{16} = 0.1 and 0.2 mixtures. Smectic order was partially recovered upon adding more **PhP16** to a mole fraction x_{16} = 0.4. The smectic order thus considerably reduced upon the loss of the SmC phase in the phase diagram, and was partially recovered upon re-entry of the SmC phase into the phase diagram.

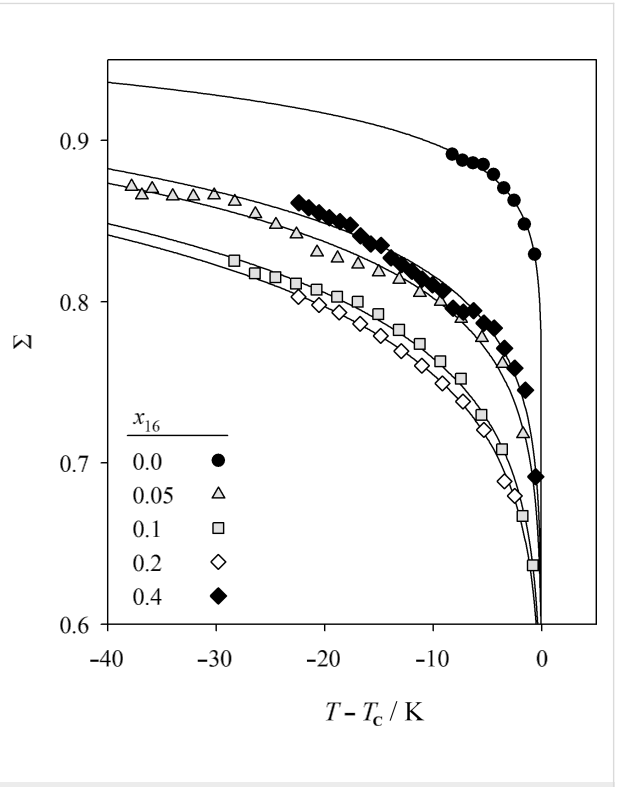

Figure 7: Translational order parameter Σ in the SmA phase versus temperature difference to the phase-transition temperature $T-T_c$ for the mixtures with x_{16} = 0.4 (filled diamonds), 0.2 (open diamonds), 0.1 (grey squares) and 0.05 (grey triangles) and for the pure compound **2PhP** (filled circles).

Besides a SmC phase, the pure material **PhP16** also forms a heretofore unidentified higher-ordered smectic phase [4]. After performing a detailed investigation of this material, we determined that this higher-ordered smectic phase in **PhP16** is a smectic F (SmF) phase, which is a tilted version of the hexatic smectic B phase. In the SmF phase, the tilt direction of the molecules is towards a face of the quasihexagonal net, i.e., halfway between nearest neighbors [14].

The textures of the higher-ordered SmF phase were investigated by polarizing microscopy. Micrographs of the textures of the SmC and SmF phase of **PhP16** are shown in Figure 8 for samples with partial planar (Figure 8a) and partial homeotropic alignments (Figure 8b). The planar aligned SmC phase shows a fan-shaped texture; after cooling of the sample to the SmF phase, a slight change of colors was observed, which indicates a slight increase in birefringence, and the fans show circular stripes. The homeotropic regions shown in Figure 8b exhibit a Schlieren texture characteristic of the SmC phase. In the SmF phase, a mosaic texture is observed. This homeotropic mosaic texture is a clear indication that the higher-ordered smectic phase is a tilted phase, since the homeotropic regions would be completely black for a nontilted phase. This homeotropic mosaic texture together with the planar circularly striped fan texture is typically found for the soft-crystalline G phases as well as for SmF phases [15]. The texture observations suggest that the higher-ordered smectic phase must be a tilted phase. A demonstration that the sample is shearable ruled out soft-crystalline phases (E, G, H, J and K), leaving only the two fluid, higher-ordered, hexatic smectic phases SmF and SmI as possibilities.

To distinguish between these two hexatic smectic phases, wide-angle X-ray scattering (WAXS) was performed in the higher-ordered smectic phase of **PhP16**. We were able to investigate the sample in three different configurations: (i) as an unoriented sample, (ii) with the smectic layer normal *k* oriented parallel to the incident X-ray beam, and (iii) with the smectic layer normal mainly oriented perpendicular to the X-ray beam. Figure 9 shows the integrated intensity profile of an unoriented sample of the SmF phase of **PhP16** at 82.5 °C, which shows three peaks. The (001)-layer peak occurs at a scattering angle $2\theta = 1.77°$, which gives a layer spacing *d* of 49.6 Å. This value differs from the value obtained from the SAXS measurements (see below in Figure 12a), which is due to the fact that the WAXS measurements are not very precise in the SAXS regime. Two distinct wide-angle peaks are observed at $2\theta = 18.4$ and 20.5°, which clearly indicate that the unidentified phase is a fluid hexatic phase, as the less-ordered smectic phases such as SmA and SmC would show a diffuse halo, and the more ordered 2-D soft-crystalline phases such as G and E would

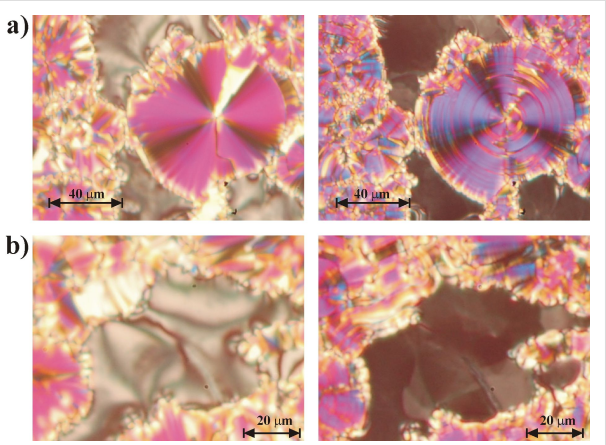

Figure 8: Textures of the pure compound **PhP16** on cooling. Left: SmC phase at 96.8 °C Right: same positions in the SmF phase at 82.7 °C. (a) In the upper part a fan-shaped texture is shown, while (b) in the lower part a homeotropic texture can be seen.

show more peaks. In the case of the SmF phase, the two peaks observed are the (200) and the (110) peaks. As the SmF phase is a tilted hexatic phase, it can be described by a centred monoclinic unit cell, with the three axes *a*, *b* and *c* and the angle $\beta \neq 90°$ [14]. The *c*-axis, which describes the height of the unit cell, is tilted at the angle $\beta = (90° + \text{tilt angle})$, with respect to the plane spanned by the *a*- and *b*-axes [14]. The unit cell parameters of the 2-D hexatic lattice can now be calculated from the (001), (200) and (110) peaks. The received parameters are $a = 10.84$ Å, $b = 4.86$ Å, $c = 56.21$ Å and $\beta = 128°$.

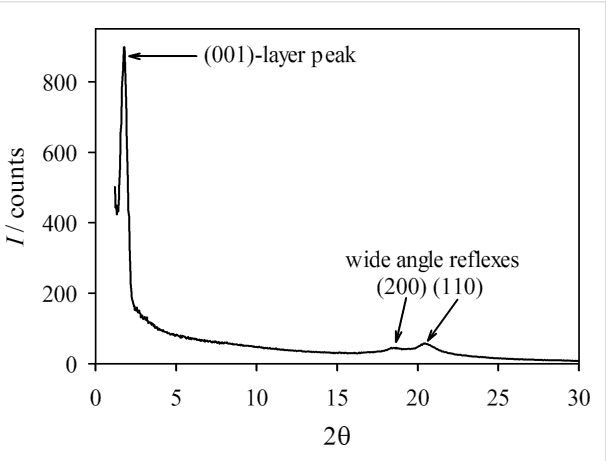

Figure 9: Integrated intensity profile of an unoriented sample of **PhP16** at *T* = 82.5 °C in the SmF phase.

WAXS measurements on a sample with the smectic-layer normal **k** oriented parallel to the X-ray beam were then performed. Figure 10 shows the 2-D diffractogram of the oriented SmF phase at *T* = 82 °C as well as the azimuthal distribution of the integrated intensity of the two wide-angle peaks.

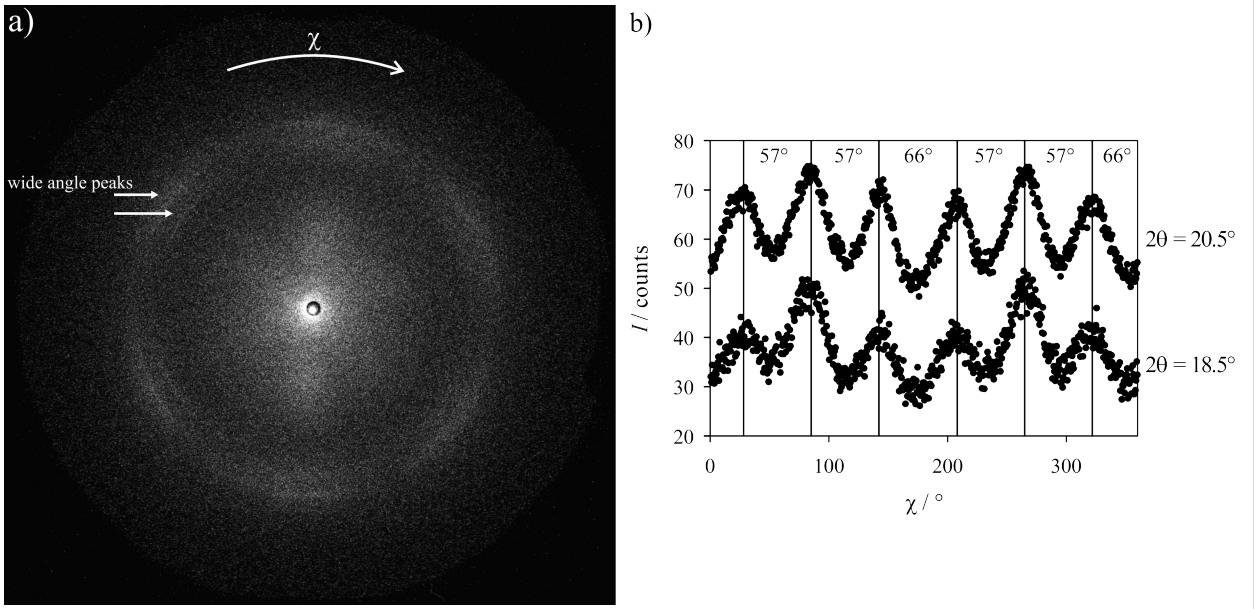

Figure 10: (a) WAXS-measurement of the SmF phase of **PhP16** at T = 82 °C with the smectic-layer normal **k** oriented parallel to the incident beam. Two wide-angle peaks can be observed, but no layer peak. (b) Integration of the two WAXS peaks in dependence of the azimuthal angle χ.

In the 2-D diffractogram (Figure 10a), no layer peak could be observed as the layer normal was oriented parallel to the beam. Again the two wide-angle peaks, which could also be seen in the unoriented sample at 2θ = 18.5 and 20.5°, are observed. They show a pseudohexagonal intensity distribution on dependence of the azimuthal angle χ. The behavior of their intensity versus the angle χ can be seen in Figure 10b. The two wide-angle peaks show six maxima separated from each other by two different angles (57 and 66°), which reflects the pseudohexagonal structure of a SmF or SmI phase.

In the 2-D diffractogram of the SmF phase of **PhP16** shown in Figure 11a, the smectic layer normal is mostly oriented perpendicular to the incident X-ray beam. In this geometry the (001) layer peak at 2θ = 1.82° as well as the (110) peak at 2θ = 20.4° were observed. We did not observe the second (200) peak, which was observed in Figure 9 at 2θ = 18.5°. This could be due to the fact that the (200) peak was less intense than the (110) peak at 2θ = 20.5° and that a different X-ray setup was used for the measurement in Figure 11a. Therefore, it may be due to the other setup that we could not detect the second, less-intense wide-angle peak. The sample used for the measurement in Figure 11a was very well oriented, as can be seen from the two sharp (001) layer peaks in the small-angle regime. The diffraction pattern in Figure 11a allows us to distinguish between SmF and SmI. Their diffraction patterns are presented schematically in Figure 11b. In the case of a SmF phase, the radial integration of the outer peak (the 110 peak) gives four maxima at the angles $\chi = \sin^{-1}(\pm 0.5 \sin\theta)$ to the equator, with θ being the tilt angle, whereas the integration in dependence of χ of the outer peak (the 020 peak) of a SmI phase would result in only two maxima, which are located at the equator [14]. In the diffraction pattern of the higher-ordered smectic phase of **PhP16** in Figure 11a, four intense maxima are found at the angles χ = 75, 107.5, 257 and 286°. These four maxima, which are not located at the equator, clearly indicate that the higher-ordered smectic phase of **PhP16** is a SmF phase. The average angular distance of the four maxima to the equator, which is defined by the position of the maxima of the small angle peaks, is χ =15.4°. The tilt angle derived from this measurement is θ = 32°, which corresponds quite well with the optical tilt angle of 28.2° in the SmF phase (see Figure 12b). There are four other less-intense maxima observed on the radial intensity distribution of the (110) wide-angle peak: χ = 31, 154, 209 and 333°. This shows that the layer normal **k** is not oriented perpendicular to the incident X-ray beam throughout the whole sample, but in some parts it is also oriented parallel. This parallel orientation gives a pseudohexagonal intensity distribution, as seen in Figure 10a. As the intensity of these peaks is much smaller than the one of the peaks coming from the perpendicular orientation, only four of the six corners of the pseudohexagon can be seen, as the other two are underneath the other peaks. In Figure 11a the pseudohexagon is marked with white lines.

Precise measurements of the smectic layer spacing d were obtained by small-angle X-ray scattering (SAXS). Figure 12a shows the smectic layer spacing d of the SmC and the SmF phases of **PhP16**. At the phase transition, we observe a clear

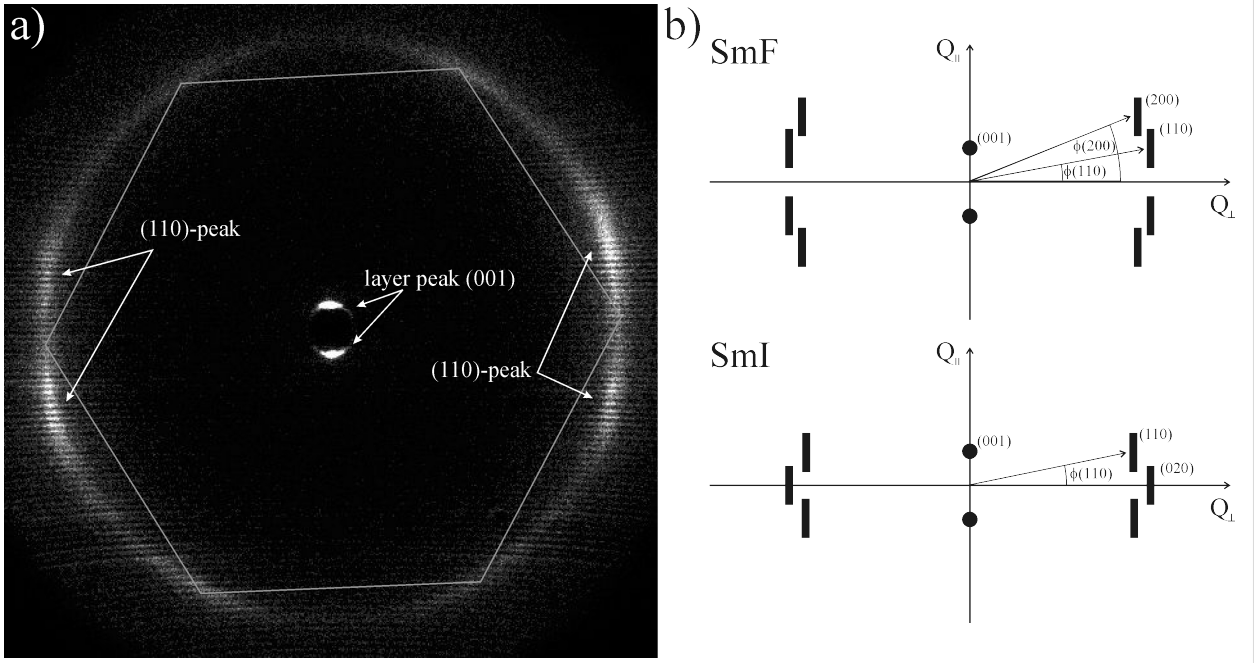

Figure 11: (a) WAXS-measurement of the SmF phase of **PhP16** at T = 88 °C with the smectic layer normal oriented mostly perpendicular to the incident beam. Only one wide-angle peak can be observed as well as the (001) layer peak. (b) Diffraction patterns of the SmF and SmI phase with the incident beam perpendicular to the layer normals (adapted from [14]).

step of the layer spacing from about 40 Å in the SmC phase to higher values of about 45 Å in the SmF phase, which suggests that the tilt angle is reduced at the phase transition. Accordingly, the optical tilt angle θ of **PhP16** was measured (Figure 12b); the tilt angle in the SmF phase is ca. 27° whereas it reaches 30° in the SmC phase. From the layer spacing d_F in the SmF phase and its tilt angle θ, the molecular length L of **PhP16** is calculated as $L = d_F/\cos\theta$. With d_F = 44.7 Å and θ = 28.2°, the effective molecular length L is 50.7 Å, which is in good agreement with the molecular length of 50.6 Å obtained by molecular modelling. In conclusion, the material **PhP16** shows a first-order phase transition from the tilted SmC phase to the tilted SmF phase at the transition temperature T_c.

Conclusion

The investigations of the phase diagram of the two phenylpyrimidines **PhP16** and **2PhP** with a length ratio of 2 is consistent with our previous study of a similar binary system with a length ratio of 1.8 [1,2]. The phenylpyrimidine **PhP16** used in this study has a greater length than the compound

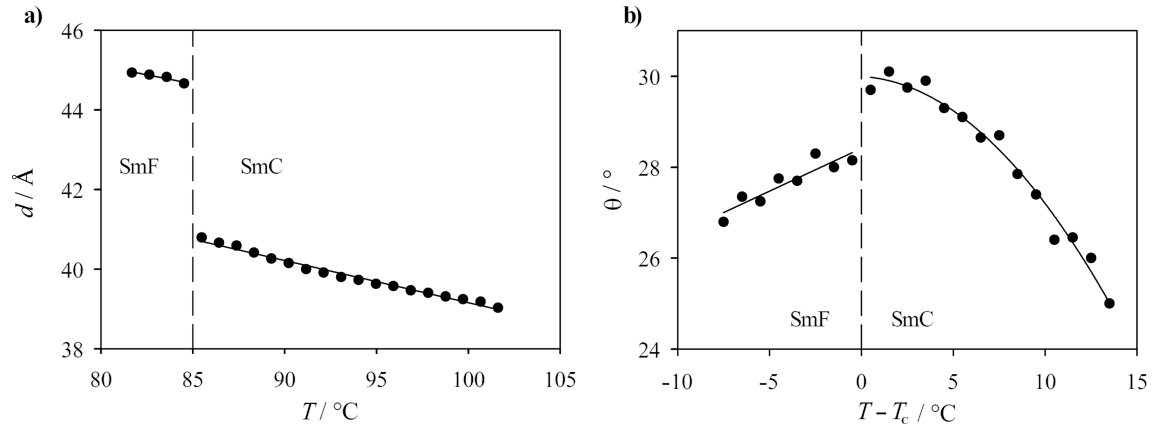

Figure 12: (a) Layer spacing of the SmF and the SmC phase of the pure compound **PhP16** in dependence of the temperature T. (b) Tilt angle θ versus reduced temperature $T-T_c$ for the pure compound **PhP16** in the SmF and in the SmC phase.

PhP14 that has been used in our earlier studies. The greater length of **PhP16** results in a different phase sequence, as **PhP16** forms a higher-ordered smectic phase in addition to the SmC phase, which is also formed by **PhP14**. Detailed investigations of this higher-ordered phase by texture analysis, shearing, and tilt-angle measurements as well as small- and wide-angle X-ray scattering confirmed that it is a smectic F phase. The greater length of **PhP16**, relative to **PhP14**, also changes the behavior of the mixtures with **2PhP**. In the system **PhP16**/**2PhP**, with the greater length difference, the stabilization of the smectic state is less pronounced. This indicates that the stability of the smectic state decreases with increasing length difference between the two molecules. This suggests that there is an optimum length difference, which is around 1.8, maximizing the stability of the smectic state.

Experimental

The compound **PhP16** [4] as well as the compound **MDW 510** [8] were synthesized according to the published procedures and showed the expected physical and spectral properties. The liquid-crystalline compound **2PhP** was purchased from a commercial source. A Kratky compact camera from Anton Paar was used to perform small-angle X-ray scattering (Ni-filtered Cu K_α radiation with wavelength $\lambda = 1.5418$ Å). The unaligned samples were filled into Mark capillary tubes of 0.7 mm diameter and put into a temperature-controlled sample holder (Anton Paar). A one-dimensional electronic detector by M. Braun was used to record the scattered intensity. Polarizing microscopy was performed by using a Leica DM-LP polarizing microscope with an Instec HS1-i hot stage. For the determination of optical tilt angles, the achiral samples were doped with 4 mol % of the chiral compound **MDW510** and filled into glass cells with a spacing of 1.6 μm, which were coated with a rubbed Nylon/ITO surface (AWAT PPW, Poland). The tilt angle θ was measured at a field strength of 12.5 $V \cdot \mu m^{-1}$.

Acknowledgements

This work was supported by the NSF/DFG program “Materials World Network” (DFG Gi 243/6) and by the Natural Sciences and Engineering Research Council of Canada.

References

1. Kapernaum, N.; Hartley, C. S.; Roberts, J. C.; Lemieux, R. P.; Giesselmann, F. *Beilstein J. Org. Chem.* **2009,** *5,* No. 65. doi:10.3762/bjoc.5.65
2. Kapernaum, N.; Hartley, C. S.; Roberts, J. C.; Schoerg, F.; Krueerke, D.; Lemieux, R. P.; Giesselmann, F. *ChemPhysChem* **2010,** *11,* 2099–2107. doi:10.1002/cphc.201000243
3. Wand, M. D.; Clark, N. A. *Proc. SPIE* **1987,** *825,* 81–87.
4. Hartley, C. S.; Kapernaum, N.; Roberts, J. C.; Giesselmann, F.; Lemieux, R. P. *J. Mater. Chem.* **2006,** *16,* 2329–2337. doi:10.1039/b515313a
5. Diele, S. *Ber. Bunsen-Ges. Phys. Chem.* **1993,** *97,* 1326–1336.
6. Bahr, C.; Heppke, G. *Ber. Bunsen-Ges. Phys. Chem.* **1987,** *91,* 925–929.
7. Giesselmann, F.; Heimann, A.; Zugenmaier, P. *Ferroelectrics* **1997,** *200,* 237–256. doi:10.1080/00150199708008609
8. Thurmes, W. N.; Wand, M. D.; Vohra, R. T.; Walba, D. M. *Mol. Cryst. Liq. Cryst.* **1991,** *204,* 1–7. doi:10.1080/00268949108046588
9. Thurmes, W. N.; Wand, M. D.; Vohra, R. T.; More, K. M.; Walba, D. M. *Liq. Cryst.* **1993,** *14,* 1061–1068. doi:10.1080/02678299308027814
10. Lagerwall, J. P. F.; Giesselmann, F. *ChemPhysChem* **2006,** *7,* 20–45. doi:10.1002/cphc.200500472
11. McMillan, W. L. *Phys. Rev. A* **1971,** *4,* 1238–1246. doi:10.1103/PhysRevA.4.1238
12. McMillan, W. L. *Phys. Rev. A* **1972,** *6,* 936–947. doi:10.1103/PhysRevA.6.936
13. Kapernaum, N.; Giesselmann, F. *Phys. Rev. E* **2008,** *78,* 062701. doi:10.1103/PhysRevE.78.062701
14. Seddon, J. M. Structural Studies of Liquid Crystals by X-Ray Diffraction. In *Handbook of liquid crystals;* Demus, D.; Goodby, J.; Gray, W.; Spiess, H.-W.; Vill, V., Eds.; Wiley-VCH: Weinheim, 1998; Vol. 1, pp 635–679. doi:10.1002/9783527620760.ch8c
15. Gray, G. W.; Goodby, J. W. *Smectic liquid crystals: Textures and Structures;* Leonard Hill: Philadelphia, PA, USA, 1984.

License and Terms

Beilstein Journal of Organic Chemistry

Synthesis of guanidinium–sulfonimide ion pairs: towards novel ionic liquid crystals

Martin Butschies, Manuel M. Neidhardt, Markus Mansueto, Sabine Laschat* and Stefan Tussetschläger

Full Research Paper

Open Access

Address:
Institut für Organische Chemie, Universität Stuttgart, Pfaffenwalring 55, 70569 Stuttgart, Germany

Email:
Sabine Laschat* - sabine.laschat@oc.uni-stuttgart.de

* Corresponding author

Keywords:
anion exchange; ionic liquid crystals; ion pairs; mesophases; sulfonimides

Beilstein J. Org. Chem. **2013,** *9,* 1093–1101.
doi:10.3762/bjoc.9.121

Received: 01 March 2013
Accepted: 21 May 2013
Published: 05 June 2013

This article is part of the Thematic Series "Progress in liquid crystal chemistry II". Dedicated to Professor Baldur Föhlisch on the occasion of his 80th birthday.

Associate Editor: P. J. Skabara

Abstract

The recently introduced concept of ionic liquid crystals (ILCs) with complementary ion pairs, consisting of both, mesogenic cation and anion, was extended from guanidinium sulfonates to guanidinium sulfonimides. In this preliminary study, the synthesis and mesomorphic properties of selected derivatives were described, which provide the first example of an ILC with the sulfonimide anion directly attached to the mesogenic unit.

Introduction

While ionic liquids, i.e., molten salts composed of either organic cation or anion (or both) with melting points far below 100 °C, are extensively used as designer solvents, electrolytes for lithium ion batteries, dye-sensitized solar cells, and the electrochemical deposition of metals [1-5], the corresponding ionic liquids with thermotropic liquid-crystalline properties, i.e., ILCs, are a much younger class of compounds [6-8]. Although Heintz was the pioneer, who observed in 1854 melting and clearing transitions upon heating of magnesium myristate [9,10], he did not recognize this as liquid-crystalline behavior. The first regular pyridinium ILCs were reported in 1938 by Knight and Shaw [11,12], followed by seminal findings by Seddon and Bruce [13]. Regarding ionic liquids, sulfonimides have been used in various ways. Particularly interesting is the symmetrical bistriflimide anion [14], which leads to desirable properties such as hydrolytic stability, low viscosity or low melting points in the ionic liquids [1,4,15-19]. By using an elongated perfluoroalkyl chain at the bistriflimide anion in combination with short chain-substituted pyrrolidinium cations MacFarlane was able to induce plastic crystal phases and liquid-crystalline phases at room temperature [20]. Ion pairs consisting of perfluorosulfonylimide anions and imidazolium cations with

short alkyl chains were studied by DesMarteau resulting in room-temperature ionic liquids [21]. In contrast, ILCs with bistriflimide anions are much less explored, because the sterically demanding anion often inhibits the formation of a mesophase [6,22]. Liquid-crystalline phases were found for viologen salts [23-28], imidazolium ILCs [29-31], pyrrolidinium ILCs [32,33] and ionic polymers [34-37]. Sulfonimides, which are directly bound to a mesogenic group, have not been described until now. We have recently described the concept of complementary ion pairs, where guanidinium sulfonate **1** with both mesogenic cation and anion displayed improved mesophase stability and increased phase widths as compared to their counterparts bearing a nonmesogenic spherical halide counterion [38,39] (Scheme 1).

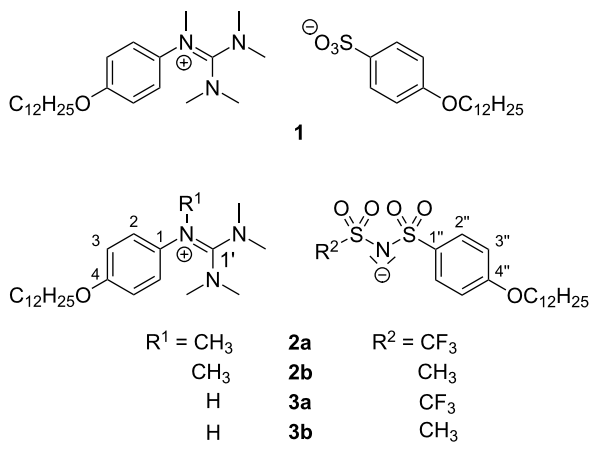

Scheme 1: Complementary guanidinium sulfonate **1** and guanidinium–sulfonimide ion pairs **2** and **3**.

We were thus interested, whether this concept could be also used to generate the corresponding sulfonimide ion pairs **2** and **3** with mesomorphic properties. The results of this preliminary study are discussed below.

Results and Discussion

The synthesis of guanidinium–sulfonimide ion pairs commenced with the commercially available sulfonyl chloride **4** [38], which was treated with trifluoromethanesulfonamide (**5a**) in the presence of NEt_3 following a procedure by Hesemann and Brunel [40]. Then the fluorinated sulfonimide was converted to the potassium salt **6a** after recrystallization from MeOH in 60% yield (Scheme 2).

The corresponding nonfluorinated sulfonimide K^+-salt **6b** was obtained by deprotonation of methanesulfonamide (**5b**) with NaH followed by treatment with sulfonyl chloride **4** according to a method by Dick and Townsend [41]. Analogous deprotonation with KOH yielded **6b** in 71%.

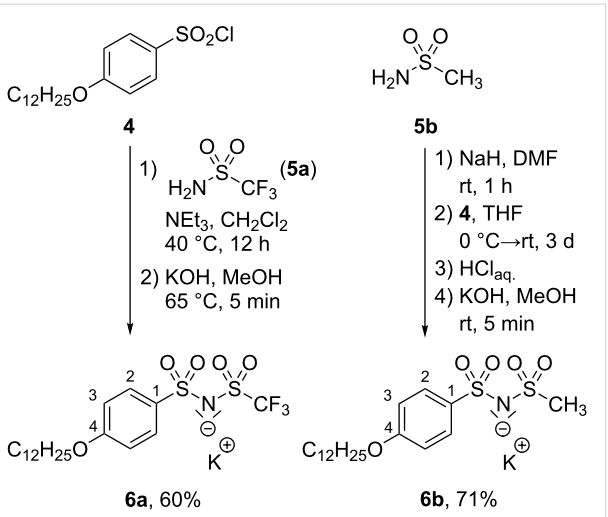

Scheme 2: Synthesis of the potassium sulfonimides **6a** and **6b**.

The K^+-salts were prepared due to their more convenient isolation as compared to the corresponding protonated compounds. However, the K^+-sulfonimides **6a**,**b** were not used for a direct methyl transfer towards the synthesis of the desired guanidinium–sulfonimide ion pairs in a similar way that the arylsulfonic acid methylesters were previously used as methyl transfer reagents [38], because we wanted to avoid the activation with dimethyl sulfate reported by DesMarteau [21]. Therefore we planned an indirect formation of the ion pairs by anion exchange via salt metathesis. In order to be successful, two requirements have to be met. First, the solubility of the sulfonimide salts **6a**,**b** in the solvent must be sufficient. Second, one of the products must be insoluble in order to shift the equilibrium towards complete conversion. In contrast to the sodium 4-alkoxyphenylsulfonates both potassium salts **6a**,**b** are soluble in boiling MeCN, so that both conditions for a successful salt metathesis are fulfilled.

The known guanidinium chloride **7**·Cl [42] was treated with MeI in the presence of K_2CO_3 to afford the N-methylated guanidinium iodide **8**·I (Scheme 3) [38,39].

However, this intermediate did not allow a salt metathesis, because the resulting KI is highly soluble in MeCN (and other organic solvents). Therefore, the intermediate was treated with $AgNO_3$ in MeOH. The resulting N-methylated guanidinium nitrate was then reacted with **6a** or **6b** in MeCN to the desired ion pairs **2a** and **2b** in 79% and 75% yield, respectively, while the precipitating KNO_3 shifted the salt metathesis to completion (Scheme 3).

The good solubility of the K^+-sulfonimide salts **6a**,**b** in MeCN was further used for a salt metathesis towards the N-protonated

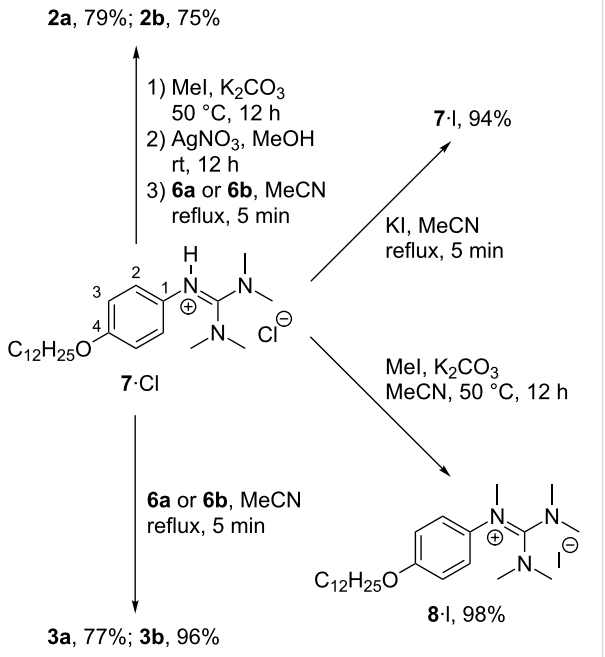

Scheme 3: Synthesis of guanidinium sulfonimides **2a**,**b**, **3a**,**b** and iodides **7·I**, **8·I**.

guanidinium–sulfonimide ion pairs **3a**,**b** by heating **7**·Cl with **6a** or **6b** under reflux. The resulting ion pairs **3a** and **3b** were isolated in 77% and 96% yield, respectively. In comparison the guanidinium iodide **7**·I was obtained in 94% yield by heating **7**·Cl with KI in MeCN under reflux (Scheme 3). The mesomorphic properties of ion pairs **2**,**3** and guanidinium halides **7**·I, **7**·Cl, **8**·I were studied by differential scanning calorimetry (DSC) and polarizing optical microscopy (POM). The results of the DSC experiments are summarized in Table 1.

N-Methylated guanidinium sulfonimides **2a**,**b** revealed only isotropic melting at 61 °C and 93 °C, respectively (Table 1, entries 1 and 2), while N-methylated guanidinium iodide **8**·I melted at 117 °C (Table 1, entry 3). In comparison, the N-methylated guanidinium sulfonate **1** displayed a melting transition at 99 °C in the SmA phase and isotropic clearing at 148 °C (Table 1, entry 8). Thus, while the presence of the sulfonimide anions in **2a**,**b** indeed led to a decrease of the melting point as compared to the corresponding iodide **8**·I, the formation of a smectic mesophase was completely suppressed. For protonated guanidinium sulfonimides **3a**,**b** again a significant decrease of the melting temperature was found (75 °C and 71 °C, respectively, Table 1, entries 4 and 5) as compared to the protonated guanidinium iodide **7**·I, which melted at 130 °C into the isotropic phase (Table 1, entry 6). The protonated chloride **7**·Cl showed a melting transition at 121 °C into the SmA phase, and a clearing transition at 128 °C (Table 1, entry 7) [42]. However, while the trifluoromethyl-substituted sulfonimide **3a** displayed only three crystal-to-crystal transitions at 8, 19 and 37 °C, respectively, besides isotropization at 75 °C, the corresponding methyl-substituted sulfonimide **3b** showed two crystal-to-crystal transitions at 5 °C and 27 °C, respectively, a melting transition into the smectic A phase at 71 °C and a clearing point at 87 °C. Thus, sulfonimide-containing ion pair **3b** indeed led to a mesophase albeit with only 16 K phase width as compared to 49 K phase width of the guanidinium sulfonate **1**. The DSC traces of **3b** are shown in Figure 1.

POM observations of **3b** upon cooling from the isotropic liquid revealed fan-shaped textures and homeotropic alignment (Figure 2) typical for SmA phases.

The mesophase of compound **3b** was investigated by X-ray scattering (WAXS and SAXS) at different temperatures. The

Table 1: Phase-transition temperatures (°C) and enthalpies (kJ mol^{-1}) of guanidinium–sulfonimide ion pairs **2** and **3** and the corresponding guanidinium salts **7**·I, **7**·Cl and **8**·I[a].

Entry	Compound	Phase transitions (onset (°C)) and transition enthalpies (given in parentheses) (kJ mol^{-1}) upon second heating
1	**2a**	Cr 61 (31.8) I[b]
2	**2b**	Cr 93 (59.1) I
3	**8**·I	Cr_1 49 (8.4) Cr_2 117 (25.8) I[c]
4	**3a**	Cr_1 8 (18.6) Cr_2 19 (0.8) Cr_3 37 (−44.9) Cr_4 75 (48.6) I
5	**3b**	Cr_1 5 (8.1) Cr_2 27 (−54.4) Cr_3 71 (73.1) SmA 87 (1.4) I
6	**7**·I	Cr_1 55 (−44.3) Cr_2 130 (37.2) I
7	**7**·Cl	Cr 121 (29.9) SmA 128 (0.7) I[b,d]
8	**1**	Cr_1 51 (−5.1) Cr_2 99 (61.6) SmA 148 (1.9) I[c]

[a]The following phases were observed: Cr Crystalline, SmA Smectic A, I Isotropic. Heating rate 10 K min^{-1}. [b]Upon 1st heating. [c]Data for compounds **8**·I and **1** were taken from [38]. [d]Data for compound **7**·Cl was taken from [42]; heating rate 5 K min^{-1}.

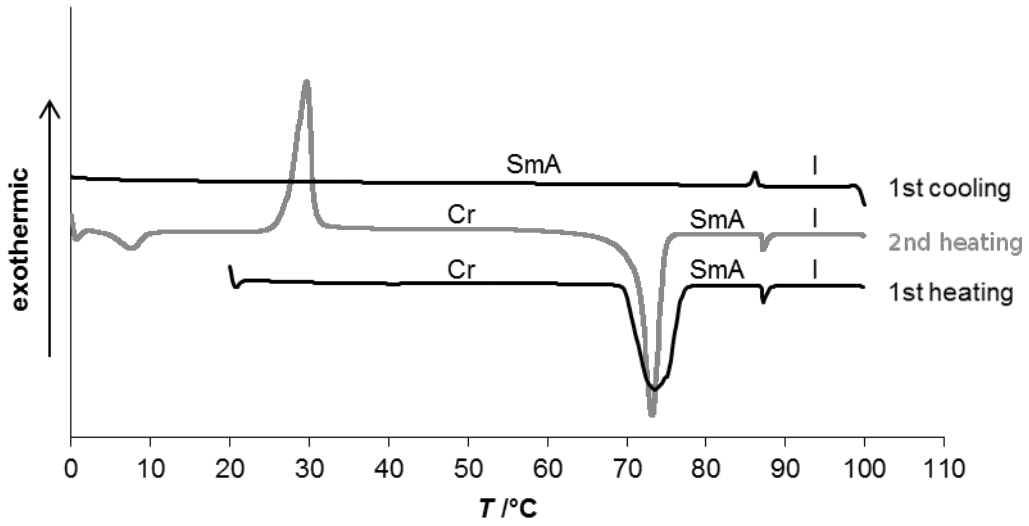

Figure 1: DSC traces of compound **3b** (heating/cooling rate 10 K min^{-1}).

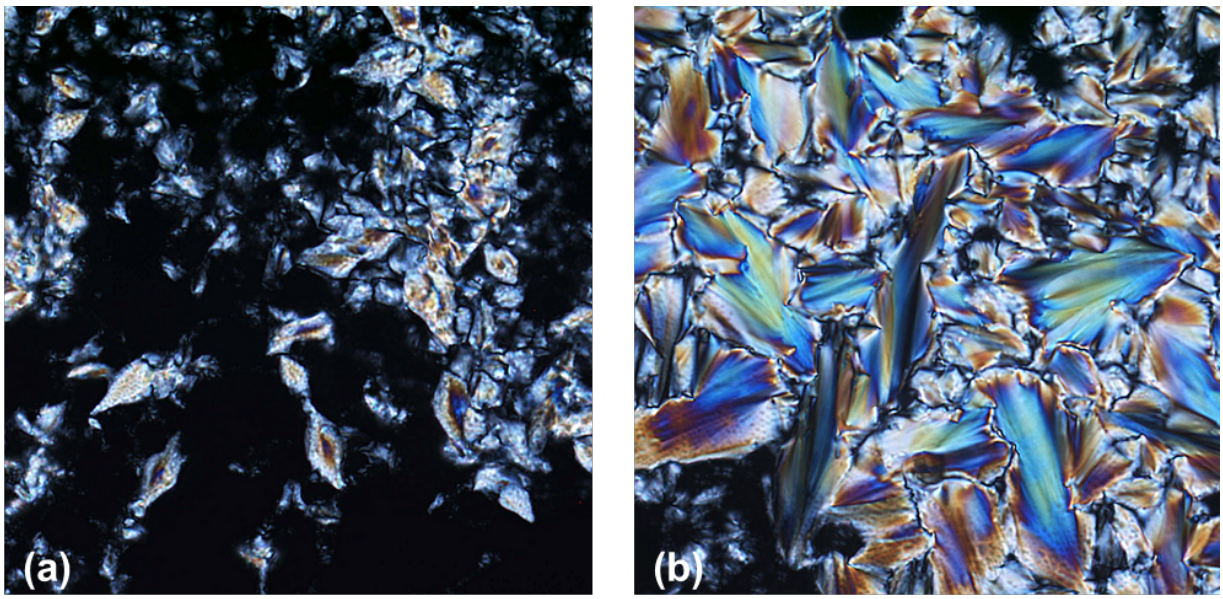

Figure 2: Compound **3b** under crossed polarizers upon cooling from the isotropic melt (200-fold magnification). (a) Homeotropic texture at 80 °C (cooling rate 10 K min^{-1}); (b) fan-shaped texture at 88 °C (cooling rate 1 K min^{-1}).

XRD experiments revealed diffraction patterns with a single diffraction peak and a diffuse halo at 4.7 Å resulting from the alkyl chains (Figure 3). These patterns are typical for smectic mesophases and further confirm the assignment of a SmA phase based on POM observations.

The exact layer spacing at each temperature was determined by fitting the first-order peak with a Gaussian distribution (Figure 3 and Supporting Information File 1, Table S1) and decreases with rising temperatures. To allow a comparison with the layer spacings of compounds **1** and **7**·Cl, the layer spacing of **3b** was determined at a reduced temperature (T_{red} = 0.95·T_{iso}) by linear extrapolation of the obtained data (Table 2). The obtained value of d_{red} = 32.6 Å (Table 2) is in good agreement with the values determined for salts **7**·Cl (34.0 Å [42]) and **1** (32.2 Å [38]) bearing the same (**7**·Cl) or nearly the same (N–Me instead of N–H) cation **1**. As the layer spacing is much larger (32.6 Å) compared to the calculated length of the cation

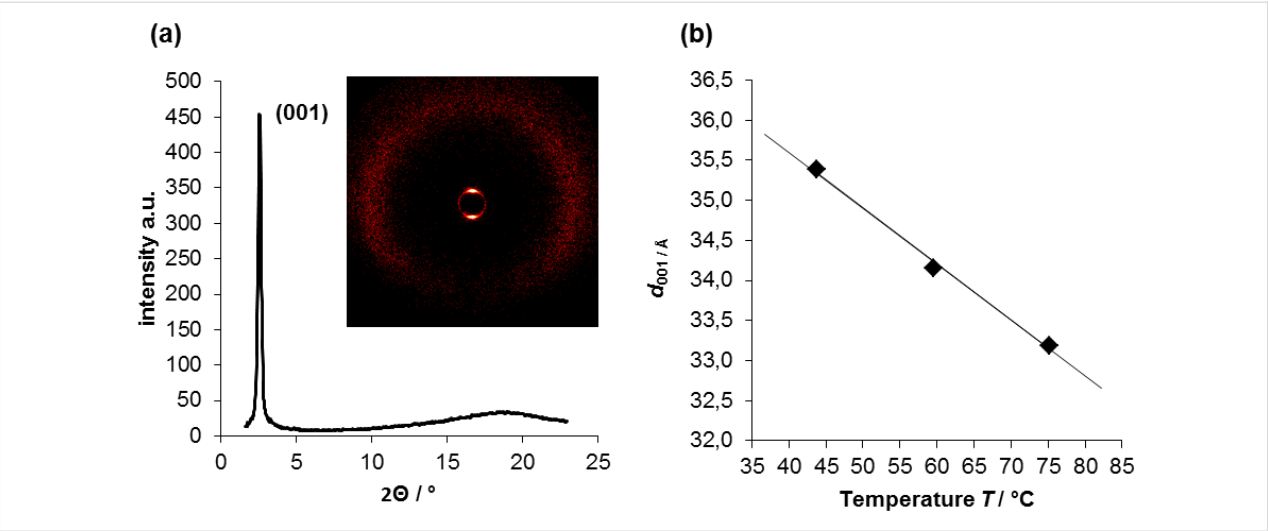

Figure 3: (a) WAXS diffraction pattern of **3b** at 59.5 °C (vertical magnetic field director); (b) temperature-dependent layer spacing of compound **3b**.

and anion (23–24 Å, Table 2), we propose the formation of mixed double layers with the charged heads of cation and anion pointing to each other. This packing behavior is in good agreement with those reported for guanidinium sulfonate **1** [38].

Table 2: Layer spacings of compounds **1**, **7**·Cl and **3b** at a common reduced temperature in comparison to the calculated molecular lengths.

Compound	T_{red}/[° C]	d_{red}/[Å]	L_{calc} (cation)/[Å]	L_{calc} (anion)/[Å]
3b	83	32.6	23.8[a]	22.7[a]
7·Cl[b]	122	34.0	23.9	1.81[c]
1[d]	141	32.2	23.0	21.0

[a]Calculated using Chem3D Ultra, Cambridgesoft, 2011. [b]Values were taken from [42]. [c]Value was taken from [43]. [d]Values were taken from [38].

Conclusion

We have developed a route towards guanidinium–sulfonimide ion pairs in which both anion and cation contain mesogenic units. The replacement of a spherical halide counterion by a calamitic sulfonimide anion indeed led to a decrease of the melting points, the effect being larger for trifluorosulfonimides **2a** and **3a** as compared to methylsulfonimides **2b** and **3b**. It should be noted that Strassner has recently introduced a different concept to tune melting points in ionic liquids by electronic effects of the aryl substituent [44,45]. However, the mesogenic sulfonimide resulted in the formation of a SmA mesophase only in the case of **3b**, while ion pairs **2a**,**b** and **3a** did not show any liquid-crystalline properties. Thus, the presence of mesogenic counterions could not overcome the known tendency of sulfonimides to inhibit mesomorphism.

Experimental

General Information. All reactions were carried out under a nitrogen atmosphere with Schlenk-type glassware and the solvents were dried and distilled under nitrogen prior to use. Characterization of the compounds was carried out by using the following instruments. Elemental analyses: Carlo Erba Strumentazione Elemental Analyzer, Modell 1106. NMR: Bruker Avance 500 (^{1}H, 500 MHz; ^{13}C, 125 MHz). IR: Bruker Vector 22 FTIR spectrometer with MKII golden gate single reflection diamond ATR system. ^{1}H and ^{13}C NMR spectra were recorded at room temperature and referenced to TMS (Me_4Si δ_H = 0.0 ppm, δ_C = 0.0 ppm) as an internal standard. The assignment of the resonances was supported by chemical shift calculations and 2D experiments (COSY and HMBC). MS (EI): Varian MAT 711 spectrometer. Polarizing optical microscopy: Olympus BX50 polarizing microscope combined with a Linkam TP93 central controller. MS (ESI): Bruker Daltonics microTOF-Q spectrometer. Differential scanning calorimetry (DSC): Mettler-Toledo DSC 822e (heating/cooling rates were 10 K min^{-1}). X-ray diffraction (WAXS, SAXS regions): Bruker AXS Nanostar C diffractometer employing Ni-filtered Cu Kα radiation (λ = 1.5418 Å). Melting points: Büchi SMP-20. Water content: Metrohm 831 Coulometric Karl Fischer Titrator, (generator electrode with a diaphragm), HYDRANAL-Coulomat AG and HYDRANAL-Coulomat CG solutions were used.

Compounds **4** and **5a,b** are commercially available. Full characterization of compounds **1** and **8**·I is given in [38], and for compound **7**·Cl in [42]. For compounds **2b**, **3a** and **7**·I the following water content was determined by Karl Fischer titration: 0.38%, 0.36% and 0.13%, respectively (see Supporting Information File 1, Table S2).

4-(Dodecyloxy)-*N*-((trifluoromethyl)sulfonyl)benzenesulfonamide, potassium salt (6a): A mixture of trifluoromethanesulfonamide (**5a**) (207 mg, 1.38 mmol) and 4-(dodecyloxy)-benzenesulfonylchloride (**4**) (500 mg, 1.39 mmol) was dissolved in abs dichloromethane (20 mL). Abs triethylamine (1 mL, 701 mg, 6.93 mmol) was added and the resulting mixture was heated under reflux for 12 h. After cooling to room temperature the solvent was removed in vacuo, the residue was taken up in ethyl acetate (100 mL), and the hot suspension was filtered. The filtrate was evaporated to dryness and the residue was purified by flash chromatography with ethyl acetate as eluent. The resulting solid was taken up in methanol (20 mL), potassium hydroxide (78 mg, 1.39 mmol) was added, and the mixture was heated under reflux for 5 min. After cooling to 0 °C product **6a** precipitated as a colorless solid. Yield: 425 mg (60%); colorless solid; mp > 300 °C; ^{1}H NMR (500 MHz, DMSO-d_6) δ 0.85 (t, J = 7.2 Hz, 3H, CH_3), 1.17–1.35 (m, 16H, CH_2), 1.36–1.43 (m, 2H, CH_2), 1.67–1.74 (m, 2H, CH_2), 4.01 (t, J = 6.5 Hz, 2H, OCH_2), 6.94–7.00 (m, 2H, 3-H), 7.62–7.68 (m, 2H, 2-H) ppm; ^{13}C NMR (125 MHz, DMSO-d_6) δ 13.9 (CH_3), 22.1, 25.4, 28.5, 28.68, 28.71, 28.95, 28.98, 29.0 31.3 (CH_2), 67.7 (OCH_2), 113.8 (C-3), 128.1 (C-2), 137.1 (C-1), 160.5 (C-4) ppm; FTIR (ATR) $\tilde{\nu}$: 2917 (m), 2848 (m), 1597 (m), 1584 (m), 1497 (m), 1467 (m), 1387 (w), 1329 (s), 1284 (m), 1254 (m), 1232 (m), 1206 (m), 1160 (vs), 1114 (m), 1093 (s), 1058 (s), 956 (w), 867 (w), 833 (m), 801 (w), 780 (s), 746 (s), 718 (w), 683 (m) cm^{-1}; ESIMS (*m*/*z*): 472 [M]$^-$, 303 [M$^-$ − $C_{12}H_{25}$]; HRMS–ESI (*m*/*z*): [M]$^-$ calcd for $C_{19}H_{29}F_3NO_5S_2^-$, 472.1445; found, 472.1427.

4-(Dodecyloxy)-*N*-((methylsulfonyl)benzenesulfonamide, potassium salt (6b): Methanesulfonamide (**5b**) (277 mg, 2.91 mmol) was given to a suspension of sodium hydride (333 mg, 8.31 mmol) in abs DMF (10 mL) and the mixture was stirred for 1 h. After cooling to 0 °C a solution of 4-(dodecyloxy)benzenesulfonylchloride (**4**, 1.00 g, 2.77 mmol) in abs THF (5 mL) was added dropwise and the reaction mixture was warmed to room temperature. After being stirred for 3 days, the mixture was brought to pH 1 by the addition of concd hydrochloric acid. The solvents were removed in vacuo and the residue was taken up in dichloromethane (50 mL). The resulting solution was dried with magnesium sulfate and filtered, and the filtrate was evaporated to dryness. The residue was taken up in methanol (30 mL) and treated with potassium hydroxide (156 mg, 2.77 mmol) for 5 min. After cooling the mixture to 0 °C the product **6b** precipitated as a colorless solid. Yield: 901 mg (71%); colorless solid; mp > 300 °C; ^{1}H NMR (500 MHz, DMSO-d_6) δ 0.86 (t, J = 6.8 Hz, 3H, CH_3), 1.18–1.35 (m, 16H, CH_2), 1.36–1.43 (m, 2H, CH_2), 1.66–1.74 (m, 2H, CH_2), 2.72 (s, 3H, SO_2CH_3), 3.98 (t, J = 6.5 Hz, 2H, OCH_2), 6.86–6.92 (m, 2H, 3-H), 7.59–7.64 (m, 2H, 2-H) ppm; ^{13}C NMR (125 MHz, DMSO-d_6) δ 13.9 (CH_3), 22.0, 25.4, 28.5, 28.6, 28.7, 28.90, 28.91, 28.94, 31.2 (CH_2), 42.6 (SO_2CH_3), 67.5 (OCH_2), 113.2 (C-3), 128.0 (C-2), 138.8 (C-1), 159.6 (C-4) ppm; FTIR (ATR) $\tilde{\nu}$: 3077 (w), 2914 (s), 2849 (m), 1595 (m), 1498 (m), 1473 (m), 1394 (m), 1274 (s), 1248 (s), 1152 (s), 1126 (s), 1089 (vs), 972 (m), 831 (s), 808 (s), 721 (s), 679 (m), 590 (s), 525 (vs) cm^{-1}; ESIMS (*m*/*z*): 418 [M]$^-$, 340 [M$^-$ − CH_3O_2S + H], 249 [M$^-$ − $C_{12}H_{25}$]; HRMS–ESI (*m*/*z*): [M]$^-$ calcd for $C_{19}H_{32}NO_5S_2^-$, 418.1727; found, 418.1728.

General procedure for the preparation of pentamethylguanidinium ion pairs (**2a,b**)

Potassium carbonate (144 mg, 971 μmol) and methyl iodide (207 mg, 1.46 mmol) were added to a solution of guanidinium chloride (**7**·Cl, 200 mg, 485 μmol) in acetonitrile (20 mL). The resulting mixture was heated to 50 °C for 12 h and then cooled to room temperature, and the solvent was removed in vacuo. The residue was taken up in dichloromethane (20 mL) and filtered, and the filtrate was concentrated to dryness. A solution of the residue in methanol (20 mL) was treated with silver nitrate (165 mg, 971 μmol) and stirred for 12 h at room temperature under the exclusion of light. The solvent was removed under reduced pressure, the residue was taken up in dichloromethane (20 mL), and the slurry was filtered by using a Rotilabo-syringe filter. After concentration of the filtrate to dryness, the residue was taken up in acetonitrile (10 mL), and sulfonimide salt **6a** or **6b** (509 μmol) was added. The mixture was heated under reflux for 5 min, the solvent was removed in vacuo, and the residue was taken up in dichloromethane (20 mL). After filtration with a Rotilabo-syringe filter the solvent was removed in vacuo, and the crude product was recrystallized from ethyl acetate.

***N*-(4-(Dodecyloxy)phenyl)-*N*,*N*',*N*',*N*",*N*"-pentamethylguanidinium ((4-(dodecyloxy)phenyl)sulfonyl)((trifluoromethyl)sulfonyl)amide (2a):** Yield: 330 mg (79%); colorless solid; ^{1}H NMR (500 MHz, $CDCl_3$) δ 0.88 (t, J = 6.8 Hz, 6H, CH_3), 1.20–1.38 (m, 32H, CH_2), 1.40–1.48 (m, 4H, CH_2), 1.73–1.82 (m, 4H, OCH_2CH_2), 2.82, 3.07 (br s, 12H, $N[CH_3]_2$), 3.39 (s, 3H, NCH_3), 3.94 (t, J = 6.5 Hz, 2H, OCH_2), 3.97 (t, J = 6.5 Hz, 2H, OCH_2), 6.87–6.95 (m, 2H, 3-H, 3"-H), 6.97–7.02 (m, 2H, 2-H), 7.88–7.92 (m, 2H, 2"-H) ppm; ^{13}C NMR (125 MHz, $CDCl_3$) δ 14.1 (CH_3), 22.7, 25.98, 26.01, 29.11, 29.18, 29.36, 29.39, 29.40, 29.57, 29.61, 29.64, 29.67, 31.9 (CH_2), 40.2 (NCH_3), 40.2, 41.1 (br s, $N(CH_3)_2$), 68.3, 68.5 (OCH_2), 114.1 (C-3"), 115.9 (C-3), 123.4 (C-2), 129.3 (C-2"), 134.65, 134.72 (C-1, C-1"), 157.7 (C-4), 162.0 (C-4"), 162.2 (C-1') ppm; ^{19}F NMR (235 MHz, $CDCl_3$) δ −77.0 (CF_3) ppm; FTIR (ATR) $\tilde{\nu}$: 2918 (s), 2850 (m), 1611 (m), 1597 (m), 1555 (m), 1511 (m), 1473 (m), 1410 (m), 1350 (m), 1323 (s), 1288 (m), 1246 (s), 1221 (m), 1173 (vs), 1132 (s), 1093 (s), 1056 (s),

999 (s), 897 (m), 837 (m), 797 (m), 720 (w), 687 (m) cm^{-1}; ESIMS (*m*/*z*): 390 $[M]^+$, 222 $[M^+ - C_{12}H_{25} + H]$; ESIMS (*m*/*z*): 472 $[M]^-$, 303 $[M^- - C_{12}H_{25}]$; HRMS–ESI (*m*/*z*): $[M]^+$ calcd for $C_{24}H_{44}N_3O^+$, 390.3479; found, 390.3456; HRMS–ESI (*m*/*z*): $[M]^-$ calcd for $C_{19}H_{29}F_3NO_5S_2^-$, 472.1434; found, 472.1438; DSC: Cr 61 °C [31.8 kJ mol^{-1}] I.

***N*-(4-(Dodecyloxy)phenyl)-*N*,*N*',*N*',*N*",*N*"-pentamethylguanidinium ((4-(dodecyloxy)phenyl)sulfonyl)(methylsulfonyl)amide (2b):** Yield: 94 mg (75%); colorless solid; ^{1}H NMR (500 MHz, $CDCl_3$) δ 0.88 (t, *J* = 6.9 Hz, 6H, CH_3), 1.20–1.39 (m, 32H, CH_2), 1.39–1.48 (m, 4H, CH_2), 1.73–1.81 (m, 4H, OCH_2CH_2), 2.82, 3.09 (br s, 12H, $N[CH_3]_2$), 3.41 (s, 3H, NCH_3), 2.90 (s, 3H, SO_2CH_3), 3.90–3.97 (m, 4H, OCH_2), 6.82–6.87 (m, 2H, 3"-H), 6.89–6.94 (m, 2H, 3-H), 7.00–7.05 (m, 2H, 2-H), 7.87–7.92 (m, 2H, 2"-H) ppm; ^{13}C NMR (125 MHz, $CDCl_3$) δ 14.1 (CH_3), 22.7, 26.0, 29.19, 29.20, 29.35, 29.40, 29.58, 29.64, 29.67, 31.9 (CH_2), 40.3 (NCH_3), 40.3, 41.2 (br s, $N(CH_3)_2$), 42.2 (SO_2CH_3), 68.1, 68.4 (OCH_2), 113.6 (C-3"), 115.8 (C-3), 123.4 (C-2), 128.7 (C-2"), 135.0 (C-1), 137.8 (C-1"), 157.4 (C-4), 160.7 (C-4"), 162.2 (C-1') ppm; FTIR (ATR) $\tilde{\nu}$: 2919 (s), 2850 (m), 1612 (m), 1552 (m), 1510 (m), 1469 (m), 1403 (m), 1296 (w), 1268 (s), 1241 (s), 1177 (m), 1143 (m), 1122 (s), 1086 (s), 1051 (s), 1001 (w), 948 (w), 897 (w), 837 (m), 801 (m), 721 (s), 653 (s), 587 (vs) cm^{-1}; ESIMS (*m*/*z*): 390 $[M]^+$, 222 $[M^+ - C_{12}H_{25} + H]$; ESIMS (*m*/*z*): 418 $[M]^-$, 249 $[M^- - C_{12}H_{25}]$; HRMS–ESI (*m*/*z*): $[M]^+$ calcd for $C_{24}H_{44}N_3O^+$, 390.3479; found, 390.3484; HRMS–ESI (*m*/*z*): $[M]^-$ calcd for $C_{19}H_{32}NO_5S_2^-$, 418.1716; found, 418.1791; Anal. calcd for $C_{43}H_{76}N_4O_6S$: C, 63.82; H, 9.47; N, 6.92; found: C, 63.83; H, 9.38; N, 6.94; DSC: Cr 93 °C [59.1 kJ mol^{-1}] I.

General procedure for the preparation of tetramethylguanidinium ion pairs (3a,b)

A mixture of guanidinium chloride (**7**·Cl, 50 mg, 0.122 mmol) and sulfonimide K^+-salt **6a** or **6b** (0.129 mmol) in acetonitrile (10 mL) was heated under reflux for 5 min. The solvent was removed under reduced pressure, the residue was taken up in dichloromethane (20 mL), and the slurry was filtered with a Rotilabo-syringe filter. After removal of all volatiles in vacuo, the residue was recrystallized from ethyl acetate to give the pure salts **3a**,**b**.

***N*-(4-(Dodecyloxy)phenyl)-*N*',*N*',*N*",*N*"-tetramethylguanidinium ((4-(dodecyloxy)phenyl)sulfonyl)((trifluoromethyl)sulfonyl)amide (3a):** Yield: 95 mg (77%), colorless solid; ^{1}H NMR (500 MHz, $CDCl_3$) δ 0.88 (t, *J* = 7.0 Hz, 6H, CH_3), 1.20–1.39 (m, 32H, CH_2), 1.40–1.49 (m, 4H, CH_2), 1.73–1.82 (m, 4H, OCH_2CH_2), 2.98 (br s, 12H, $N(CH_3)_2$), 3.92 (t, *J* = 6.6 Hz, 2H, OCH_2), 3.97 (t, *J* = 6.6 Hz, 2H, OCH_2), 6.85–6.91 (m, 4H, 3-H, 3"-H), 6.95–7.00 (m, 2H, 2-H), 7.85–7.90 (m, 2H, 2"-H) ppm; ^{13}C NMR (125 MHz, $CDCl_3$) δ 14.1 (CH_3), 22.7, 25.99, 26.04, 29.13, 29.24, 29.36, 29.39, 29.42, 29.57, 29.59, 29.61, 29.64, 29.67, 31.9 (CH_2), 40.3 ($N(CH_3)_2$), 66.3, 66.4 (OCH_2), 113.9 (C-3"), 115.7 (C-3), 122.3 (C-2), 128.7 (C-2"), 130.2 (C-1), 135.6 (C-1"), 157.0 (C-4), 159.1 (C-4"), 161.6 (C-1') ppm; ^{19}F NMR (235 MHz, $CDCl_3$) δ −78.1 (CF_3) ppm; FTIR (ATR) $\tilde{\nu}$: 2917 (s), 2850 (m), 1620 (m), 1595 (m), 1572 (m), 1512 (m), 1474 (m), 1423 (w), 1403 (m), 1335 (s), 1311 (m), 1296 (m), 1257 (m), 1241 (m), 1223 (m), 1195 (s), 1163 (s), 1137 (s), 1111 (w), 1091 (m), 1032 (vs), 915 (w), 828 (s), 782 (m), 752 (m), 723 (m), 685 (m), 640 (m), 598 (s), 562 (s) cm^{-1}; ESIMS (*m*/*z*): 376 $[M]^+$, 331 $[M^+ - C_2H_6N - H]$; ESIMS (*m*/*z*): 472 $[M]^-$, 303 $[M^- - C_{12}H_{25}]$; HRMS–ESI (*m*/*z*): $[M]^+$ calcd for $C_{23}H_{42}N_3O^+$, 376.3322; found: 376.3334; HRMS–ESI (*m*/*z*): $[M]^-$ calcd for $C_{19}H_{29}F_3NO_5S_2^-$, 472.1434; found, 472.1425; Anal. calcd for $C_{42}H_{71}F_3N_4O_6S_2$ (849.2): C, 59.41; H, 8.43; N, 6.60; found: C, 59.53; H, 8.36; N, 6.60; DSC: Cr_1 8 °C [18.6 kJ mol^{-1}] Cr_2 19 °C [0.8 kJ mol^{-1}] Cr_3 37 °C [−44.9 kJ mol^{-1}] Cr_4 75 °C [48.6 kJ mol^{-1}] I.

***N*-(4-(Dodecyloxy)phenyl)-*N*',*N*',*N*",*N*"-tetramethylguanidinium ((4-(dodecyloxy)phenyl)sulfonyl)(methylsulfonyl)amide (3b):** Yield: 93 mg (96%); colorless solid; ^{1}H NMR (500 MHz, $CDCl_3$) δ 0.88 (t, *J* = 6.9 Hz, 6H, CH_3), 1.20–1.39 (m, 32H, CH_2), 1.40–1.48 (m, 4H, CH_2), 1.72–1.81 (m, 4H, OCH_2CH_2), 2.86–3.08 (m, 12H, $N(CH_3)_2$), 2.90 (s, 3H, SO_2CH_3), 3.92 (t, *J* = 6.5 Hz, 2H, OCH_2), 3.96 (t, *J* = 6.6 Hz, 2H, OCH_2), 6.83–6.89 (m, 4H, 3-H, 3"-H), 6.96–7.02 (m, 2H, 2-H), 7.85–7.90 (m, 2H, 2"-H) ppm; ^{13}C NMR (125 MHz, $CDCl_3$) δ 14.1 (CH_3), 22.7, 26.0, 26.1, 29.16, 29.25, 29.36, 29.40, 29.42, 29.58, 29.59, 29.61, 29.64, 29.67, 31.9 (CH_2), 40.4 ($N(CH_3)_2$), 42.4 (SO_2CH_3), 66.2, 66.3 (OCH_2), 113.8 (C-3"), 115.6 (C-3), 122.2 (C-2), 128.7 (C-2"), 130.7 (C-1), 136.7 (C-1"), 156.8 (C-4), 159.2 (C-4"), 161.1 (C-1') ppm; FTIR (ATR) $\tilde{\nu}$: 2915 (s), 2850 (m), 1631 (m), 1597 (m), 1567 (s), 1513 (m), 1467 (m), 1434 (m), 1417 (m), 1401 (m), 1301 (w), 1271 (s), 1239 (s), 1170 (w), 1114 (s), 1079 (vs), 1061 (s), 1004 (m), 972 (m), 913 (w), 835 (s), 800 (m), 714 (s) cm^{-1}; ESIMS (*m*/*z*): 376 $[M]^+$, 331 $[M^+ - C_2H_6N - H]$; ESIMS (*m*/*z*): 418 $[M]^-$, 249 $[M^- - C_{12}H_{25}]$; HRMS–ESI (*m*/*z*): $[M]^+$ calcd for $C_{23}H_{42}N_3O^+$, 376.3322; found, 376.3331; HRMS–ESI (*m*/*z*): $[M]^-$ calcd for $C_{19}H_{32}NO_5S_2^-$, 418.1716; found, 418.1724; Anal. calcd for $C_{42}H_{74}N_4O_6S_2$ (795.2): C, 63.44; H, 9.38; N, 7.05; found: C, 63.55; H, 9.31; N, 7.07; DSC: Cr_1 5 °C [8.1 kJ mol^{-1}] Cr_2 27 °C [−54.4 kJ mol^{-1}] Cr_3 71 °C [73.1 kJ mol^{-1}] SmA 87 °C [1.4 kJ mol^{-1}] I.

***N*-(4-(Dodecyloxy)phenyl)-*N*',*N*',*N*",*N*"-tetramethylguanidinium iodide (7·I):** A mixture of guanidinium chloride (**7**·Cl,

400 mg, 971 μmol) and potassium iodide (493 mg, 2.97 mmol) in acetonitrile (15 mL) was heated under reflux for 5 min. After being cooled to room temperature, the solvent was removed under reduced pressure. The residue was taken up in dichloromethane (20 mL), and the resulting slurry was filtered. After evaporation of the filtrate to dryness the residue was recrystallized from ethyl acetate/acetonitrile (20:1). Yield: 446 mg (94%); colorless solid; ^{1}H NMR (500 MHz, $CDCl_3$) δ 0.88 (t, J = 6.9 Hz, 3H, CH_3), 1.73–1.80 (m, 2H, OCH_2CH_2), 2.98 (br s, 12H, $N(CH_3)_2$), 3.91 (t, J = 6.6 Hz, 2H, OCH_2), 6.84–6.91 (m, 2H, 3-H), 7.11–7.17 (m, 2H, 3-H), 9.93 (s, 1H, NH) ppm; ^{13}C NMR (125 MHz, $CDCl_3$) δ 14.1 (CH_3), 22.7, 26.0, 29.22, 29.36, 29.41, 29.58, 29.61, 29.64, 29.67, 31.9 (CH_2), 41.0 (br s, $N(CH_3)_2$), 68.4 (OCH_2), 115.6 (C-3), 122.6 (C-2), 129.8 (C-1), 157.1, 158.4 (C-4, C-1) ppm; FTIR (ATR) $\tilde{\nu}$: 2917 (s), 2847 (m), 1620 (s), 1558 (s), 1510 (s), 1467 (s), 1452 (m), 1417 (s), 1398 (s), 1312 (m), 1261 (m), 1229 (s), 1167 (m), 1115 (m), 1067 (m), 1024 (m), 1000 (m), 907 (w), 837 (s), 798 (w), 782 (w), 719 (m), 683 (s), 635 (m), 603 (m), 537 (m) cm^{-1}; ESIMS (m/z): 376 $[M]^+$, 331 $[M^+ - C_2H_6 - H]$; ESIMS (m/z): 127 $[M]^-$; HRMS–ESI (m/z): $[M]^+$ calcd for $C_{23}H_{42}N_3O^+$, 376.3323; found, 376.3343; Anal. calcd for $C_{23}H_{42}IN_3O$ (503.5): C, 54.86; H, 8.41; N, 8.35; found: C, 54.91; H, 8.23; N, 7.97; DSC: Cr_1 55 °C [−44.3 kJ mol^{-1}] Cr_2 130 °C [37.2 kJ mol^{-1}] I.

Supporting Information

Supporting Information File 1

DSC traces of compounds **2a**,**b**, **3a** and X-ray data of compound **3b**.
[http://www.beilstein-journals.org/bjoc/content/supplementary/1860-5397-9-121-S1.pdf]

Acknowledgements

Generous financial support by the Studienstiftung des Deutschen Volkes (Fellowship for M.B.), the Deutsche Forschungsgemeinschaft, the Ministerium für Wissenschaft, Forschung und Kunst des Landes Baden-Württemberg, the Fonds der Chemischen Industrie and the Forschungsfonds der Universität Stuttgart is gratefully acknowledged.

References

1. Endres, F.; MacFarlane, D.; Abbott, A. P., Eds. *Electrodeposition from Ionic Liquids;* Wiley-VCH: Weinheim, Germany, 2008. doi:10.1002/9783527622917
2. *Ionic Liquids IIIA: Fundamentals, Progress, Challenges, and Opportunities;* Seddon, K. R.; Rogers, R. D., Eds.; *ACS Symposium Series*, Vol. 901; American Chemical Society: Washington, 2005. doi:10.1021/bk-2005-0901
3. *Ionic Liquids IIIB: Fundamentals, Progress, Challenges, and Opportunities–Transformations and Processes;* Seddon, K. R.; Rogers, R. D., Eds.; *ACS Symposium Series*, Vol. 902; American Chemical Society: Washington, 2005. doi:10.1021/bk-2005-0902
4. Wasserscheid, P.; Welton, T., Eds. *Ionic Liquids in Synthesis,* 2nd ed.; Wiley-VCH: Weinheim, Germany, 2008. doi:10.1002/9783527621194
5. Dupont, J.; de Souza, R. F.; Suarez, P. A. Z. *Chem. Rev.* **2002,** *102,* 3667–3692. doi:10.1021/cr010338r
6. Axenov, K. V.; Laschat, S. *Materials* **2011,** *4,* 206–259. doi:10.3390/ma4010206
7. Kato, T.; Mizoshita, N.; Kishimoto, K. *Angew. Chem.* **2006,** *118,* 44–74. doi:10.1002/ange.200501384
Angew. Chem., Int. Ed. **2006,** *45,* 38–68. doi:10.1002/anie.200501384
8. Binnemans, K. *Chem. Rev.* **2005,** *105,* 4148–4204. doi:10.1021/cr0400919
9. Heintz, W. *Justus Liebigs Ann. Chem.* **1854,** *92,* 291–299. doi:10.1002/jlac.18540920306
10. Heintz, W. *J. Prakt. Chem.* **1855,** *66,* 1–51. doi:10.1002/prac.18550660101
11. Knight, G. A.; Shaw, B. D. *J. Chem. Soc.* **1938,** 682–683. doi:10.1039/jr9380000682
12. Somashekar, R. *Mol. Cryst. Liq. Cryst.* **1987,** *146,* 225–233. doi:10.1080/00268948708071815
13. Bowlas, C. J.; Bruce, D. W.; Seddon, K. R. *Chem. Commun.* **1996,** 1625–1626. doi:10.1039/cc9960001625
14. Jákli, A.; Saupe, A. *One- and Two-Dimensional Fluids: Properties of Smectic, Lamellar and Columnar Liquid Crystals;* CRC Press: Boca Raton, 2006. doi:10.1201/9781420012200
15. Welton, T. *Chem. Rev.* **1999,** *99,* 2071–2084. doi:10.1021/cr980032t
16. Plechkova, N. V.; Seddon, K. R. *Chem. Soc. Rev.* **2008,** *37,* 123–150. doi:10.1039/b006677j
17. Bonhôte, P.; Dias, A.-P.; Papageorgiou, N.; Kalyanasundaram, K.; Grätzel, M. *Inorg. Chem.* **1996,** *35,* 1168–1175. doi:10.1021/ic951325x
18. Jacquemin, J.; Husson, P.; Padua, A. A. H.; Majer, V. *Green Chem.* **2006,** *8,* 172–180. doi:10.1039/b513231b
19. Keskin, S.; Kayrak-Talay, D.; Akman, U.; Hortaçsu, Ö. *J. Supercrit. Fluids* **2007,** *43,* 150–180. doi:10.1016/j.supflu.2007.05.013
20. Johansson, K. M.; Adebahr, J.; Howlett, P. C.; Forsyth, M.; MacFarlane, D. R. *Aust. J. Chem.* **2007,** *60,* 57–63. doi:10.1071/CH06299
21. Hickman, T.; DesMarteau, D. D. *J. Fluorine Chem.* **2012,** *133,* 11–15. doi:10.1016/j.jfluchem.2011.11.001
22. Gao, Y.; Slattery, J. M.; Bruce, D. W. *New J. Chem.* **2011,** *35,* 2910–2918. doi:10.1039/c1nj20715f
23. Bhowmik, P. K.; Han, H.; Cebe, J. J.; Nedeltchev, I. K. *Polym. Prepr. (Am. Chem. Soc., Div. Polym. Chem.)* **2002,** *43,* 1385–1386.
24. Bhowmik, P. K.; Han, H.; Cebe, J. J.; Burchett, R. A.; Acharya, B.; Kumar, S. *Liq. Cryst.* **2003,** *30,* 1433–1440. doi:10.1080/02678290310001621895
25. Bhowmik, P. K.; Han, H.; Nedeltchev, I. K.; Cebe, J. J. *Mol. Cryst. Liq. Cryst.* **2004,** *419,* 27–46. doi:10.1080/15421400490478272
26. Causin, V.; Saielli, G. *J. Mater. Chem.* **2009,** *19,* 9153–9162. doi:10.1039/b915559g
27. Jo, T. S.; Wray, J. K.; Tanthmanatham, O.; Han, H.; Bhowmik, P. K. *Polym. Prepr. (Am. Chem. Soc., Div. Polym. Chem.)* **2011,** *52,* 387–388.

28. Bonchio, M.; Carraro, M.; Casella, G.; Causin, V.; Rastrelli, F.; Saielli, G. *Phys. Chem. Chem. Phys.* **2012,** *14,* 2710–2717. doi:10.1039/c2cp23580c
29. Fernandez, A. A.; de Haan, L. T.; Kouwer, P. H. J. *J. Mater. Chem. A* **2013,** *1,* 354–357. doi:10.1039/c2ta00133k
30. Alam, M. A.; Motoyanagi, J.; Yamamoto, Y.; Fukushima, T.; Kim, J.; Kato, K.; Takata, M.; Saeki, A.; Seki, S.; Tagawa, S.; Aida, T. *J. Am. Chem. Soc.* **2009,** *131,* 17722–17723. doi:10.1021/ja905373d
31. Goossens, K.; Nockemann, P.; Driesen, K.; Goderis, B.; Görller-Walrand, C.; Van Hecke, K.; Van Meervelt, L.; Pouzet, E.; Binnemans, K.; Cardinaels, T. *Chem. Mater.* **2008,** *20,* 157–168. doi:10.1021/cm702321c
32. Goossens, K.; Lava, K.; Nockemann, P.; Van Hecke, K.; Van Meervelt, L.; Pattison, P.; Binnemans, K.; Cardinaels, T. *Langmuir* **2009,** *25,* 5881–5897. doi:10.1021/la900048h
33. Goossens, K.; Lava, K.; Nockemann, P.; Van Hecke, K.; Van Meervelt, L.; Driesen, K.; Görller-Walrand, C.; Binnemans, K.; Cardinaels, T. *Chem.–Eur. J.* **2009,** *15,* 656–674. doi:10.1002/chem.200801566
34. Bhowmik, P. K.; Han, H.; Cebe, J. J.; Burchett, R. A.; Sarker, A. M. *J. Polym. Sci., Part A: Polym. Chem.* **2002,** *40,* 659–674. doi:10.1002/pola.10134
35. Bhowmik, P. K.; Han, H.; Cebe, J. J.; Nedeltchev, I. K.; Kang, S.-W.; Kumar, S. *Macromolecules* **2004,** *37,* 2688–2694. doi:10.1021/ma030460n
36. Bhowmik, P. K.; Han, H.; Nedeltchev, A. K. *J. Polym. Sci., Part A: Polym. Chem.* **2006,** *44,* 1028–1041. doi:10.1002/pola.21181
37. Han, H.; Vantine, P. R.; Nedeltchev, A. K.; Bhowmik, P. K. *J. Polym. Sci., Part A: Polym. Chem.* **2006,** *44,* 1541–1554. doi:10.1002/pola.21259
38. Butschies, M.; Frey, W.; Laschat, S. *Chem.–Eur. J.* **2012,** *18,* 3014–3022. doi:10.1002/chem.201101925
39. Lo Celso, F.; Pibiri, I.; Triolo, A.; Triolo, R.; Pace, A.; Buscemi, S.; Vivona, N. *J. Mater. Chem.* **2007,** *17,* 1201–1208. doi:10.1039/B615190F
    See for example for ILCs with trifluoromethanesulfonate counterion.
40. El Kadib, A.; Hesemann, P.; Molvinger, K.; Brandner, J.; Biolley, C.; Gaveau, P.; Moreau, J. J. E.; Brunel, D. *J. Am. Chem. Soc.* **2009,** *131,* 2882–2892. doi:10.1021/ja807630j
41. Jones, P. B.; Parrish, N. M.; Houston, T. A.; Stapon, A.; Bansal, N. P.; Dick, J. D.; Townsend, C. A. *J. Med. Chem.* **2000,** *43,* 3304–3314. doi:10.1021/jm000149l
42. Sauer, S.; Saliba, S.; Tussetschläger, S.; Baro, A.; Frey, W.; Giesselmann, F.; Laschat, S.; Kantlehner, W. *Liq. Cryst.* **2009,** *36,* 275–299. doi:10.1080/02678290902850027
43. Marcus, Y. *J. Chem. Soc., Faraday Trans.* **1993,** *89,* 713–718. doi:10.1039/ft9938900713
44. Schulz, T.; Ahrens, S.; Meyer, D.; Allolio, C.; Peritz, A.; Strassner, T. *Chem.–Asian J.* **2011,** *6,* 863–867. doi:10.1002/asia.201000744
45. Ahrens, S.; Peritz, A.; Strassner, T. *Angew. Chem.* **2009,** *121,* 8048–8051. doi:10.1002/ange.200903399
    Angew. Chem., Int. Ed. **2009,** *48,* 7908–7910. doi:10.1002/anie.200903399

License and Terms